# TRANSCELLULAR CYCLES UNDERLYING NEUROTRANSMISSION

EDITED BY: Sebastian Cerdan
PUBLISHED IN: Frontiers in Neuroenergetics

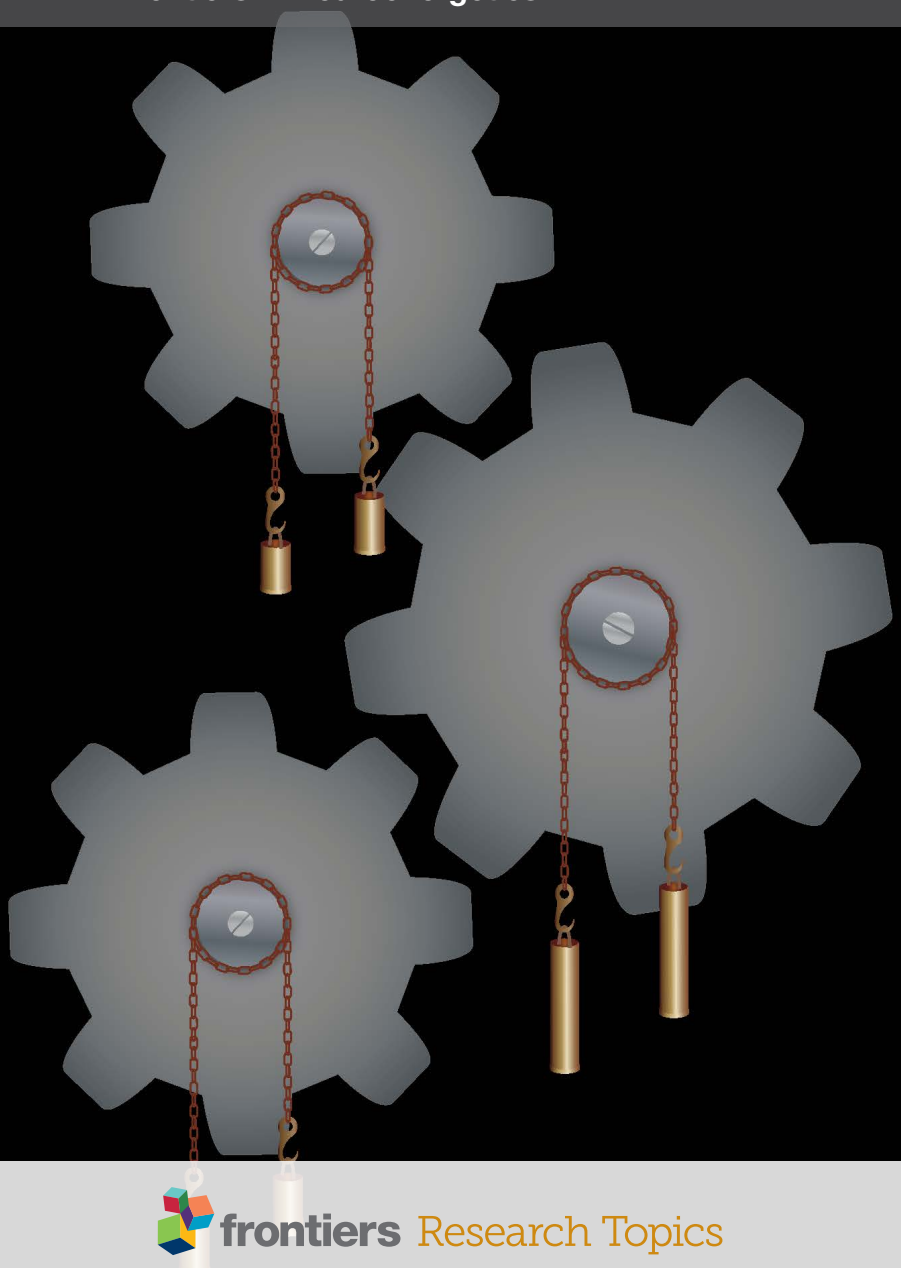

frontiers Research Topics

# frontiers



**ISSN 1664-8714**
**ISBN 978-2-88919-654-8**
**DOI 10.3389/978-2-88919-654-8**

## About Frontiers

Frontiers is more than just an open-access publisher of scholarly articles: it is a pioneering approach to the world of academia, radically improving the way scholarly research is managed. The grand vision of Frontiers is a world where all people have an equal opportunity to seek, share and generate knowledge. Frontiers provides immediate and permanent online open access to all its publications, but this alone is not enough to realize our grand goals.

## Frontiers Journal Series

The Frontiers Journal Series is a multi-tier and interdisciplinary set of open-access, online journals, promising a paradigm shift from the current review, selection and dissemination processes in academic publishing. All Frontiers journals are driven by researchers for researchers; therefore, they constitute a service to the scholarly community. At the same time, the Frontiers Journal Series operates on a revolutionary invention, the tiered publishing system, initially addressing specific communities of scholars, and gradually climbing up to broader public understanding, thus serving the interests of the lay society, too.

## Dedication to Quality

Each Frontiers article is a landmark of the highest quality, thanks to genuinely collaborative interactions between authors and review editors, who include some of the world's best academicians. Research must be certified by peers before entering a stream of knowledge that may eventually reach the public - and shape society; therefore, Frontiers only applies the most rigorous and unbiased reviews.
Frontiers revolutionizes research publishing by freely delivering the most outstanding research, evaluated with no bias from both the academic and social point of view.
By applying the most advanced information technologies, Frontiers is catapulting scholarly publishing into a new generation.

## What are Frontiers Research Topics?

Frontiers Research Topics are very popular trademarks of the Frontiers Journals Series: they are collections of at least ten articles, all centered on a particular subject. With their unique mix of varied contributions from Original Research to Review Articles, Frontiers Research Topics unify the most influential researchers, the latest key findings and historical advances in a hot research area! Find out more on how to host your own Frontiers Research Topic or contribute to one as an author by contacting the Frontiers Editorial Office: **researchtopics@frontiersin.org**

# TRANSCELLULAR CYCLES UNDERLYING NEUROTRANSMISSION

Topic Editor:
**Sebastian Cerdan,** Instituto de Investigaciones Biomédicas "Alberto Sols" CSIC/UAM, Spain

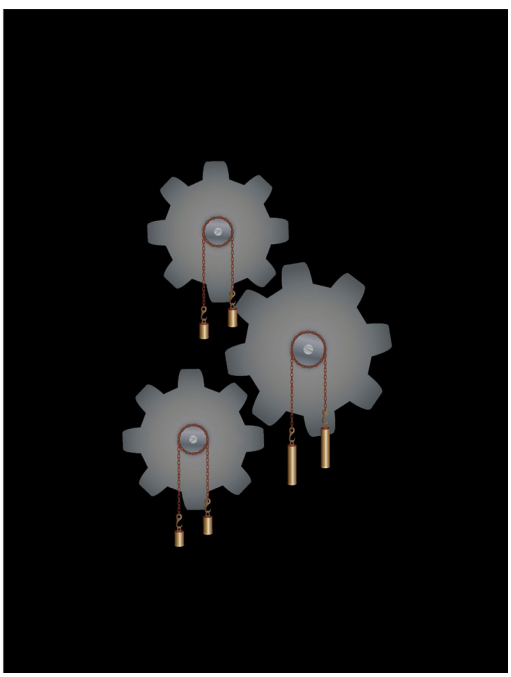

The mechanisms underlying cerebral activation may be envisioned mechanically as high precision clockwork machinery, composed of three closely coupled and reversible gears, representing blood vessels (top gear), astrocytes (central gear) and neurons (bottom gear), respectively. The rotation of these gears is driven ultimately by the energy requirements of the system, coupling mechanically the neuronal needs to the vascular supplies, through the central astrocyte gear. The mechanisms ultimately responsible for the rotation of these gears, those coupling one gear to the next, or the weights necessary to maintain the system in continuous operation, remain insufficiently understood. The present e-book addresses these topics.

Synaptic transmission demands the operation of a highly specialized metabolic machinery involving the transfer of metabolites and neurotransmitters between neurons, astrocytes and microvessels. In the last years, important advances have occurred in our understanding of the mechanisms underlying cerebral activation, neuroglial coupling and the associated neurovas-

cular response. Briefly, exacerbated oxygen consumption in stimulated neurons is thought to trigger glycolytic lactate and glucose transfer from astrocytes which, in turn, obtain these fuels from the microvasculature.

Neurotransmitter release is made possible by a combination of transcellular cycles exchanging metabolites between these three compartments, returning eventually the synapsis to its pre-firing situation in the resting periods. In spite of the enormous progresses achieved in recent years, the drivers determining the predominant direction of the fluxes, their quantitative contribution and their energy requirements, have remained until today incompletely understood, more particularly under the circumstances prevailing in vivo.

In many instances, progress derived from the implementation of novel methodological approaches including advanced neuroimaging and neurospectroscopy methods. As a consequence, literature in the field became vast, diverse and spread within journals of different specialities. The e-book "Transcellular cycles underlying neurotransmission" aims to summaryze in a single volume, recent progress achieved in hypothesis, methods and interpretations on the trafficking of metabolites between neurons and glial cells, and the associated mechanisms of neurovascular coupling.

**Citation:** Cerdan, S., ed. (2015). Transcellular Cycles Underlying Neurotransmission. Lausanne: Frontiers Media. doi: 10.3389/978-2-88919-654-8

# Table of Contents

frontiers in Nutrition

EDITORIAL
published: 29 June 2015
doi: 10.3389/fnut.2015.00018

# Editorial: "Transcellular cycles underlying neurotransmission"

*Sebastián Cerdan*[1]* *and Blanca Lizarbe*[2]

[1] *Instituto Investigaciones Biomédicas "Alberto Sols" CSIC-UAM, Madrid, Spain,* [2] *Laboratory for Functional and Metabolic Imaging (LIFMET), SB IPSB, École Polytechnique Fédéral de Lausanne, Lausanne, Switzerland*

**Keywords: magnetic resonance imaging, magnetic resonance spectroscopy, glutamate–glutamine cycle, neuroglial interactions, neurovascular coupling**

Neuronal action potentials and neurotransmitter releases induce important alterations in the extracellular *millieu*, including increased $K^+$ concentrations from membrane repolarization and increased neurotransmitter levels from trans-synaptic signaling (1, 2). It becomes crucial then to remove, fast and efficiently, these ionic and neurotransmitter surges and to prepare the synapsis for a new neurotransmission event (3). In parallel, the energy demands of these metabolic movements must be fulfilled from substrates, such as glucose and lactate, obtained from cerebrovascular supplies (4, 5). Surrounding astrocytes coordinate all these tasks, playing a central role during neurotransmission, many times operating intercellularly as astrocytic networks (6, 7). Summarizing, the adequate operation of neurotransmission requires the transcellular coupling of neuronal and astrocytic metabolisms to a suitable supply of metabolic substrates from the microvasculature. Pathological alterations in these processes underlie the most morbid and prevalent neurological disorders, including ischemic or traumatic episodes and neurodegeneration.

Despite enormous progress in our understanding of neurotransmission during the last decades, important questions remain insufficiently explored including the quantitative assessment of transcellular cycles of glutamate, glutamine, and GABA supporting glutamatergic or gabaergic neurotransmissions, the preferred metabolic substrates, as glucose and/or lactate, supporting the energy demands under resting or stimulated conditions, and the mechanisms underlying neurovascular coupling. In addition, the important question on how all these processes occur and integrate under the *in vivo* situation reaches, in this context, vital relevance.

Recently, a variety of non-invasive approaches have allowed the investigation of these aspects *in vivo* (8), outstandingly, those involving functional magnetic resonance imaging and $^{13}C$ magnetic resonance spectroscopy methods. The following e-book entitled "Transcellular Cycles Underlying Neurotransmission" provides an authoritative overview of these issues, compiling contributions from leading scientists in this field.

In the study of neuroglial interactions *in vivo*, Rodrigues et al. (9) provide a convenient introduction to the fundamentals of $^{13}C$ NMR spectroscopy and its applications to cerebral energy metabolism, Duarte et al. (10) report on the compartmentalized metabolism of (1,6-$^{13}C_2$) glucose in the brain *in vivo*, Shen (11) reviews the mathematical modeling strategies used to simulate quantitatively the operation glutamate–glutamine cycle *in vivo*, and Sampol et al. (12) address the metabolism of glucose and lactate in the stimulated, awake, rat brain. Similarly, Bartnick-Olson et al. (13) illustrate the use of $^{13}C$ NMR to evaluate the altered neuroglial interactions in response to traumatic brain injury.

The neurophysiological, metabolic, and cellular compartmentation events underlying functional neuroimaging by MRI are discussed by Moreno et al. (14), while Lizarbe et al. (15) cover the use of different MRI and MRS strategies to evaluate the ionic responses during hypothalamic activation by appetite stimulation. The role of astrocytic metabolic networks in metabolic coupling is discussed

OPEN ACCESS

***Edited and reviewed by:***
*Pierre J. Magistretti, École Polytechnique Fédéral de Lausanne, Switzerland*

***Correspondence:**
*Sebastián Cerdan*
*scerdan@iib.uam.es*

***Specialty section:***
*This article was submitted to Neuroenergetics, Nutrition and Brain Health, a section of the journal Frontiers in Nutrition*

***Received:*** *02 June 2015*
***Accepted:*** *11 June 2015*
***Published:*** *29 June 2015*

***Citation:***
*Cerdan S and Lizarbe B (2015) Editorial: "Transcellular cycles underlying neurotransmission". Front. Nutr. 2:18. doi: 10.3389/fnut.2015.00018*

by Escartin and Rouach (16), whereas Bergessen and Gjedde (17) elaborate on the interesting hypothesis of lactate becoming a volume transmitter of metabolic states through the brain.

In summary, this e-book provides a broad coverage of recent progress in neuroglial coupling mechanisms underlying neuronal firing under physiological or pathological situations and their integration within astrocytic networks and associated neurovascular responses, as observed by advanced magnetic resonance imaging and spectroscopy methods *in vivo*.

We hope that this compilation becomes useful for a wide range of neuroscientists, from young students entering the field and looking for a global perspective, to established scientists, searching for specialized views on critical issues of cerebral neurotransmission *in vivo*.

## References


1. Hertz L, Xu J, Song D, Yan E, Gu L, Peng L. Astrocytic and neuronal accumulation of elevated extracellular $K^+$ with a 2/3 $K^+/Na^+$ flux ratio-consequences for energy metabolism, osmolarity and higher brain function. *Front Comput Neurosci* (2013) **7**:114. doi:10.3389/fncom.2013.00114
2. Koester J. Voltage-gated ion channels and the generation of the action potential. In: Kandel E, Schwartz JH, Jessel TM, editors. *Principles of Neural Science*. Englewood Cliffs, NJ: Prentice Hall (1991). p. 104–18.
3. Kandel E, Siegelbaum SA, Schwartz JH. Synaptic transmission. In: Kandel E, Schwartz JH, Jessel TM, editors. *Principles of Neural Science*. Englewood Cliffs, NJ: Prentice Hall (1991). p. 123–34.
4. Dienel GA. Energy generation in the central nervous system. In: Edvinson L, Krause DN, editors. *Cerebral Blood Flow and Metabolism*. Philadelphia, PA: Lippincott Williams & Wilkins (2002). p. 140–61.
5. Attwell D, Laughlin SB. An energy budget for signaling in the grey matter of the brain. *J Cereb Blood Flow Metab* (2001) **21**:1133–45. doi:10.1097/00004647-200110000-00001
6. Belanger M, Allaman I, Magistretti PG. Brain energy metabolism: focus on astrocyte-neuron metabolic cooperation. *Cell Metab* (2015) **14**:724–38. doi:10.1016/j.cmet.2011.08.016
7. Giaume C, Koulakoff A, Roux L, Holcman D, Rouach N. Astroglial networks: a step further in neuroglial and gliovascular interactions. *Nat Rev Neurosci* (2010) **11**:87–99. doi:10.1038/nrn2757
8. Song AW, Merkle H, Neil JJ, Linden A, Graaf RA, Cady EB, et al. Advances in neurobiology. In: Choi I-Y, Gruetter R, editors. *Neural Metabolism in vivo*. Vol. 4. New York, NY: Springer (2012). doi:10.1007/978-1-4614-1788-0
9. Rodrigues TB, Valette J, Bouzier-Sore AK. $^{13}C$ NMR spectroscopy applications to brain energy metabolism. *Front Neuroenergetics* (2013) **5**:9. doi:10.3389/fnene.2013.00009
10. Duarte JM, Lanz B, Gruetter R. Compartmentalized cerebral metabolism of [1,6-$^{13}C$]glucose determined by in vivo $^{13}C$ NMR spectroscopy at 14.1 T. *Front Neuroenergetics* (2013) **3**:3. doi:10.3389/fnene.2011.00003
11. Shen J. Modeling the glutamate-glutamine neurotransmitter cycle. *Front Neuroenergetics* (2013) **5**:1. doi:10.3389/fnene.2013.00001
12. Sampol D, Ostrofet E, Jobin ML, Raffard G, Sanchez S, Bouchaud V, et al. Glucose and lactate metabolism in the awake and stimulated rat: a $^{13}C$-NMR study. *Front Neuroenergetics* (2013) **5**:5. doi:10.3389/fnene.2013.00005
13. Bartnik-Olson BL, Harris NG, Shijo K, Sutton RL. Insights into the metabolic response to traumatic brain injury as revealed by $^{13}C$ NMR spectroscopy. *Front Neuroenergetics* (2013) **5**:8. doi:10.3389/fnene.2013.00008
14. Moreno A, Jego P, de la Cruz F, Canals S. Neurophysiological, metabolic and cellular compartments that drive neurovascular coupling and neuroimaging signals. *Front Neuroenergetics* (2013) **5**:3. doi:10.3389/fnene.2013.00003
15. Lizarbe B, Benítez A, Pelaez-Brioso GA, Sanchez-Montanes M, López-Larrubia P, Ballesteros P, et al. Hypothalamic metabolic compartmentation during appetite regulation as revealed by magnetic resonance imaging and spectroscopy methods. *Front Neuroenergetics* (2013) **5**:6. doi:10.3389/fnene.2013.00006
16. Escartin C, Rouach N. Astroglial networking contributes to neurometabolic coupling. *Front Neuroenergetics* (2013) **5**:4. doi:10.3389/fnene.2013.00004
17. Bergersen LH, Gjedde A. Is lactate a volume transmitter of metabolic states of the brain? *Front Neuroenergetics* (2012) **4**:5. doi:10.3389/fnene.2012.00005


**Conflict of Interest Statement:** The authors declare that the research was conducted in the absence of any commercial or financial relationships that could be construed as a potential conflict of interest. The handling editor, Pierre J. Magistretti, declares that, despite being affiliated to the same institution as author, Blanca Lizarbe, the review was handled objectively and no conflict of interest exists.

frontiers in
NEUROENERGETICS

REVIEW ARTICLE
published: 09 December 2013
doi: 10.3389/fnene.2013.00009

# $^{13}$C NMR spectroscopy applications to brain energy metabolism

***Tiago B. Rodrigues[1]*, Julien Valette[2] and Anne-Karine Bouzier-Sore[3]***

[1] *Cancer Research UK Cambridge Institute and Department of Biochemistry, University of Cambridge, Cambridge, UK*
[2] *Commissariat à l'Energie Atomique, Institut d'Imagerie Biomédicale, Molecular Imaging Research Center, Fontenay-Aux-Roses, France*
[3] *Centre de Résonance Magnétique des Systèmes Biologiques, UMR 5536, Université Bordeaux Segalen - Centre National de la Recherche Scientifique, Bordeaux, France*

***Edited by:***
*Sebastian Cerdan, Instituto de Investigaciones Biomedicas Alberto Sols, Spain*

***Reviewed by:***
*Sebastian Cerdan, Instituto de Investigaciones Biomedicas Alberto Sols, Spain*
*Ursula Sonnewald, Norwegian University of Science and Technology, Norway*

****Correspondence:***
*Tiago B. Rodrigues, Cancer Research UK Cambridge Institute and Department of Biochemistry, University of Cambridge, Robinson Way, Cambridge CB2 0RE, UK*
*e-mail: tiago.rodrigues@cruk.cam.ac.uk*

$^{13}$C nuclear magnetic resonance (NMR) spectroscopy is the method of choice for studying brain metabolism. Indeed, the most convincing data obtained to decipher metabolic exchanges between neurons and astrocytes have been obtained using this technique, thus illustrating its power. It may be difficult for non-specialists, however, to grasp the full implication of data presented in articles written by spectroscopists. The aim of the review is, therefore, to provide a fundamental understanding of this topic to facilitate the non-specialists in their reading of this literature. In the first part of this review, we present the metabolic fate of $^{13}$C-labeled substrates in the brain in a detailed way, including an overview of some general neurochemical principles. We also address and compare the various spectroscopic strategies that can be used to study brain metabolism. Then, we provide an overview of the $^{13}$C NMR experiments performed to analyze both intracellular and intercellular metabolic fluxes. More particularly, the role of lactate as a potential energy substrate for neurons is discussed in the light of $^{13}$C NMR data. Finally, new perspectives and applications offered by $^{13}$C hyperpolarization are described.

**Keywords: $^{13}$C NMR spectroscopy, brain metabolism, neuron, astrocyte, neuroglial coupling, metabolic modeling, hyperpolarized NMR**

## INTRODUCTION

The brain is metabolically the most energy-consuming organ. Adequate brain physiology depends on the unceasing supply of proper amounts of oxygen and plasma glucose (Glc). Consequently, limitations in the delivery of these two cerebral substrates cause most physiopathological states (Nicholls, 2007; Okada and Lipton, 2007).

Classical approaches to study cerebral metabolism, both in physiological and in physiopathological conditions, required the use of optical methods or radioactive isotopes and the isolation and purification of the enzymes or transport systems involved to study the corresponding *in vitro* kinetics (Bachelard, 1989; Clark and Lai, 1989; Sokoloff, 1989). This reductionist approach provided essential information on the operation of the central nervous system (CNS), despite the limitations brought by the small amounts of the involved proteins present in cerebral tissues and by the fact that its utilization was circumscribed to *postmortem* biopsies or cerebral extracts.

The remarkable advance during the past decades of powerful tools for investigating the human brain has had a tremendous impact on our ability to investigate and understand brain function. Autoradiography and positron emission tomography (PET) methods have been developed based on the measurement of regional Glc consumption, after the administration of 2-deoxyglucose, either labeled with $^{14}$C or with $^{18}$F, respectively (Sokoloff, 1981; Wienhard, 2002; Herholz and Heiss, 2004). These methodologies can be used to determine the regional accumulation of 2-($^{14}$C or $^{18}$F)-deoxyglucose-6-phosphate, virtually unmetabolizable analogs of glucose-6-phosphate, using autoradiography or PET. Autoradiography provides *ex vivo* images of the regional accumulation of radioactive 2-deoxyglucose-6-phosphate (or other radioactive substrates such as acetate and butyrate, among others), as reflected in photographic plates obtained from sections of fixed brain tissue. PET produces *in vivo*, possibly dynamic, images of the regional uptake of 2-($^{18}$F)-deoxyglucose (FDG, or other positron emitters) in different brain sections, as resolved tomographically by a coronal arrangement of positron selective gamma cameras. Both approaches allow

**Abbreviations:** AcCoA, acetyl-CoA; αKG, α-ketoglutarate; ANLS, astrocyte–neuron lactate shuttle; Asp, aspartate; ATP, adenosine triphosphate; $B_0$, external magnetic field; BBB, blood–brain barrier; Cho, choline; $CMR_{glc}$, cerebral metabolic rates for glucose; CNS, central nervous system; CP, cross-polarization; Cr, creatine; CSI, chemical shift imaging; DNP, dynamic nuclear polarization; FDG, 2-($^{18}$F)-deoxyglucose-6-phosphate; fMRI, functional magnetic resonance imaging; GABA, γ-aminobutyric acid, Glc, glucose; Gln, glutamine; Glu, glutamate; GLUT, glucose transporter; GS, glutamine synthetase; Ins, *myo*-inositol; KIC, 2-ketoisocaproate; Lac, lactate; LDH, lactate dehydrogenase; Mal, malate; MCT, monocarboxylate transporter; MRI, magnetic resonance imaging; NAA, *N*-acetyl-aspartic acid; NMR, nuclear magnetic resonance; nOe, nuclear Overhauser effect; OAA, oxaloacetate; $OAA_n$, neuronal OAA; PC, pyruvate carboxylase; PCr, phosphocreatine; PDE, phosphodiesters; PDH, pyruvate dehydrogenase; PET, positron emission tomography; PGK, phosphoglycerate kinase; PHIP, parahydrogen-induced polarization; $P_i$, inorganic phosphate; PME, phosphomonoesters; POCE, proton-observed carbon-edited; PPT, pulsed polarization transfer; Pyr, pyruvate; RF, radiofrequency; SNR, signal-to-noise ratio; Suc, succinate; TCA, tricarboxylic acid; $V_{NT}$, glutamatergic neurotransmission flux; $V_{TCA}$, TCA cycle flux; $V_X$, rate of exchange between α-ketoglutarate and glutamate.

the determination of cerebral metabolic rates for Glc transport and phosphorylation ($CMR_{glc}$) in different cerebral regions after appropriate modeling of the underlying tracer kinetics (Price, 2003). However, these radioactive approaches are limited in resolution and chemical specificity, making it not possible to investigate the downstream metabolism of Glc after the first glycolytic enzymatic step. Similarly, functional magnetic resonance imaging (fMRI) indirectly allowed the investigation of the hemodynamic and blood oxygenation changes associated with sensory or motor stimulation (Heeger and Ress, 2002). Despite their importance, FDG uptake or fMRI provided no information on the pathways and metabolic interactions underlying the cerebral activation process. This implies that further advances in this area would involve necessarily the use of additional methodologies. From this perspective, genome cloning and sequencing techniques, as well as the important development of novel nuclear magnetic resonance (NMR) approaches have overcome many of the limitations of the traditional strategies, as explained below. In particular, sequencing of the human and mouse genomes has provided a broad understanding of the different isoforms of enzymes and transporters present in the brain, without the need to isolate and purify the corresponding proteins (International Human Genome Sequencing Consortium, 2001; Mouse Genome Sequencing Consortium, 2002). These genomic methods, however, do not allow the investigation of the function and *in vivo* performance of the genes sequenced or cloned. It is in this respect that NMR technologies have become more helpful, providing the quantitative assessment of transport steps, metabolic fluxes and cellular compartmentalization of glycolysis, pyruvate (Pyr) oxidation, and tricarboxylic acid (TCA) cycle, among other pathways, in a plethora of neural systems ranging from primary cell cultures to the intact rodent or human brain (Gruetter et al., 2003; Shulman et al., 2004; Rodrigues and Cerdán, 2005).

Pioneering NMR approaches to cerebral energetics begun with the application of $^{31}$P NMR (Moore et al., 1999). These $^{31}$P NMR spectra from rodent, cat, dog, or human brain – depicted resonances from adenosine triphosphate (ATP), phosphocreatine (PCr), inorganic phosphate (Pi), phosphomonoesters (PME, mainly phosphorylethanolamine), and phosphodiesters (PDE, glycerophosphorylcholine; Hilberman et al., 1984; Komatsumoto et al., 1987; Nioka et al., 1991). With this technique it was possible to follow non-invasively the rates of PCr breakdown and recovery after hypoxic and ischemic episodes.

Nowadays, the most extended NMR approach to explore brain in the clinic is $^{1}$H NMR spectroscopy (Burtscher and Holtas, 2001). $^{1}$H NMR spectra from human or rodent brain show resonances from the methyl group of *N*-acetyl-aspartic acid (NAA), the methyl groups of creatine (Cr) and PCr, the trimethylammonium groups of choline (Cho) containing compounds and the *myo*-inositol (Ins), glutamate (Glu), glutamine (Gln), and γ-aminobutyric acid (GABA) resonances, among others. Ins and NAA are thought to represent the glial and neuronal contributions to the observed voxel, respectively. Remarkably, lactate (Lac) becomes evidently observable under hypoxic or ischemic conditions, providing a proof of augmented net glycolytic flux under these conditions. However, $^{1}$H NMR spectroscopy has the limitation of poor signal dispersion, compared to other commonly used spin nuclei, with the consequent severe overlap problems.

$^{13}$C NMR approaches constitute probably the most elaborated, chemically specific, tool to follow the metabolic fate of $^{13}$C-labeled substrates in the brain, both *in vivo* and *in vitro* (de Graaf et al., 2003b; Gruetter et al., 2003; Garcia-Espinosa et al., 2004; Rodrigues et al., 2009). Since the first $^{13}$C NMR spectroscopy study of a living organism, describing the metabolism of [1-$^{13}$C]Glc by an eukaryotic cell system (Eakin et al., 1972), this approach developed into a powerful method for metabolic research with cells, perfused organs, *in vivo* animals and humans (Morris and Bachelard, 2003). It enabled measuring metabolic processes as they occur in their intracellular environment. Furthermore, it continues to provide unique information, not accessible from previously used approaches.

$^{13}$C NMR spectroscopy allows detecting resonances from $^{13}$C, the only stable isotope of carbon having a magnetic moment. The natural abundance (NA) for $^{13}$C is approximately 1.1% of the total carbon and its magnetogyric ratio is approximately one-fourth of that of the proton. These two circumstances make $^{13}$C NMR spectroscopy a relatively insensitive technique (Friebolin, 1991). The sensitivity can be improved noticeably by using $^{13}$C-enriched substrates. The combination of $^{13}$C NMR spectroscopy detection and substrates selectively enriched in $^{13}$C in specific carbon positions has made it possible to follow *in vitro* and *in vivo* the activity of a large variety of metabolic pathways. These include glycolysis and the pentose phosphate pathway, glycogen synthesis and degradation, gluconeogenesis, the TCA cycle, ketogenesis, ureogenesis, and the Glu–Gln/GABA cycle in brain, among others (Cerdan and Seelig, 1990; Kunnecke, 1995; Morris and Bachelard, 2003; Rodrigues et al., 2007). The $^{13}$C NMR approach also enables to investigate the activities of the neuronal and glial TCA cycles *in vitro* and *in vivo*, providing direct insight into cerebral metabolic compartmentalization (Cerdan et al., 2009).

The design of $^{13}$C NMR experiments with selectively $^{13}$C-enriched substrates is similar to the classical radiolabeling experiments using $^{14}$C. An important difference is that $^{13}$C precursors are administered in substrate amounts, while $^{14}$C substrates are used in tracer amounts. Despite this, $^{13}$C NMR presents important advantages over methodologies using $^{14}$C: (i) the metabolism of the $^{13}$C-labeled substrate can be followed in real-time, *in situ* and non-invasively (Szyperski, 1998; Morris and Bachelard, 2003); (ii) even if tissue extracts are prepared, the detection of $^{13}$C in the different carbon resonances of a specific metabolite does not require separation and carbon by carbon degradation, a prerequisite in the experiments with radioactive $^{14}$C (Dobbins and Malloy, 2003); and (iii) when two or more $^{13}$C atoms occupy contiguous positions *in the same metabolite molecule* it will give rise to isotope effects, called homonuclear spin-coupling, that lead to the appearance of multiplets (instead of single resonances). The analysis by $^{13}$C NMR of these homonuclear spin-coupling patterns represents an enormous gain in the information obtained as compared to the classical radioactive $^{14}$C experiments (Dobbins and Malloy, 2003). As a counterpart to these advantages, $^{13}$C NMR is significantly less sensitive than

other conventional metabolic techniques like radioactive counting, mass spectrometry, and fluorimetric or spectrophotometric methods.

Investigation of metabolic pathways using $^{13}$C NMR spectroscopy is comprised of three main tasks: (i) the infusion of a $^{13}$C-labeled substrate; (ii) the detection of $^{13}$C-labeled metabolites following substrate consumption; and (iii) the metabolic modeling of measured $^{13}$C enrichments to quantitatively derive metabolic fluxes. In general, these three tasks are closely interconnected. Each of them imposes constraints on the two others, and all three must be designed depending on metabolic pathways that are to be investigated. The choice of the substrate (such as Glc, acetate, Pyr, among others) will allow more or less specific feeding of a specific cell type (such as neurons and astrocytes). This will, in-turn, impose the choice of modeling for these cells, and may drive the NMR methodological choices to measure $^{13}$C labeling for cell-specific metabolites (such as Glu, Gln, GABA, among others). Alternatively, the ability of $^{13}$C spectroscopy methods to resolve certain peaks on NMR spectra may lead to the refinement of metabolic models, while the inability to resolve peaks may impose the choice of a labeled substrate whose consumption does not lead to the formation of species with spectral overlap.

Due to the connection between biological questions and methodological issues, a good understanding of the practical implementation of $^{13}$C experiments, with associated caveats and pitfalls, is a prerequisite to any investigation and discussion of metabolism based on $^{13}$C studies. In this review, we will initially provide a simple picture of brain energy metabolism, with a level of details commensurable with NMR accessible information, and explain how $^{13}$C nuclei from different substrates flow through metabolic pathways. Then, spectroscopic acquisition techniques will be reviewed, with associated advantages, drawbacks, and technical difficulties. The basis of metabolic modeling to derive quantitative flux values will be then explained. Finally, we will address two different models of neuroglial coupling : the astrocyte–neuron lactate shuttle (ANLS) model (Pellerin and Magistretti, 1994; Pellerin et al., 2007) and the redox switch/redox coupling hypothesis (Cerdan et al., 2006; Ramirez et al., 2007).

## THE JOURNEY OF CARBON: METABOLIC FATES OF LABELED SUBSTRATES

### FUELS FOR THE BRAIN

The quasi-universal energy molecule of living systems is ATP, which is predominantly synthesized during aerobic cellular respiration (Gjedde, 2007). A central mechanism of aerobic cellular respiration is the TCA cycle, where fuel molecules undergo complete oxidation, ultimately leading to ATP synthesis through oxidative phosphorylation in mitochondrial cristae. When these fuel molecules are labeled with $^{13}$C and continuously infused, their degradation in the TCA cycle will lead to the progressive incorporation of $^{13}$C into metabolic intermediates and by-products (Rodrigues and Cerdán, 2007). The journey of $^{13}$C nuclei is summarized in **Figure 1**.

Under physiological conditions, the main cerebral substrate is Glc. After crossing the blood–brain barrier (BBB), a Glc molecule originates two Pyr molecules through glycolysis (**Figure 1A**). Pyr

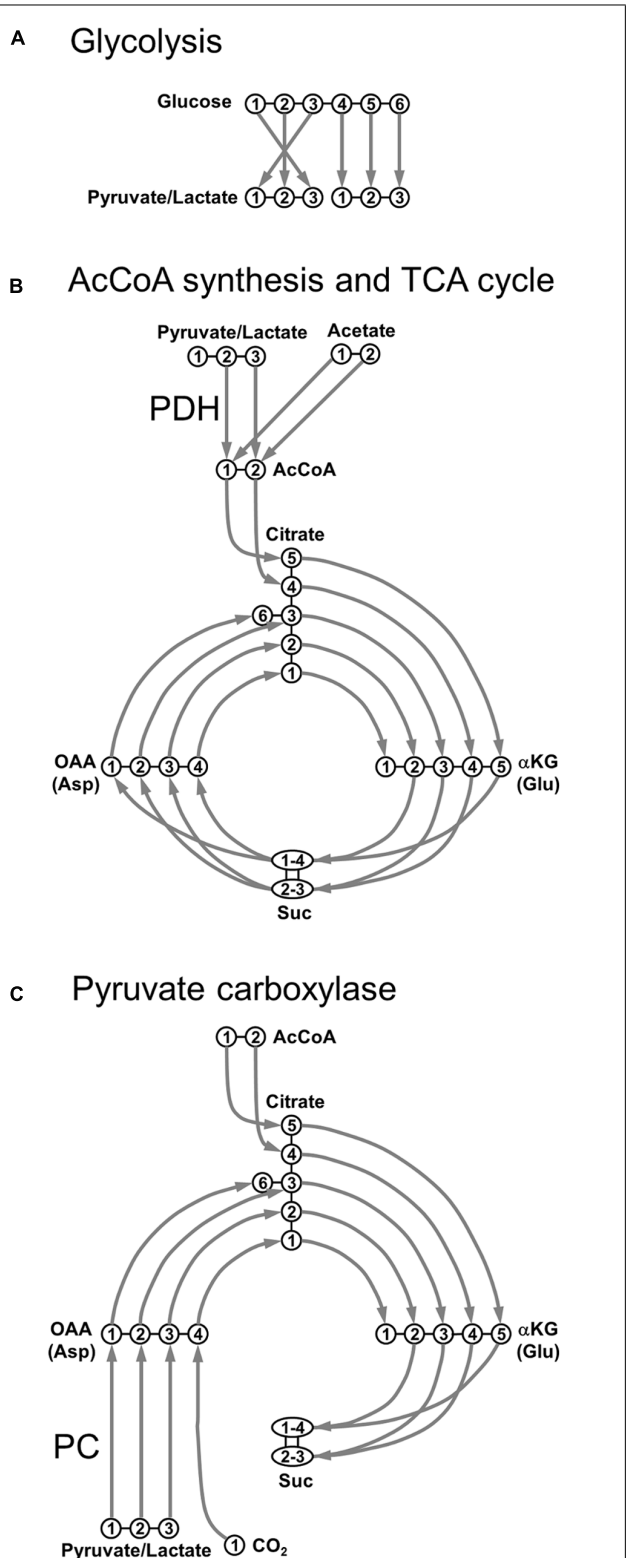


**FIGURE 1 | Transfer of individual $^{13}$C nuclei during the main steps of oxidative metabolism**. **(A)** Glycolysis; **(B)** acetyl-CoA synthesis through pyruvate dehydrogenase (PDH) and TCA cycle; **(C)** pyruvate carboxylase (PC). AcCoA, acetyl-CoA; αKG, α-ketoglutarate; Asp, aspartate; Glu, glutamate; OAA, oxaloacetate; Suc, succinate.

can be reduced to Lac by the lactate dehydrogenase (LDH, fast exchange) with the following reversible reaction:

$$\text{Pyruvate} + \text{NADH} + \text{H}^+ \leftrightarrow \text{lactate} + \text{NAD}^+ \quad (1)$$

Lactate dehydrogenase is a tetramer composed of different combinations of two subunits, H (isolated from heart) and M (from muscle): H4 (LDH1), H3M (LDH2), H2M2 (LDH3), HM3 (LDH4), and M4 (LDH5). LDH1 is mostly neuronal and its kinetic properties promote the formation of Pyr (Bittar et al., 1996). Conversely, LDH5 is primarily astrocytic and its kinetic characteristics favor mainly Lac formation. Pyr is also transported into mitochondria and decarboxylated to acetyl-CoA (AcCoA) *via* the oxidative pathway (pyruvate dehydrogenase, PDH), as shown in **Figure 1B**. AcCoA enters TCA cycle by irreversibly condensating with oxaloacetate (OAA) to form citrate, which is subsequently converted to α-ketoglutarate (αKG) via isocitrate. αKG is then degraded into succinate (Suc) via succinyl-CoA, where scrambling occurs between C1 and C4 positions, and between C2 and C3 positions, due to the symmetry of the Suc molecule. Suc is then oxidized to fumarate, with flavin adenine dinucleotide ($FADH_2$) used as the hydrogen acceptor. The next step is the hydration of fumarate to form malate, and the cycle becoming complete with the oxidation of malate to OAA (**Figure 1B**). Pyr, or even Lac, can be directly supplied to the brain as fuels for TCA cycle. An alternative fuel is acetate, which can be directly converted to AcCoA. This was primarily suggested to happen in astrocytes (Waniewski and Martin, 1998). It was proposed that the main reason acetate is a relatively poor substrate for neurons was due to transporter affinity. This study was based on poor uptake of acetate by synaptosomal fractions compared to astrocytes, not measuring the uptake of acetate by neurons in this work. Further studies revealed that metabolism of acetate is tightly controlled at the enzyme level, via changes in the acetylation status of AcCoA and is not regulated by restriction of uptake (Rae et al., 2012).

In addition to PDH, Pyr may also enter the TCA cycle via the anaplerotic pathway, after its carboxylation to OAA, through the pyruvate carboxylase (PC), as depicted in **Figure 1C**. In contrast to PDH metabolism, which preserves the source of carbon skeletons in TCA cycle, OAA is synthesized *de novo* by PC. The total number of carbon skeletons in the TCA cycle is therefore increased, consequently requiring a net efflux before a turn has been completed. This anaplerotic pathway is mainly glial, due to the specific astrocytic localization of PC (Shank et al., 1985; Sonnewald and Rae, 2010).

## LABELING OF NMR-VISIBLE AMINO ACIDS

Nuclear magnetic resonance detection threshold is typically in the millimolar (mM) range, which is above the typical concentration of most TCA cycle intermediates, including αKG and OAA. However, these intermediates are in fast exchange with amino acids, which exist in concentrations that are above the detection threshold, making $^{13}$C-labeling measurements possible. In particular, αKG is in fast exchange with Glu through aspartate aminotransferase, with identical labeling patterns for the keto acid and the amino acid pools. In neurons, neuronal OAA ($OAA_n$) is in exchange with a pool of Asp, with identical labeling patterns as well.

Exploring **Figure 1**, it is relatively easy to track $^{13}$C labeling along metabolic pathways from labeled substrates to amino acids. For example, following [1-$^{13}$C]Glc or [1,6-$^{13}C_2$]Glc infusions, generation of [3-$^{13}$C]pyruvate is observed, which via PDH leads to the labeling of αKG and Glu at the C4 position during the first turn of the TCA cycle. During the second turn of the TCA cycle, $^{13}$C label is then transferred to Glu C2 and Glu C3. Note that comparing to [1,6-$^{13}C_2$]Glc, the use of [1-$^{13}$C]Glc as precursor will lead to a 50%-dilution in the $^{13}$C enrichment of Pyr at the end of the glycolysis.

## NEUROTRANSMISSION AND METABOLIC INTERACTIONS BETWEEN NEURONS AND ASTROCYTES

The TCA cycle plays a central role in brain metabolism because sugars, fatty acids, and amino acids are oxidized in this pathway. This metabolic route provides numerous intermediates for cerebral biosynthetic pathways, including the neurotransmitters Glu and GABA. In the case of brain cell compartmentalization, two different TCA cycles may be considered as functioning in parallel: an astrocytic and a neuronal cycle. The existence of these two cycles, with different kinetics, was firstly demonstrated in the 1960s. When $^{14}$C-labeled Glu was administered to rats, brain radioactivity was mainly found in the form of Gln (Berl et al., 1961), showing that there is an exchange between Glu and Gln. In addition, the specific activity recovered was higher for Gln than for Glu. Therefore, a pool of Glu exists in the brain that is not exchanged. The use of $^{15}$N-labeled ammonium confirmed the existence of two pools of Glu (Berl et al., 1962), originating the concept that there are two different Glu compartments: a "small" compartment where the Glu–Gln conversion is fast, and a "large" compartment in which the renewal of Glu is much slower. Subsequently, it was shown that glutamine synthetase (GS), an enzyme responsible for the synthesis of Gln, was found mainly in astrocytes (Norenberg and Martinez-Hernandez, 1979). On the other hand, the enzyme responsible for its conversion to Glu, glutaminase, was found mainly in the neurons (Patel et al., 1982). Thereafter, the two compartments were assigned to the two cell types: neurons representing the "large" compartment and astrocytes the "small" one. One of the main consequences of the metabolic compartmentation concept is that there is a Glu–Gln cycle between neurons and astrocytes (cf. **Figure 2B**). In this intercellular metabolic exchange, Gln is synthesized by astrocytes and then transferred to the neuronal compartment, where it is converted to Glu. The Glu, a major neuronal signaling molecule, is released by the neurons into the synaptic cleft during neuronal activity, and then taken up by astrocytes, where it is transformed back into Gln (Badar-Goffer et al., 1990; Cerdan et al., 1990; Shank et al., 1993; Lapidot and Gopher, 1994). This exchange has been widely studied (Schousboe and Hertz, 1981; Waniewski and Martin, 1986; Erecinska and Silver, 1990), including *in vivo* using $^{13}$C NMR spectroscopy (for review, see Rothman et al., 2011), and various Glu transporters have been found on astrocytes (Erecinska and Silver, 1990; Flott and Seifert, 1991; Danbolt, 2001; Huang and Bergles, 2004).

The metabolic relationship between neurons and astrocytes appears, however, to be much more complex than the existence of a simple Glu–Gln cycle. Indeed, it is possible to show that the uptake of Gln by neurons does not offset the continuous loss of Glu

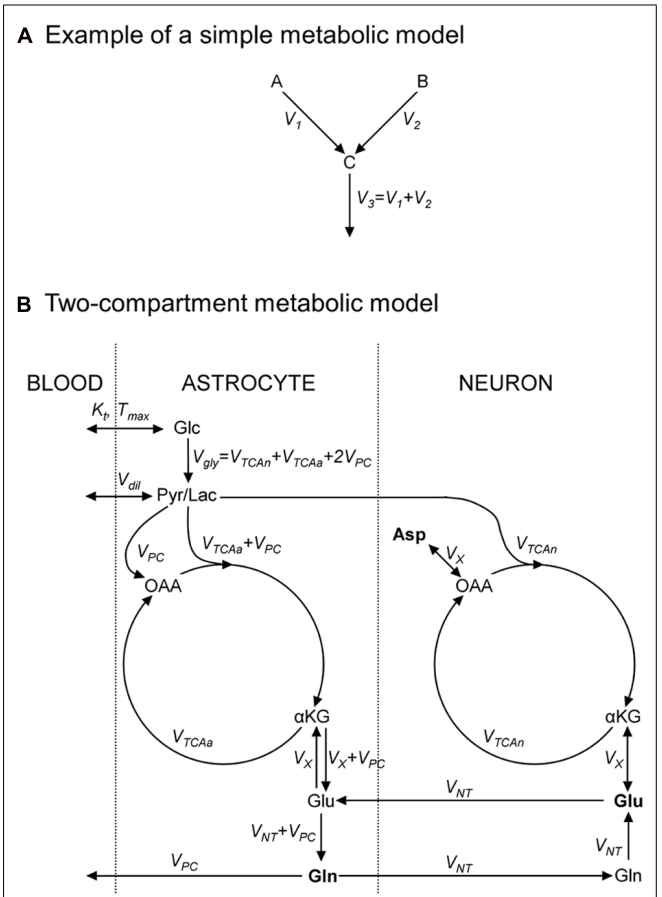


**FIGURE 2 | Metabolic models consist in an ensemble of metabolic pools, connected by metabolic fluxes respecting the steady-state condition for metabolic pools. (A)** Example of a simple metabolic model used to illustrate how to write $^{13}$C-labeling equations; metabolic pools A and B yield C at rates $V_1$ and $V_2$, respectively; **(B)** a "classical" two-compartment metabolic model (see main text for model's description). αKG, α-ketoglutarate; Asp, aspartate; Glc, glucose; Gln, glutamine; Glu, glutamate; Lac, lactate; OAA, oxaloacetate; Pyr, pyruvate; Suc, succinate.

(Hertz, 1979). Therefore, the neurons must use other metabolites that are precursors of the synthesis of Glu, as the components of the TCA cycle, and must therefore be equipped with an enzymatic route to allow their net synthesis from Glc. As briefly addressed above, this synthesis occurs mainly through the PC activity (Voet and Voet, 1990). However, it turns out that this enzymatic activity is present only in astrocytes (Yu et al., 1983; Shank et al., 1985), imposing a necessary anaplerotic transfer of carbons from astrocytes to neurons to replenish the neuronal pools of oxidized TCA intermediates.

In GABAergic neurons, Glu is converted to GABA by glutamate decarboxylase, which is subsequently released in the synaptic cleft. Most GABA molecules are recaptured by neurons, but a small fraction is also recaptured by astrocytes and incorporated into the glial TCA cycle.

Additional pathways exist that may impact the $^{13}$C labeling of NMR-visible metabolites such as Pyr recycling, the transfer of Lac from astrocytes to neurons and the alanine–lactate shuttle between neurons and astrocytes (Waagepetersen et al., 2000; Zwingmann and Leibfritz, 2003).

## $^{13}$C NMR SPECTROSCOPY ACQUISITION TECHNIQUES

The ability to detect $^{13}$C enrichment in brain amino acids is governed by two parameters: sensitivity and spectral resolution. High signal-to-noise ratio (SNR) means that metabolites can potentially be quantified with lower concentrations or enrichments, in smaller volumes, or in shorter periods. Good spectral resolution means that more resonances (corresponding to more metabolites or more specific positions) can be individually quantified, resulting in a higher chemical specificity. SNR and spectral resolution increase linearly with the magnetic field, although technical challenges become significant *in vivo* (shorter $T_2$ relaxation times, increased energy deposition in tissues, higher demand on radiofrequency (RF) pulse bandwidth, and poor homogeneity of the RF field). Essentially, two main approaches can be distinguished for $^{13}$C detection, each trading one of these parameters against the others: direct $^{13}$C detection and indirect $^{13}$C detection.

### DIRECT $^{13}$C DETECTION: CHEMICAL SPECIFICITY

$^{13}$C NMR resonances of brain metabolites span a very broad chemical shift range (~250 ppm), in which conveys the ability to resolve virtually all carbon positions in the detectable metabolites. In particular, direct $^{13}$C spectroscopy allows simultaneously resolving Glu and Gln at C2, C3, and C4 positions, as well as Asp and GABA at positions C2 and C3, even *in vivo* (Gruetter et al., 2003; Henry et al., 2003a). The carboxylic carbons are, in all cases, more difficult to observe because of their long $T_1$s and significant saturation effects.

Beyond the information about positional enrichment, direct $^{13}$C spectroscopy allows quantifying isotopomers (i.e., individual molecules labeled at different atomic positions), since it is sensitive to a constant value – called scalar $J$ coupling – that is different for each $^{13}$C neighborhood type. Indeed, the scalar $J$ coupling will result in the splitting of singlet resonances, corresponding to a given enriched position, into multiplets for $^{13}$C nuclei coupled with neighboring $^{13}$C. This additional information about isotopomers allows one to resolve the activity of different metabolic pathways, as discussed below.

One-bond heteronuclear coupling between $^{13}$C and $^{1}$H may compromise spectral resolution and SNR, since it results in the splitting of $^{13}$C resonances in doublets or multiplets ($J \sim 130$ Hz), with reduced peak heights. Therefore, it is generally desirable to perform heteronuclear decoupling during $^{13}$C acquisition. This is achieved by the application of a RF train at $^{1}$H frequency, resulting in the effective suppression of the effects of $^{1}$H–$^{13}$C coupling on $^{13}$C spectra. Besides technical difficulties associated with the necessity to control two RF chains and to prevent noise injection from the $^{1}$H transmission chain into the $^{13}$C acquisition chain, decoupling may become problematic for *in vivo* application at high field due to the large power deposition in tissues (de Graaf, 2005). It has, however, been shown that detection without decoupling could be achieved in the human brain at 9.4 T with acceptable accuracy (concentration uncertainty was 35–90% higher; Deelchand et al., 2006).

The main disadvantage of direct $^{13}$C spectroscopy is its low sensitivity, derived from the low gyromagnetic ratio of $^{13}$C. Three different strategies, namely nuclear Overhauser effect (nOe), pulsed polarization transfer (PPT), and cross-polarization (CP; Ernst et al., 1987) have been proposed to transfer polarization (or magnetization) from neighboring $^{1}$H to $^{13}$C, both in liquids and *in vivo*. This implies an increase in the $^{13}$C polarization, ultimately resulting in higher SNR. Like heteronuclear decoupling, these strategies require two transmission channels at $^{1}$H and $^{13}$C frequencies.

Nuclear Overhauser effect relies on direct (through-space) dipolar coupling between spins, and refers to the transfer of polarization from $^{1}$H to $^{13}$C due to cross-relaxation. This is achieved when RF irradiation is performed at the $^{1}$H frequency while longitudinal relaxation occurs, which drives the $^{13}$C thermodynamic equilibrium polarization to a higher value. Assuming that $^{13}$C relaxation is entirely due to dipolar interaction with $^{1}$H, nOe increases $^{13}$C polarization up to a factor $1 + 0.5 \times \gamma_I/\gamma_S = 3$, where $\gamma_I$ and $\gamma_S$ are $^{1}$H and $^{13}$C gyromagnetic ratios. Excitation is thus performed both in the $^{1}$H and $^{13}$C frequencies, while detection is obtained only in the $^{13}$C channel.

Cross-polarization and PPT rely on indirect (through-bond) scalar coupling between spins (*J*-coupling), the excitation being initially performed for $^{1}$H. Then, under the combined effect of *J*-coupling and RF perturbation, polarization is driven to an observable $^{13}$C state with amplitude corresponding to $\gamma_I$ instead of $\gamma_S$, as would result from direct $^{13}$C excitation. Ideal CPT and PPT therefore yield up to a $\gamma_I/\gamma_S = 4$-fold gain in SNR. For CPT, this is optimally achieved after RF irradiation of $^{1}$H and $^{13}$C frequencies during a $1/J$ delay, when the Hartmann–Hahn condition is met ($\gamma_I B_{1I} = \gamma_S B_{1S}$; Hartmann and Hahn, 1962) and high $B_1$ amplitudes are used. On the other hand, PPT only requires short RF perturbations (simultaneous 90° pulse at both frequencies at time $1/2J$ after initial excitation). It is therefore particularly interesting for *in vivo* applications due to the limited power deposition, while CPT can yield slightly larger SNR gains. An important feature for the *in vivo* application is that the localization can be fully achieved at the $^{1}$H frequency before transferring polarization, resulting in better localization accuracy compared to the direct $^{13}$C localization, due to the narrower $^{1}$H chemical shift range.

In practice, gains in SNR are significantly smaller than predicted under ideal conditions and vary between different resonances, complicating the quantification process. SNR gains up to 3.5 have been reported in the human brain at 3 T, combining nOe and CPT (Klomp et al., 2006).

## INDIRECT $^{13}$C DETECTION: HIGH SENSITIVITY

As an alternative to detecting $^{13}$C signal directly, an efficient way to increase these measurements sensitivity is to detect $^{1}$H bound to $^{13}$C. SNR gains result mostly from the increased signal voltage, which is proportional to the higher $^{1}$H thermal equilibrium magnetization – by a factor $(\gamma_I/\gamma_S)^2$ – and to the higher precession frequency – by a factor $\gamma_I/\gamma_S$ – compared to $^{13}$C. At the same time, state-of-the-art coils yield noise voltage increasing roughly linearly with the frequency, i.e., as $\gamma_I/\gamma_S$. Therefore, a $(\gamma_I/\gamma_S)^2 \sim 16$-fold increase in SNR can be expected when going from direct detection (without polarization transfer) to indirect detection.

Indirect detection is usually based on a proton-observed carbon-edited (POCE) strategy, requiring two transmission channels at $^{1}$H and $^{13}$C frequencies. The strategy is based on a standard $^{1}$H spectroscopy sequence with an additional 180° pulse at $^{13}$C frequency, being ON or OFF every other scan (Rothman et al., 1985). When the $^{13}$C pulse is ON, satellite resonances due to coupling between $^{1}$H and $^{13}$C nuclei are of opposite sign when compared with the OFF case, while resonances corresponding to $^{1}$H bound to $^{12}$C nuclei are unaffected. Therefore, subtracting odd from even scans will result in the cancellation of signal from $^{1}$H bound to $^{12}$C, while signal from $^{1}$H bound to $^{13}$C will build up.

Heteronuclear decoupling is generally performed by the application of a RF train at $^{13}$C frequency during the $^{1}$H acquisition. This is complicated by the large chemical shift range of $^{13}$C, which imposes a requirement for ultra-broadband decoupling (resulting in high-power deposition) if all resonances on the $^{1}$H spectra have to be decoupled. Decoupling is performed to increase SNR but also to improve spectral resolution, which is critical when observing $^{1}$H resonances. Indeed, the $^{1}$H chemical shift range only spans ∼3 ppm for the aliphatic portion which covers the metabolites' resonances of interest. It is generally accepted that resolution of Glu and Gln C4 becomes possible only for $B_0 > 3$ T, while resolving Glu and Gln C3 remains problematic even at much higher field (Pfeuffer et al., 1999). Indirect detection of GABA and Asp labeling remains problematic and has only been reported at $B_0 = 7$ T or above in the rodent brain (Pfeuffer et al., 1999; de Graaf et al., 2003a; Yang et al., 2005; van Eijsden et al., 2010). Therefore, the loss of chemical specificity associated with indirect detection is acceptable mostly for *in vivo* applications where sensitivity is critical, especially when performing a dynamic measurement: collecting multiple spectra during $^{13}$C-labeled substrate infusion. Indirect $^{13}$C spectroscopy *in vivo* was extensively reviewed by de Graaf et al. (2003b).

An alternative method has been recently proposed for *in vivo* applications, which presents the unique characteristic of requiring no $^{13}$C RF pulse-chain. The method is based on the subtraction of $^{1}$H spectra collected during the $^{13}$C infusion from a baseline spectra acquired prior to infusion (Boumezbeur et al., 2004). Using this approach, C4 and C3 positions could be resolved for the total "Glu + Gln" pool at 3 T. Note that the technique demands extremely stable acquisition (including shimming and coil sensitivity) over the entire experiment.

## NOTE ON SPECTRAL QUANTIFICATION

Analysis of $^{13}$C spectra has long been performed by simple peak integration, which is possible due to the limited spectral overlap on direct $^{13}$C spectra. More recently, spectral quantification based on prior knowledge has been introduced, using for example the LCModel software (Provencher, 1993). In this approach, individual spectra of labeled molecules (obtained by experimental measurement or numerical simulation) are linearly combined to fit experimental data. This allows accurate quantification despite partial overlap, which becomes particularly interesting to discriminate different isotopomers around a given resonance, being possible to perform it even *in vivo*, where lines are broader (Henry et al., 2003a). Although still uncommon in direct $^{13}$C spectroscopy, prior knowledge spectral fitting is now routinely implemented

in indirect $^{13}$C spectroscopy, due to unavoidable overlap on $^{1}$H spectra.

Absolute quantification, i.e., the determination of metabolite concentration and enrichment (in mM and %$^{13}$C), as required for dynamic metabolic modeling (see below), is generally easier using indirect spectroscopy, due to the presence of internal references of known concentration, such as unlabeled Cr or water. With direct spectroscopy, absolute quantification can be complicated by the different polarization transfer efficiency for the different resonances, and for *in vivo* experiments by the absence of a suitable internal $^{13}$C reference of known concentration.

## METABOLIC MODELING

Examination of $^{13}$C enrichment can yield qualitative information about metabolite compartmentalization and the existence and relative importance of metabolic pathways. When seeking quantitative information, one must turn to metabolic modeling, whose basic principle is to mathematically express $^{13}$C labeling of detected metabolites as a function of the metabolic fluxes underlying the labeling process.

### WRITING EQUATIONS: MASS CONSERVATION AND LABEL INCORPORATION

As an exercise, we should consider two metabolite pools, A and B, yielding a third pool, C, at rates $V_1$ and $V_2$ (in μmol/g/min), respectively, and C being then consumed at rate $V_3$ (**Figure 2A**). A usual assumption is that the size of pool C remains constant:

$$\frac{d[C]}{dt} = V_1 + V_2 - V_3 = 0 \tag{2}$$

This imposes that the total influx in the pool is equal to the total efflux from the pool, $V_3 = V_1 + V_2$. We should also assume that $^{13}$C nuclei, at position $i$ in A and $j$ in B, both enter the C pool at position $k$. We use $A_i^*$, $B_j^*$, and $C_k^*$ to denote molecules labeled at these positions. $^{13}$C mass conservation imposes that the increase in the $C_k^*$ pool size is equal to the amount of $^{13}$C entering the pool *minus* what exits the pool at each instant:

$$\frac{d[C_k^*]}{dt} = V_1\frac{[A_i^*]}{[A]} + V_2\frac{B_j^*}{[B]} - (V_1 + V_2)\frac{[C_k^*]}{[C]} \tag{3}$$

A metabolic model typically consists in several equations of the previous type, describing label transfer from infused substrates to metabolic intermediates and, ultimately, to detected metabolites. To favor an efficient solution, the number of differential equations describing the model should be minimized. Equations describing low-concentration intermediates can generally be omitted since their enrichment mimics that of the immediately preceding high-concentration metabolite. Except at steady-state, these systems of differential equations can generally not be solved analytically and require numerical computing to determine what flux values yield the best fit to experimental data.

### TEMPORAL RESOLUTION: STEADY-STATE *VERSUS* DYNAMIC MODELING

To illustrate the impact of temporal resolution on a model, we can assume constant, but different, fractional enrichments for A and B ($[A_i^*]/[A] = FE_A$, $[B_j^*]/[B] = FE_B$). A common procedure in acquiring these data is to wait a period of time after the start of the $^{13}$C infusion, ensuring that isotopic steady-state has been reached for $[C_k^*]$. In this case, Eq. 2 immediately yields, with $FE_C = [C_k^*](t = \infty)/[C]$:

$$\frac{V_1}{V_2} = \frac{FE_C - FE_B}{FE_A - FE_C} \tag{4}$$

The ratio $V_1$ to $V_2$ can therefore be determined from known values of $FE_A$, $FE_B$, and $FE_C$. In general, metabolic models at steady-state only yield flux ratios, not absolute values.

In contrast, we can also explore how dynamic modeling (i.e., using data collected at different time points) carries richer information. We solve Eq. 2 assuming fractional enrichment (also called specific enrichment) for A and B going instantaneously from $^{13}$C NA = 1.1% to $FE_A$ and $FE_B$ at $t > 0$:

$$\frac{[C_k^*](t)}{[C]} = \frac{V_1FE_A + V_2FE_B}{V_1 + V_2} + \left(NA - \frac{V_1FE_A + V_2FE_B}{V_1 + V_2}\right)e^{-\frac{V_1+V_2}{[C]}t} \tag{5}$$

It appears that the enrichment curve will again carry information about the ratio $V_1/V_2$ from long-time enrichment, and independently $V_1 + V_2$ from the exponential rise (provided [C] is known). This means that the absolute values of $V_1$ and $V_2$ (in μmol/g/min) can now be determined. The ability to assess absolute flux values and, potentially, for a number of fluxes greater than the number of equations is a unique feature of dynamic modeling. However, absolute quantification of concentrations is required.

### FEEDING DYNAMIC MODELS: SUBSTRATE ENTRY INTO THE BRAIN

Dynamic metabolic modeling is complicated by the need to estimate the temporal evolution of substrate's intracellular concentration and the enrichment as an entry function. Since, in general, these parameters cannot be directly measured, they are calculated from plasma concentrations and enrichments by modeling transport through the BBB. Transport of Glc and monocarboxylic acids through the BBB is a bidirectional process and is best modeled by reversible Michaelis–Menten transport equations (Simpson et al., 2007). Kinetic parameters have been estimated in the mammalian brain for Glc (Gruetter et al., 1998), acetate (Deelchand et al., 2009), and Lac (Boumezbeur et al., 2010). Blood sampling throughout the infusion is required to determine plasmatic concentration and enrichment of the investigated substrate. However, it has been shown for Glc that, provided the infusion protocol yields "reasonably" stable plasmatic fractional enrichment, blood sampling, as well as Michaelis–Menten kinetics, can be omitted. Cerebral Pyr/Lac fractional enrichment can be directly fitted as an additional unknown parameter (Valette et al., 2009).

### TOWARD DYNAMIC MODELING OF ISOTOPOMERS

For a given set of metabolic pathways, dynamic modeling of isotopomer time courses should, in theory, allow the derivation of metabolic fluxes with the highest achievable reliability, due to the higher information content (provided SNR is high enough). In practice, this has been performed in a very limited number of studies (e.g., Haberg et al., 1998; Serres et al., 2007), and never *in vivo*. Isotopomer modeling is regularly performed *in vitro* and

*ex vivo* at steady-state (see Wiechert, 2001 for a review). Conversely, *in vivo* modeling in the brain has been almost exclusively performed using dynamic positional enrichments (for review of this, see de Graaf et al., 2003b; Gruetter et al., 2003; Henry et al., 2006; Rothman et al., 2011). As far as we know, isotopomer modeling has not been successfully achieved in the brain *in vivo*, although it can theoretically yield flux values with unparalleled accuracy (Shestov et al., 2012). This is probably due to the difficulty of measuring $^{13}$C spectra fine structure *in vivo*, especially with a high-temporal resolution to perform dynamic modeling. However, it has been shown that using high-field NMR systems allowed the dynamic detection of $^{13}$C isotopomers in the rat brain during an infusion of [1,6-$^{13}C_2$]Glc (Henry et al., 2003b) and double infusion of [1,2-$^{13}C_2$]acetate and [1,6-$^{13}C_2$]Glc (Deelchand et al., 2009). Recent modeling of these data suggests that current metabolic models are incomplete to account for the dynamics of all isotopomer time-curves (Jeffrey et al., 2013), appealing for new refined models.

#### SINGLE- OR TWO-COMPARTMENT MODEL

A detailed description of models found in the literature is beyond the scope of this review. We will only briefly present the main metabolic pathways and assumptions in two popular models. The first one is the single-compartment model, which allows the measurement of TCA cycle flux ($V_{TCA}$) following infusion of [1-$^{13}$C]Glc or [1,6-$^{13}C_2$]Glc. The Pyr/Lac pool is in exchange with the blood pool at the rate $V_{dil}$, leading to label dilution (**Figure 2B**). Measuring Glu C4 and C3 is required to derive both the $V_{TCA}$ and the rate of exchange ($V_X$) between αKG and Glu. Some early works proposed that $V_X$ was much higher than $V_{TCA}$ (Mason et al., 1992), allowing $V_{TCA}$ estimation from Glu C4 only. There is still some controversy about the value of $V_X$, and modeling of Glu C3 and C4 should be considered safer if no assumption is done on $V_X$ (Henry et al., 2006). An Asp pool can be added to the model, in exchange with OAA at the same rate $V_X$, to ensure nitrogen mass balance through the malate–aspartate shuttle. In this model, the Glu–Gln cycle is usually modeled by a simple exchange between both pools at a rate usually set to $\sim 0.5 \times V_{TCA}$. Since most Glu is neuronal, this model essentially reflects neuronal $V_{TCA}$. Extensive review of this model for *in vivo* applications was provided by Henry et al. (2003a).

An increasingly popular model (including *in vivo*) is the so-called two-compartment model, where neurons and astrocytes are explicitly considered (**Figure 2B**). Infusion of various substrates ([1-$^{13}$C]Glc, [1,6-$^{13}C_2$]Glc, [2-$^{13}$C]Glc, [1,2-$^{13}C_2$]acetate) may be performed to calculate simultaneously neuronal TCA cycle, glial PDH and PC fluxes, and the glutamatergic neurotransmission flux $V_{NT}$ (Glu–Gln cycle). A net efflux of Gln in the blood is generally considered to remove extra carbon skeletons added by PC. Robustness of the model requires the measurement of Glu and Gln at position C4 and C3, and measurement of Asp C2 and C3 may help stabilize the model (Gruetter et al., 2001). Isotopomer modeling may significantly improve model's reliability.

Some publications have sought to refine single-compartment or two-compartment models by including conversion of Glu to GABA and its reentry into TCA cycle, which is associated with GABAergic neurotransmission (Lapidot and Gopher, 1994; Patel et al., 2005; van Eijsden et al., 2010; Duarte and Gruetter, 2013).

#### ASSESSING A MODEL'S RELIABILITY

When performing modeling, the quality and amount of measured $^{13}$C enrichments should be high enough for the problem to be well determined (i.e., estimated flux values should be close to the real values), and standard deviation on fluxes, as well as covariance between fluxes should be low. A method of choice to explore model's reliability is Monte Carlo simulations. Enrichments are simulated for to-be-infused substrates and to-be-measured metabolites, using the metabolic model and given flux values. Noise is then added to yield SNR comparable to experimental SNR, and noised enrichments are fitted using the model. This procedure is repeated hundreds of times to derive mean and standard deviation for the estimated fluxes. The degree of confidence one can have in flux values can therefore be assessed for a given metabolic model and given experimental conditions. It allowed showing that estimation of $V_{TCA}$ and $V_X$ from the Glu C4 time-course only is very uncertain (Henry et al., 2006), and that the glutamatergic neurotransmission $V_{NT}$ may not be reliable when only [1-$^{13}$C]Glc or [1,6-$^{13}C_2$]Glc infusion is performed (Shestov et al., 2007).

## METABOLIC COOPERATION BETWEEN NEURONS AND ASTROCYTES STUDIED BY NMR SPECTROSCOPY

### ASTROCYTE–NEURON LACTATE SHUTTLE HYPOTHESIS: FOLLOWING LACTATE PRODUCTION AND CONSUMPTION BY THE BRAIN

Since the astrocytes are located between blood vessels and neurons, the question arises whether the astrocytes play the role of intermediary in the flow of substrates from blood to neurons. Indeed, Glc can reach neurons (i) directly, by diffusing from the capillaries through the intercellular space using the Glc transporters present in each of these cells (GLUT-1 and GLUT-3; Vannucci et al., 1997); or (ii) through the astrocytes, since astrocytic end-feet continuously cover blood vessel walls (Mathiisen et al., 2010). In this latter option, Glc that enters the astrocytic end-feet can be metabolized and the product can be subsequently transferred to the neurons and used as a substrate. A growing body of evidence supports this latter hypothesis and indicates that the astrocytic metabolic supply for neurons could be Lac (Dringen et al., 1993; Pellerin and Magistretti, 1994; Larrabee, 1995; Poitry-Yamate et al., 1995; Waagepetersen et al., 1998). Indeed, it has been shown that the presence of Lac in a Glc-free medium maintains synaptic activity in brain slices (Schurr et al., 1988). In addition, Lac has a protective effect and allows better recovery of neurons after hypoxia (Schurr et al., 1997). Although Lac has relatively low permeability at the BBB, different isoforms of monocarboxylate transporters have been localized on endothelial cells (MCT1; Leino et al., 1999), astrocytes (MCT1), and neurons (MCT2; Bröer et al., 1997, 1999). Moreover, the isoenzymes of LDH, LDH1 and LDH5, have been found in different cellular locations (Bittar et al., 1996), supporting the hypothesis of astrocytic Lac utilization by neurons.

The traditional metabolic coupling theory (ANLSH for the astrocyte–neuron lactate shuttle hypothesis), firstly proposed by Pellerin and Magistretti in the mid-1990s (Pellerin and Magistretti, 1994), describes that neurotransmitter Glu released to the synaptic

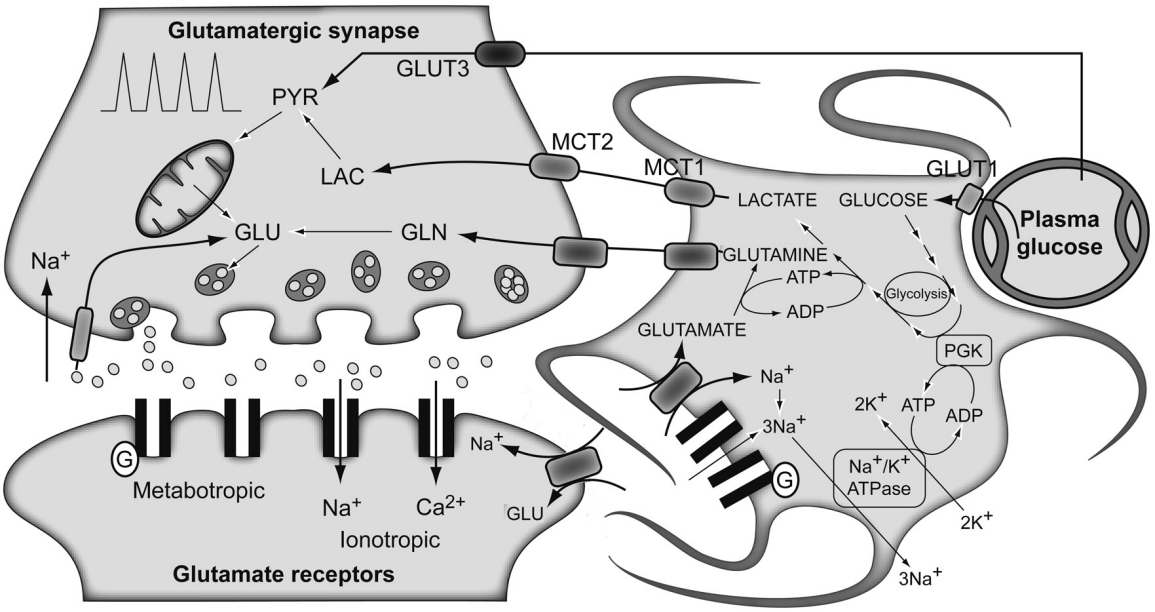


**FIGURE 3 | The traditional metabolic coupling hypothesis between neurons and astrocytes during glutamatergic neurotransmission.** Glutamate released to the synaptic cleft during glutamatergic neurotransmission is co-transported with $Na^+$ to the astrocytes. Astrocytic $Na^+$ is exchanged by extracellular $K^+$ through the $Na^+/K^+$ ATPase, consuming one ATP molecule. Astrocytic glutamate produces glutamine through glutamine synthetase, consuming one additional ATP molecule. Lactate produced exclusively in astrocytic glycolysis to support these energy demands, is extruded to the extracellular medium, taken up by the surrounding neurons and oxidized as their main metabolic fuel. Note the apparent stoichiometric coupling between glutamate–glutamine cycling and glucose uptake as well as the exclusive *glycolytic* or *oxidative* metabolisms in astrocytes and neurons, respectively. Gln, glutamine; Glu, glutamate; GLUT 1 and GLUT 3, glucose transporters 1 and 3; Lac, lactate; MCT1 and MCT2, monocarboxylate transporters 1 and 2; PGK, phosphoglycerate kinase; Pyr, pyruvate. Adapted with permission from Tsacopoulos and Magistretti (1996).

cleft, following an action potential, is recaptured predominantly by the high-affinity Glu transporters of surrounding astrocytes in the neuropil (**Figure 3**). Three $Na^+$ atoms are co-transported with each Glu molecule to the astrocytic cytosol and metabolized into Gln by GS. The $Na^+$ atoms are extruded from the cytosol through the $Na^+/K^+$ ATPase, at the expense of one ATP molecule, and GS consumes one additional ATP molecule. These two ATP molecules were originally proposed to be compensated for by the degradation of one Glc molecule in the astrocyte through the glycolytic pathway. Gln is then extruded to the extracellular space, being recaptured by the neurons to regenerate Glu. Therefore, in this particular process, we assist in the consumption of one Glc molecule from plasma, with the subsequent generation of two molecules of astrocytic Lac. These Lac molecules are exported to the neurons to become their main metabolic fuel. Thus, Gln production appears to be stoichiometrically coupled to Glc uptake (1:1 stoichiometry), glycolysis occurring mainly in the astrocytes while Pyr oxidation remaining as a predominantly neuronal process. These findings fit well with early $^{13}$C NMR results, which determined the cerebral Gln cycle and the TCA cycle fluxes from a minimal mathematical model. This model assumed that [4-$^{13}$C]Glu and [4-$^{13}$C]Gln turnover curves reflected the neuronal TCA cycle and the Gln cycle fluxes, respectively (Sibson et al., 1998). Later, Rothman et al. (2003) proposed Gln as the major precursor of cerebral Glu and the Gln cycle was found to be stoichiometrically coupled to Glc uptake, accounting for 60–80% of the energy derived from Glc metabolism.

Importantly, a thorough examination of the earlier evidences led several authors to challenge the traditional approach proposed by the ANLSH (Chih et al., 2001; Dienel and Hertz, 2001; Chih and Roberts, 2003; Dienel and Cruz, 2003). In response to these criticisms, Pellerin and Magistretti (2003) presented a revised version of their proposal. The main differences are that this newer proposal does not exclude the activation of glycolysis and production of Lac in active neurons. Additionally, it does not require a direct coupling between astrocytic Lac release and neuronal Lac oxidation, proposing that Lac from both active astrocytes and neurons is released into the extracellular space. This Lac is eventually used by neurons (at rest or during activity). The current version of the ANLSH has been also critically reviewed (Hertz, 2004).

In the context of this review, it is important to remark that both $^1$H (Prichard, 1991; Prichard et al., 1991; Merboldt et al., 1992; Sappey-Marinier et al., 1992) and $^{13}$C NMR spectroscopy studies have been used to explore the ANLSH/metabolic coupling theory by monitoring and comparing the fate of $^{13}$C-glucose and $^{13}$C-lactate metabolism in neurons (Sonnewald et al., 1991; Schousboe et al., 1997; Bouzier-Sore et al., 2003), astrocytes (Alves et al., 1995), rat brain (Bouzier et al., 2000; Hassel and Brathe, 2000; Serres et al., 2004; Sampol et al., 2013) and human brain (Boumezbeur et al., 2010).

## THE REDOX SWITCH/REDOX COUPLING HYPOTHESIS

Several other convincing evidences have accumulated since the above explained interpretations of metabolic neuroglial

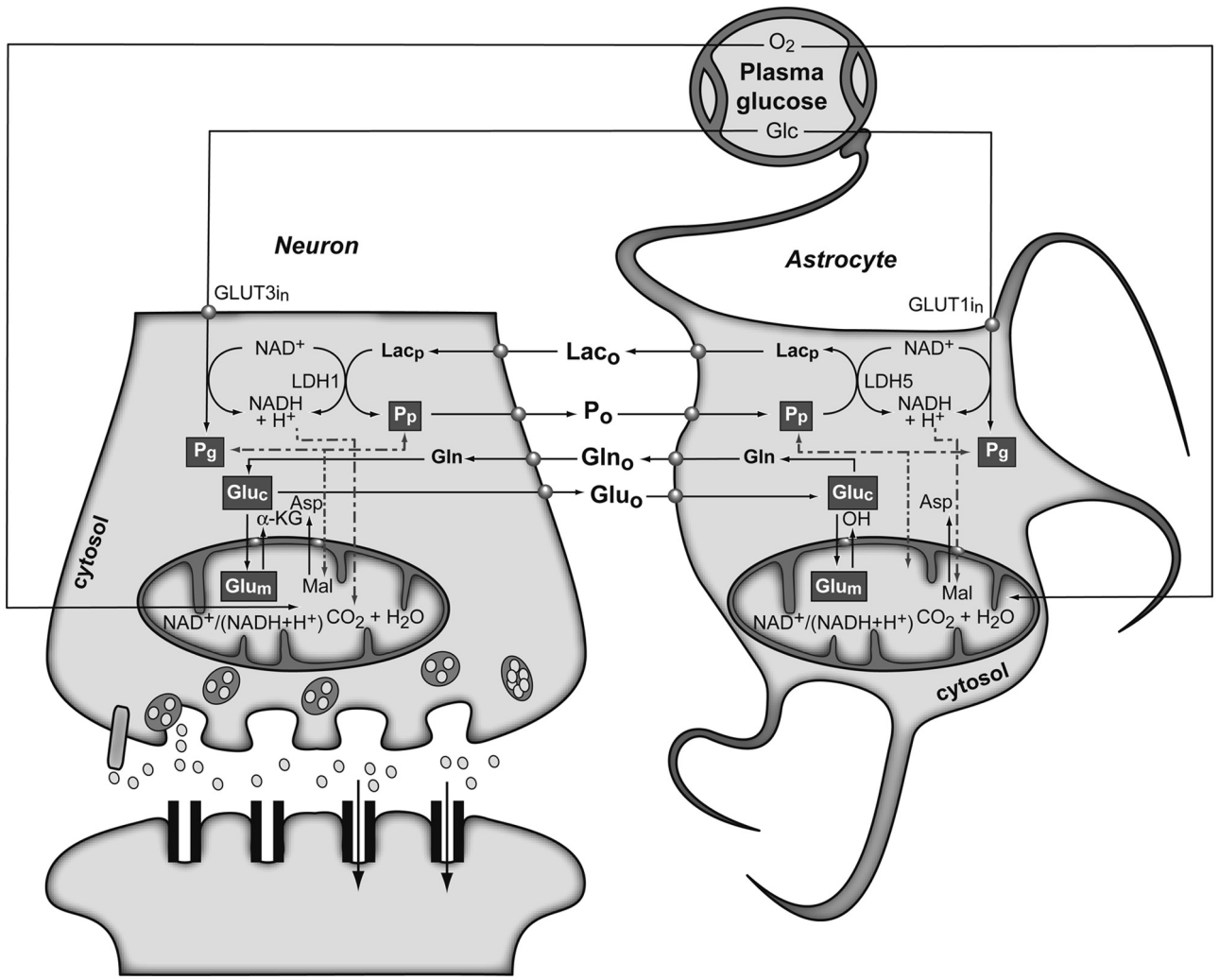


**FIGURE 4 | The subcellular compartmentation of pyruvate and glutamate and the redox switch/redox coupling hypothesis.** Two pools of pyruvate exist in neurons and astrocytes derived from extracellular monocarboxylates (Pp) or glucose (Pg). A lactate/pyruvate redox shuttle is able to transfer continuously lactate from astrocytes to neurons, taking advantage of the kinetics of plasma membrane transporters and lactate dehydrogenase isoenzymes. High cytosolic lactate concentration inhibits neuronal glycolysis at the glyceraldehyde-3-phosphate dehydrogenase step by competition with cytosolic $NAD^+$, favoring the oxidation of extracellular Lac. Neuronal pyruvate is transferred back to the astrocyte to close the transcellular exchange of reducing equivalents. Two α-ketoglutarate/glutamate pools exist in neurons and astrocytes, associated probably to cytosolic and mitochondrial compartments. Exchange of α-ketoglutarate/glutamate between mitochondria and cytosol appears to be slow in the H3 glutamate hydrogen exchange timescale and dependent of the cytosolic and mitochondrial $NAD(P)^+/NAD(P)H$ ratios, as determined by the malate–aspartate shuttle. Both glycolysis and oxidative astrocytic metabolism contribute the energy for glutamine production in the astrocytes, indicating that this coupling involves both transcellular and intracellular redox coupling mechanisms that allow the simultaneous operation of glycolysis and oxidation in astrocytes. Asp, aspartate; Glc, glucose; Gln, glutamine; Glu, glutamate; GLUT1 and GLUT3, glutamate transporters 1 and 3; α-KG, α-ketoglutarate; Lac, lactate; LDH1 and LDH5, lactate dehydrogenase 1 and 5; Mal, malate. Reproduced with permission from Rodrigues et al. (2012).

coupling during glutamatergic neurotransmission, with relevant consequences. These new pieces of evidence showed that: (i) an important portion of the energy used to synthesize Gln is derived from the astroglial TCA cycle (Garcia-Espinosa et al., 2003); (ii) up to 40% of cerebral Glu is derived from alternative sources to Gln (Garcia-Espinosa et al., 2003); (iii) Gln cycling may not present a 1:1 stoichiometry with Glc uptake (Gruetter et al., 2001; McKenna, 2007); (iv) different kinetic pools of Lac, Pyr, Gln, Glu, and GABA exist both in astrocytes and in neurons (Cruz et al., 2001; Zwingmann et al., 2001; Rodrigues et al., 2005; Cerdan et al., 2009). All the previous described findings indicate that the coupling mechanisms between neuronal and glial metabolisms are more complex than previously envisioned.

**Figure 4** shows the conception of metabolic coupling between neurons and astrocytic during glutamatergic neurotransmission proposed by Cerdan and colleagues (Cerdan et al., 2006; Ramirez et al., 2007). This hypothesis is based on the existence of transcellular coupling of oxidative and non-oxidative metabolisms in both neurons and astrocytes through the exchange of monocarboxylate reducing equivalents and on the operation of intracellular

redox switches. So, after presynaptic Glu release, astrocytes incorporate Glu and three $Na^+$ ions, being the latter removed subsequently through the plasma membrane $Na^+/K^+$ ATPase. The energetic cost of this process implies reduced astrocytic ATP/ADP concentrations, stimulating astroglial glycolysis and TCA cycle. Both astrocytic metabolic pathways contribute the energy required by GS, with a major contribution of the oxidative metabolism. However, the energy demands during glutamatergic neurotransmission eventually exceed the reduced capacity of the astrocytic TCA cycle, what could result in a net activation of the glycolytic flux and a net production of astrocytic Lac, which is rapidly extruded to the extracellular space. The resulting extracellular Lac is taken up by neurons with a consequent reduction of the cytosolic redox state to a point where neuronal glycolysis could be inhibited at the glyceraldehyde 3-phosphate dehydrogenase step. An opposite flux of Pyr, from neurons to astrocytes, is proposed to connect and balance the redox state in both neurons and glial cells. Under these conditions, extracellular Lac is predominantly consumed by neuronal oxidation until its extracellular concentration reaches the pre-activation levels, preparing the stage for a new glutamatergic event.

This redox switch/redox coupling hypothesis integrates basically the described experimental findings, both obtained *in vivo* and *in vitro*. More specifically, it includes: (i) the simultaneous operation of both astrocytic and neuronal glycolysis and TCA cycles during neuronal activation; (ii) the fact that both astrocytes and neurons may potentially use Glc or Lac as complementary, or even alternative, substrates; this depends on the extracellular redox state and availability; (iii) the stoichiometric or non-stoichiometric coupling of the Glu cycle and Glc uptake; (iv) the intracellular compartmentalization of cytosolic monocarboxylates; and, finally, (v) the intracellular Glu compartmentalization also both in neurons and astrocytes (Cruz et al., 2005; Dienel and Hertz, 2005). The transcellular redox switch/redox coupling proposal mimics the intracellular coupling mechanisms existing between cytosolic glycolysis and the TCA cycle which involves the transfer of reducing equivalents through the inner mitochondrial membrane. During transcellular redox coupling, however, reducing equivalents are reversibly exchanged between neurons and astrocytes in the form of Lac and Pyr (Arco and Satrustegui, 2005; McKenna et al., 2006).

## PERSPECTIVE: HYPERPOLARIZED $^{13}$C NMR APPROACHES

As explained before, one of the most limiting features of NMR is its lack of sensitivity. Therefore, magnetic resonance imaging (MRI) has relied primarily on imaging of water protons. This results from the fact that the SNR ratio of the NMR signal is proportional to the equilibrium polarization between the two proton spin states under thermal equilibrium conditions in an external magnetic field ($B_0$), as well as the proton concentration. Clinical imaging applications have until now been restricted to $^1$H MRI because the existence of a high concentration of protons in biological tissue is able to counterbalance the inherent low sensitivity. Unfortunately, MR sensitivity of $^{13}$C is too low to allow conventional $^{13}$C MRI due to the vestigial *in vivo* abundance of this nucleus and its lower magnetogyric ratio.

Although it is possible to improve the sensitivity using MRI systems at high $B_0$ and extremely low temperatures, a maximum polarization (and corresponding SNR) increase ($\sim 10^3$), obtained by cooling down the sample to liquid He temperature at a field strength of 20 T, would not be sufficient for clinical $^{13}$C MRI applications. Alternatively, it is possible to improve the sensitivity by transferring polarization from an electron or nuclear spin that has a higher polarization, creating a non-equilibrium distribution of nuclear spins called the hyperpolarized state (Månsson et al., 2006). In this state, the polarization of spins can be increased by a factor of $\sim 10^5$ compared with that in the thermal equilibrium state and independently of the $B_0$ value, leading to a corresponding gain in signal strength for MRI. This allows imaging of nuclei other than protons, namely $^{13}$C, and their molecular distribution *in vivo* can be visualized in a clinically relevant time window (Ardenkjær-Larsen et al., 2003).

The hyperpolarized state is created by an external device followed by rapid administration of the agent to the subject to be imaged. However, the lifetime of the hyperpolarized state is limited by the $T_1$ relaxation time which depends on the chemical structure and environment of the hyperpolarized compound. In the case of $^{13}$C, it can range from a few seconds to several minutes, depending on the functional groups where the $^{13}$C nucleus is present.

Both parahydrogen-induced polarization (PHIP) and dynamic nuclear polarization (DNP) techniques have been able to hyperpolarize a wide range of organic $^{13}$C-labeled substances. As the polarization of electrons is much higher than the $^{13}$C nuclear polarization, due to the much larger gyromagnetic ratio of the electron, the DNP approach implies transferring polarization from hyperpolarized electron spins in a solid to the coupled $^{13}$C nuclear spins in a doping substance ($\sim$3 T and $\sim$1 K; Månsson et al., 2006). Microwave irradiation near the electron resonance frequency transfers the polarization from the unpaired electrons to the $^{13}$C nuclei. After reaching an appropriate polarization, the solid is rapidly dissolved and injected with small polarization losses (Ardenkjær-Larsen et al., 2003).

An interesting use of $^{13}$C-labeled endogenous compounds is metabolic imaging. Chemical shift imaging (CSI) has been traditionally used to image the cerebral distribution of metabolites from $^{13}$C-labeled substances, such as Glc (van der Zijden et al., 2008). However, without using hyperpolarization techniques, such images can only be obtained using long scan times (minutes). Using the previously described hyperpolarization approaches, images of the metabolic processes can be generated in a significant faster time scale (seconds). Endogenous compounds selectively labeled with $^{13}$C have been hyperpolarized by the DNP technique, extending substantially the applications of cerebral metabolic imaging. Basically, enzymatic processes can be non-invasively quantified and imaged *in vivo* using these hyperpolarized $^{13}$C-labeled metabolites. The metabolic fate of [1-$^{13}$C]Pyr in images of tumor-bearing animals injected with hyperpolarized labeled Pyr has been followed using the DNP approach, and allowed mapping the metabolic pattern of labeled Pyr, as well as of Lac and alanine. It was confirmed that gliomas abundantly transform Pyr into Lac through anaerobic glycolysis. Using this strategy, it was shown that exchange of hyperpolarized $^{13}$C

label between Pyr and Lac could be imaged in tumors (Day et al., 2011). This flux was decreased in tumors receiving treatment undergoing drug-induced cell death. Using the same substrate, fast dynamic spiral CSI and transport modeling were combined to better characterize the bolus, transport, and metabolic effects, separating the metabolites in the cerebral blood volume from the metabolites in the brain tissue. This allowed developing a repeatable non-invasive measurement of regional BBB transport kinetics and regional cerebral Lac levels (Hurd et al., 2010). A novel non-invasive method for imaging tissue pH *in vivo* was also demonstrated (Gallagher et al., 2008). It was shown that interstitial tumor pH can be imaged *in vivo* from the ratio of the signal intensities of hyperpolarized bicarbonate ($H^{13}CO_3^-$) and $^{13}CO_2$, after the intravenous injection of hyperpolarized $H^{13}CO_3^-$. Additionally, other neurochemical pathways have been exploited using this approach. Conversion of $^{13}C$-labeled acetate to 2-oxoglutarate, a key biomolecule connecting metabolism to neuronal activity, was recently shown using the DNP approach, reporting a direct *in vivo* observation of a TCA cycle intermediate in intact brain (Mishkovsky et al., 2012). The cerebral distribution and metabolism of hyperpolarized 2-keto[1-$^{13}C$]isocaproate (KIC) has also been described in the normal rat using MR (Butt et al., 2012). Hyperpolarized KIC is metabolized to [1-$^{13}C$]leucine by branched chain amino acid transaminase, having this enzyme an important role in nitrogen shuttling and glutamate metabolism in the brain. Another group was able to show how sodium 1-$^{13}C$ acetylenedicarboxylate, which after hydrogenation by PASADENA (Parahydrogen and Synthesis Allows Dramatically Enhanced Nuclear Alignment), becomes $^{13}C$ sodium succinate. Fast *in vivo* imaging demonstrated that, following carotid arterial injection, the hyperpolarized $^{13}C$-succinate appeared in the head and cerebral circulation of normal and tumor-bearing rats (Bhattacharya et al., 2007). Even more recently, the injection of hyperpolarized [U-$^{2}H$,U-$^{13}C$]Glc allowed real-time imaging of the glycolytic flux in two non-cerebral murine tumor models *in vivo*, due to the clear detection of labeled Lac (Rodrigues et al., in press). Low levels of dihydroxyacetone phosphate, 6-phosphogluconate and bicarbonate were also observed, with the latter two synthesized by the pentose phosphate pathway activity. The possible use of labeled Glc in cerebral studies could open a very important avenue in neurochemistry, mainly because of the possibility to investigate a completely new metabolic timeframe with this approach. Therefore, the application of $^{13}C$ metabolic imaging using hyperpolarized $^{13}C$-labeled substrates to neurochemistry is an open field of research.

## ACKNOWLEDGMENTS

Tiago B. Rodrigues was in receipt of an Intra-European Marie Curie (FP7-PEOPLE-2009-IEF, Imaging Lymphoma) and a Long-Term EMBO (EMBO-ALT-1145-2009) fellowships. Anne-Karine Bouzier-Sore is supported by a public grant from the French "Agence Nationale de la Recherche" within the context of the Investments for the Future Program, referenced ANR-10-LABX-57 and named TRAIL. The authors would like to thank Dr. Mikko I. Kettunen and Dr. Alan J. Wright for the critical reading of the manuscript.

## REFERENCES

Alves, P. M., Mckenna, M. C., and Sonnewald, U. (1995). Lactate metabolism in mouse brain astrocytes studied by [13C]NMR spectroscopy. *Neuroreport* 6, 2201–2204. doi: 10.1097/00001756-199511000-00024

Arco, A. D., and Satrustegui, J. (2005). New mitochondrial carriers: an overview. *Cell. Mol. Life Sci.* 62, 2204–2227. doi: 10.1007/s00018-005-5197-x

Ardenkjær-Larsen, J. H., Fridlund, B., Gram, A., Hansson, G., Hansson, L., Lerche, M. H., et al. (2003). Increase in signal-to-noise ratio of >10,000 times in liquid-state NMR. *Proc. Natl. Acad. Sci. U.S.A.* 100, 10158–10163. doi: 10.1073/pnas.1733835100

Bachelard, H. S. (1989). "Measurement of carbohydrates and their derivatives in neuronal tissues," in *Carbohydrates and Energy Metabolism*, eds A. A. Boulton, G. B. Baker, and R. F. Butterworth (Clifton, NJ: Humana Press), 133–154.

Badar-Goffer, R. S., Bachelard, H. S., and Morris, P. G. (1990). Cerebral metabolism of acetate and glucose studied by $^{13}C$-n.m.r. spectroscopy. A technique for investigating metabolic compartmentation in the brain. *Biochem. J.* 266, 133–139.

Berl, S., Lajtha, A., and Waelsch, H. (1961). Amino acid and protein metabolism. VI. Cerebral compartments of glutamic acid metabolism. *J. Neurochem.* 7, 186–197. doi: 10.1111/j.1471-4159.1961.tb13503.x

Berl, S., Takagaki, G., Clarke, D. D., and Waelsch, H. (1962). Metabolic compartments in vivo. Ammonia and glutamic acid metabolism in brain and liver. *J. Biol. Chem.* 237, 2562–2569.

Bhattacharya, P., Chekmenev, E. Y., Perman, W. H., Harris, K. C., Lin, A. P., Norton, V. A., et al. (2007). Towards hyperpolarized $^{13}C$-succinate imaging of brain cancer. *J. Magn. Reson.* 186, 150–155. doi: 10.1016/j.jmr.2007.01.017

Bittar, P. G., Charnay, Y., Pellerin, L., Bouras, C., and Magistretti, P. J. (1996). Selective distribution of lactate dehydrogenase isoenzymes in neurons and astrocytes of human brain. *J. Cereb. Blood Flow Metab.* 16, 1079–1089. doi: 10.1097/00004647-199611000-00001

Boumezbeur, F., Besret, L., Valette, J., Vaufrey, F., Henry, P. G., Slavov, V., et al. (2004). NMR measurement of brain oxidative metabolism in monkeys using $^{13}C$-labeled glucose without a $^{13}C$ radiofrequency channel. *Magn. Reson.* 52, 33–40. doi: 10.1002/mrm.20129

Boumezbeur, F., Petersen, K. F., Cline, G. W., Mason, G. F., Behar, K. L., Shulman, G. I., et al. (2010). The contribution of blood lactate to brain energy metabolism in humans measured by dynamic $^{13}C$ nuclear magnetic resonance spectroscopy. *J. Neurosci.* 30, 13983–13991. doi: 10.1523/JNEUROSCI.2040-10.2010

Bouzier, A. K., Thiaudiere, E., Biran, M., Rouland, R., Canioni, P., and Merle, M. (2000). The metabolism of [3-(13)C]lactate in the rat brain is specific of a pyruvate carboxylase-deprived compartment. *J. Neurochem.* 75, 480–486. doi: 10.1046/j.1471-4159.2000.0750480.x

Bouzier-Sore, A. K., Voisin, P., Canioni, P., Magistretti, P. J., and Pellerin, L. (2003). Lactate is a preferential oxidative energy substrate over glucose for neurons in culture. *J. Cereb. Blood Flow Metab.* 23, 1298–1306. doi: 10.1097/01.WCB.0000091761.61714.25

Bröer, S., Bröer, A., Schneider, H. P., Stegen, C., Halestrap, A. P., and Deitmer, J. W. (1999). Characterization of the high-affinity monocarboxylate transporter MCT2 in *Xenopus laevis* oocytes. *Biochem. J.* 341, 529–535. doi: 10.1042/0264-6021:3410529

Bröer, S., Rahman, B., Pellegri, G., Pellerin, L., Martin, J. L., Verleysdonk, S., et al. (1997). Comparison of lactate transport in astroglial cells and monocarboxylate transporter 1 (MCT 1) expressing *Xenopus laevis* oocytes. Expression of two different monocarboxylate transporters in astroglial cells and neurons. *J. Biol. Chem.* 272, 30096–30102. doi: 10.1074/jbc.272.48.30096

Burtscher, I. M., and Holtas, S. (2001). Proton MR spectroscopy in clinical routine. *J. Magn. Reson. Imaging* 13, 560–567. doi: 10.1002/jmri.1079

Butt, S. A., Søgaard, L. V., Magnusson, P. O., Lauritzen, M. H., Laustsen, C., Åkeson, P., et al. (2012). Imaging cerebral 2-ketoisocaproate metabolism with hyperpolarized (13)C magnetic resonance spectroscopic imaging. *J. Cereb. Blood Flow Metab.* 32, 1508–1514. doi: 10.1038/jcbfm.2012.34

Cerdan, S., Kunnecke, B., and Seelig, J. (1990). Cerebral metabolism of [1,2-$^{13}C_2$]acetate as detected by in vivo and in vitro $^{13}C$ NMR. *J. Biol. Chem.* 265, 12916–12926.

Cerdan, S., Rodrigues, T. B., Sierra, A., Benito, M., Fonseca, L. L., Fonseca, C. P., et al. (2006). The redox switch/redox coupling hypothesis. *Neurochem. Int.* 48, 523–530. doi: 10.1016/j.neuint.2005.12.036

Cerdan, S., and Seelig, J. (1990). NMR studies of metabolism. *Annu. Rev. Biophys. Biophys. Chem.* 19, 43–67. doi: 10.1146/annurev.bb.19.060190.000355

Cerdan, S., Sierra, A., Fonseca, L. L., Ballesteros, P., and Rodrigues, T. B. (2009). The turnover of the H3 deuterons from (2-$^{13}$C) glutamate and (2-$^{13}$C) glutamine reveals subcellular trafficking in the brain of partially deuterated rats. *J. Neurochem.* 109(Suppl. 1), 63–72. doi: 10.1111/j.1471-4159.2009.05962.x

Chih, C.-P., Lipton, P., and Roberts, E. L. Jr. (2001). Do active cerebral neurons really use lactate rather than glucose? *Trends Neurosci.* 24, 573–578. doi: 10.1016/S0166-2236(00)01920-2

Chih, C. P., and Roberts, E. L. Jr. (2003). Energy substrates for neurons during neural activity: a critical review of the astrocyte–neuron lactate shuttle hypothesis. *J. Cereb. Blood Flow Metab.* 23, 1263–1281. doi: 10.1097/01.WCB.0000081369.51727.6F

Clark, J. B., and Lai, J. C. K. (1989). "Glycolytic, tricarboxylic acid cycle and related enzymes in brain," in *Carbohydrates and Energy Metabolism*, eds A. A. Boulton, G. B. Baker, and R. F. Butterworth (Clifton, NJ: Humana Press), 233–281.

Cruz, F., Villalba, M., Garcia-Espinosa, M. A., Ballesteros, P., Bogonez, E., Satrustegui, J., et al. (2001). Intracellular compartmentation of pyruvate in primary cultures of cortical neurons as detected by (13)C NMR spectroscopy with multiple (13)C labels. *J. Neurosci. Res.* 66, 771–781. doi: 10.1002/jnr.10048

Cruz, N. F., Lasater, A., Zielke, H. R., and Dienel, G. A. (2005). Activation of astrocytes in brain of conscious rats during acoustic stimulation: acetate utilization in working brain. *J. Neurochem.* 92, 934–947. doi: 10.1111/j.1471-4159.2004.02935.x

Danbolt, N. C. (2001). Glutamate uptake. *Prog. Neurobiol.* 65, 1–105. doi: 10.1016/S0301-0082(00)00067-8

Day, S. E., Kettunen, M. I., Cherukuri, M. K., Mitchell, J. B., Lizak, M. J., Morris, H. D., et al. (2011). Detecting response of rat C6 glioma tumors to radiotherapy using hyperpolarized [1-$^{13}$C]pyruvate and $^{13}$C magnetic resonance spectroscopic imaging. *Magn. Reson. Med.* 65, 557–563. doi: 10.1002/mrm.22698

Deelchand, D. K., Shestov, A. A., Koski, D. M., Ugurbil, K., and Henry, P. G. (2009). Acetate transport and utilization in the rat brain. *J. Neurochem.* 109(Suppl. 1), 46–54. doi: 10.1111/j.1471-4159.2009.05895.x

Deelchand, D. K., Ugurbil, K., and Henry, P. G. (2006). Investigating brain metabolism at high fields using localized $^{13}$C NMR spectroscopy without $^{1}$H decoupling. *Magn. Reson. Med.* 55, 279–286. doi: 10.1002/mrm.20756

de Graaf, R. A. (2005). Theoretical and experimental evaluation of broadband decoupling techniques for in vivo nuclear magnetic resonance spectroscopy. *Magn. Reson. Med.* 53, 1297–1306. doi: 10.1002/mrm.20507

de Graaf, R. A., Brown, P. B., Mason, G. F., Rothman, D. L., and Behar, K. L. (2003a). Detection of [1,6-$^{13}C_2$]-glucose metabolism in rat brain by in vivo $^{1}$H-[$^{13}$C]-NMR spectroscopy. *Magn. Reson. Med.* 49, 37–46. doi: 10.1002/mrm.10348

de Graaf, R. A., Mason, G. F., Patel, A. B., Behar, K. L., and Rothman, D. L. (2003b). In vivo $^{1}$H-[$^{13}$C]-NMR spectroscopy of cerebral metabolism. *NMR Biomed.* 16, 339–357. doi: 10.1002/nbm.847

Dienel, G. A., and Cruz, N. F. (2003). Neighborly interactions of metabolically-activated astrocytes in vivo. *Neurochem. Int.* 43, 339–354. doi: 10.1016/S0197-0186(03)00021-4

Dienel, G. A., and Hertz, L. (2001). Glucose and lactate metabolism during brain activation. *J. Neurosci. Res.* 66, 824–838. doi: 10.1002/jnr.10079

Dienel, G. A., and Hertz, L. (2005). Astrocytic contributions to bioenergetics of cerebral ischemia. *Glia* 50, 362–388. doi: 10.1002/glia.20157

Dobbins, R. L., and Malloy, C. R. (2003). Measuring in-vivo metabolism using nuclear magnetic resonance. *Curr. Opin. Clin. Nutr. Metab. Care* 6, 501–509. doi: 10.1097/00075197-200309000-00003

Dringen, R., Gebhardt, R., and Hamprecht, B. (1993). Glycogen in astrocytes: possible function as lactate supply for neighboring cells. *Brain Res.* 623, 208–214. doi: 10.1016/0006-8993(93)91429-V

Duarte, J. M., and Gruetter, R. (2013). Glutamatergic and GABAergic energy metabolism measured in the rat brain by $^{13}$C NMR spectroscopy at 14.1 T. *J. Neurochem.* 126, 579–590. doi: 10.1111/jnc.12333

Eakin, R. T., Morgan, L. O., Gregg, C. T., and Matwiyoff, N. A. (1972). Carbon-13 nuclear magnetic resonance spectroscopy of living cells and their metabolism of a specifically labeled $^{13}$C substrate. *FEBS Lett.* 28, 259–264. doi: 10.1016/0014-5793(72)80726-9

Erecinska, M., and Silver, I. A. (1990). Metabolism and role of glutamate in mammalian brain. *Prog. Neurobiol.* 35, 245–296. doi: 10.1016/0301-0082(90)90013-7

Ernst, R. R., Bodenhausen, G., and Wokaun, A. (1987). *Principles of Nuclear Magnetic Resonance in One and Two Dimensions*. Oxford: Clarendon Press/Oxford University Press.

Flott, B., and Seifert, W. (1991). Characterization of glutamate uptake systems in astrocyte primary cultures from rat brain. *Glia* 4, 293–304. doi: 10.1002/glia.440040307

Friebolin, H. (1991). *Basic One- and Two-dimensional NMR Spectroscopy*. Weinheim: VCH Publishers.

Gallagher, F. A., Kettunen, M. I., Day, S. E., Hu, D. E., Ardenkjaer-Larsen, J. H., Zandt, R., et al. (2008). Magnetic resonance imaging of pH in vivo using hyperpolarized $^{13}$C-labelled bicarbonate. *Nature* 453, 940–943. doi: 10.1038/nature07017

Garcia-Espinosa, M. A., Garcia-Martin, M. L., and Cerdan, S. (2003). Role of glial metabolism in diabetic encephalopathy as detected by high resolution $^{13}$C NMR. *NMR Biomed.* 16, 440–449. doi: 10.1002/nbm.843

Garcia-Espinosa, M. A., Rodrigues, T. B., Sierra, A., Benito, M., Fonseca, C., Gray, H. L., et al. (2004). Cerebral glucose metabolism and the glutamine cycle as detected by in vivo and in vitro $^{13}$C NMR spectroscopy. *Neurochem. Int.* 45, 297–303. doi: 10.1016/j.neuint.2003.08.014

Gjedde, A. (2007). "Coupling of brain function to metabolism: evaluation of energy requirements," in *Handbook of Neurochemistry and Molecular Neurobiology*, eds A. Lajtha, G. Gibson, and G. Dienel (New York: Springer), 343–400.

Gruetter, R., Adriany, G., Choi, I. Y., Henry, P. G., Lei, H., and Oz, G. (2003). Localized in vivo $^{13}$C NMR spectroscopy of the brain. *NMR Biomed.* 16, 313–338. doi: 10.1002/nbm.841

Gruetter, R., Seaquist, E. R., and Ugurbil, K. (2001). A mathematical model of compartmentalized neurotransmitter metabolism in the human brain. *Am. J. Physiol. Endocrinol. Metab.* 281, E100–E112.

Gruetter, R., Ugurbil, K., and Seaquist, E. R. (1998). Steady-state cerebral glucose concentrations and transport in the human brain. *J. Neurochem.* 70, 397–408. doi: 10.1046/j.1471-4159.1998.70010397.x

Haberg, A., Qu, H., Haraldseth, O., Unsgard, G., and Sonnewald, U. (1998). In vivo injection of [1-$^{13}$C]glucose and [1,2-$^{13}$C]acetate combined with ex vivo $^{13}$C nuclear magnetic resonance spectroscopy: a novel approach to the study of middle cerebral artery occlusion in the rat. *J. Cereb. Blood Flow Metab.* 18, 1223–1232. doi: 10.1097/00004647-199811000-00008

Hartmann, S. R., and Hahn, E. L. (1962). Nuclear double resonance in the rotating frame. *Phys. Rev.* 128, 2042–2053. doi: 10.1103/PhysRev.128.2042

Hassel, B., and Bråthe, A. (2000). Cerebral metabolism of lactate in vivo: evidence for neuronal pyruvate carboxylation. *J. Cereb. Blood Flow Metab.* 20, 327–336. doi: 10.1097/00004647-200002000-00014

Heeger, D. J., and Ress, D. (2002). What does fMRI tell us about neuronal activity. *Nat. Rev. Neurosci.* 3, 142–151. doi: 10.1038/nrn730

Henry, P. G., Adriany, G., Deelchand, D., Gruetter, R., Marjanska, M., Oz, G., et al. (2006). In vivo $^{13}$C NMR spectroscopy and metabolic modeling in the brain: a practical perspective. *Magn. Reson. Imaging* 24, 527–539. doi: 10.1016/j.mri.2006.01.003

Henry, P. G., Oz, G., Provencher, S., and Gruetter, R. (2003a). Toward dynamic isotopomer analysis in the rat brain in vivo: automatic quantitation of $^{13}$C NMR spectra using LCModel. *NMR Biomed.* 16, 400–412. doi: 10.1002/nbm.840

Henry, P. G., Tkac, I., and Gruetter, R. (2003b). $^{1}$H-localized broadband $^{13}$C NMR spectroscopy of the rat brain in vivo at 9.4 T. *Magn. Reson. Med.* 50, 684–692. doi: 10.1002/mrm.10601

Herholz, K., and Heiss, W. D. (2004). Positron emission tomography in clinical neurology. *Mol. Imaging Biol.* 6, 239–269. doi: 10.1016/j.mibio.2004.05.002

Hertz, L. (1979). Functional interactions between neurons and astrocytes. I. Turnover and metabolism of putative amino acid transmitters. *Prog. Neurobiol.* 13, 277–323. doi: 10.1016/0301-0082(79)90018-2

Hertz, L. (2004). The astrocyte–neuron lactate shuttle: a challenge of a challenge. *J. Cereb. Blood Flow Metab.* 24, 1241–1248. doi: 10.1097/00004647-200411000-00008

Hilberman, M., Subramanian, V. H., Haselgrove, J., Cone, J. B., Egan, J. W., Gyulai, L., et al. (1984). In vivo time-resolved brain phosphorus nuclear magnetic resonance. *J. Cereb. Blood Flow Metab.* 4, 334–342. doi: 10.1038/jcbfm.1984.50

Huang, Y. H., and Bergles, D. E. (2004). Glutamate transporters bring competition to the synapse. *Curr. Opin. Neurobiol.* 14, 346–352. doi: 10.1016/j.conb.2004.05.007

Hurd, R. E., Yen, Y. F., Tropp, J., Pfefferbaum, A., Spielman, D. M., and Mayer, D. (2010). Cerebral dynamics and metabolism of hyperpolarized [1-(13)C]pyruvate using time-resolved MR spectroscopic imaging. *J. Cereb. Blood Flow Metab.* 30, 1734–1741. doi: 10.1038/jcbfm.2010.93

International Human Genome Sequencing Consortium. (2001). Initial sequencing and analysis of the human genome. *Nature* 409, 860–921. doi: 10.1038/35057062

Jeffrey, F. M., Marin-Valencia, I., Good, L. B., Shestov, A. A., Henry, P. G., Pascual, J. M., et al. (2013). Modeling of brain metabolism and pyruvate compartmentation using $^{13}$C NMR in vivo: caution required. *J. Cereb. Blood Flow Metab.* 33, 1160–1167. doi: 10.1038/jcbfm.2013.67

Klomp, D. W., Renema, W. K., Van Der Graaf, M., De Galan, B. E., Kentgens, A. P., and Heerschap, A. (2006). Sensitivity-enhanced $^{13}$C MR spectroscopy of the human brain at 3 Tesla. *Magn. Reson. Med.* 55, 271–278. doi: 10.1002/mrm.20745

Komatsumoto, S., Nioka, S., Greenberg, J. H., Yoshizaki, K., Subramanian, V. H., Chance, B., et al. (1987). Cerebral energy metabolism measured in vivo by $^{31}$P-NMR in middle cerebral artery occlusion in the cat – relation to severity of stroke. *J. Cereb. Blood Flow Metab.* 7, 557–562. doi: 10.1038/jcbfm.1987.105

Kunnecke, B. (1995). "Application of $^{13}$C NMR spectroscopy to metabolic studies on animals," in *Carbon-13 NMR Spectroscopy of Biological Systems*, ed. N. Beckman (New York: Academic Press, Inc.), 159–267.

Lapidot, A., and Gopher, A. (1994). Cerebral metabolic compartmentation. Estimation of glucose flux via pyruvate carboxylase/pyruvate dehydrogenase by $^{13}$C NMR isotopomer analysis of D-[U-$^{13}$C]glucose metabolites. *J. Biol. Chem.* 269, 27198–27208.

Larrabee, M. G. (1995). Lactate metabolism and its effects on glucose metabolism in an excised neural tissue. *J. Neurochem.* 64, 1734–1741. doi: 10.1046/j.1471-4159.1995.64041734.x

Leino, R. L., Gerhart, D. Z., and Drewes, L. R. (1999). Monocarboxylate transporter (MCT1) abundance in brains of suckling and adult rats: a quantitative electron microscopic immunogold study. *Brain Res. Dev. Brain Res.* 113, 47–54. doi: 10.1016/S0165-3806(98)00188-6

Månsson, S., Johansson, E., Magnusson, P., Chai, C.-M., Hansson, G., Petersson, J. S., et al. (2006). $^{13}$C imaging – a new diagnostic platform. *Eur. Radiol.* 16, 57–67. doi: 10.1007/s00330-005-2806-x

Mason, G. F., Rothman, D. L., Behar, K. L., and Shulman, R. G. (1992). NMR determination of the TCA cycle rate and alpha-ketoglutarate/glutamate exchange rate in rat brain. *J. Cereb. Blood Flow Metab.* 12, 434–447. doi: 10.1038/jcbfm.1992.61

Mathiisen, T. M., Lehre, K. P., Danbolt, N. C., and Ottersen, O. P. (2010). The perivascular astroglial sheath provides a complete covering of the brain microvessels: an electron microscopic 3D reconstruction. *Glia* 58, 1094–1103. doi: 10.1002/glia.20990

McKenna, M. C. (2007). The glutamate–glutamine cycle is not stoichiometric: fates of glutamate in brain. *J. Neurosci. Res.* 85, 3347–3358. doi: 10.1002/jnr.21444

McKenna, M. C., Waagepetersen, H. S., Schousboe, A., and Sonnewald, U. (2006). Neuronal and astrocytic shuttle mechanisms for cytosolic-mitochondrial transfer of reducing equivalents: current evidence and pharmacological tools. *Biochem. Pharmacol.* 71, 399–407. doi: 10.1016/j.bcp.2005.10.011

Merboldt, K. D., Bruhn, H., Hanicke, W., Michaelis, T., and Frahm, J. (1992). Decrease of glucose in the human visual cortex during photic stimulation. *Magn. Reson. Med.* 25, 187–194. doi: 10.1002/mrm.1910250119

Mishkovsky, M., Comment, A., and Gruetter, R. (2012). In vivo detection of brain Krebs cycle intermediate by hyperpolarized magnetic resonance. *J. Cereb. Blood Flow Metab.* 32, 2108–2113. doi: 10.1038/jcbfm.2012.136

Moore, C. M., Frederick, B. B., and Renshaw, P. F. (1999). Brain biochemistry using magnetic resonance spectroscopy: relevance to psychiatric illness in the elderly. *J. Geriatr. Psychiatry Neurol.* 12, 107–117. doi: 10.1177/089198879901200304

Morris, P., and Bachelard, H. (2003). Reflections on the application of C-13-MRS to research on brain metabolism. *NMR Biomed.* 16, 303–312. doi: 10.1002/nbm.844

Mouse Genome Sequencing Consortium. (2002). Initial sequencing and comparative analysis of the mouse genome. *Nature* 420, 520–562. doi: 10.1038/nature01262

Nicholls, D. (2007). "Bioenergetics," in *Brain Energetics. Integration of Molecular and Cellular Processes*, 3rd Edn, eds A. Lajhta, G. Gibson, and G. Dienel (New York: Springer), 3–16.

Nioka, S., Zaman, A., Yoshioka, H., Masumura, M., Miyake, H., Lockard, S., et al. (1991). $^{31}$P magnetic resonance spectroscopy study of cerebral metabolism in developing dog brain and its relationship to neuronal function. *Dev. Neurosci.* 13, 61–68. doi: 10.1159/000112142

Norenberg, M. D., and Martinez-Hernandez, A. (1979). Fine structural localization of glutamine synthetase in astrocytes of rat brain. *Brain Res.* 161, 303–310. doi: 10.1016/0006-8993(79)90071-4

Okada, Y., and Lipton, P. (2007). "Glucose, oxidative energy metabolism, and neural function in brain slices – glycolysis plays a key role in neural activity," in *Brain Energetics. Integration of Molecular and Cellular Processes*, 3rd Edn, eds A. Lajhta, G. Gibson, and G. Dienel (New York: Springer), 17–39.

Patel, A. B., De Graaf, R. A., Mason, G. F., Rothman, D. L., Shulman, R. G., and Behar, K. L. (2005). The contribution of GABA to glutamate/glutamine cycling and energy metabolism in the rat cortex in vivo. *Proc. Natl. Acad. Sci. U.S.A.* 102, 5588–5593. doi: 10.1073/pnas.0501703102

Patel, A. J., Hunt, A., Gordon, R. D., and Balazs, R. (1982). The activities in different neural cell types of certain enzymes associated with the metabolic compartmentation glutamate. *Brain Res.* 256, 3–11.

Pellerin, L., Bouzier-Sore, A. K., Aubert, A., Serres, S., Merle, M., Costalat, R., et al. (2007). Activity-dependent regulation of energy metabolism by astrocytes: an update. *Glia* 55, 1251–1262. doi: 10.1002/glia.20528

Pellerin, L., and Magistretti, P. J. (1994). Glutamate uptake into astrocytes stimulates aerobic glycolysis: a mechanism coupling neuronal activity to glucose utilization. *Proc. Natl. Acad. Sci. U.S.A.* 91, 10625–10629. doi: 10.1073/pnas.91.22.10625

Pellerin, L., and Magistretti, P. J. (2003). Food for thought: challenging the dogmas. *J. Cereb. Blood Flow Metab.* 23, 1282–1286. doi: 10.1097/01.WCB.0000096064.12129.3D

Pfeuffer, J., Tkac, I., Choi, I. Y., Merkle, H., Ugurbil, K., Garwood, M., et al. (1999). Localized in vivo $^{1}$H NMR detection of neurotransmitter labeling in rat brain during infusion of [1-$^{13}$C] D-glucose. *Magn. Reson. Med.* 41, 1077–1083. doi: 10.1002/(SICI)1522-2594(199906)41:6<1077::AID-MRM1>3.0.CO;2-#

Poitry-Yamate, C. L., Poitry, S., and Tsacopoulos, M. (1995). Lactate released by Muller glial cells is metabolized by photoreceptors from mammalian retina. *J. Neurosci.* 15, 5179–5191.

Price, J. C. (2003). Principles of tracer kinetic analysis. *Neuroimaging Clin. N. Am.* 13, 689–704. doi: 10.1016/S1052-5149(03)00107-2

Prichard, J., Rothman, D., Novotny, E., Petroff, O., Kuwabara, T., Avison, M., et al. (1991). Lactate rise detected by $^{1}$H NMR in human visual cortex during physiologic stimulation. *Proc. Natl. Acad. Sci. U.S.A.* 88, 5829–5831. doi: 10.1073/pnas.88.13.5829

Prichard, J. W. (1991). What the clinician can learn from MRS lactate measurements. *NMR Biomed.* 4, 99–102. doi: 10.1002/nbm.1940040212

Provencher, S. W. (1993). Estimation of metabolite concentrations from localized in vivo proton NMR spectra. *Magn. Reson. Med.* 30, 672–679. doi: 10.1002/mrm.1910300604

Rae, C., Fekete, A., Kashem, M., Nasrallah, F., and Bröer, S. (2012). Metabolism, compartmentation, transport and production of acetate in the cortical brain tissue slice. *Neurochem. Res.* 37, 2541–2553. doi: 10.1007/s11064-012-0847-5

Ramirez, B. G., Rodrigues, T. B., Violante, I. R., Cruz, F., Fonseca, L. L., Ballesteros, P., et al. (2007). Kinetic properties of the redox switch/redox coupling mechanism as determined in primary cultures of cortical neurons and astrocytes from rat brain. *J. Neurosci. Res.* 85, 3244–3253. doi: 10.1002/jnr.21386

Rodrigues, T. B., and Cerdán, S. (2005). $^{13}$C MRS: an outstanding tool for metabolic studies. *Concepts Magn. Reson. Part A* 27A, 1–16. doi: 10.1002/cmr.a.20039

Rodrigues, T. B., and Cerdán, S. (2007). "The cerebral tricarboxylic acid cycles," in *Handbook of Neurochemistry and Molecular Neurobiology*, eds A. Lajtha, G. Gibson, and G. Dienel (New York: Springer), 63–91.

Rodrigues, T. B., Granado, N., Ortiz, O., Cerdan, S., and Moratalla, R. (2007). Metabolic interactions between glutamatergic and dopaminergic neurotransmitter systems are mediated through D(1) dopamine receptors. *J. Neurosci. Res.* 85, 3284–3293. doi: 10.1002/jnr.21302

Rodrigues, T. B., Gray, H. L., Benito, M., Garrido, S., Sierra, A., Geraldes, C. F., et al. (2005). Futile cycling of lactate through the plasma membrane of C6

glioma cells as detected by ($^{13}$C, $^{2}$H) NMR. *J. Neurosci. Res.* 79, 119–127. doi: 10.1002/jnr.20308

Rodrigues, T. B., Lopez-Larrubia, P., and Cerdan, S. (2009). Redox dependence and compartmentation of [$^{13}$C]pyruvate in the brain of deuterated rats bearing implanted C6 gliomas. *J. Neurochem.* 109(Suppl. 1), 237–245. doi: 10.1111/j.1471-4159.2009.05935.x

Rodrigues, T. B., Serrao, E. M., Kennedy, B. W. C., Hu, D. E., Kettunen, M. I., and Brindle, K. M. (in press). Magnetic resonance imaging of tumor glycolysis using hyperpolarized $^{13}$C-labeled glucose. *Nat. Med.* doi: 10.1038/nm.3416

Rodrigues, T. B., Sierra, A., Ballesteros, P., and Cerdán, S. (2012). "Pyruvate transport and metabolism in the central nervous system," in *Neural Metabolism In Vivo*, eds I.-Y. Choi and R. Gruetter (Berlin: Springer), 715–753.

Rothman, D. L., Behar, K. L., Hetherington, H. P., Den Hollander, J. A., Bendall, M. R., Petroff, O. A., et al. (1985). $^{1}$H-observe/$^{13}$C-decouple spectroscopic measurements of lactate and glutamate in the rat brain in vivo. *Proc. Natl. Acad. Sci. U.S.A.* 82, 1633–1637. doi: 10.1073/pnas.82.6.1633

Rothman, D. L., Behar, K. L., Hyder, F., and Shulman, R. G. (2003). In vivo NMR studies of the glutamate neurotransmitter flux and neuroenergetics: implications for brain function. *Annu. Rev. Physiol.* 65, 401–427. doi: 10.1146/annurev.physiol.65.092101.142131

Rothman, D. L., De Feyter, H. M., De Graaf, R. A., Mason, G. F., and Behar, K. L. (2011). $^{13}$C MRS studies of neuroenergetics and neurotransmitter cycling in humans. *NMR Biomed.* 24, 943–957. doi: 10.1002/nbm.1772

Sampol, D., Ostrofet, E., Jobin, M. L., Raffard, G., Sanchez, S., Bouchaud, V., et al. (2013). Glucose and lactate metabolism in the awake and stimulated rat: a (13)C-NMR study. *Front. Neuroenergetics* 5:5. doi: 10.3389/fnene.2013.00005

Sappey-Marinier, D., Calabrese, G., Fein, G., Hugg, J. W., Biggins, C., and Weiner, M. W. (1992). Effect of photic stimulation on human visual cortex lactate and phosphates using $^{1}$H and $^{31}$P magnetic resonance spectroscopy. *J. Cereb. Blood Flow Metab.* 12, 584–592. doi: 10.1038/jcbfm.1992.82

Schousboe, A., and Hertz, L. (1981). Role of astroglial cells in glutamate homeostasis. *Adv. Biochem. Psychopharmacol.* 27, 103–113. doi: 10.1007/BF03033975

Schousboe, A., Westergaard, N., Waagepetersen, H. S., Larsson, O. M., Bakken, I. J., and Sonnewald, U. (1997). Trafficking between glia and neurons of TCA cycle intermediates and related metabolites. *Glia* 21, 99–105. doi: 10.1002/(SICI)1098-1136(199709)21:1<99::AID-GLIA11>3.0.CO;2-W

Schurr, A., Dong, W. Q., Reid, K. H., West, C. A., and Rigor, B. M. (1988). Lactic acidosis and recovery of neuronal function following cerebral hypoxia in vitro. *Brain Res.* 438, 311–314. doi: 10.1016/0006-8993(88)91354-6

Schurr, A., Payne, R. S., Miller, J. J., and Rigor, B. M. (1997). Brain lactate, not glucose, fuels the recovery of synaptic function from hypoxia upon reoxygenation: an in vitro study. *Brain Res.* 744, 105–111. doi: 10.1016/S0006-8993(96)01106-7

Serres, S., Bezancon, E., Franconi, J. M., and Merle, M. (2004). Ex vivo analysis of lactate and glucose metabolism in the rat brain under different states of depressed activity. *J. Biol. Chem.* 279, 47881–47889. doi: 10.1074/jbc.M409429200

Serres, S., Bezancon, E., Franconi, J. M., and Merle, M. (2007). Brain pyruvate recycling and peripheral metabolism: an NMR analysis ex vivo of acetate and glucose metabolism in the rat. *J. Neurochem.* 101, 1428–1440. doi: 10.1111/j.1471-4159.2006.04442.x

Shank, R. P., Bennett, G. S., Freytag, S. O., and Campbell, G. L. (1985). Pyruvate carboxylase: an astrocyte-specific enzyme implicated in the replenishment of amino acid neurotransmitter pools. *Brain Res.* 329, 364–367. doi: 10.1016/0006-8993(85)90552-9

Shank, R. P., Leo, G. C., and Zielke, H. R. (1993). Cerebral metabolic compartmentation as revealed by nuclear magnetic resonance analysis of D-[1-$^{13}$C]glucose metabolism. *J. Neurochem.* 61, 315–323. doi: 10.1111/j.1471-4159.1993.tb03570.x

Shestov, A. A., Valette, J., Deelchand, D. K., Ugurbil, K., and Henry, P. G. (2012). Metabolic modeling of dynamic brain $^{13}$C NMR multiplet data: concepts and simulations with a two-compartment neuronal-glial model. *Neurochem. Res.* 37, 2388–2401. doi: 10.1007/s11064-012-0782-5

Shestov, A. A., Valette, J., Ugurbil, K., and Henry, P. G. (2007). On the reliability of $^{13}$C metabolic modeling with two-compartment neuronal-glial models. *J. Neurosci. Res.* 85, 3294–3303. doi: 10.1002/jnr.21269

Shulman, R. G., Rothman, D. L., Behar, K. L., and Hyder, F. (2004). Energetic basis of brain activity: implications for neuroimaging. *Trends Neurosci.* 27, 489–495. doi: 10.1016/j.tins.2004.06.005

Sibson, N. R., Dhankhar, A., Mason, G. F., Rothman, D. L., Behar, K. L., and Shulman, R. G. (1998). Stoichiometric coupling of brain glucose metabolism and glutamatergic neuronal activity. *Proc. Natl. Acad. Sci. U.S.A.* 95, 316–321. doi: 10.1073/pnas.95.1.316

Simpson, I. A., Carruthers, A., and Vannucci, S. J. (2007). Supply and demand in cerebral energy metabolism: the role of nutrient transporters. *J. Cereb. Blood Flow Metab.* 27, 1766–1791. doi: 10.1038/sj.jcbfm.9600521

Sokoloff, L. (1981). Localization of functional activity in the central nervous system by measurement of glucose utilization with radioactive deoxyglucose. *J. Cereb. Blood Flow Metab.* 1, 7–36. doi: 10.1038/jcbfm.1981.4

Sokoloff, L. (1989). "Circulation and energy metabolism of the brain," in *Basic Neurochemistry*, eds G. Siegel, B. Agranoff, R. W. Albers, and P. Molinoff (New York: Raven Press), 565–590.

Sonnewald, U., and Rae, C. (2010). Pyruvate carboxylation in different model systems studied by $^{13}$C MRS. *Neurochem. Res.* 35, 1916–1921. doi: 10.1007/s11064-010-0257-5

Sonnewald, U., Westergaard, N., Krane, J., Unsgard, G., Petersen, S. B., and Schousboe, A. (1991). First direct demonstration of preferential release of citrate from astrocytes using [13C]NMR spectroscopy of cultured neurons and astrocytes. *Neurosci. Lett.* 128, 235–239. doi: 10.1016/0304-3940(91)90268-X

Szyperski, T. (1998). $^{13}$C-NMR, MS and metabolic flux balancing in biotechnology research. *Q. Rev. Biophys.* 31, 41–106. doi: 10.1017/S0033583598003412

Tsacopoulos, M., and Magistretti, P. J. (1996). Metabolic coupling between glia and neurons. *J. Neurosci.* 16, 877–885.

Valette, J., Boumezbeur, F., Hantraye, P., and Lebon, V. (2009). Simplified $^{13}$C metabolic modeling for simplified measurements of cerebral TCA cycle rate in vivo. *Magn. Reson. Med.* 62, 1641–1645. doi: 10.1002/mrm.22160

van der Zijden, J. P., Van Eijsden, P., De Graaf, R. A., and Dijkhuizen, R. M. (2008). $^{1}$H/$^{13}$C MR spectroscopic imaging of regionally specific metabolic alterations after experimental stroke. *Brain* 131, 2209–2219. doi: 10.1093/brain/awn139

van Eijsden, P., Behar, K. L., Mason, G. F., Braun, K. P., and De Graaf, R. A. (2010). In vivo neurochemical profiling of rat brain by $^{1}$H-[$^{13}$C] NMR spectroscopy: cerebral energetics and glutamatergic/GABAergic neurotransmission. *J. Neurochem.* 112, 24–33. doi: 10.1111/j.1471-4159.2009.06428.x

Vannucci, S. J., Maher, F., and Simpson, I. A. (1997). Glucose transporter proteins in brain: delivery of glucose to neurons and glia. *Glia* 21, 2–21. doi: 10.1002/(SICI)1098-1136(199709)21:1<2::AID-GLIA2>3.0.CO;2-C

Voet, D., and Voet, J. G. (1990). "Regulation of the citric acid cycle," in *Biochemistry* (Hoboken: John Wiley), 522–527.

Waagepetersen, H. S., Bakken, I. J., Larsson, O. M., Sonnewald, U., and Schousboe, A. (1998). Comparison of lactate and glucose metabolism in cultured neocortical neurons and astrocytes using $^{13}$C-NMR spectroscopy. *Dev. Neurosci.* 20, 310–320. doi: 10.1159/000017326

Waagepetersen, H. S., Sonnewald, U., Larsson, O. M., and Schousboe, A. (2000). A possible role of alanine for ammonia transfer between astrocytes and glutamatergic neurons. *J. Neurochem.* 75, 471–479. doi: 10.1046/j.1471-4159.2000.0750471.x

Waniewski, R. A., and Martin, D. L. (1986). Exogenous glutamate is metabolized to glutamine and exported by rat primary astrocyte cultures. *J. Neurochem.* 47, 304–313. doi: 10.1111/j.1471-4159.1986.tb02863.x

Waniewski, R. A., and Martin, D. L. (1998). Preferential utilization of acetate by astrocytes is attributable to transport. *J. Neurosci.* 18, 5225–5233.

Wiechert, W. (2001). $^{13}$C metabolic flux analysis. *Metab. Eng.* 3, 195–206. doi: 10.1006/mben.2001.0187

Wienhard, K. (2002). Measurement of glucose consumption using [(18)F]fluorodeoxyglucose. *Methods* 27, 218–225. doi: 10.1016/S1046-2023(02)00077-4

Yang, J., Li, C. Q., and Shen, J. (2005). In vivo detection of cortical GABA turnover from intravenously infused [1-$^{13}$C]D-glucose. *Magn. Reson. Med.* 53, 1258–1267. doi: 10.1002/mrm.20473

Yu, A. C., Drejer, J., Hertz, L., and Schousboe, A. (1983). Pyruvate carboxylase activity in primary cultures of astrocytes and neurons. *J. Neurochem.* 41, 1484–1487. doi: 10.1111/j.1471-4159.1983.tb00849.x

Zwingmann, C., and Leibfritz, D. (2003). Regulation of glial metabolism studied by $^{13}$C-NMR. *NMR Biomed.* 16, 370–399. doi: 10.1002/nbm.850

Zwingmann, C., Richter-Landsberg, C., and Leibfritz, D. (2001). $^{13}$C isotopomer analysis of glucose and alanine metabolism reveals cytosolic pyruvate compartmentation as part of energy metabolism in astrocytes. *Glia* 34, 200–212. doi: 10.1002/glia.1054

**Conflict of Interest Statement:** The authors declare that the research was conducted in the absence of any commercial or financial relationships that could be construed as a potential conflict of interest.

*Received: 31 July 2013; accepted: 15 November 2013; published online: 09 December 2013.*

*Citation: Rodrigues TB, Valette J and Bouzier-Sore A-K (2013) $^{13}$C NMR spectroscopy applications to brain energy metabolism. Front. Neuroenergetics **5**:9. doi: 10.3389/fnene.2013.00009*

*This article was submitted to the journal Frontiers in Neuroenergetics.*

frontiers in
NEUROENERGETICS

ORIGINAL RESEARCH ARTICLE
published: 06 June 2011
doi: 10.3389/fnene.2011.00003

# Compartmentalized cerebral metabolism of [1,6-$^{13}$C]glucose determined by *in vivo* $^{13}$C NMR spectroscopy at 14.1 T

***João M. N. Duarte[1,2]*, Bernard Lanz[1] and Rolf Gruetter[1,3,4]***

[1] *Center for Biomedical Imaging, Ecole Polytechnique Fédérale de Lausanne, Lausanne, Switzerland*
[2] *Faculty of Biology and Medicine, University of Lausanne, Lausanne, Switzerland*
[3] *Department of Radiology, University of Lausanne, Lausanne, Switzerland*
[4] *Department of Radiology, University of Geneva, Geneva, Switzerland*

***Edited by:***
*Sebastián Cerdán, Instituto de Investigaciones Biomédicas Alberto Sols, Spain*

***Reviewed by:***
*Sebastián Cerdán, Instituto de Investigaciones Biomédicas Alberto Sols, Spain*
*Kevin L. Behar, Yale University, School of Medicine, USA*
*Tiago B. Rodrigues, Cancer Research UK (Cambridge Research Institute) and University of Cambridge, UK*

****Correspondence:***
*João M. N. Duarte, Ecole Polytechnique Fédérale de Lausanne, SB IPMC LIFMET (Bâtiment CH), Station 6, CH-1015 Lausanne, Switzerland.*
*e-mail: joao.duarte@epfl.ch*

Cerebral metabolism is compartmentalized between neurons and glia. Although glial glycolysis is thought to largely sustain the energetic requirements of neurotransmission while oxidative metabolism takes place mainly in neurons, this hypothesis is matter of debate. The compartmentalization of cerebral metabolic fluxes can be determined by $^{13}$C nuclear magnetic resonance (NMR) spectroscopy upon infusion of $^{13}$C-enriched compounds, especially glucose. Rats under light α-chloralose anesthesia were infused with [1,6-$^{13}$C]glucose and $^{13}$C enrichment in the brain metabolites was measured by $^{13}$C NMR spectroscopy with high sensitivity and spectral resolution at 14.1 T. This allowed determining $^{13}$C enrichment curves of amino acid carbons with high reproducibility and to reliably estimate cerebral metabolic fluxes (mean error of 8%). We further found that TCA cycle intermediates are not required for flux determination in mathematical models of brain metabolism. Neuronal tricarboxylic acid cycle rate ($V_{TCA}$) and neurotransmission rate ($V_{NT}$) were $0.45 \pm 0.01$ and $0.11 \pm 0.01$ μmol/g/min, respectively. Glial $V_{TCA}$ was found to be $38 \pm 3$% of total cerebral oxidative metabolism, accounting for more than half of neuronal oxidative metabolism. Furthermore, glial anaplerotic pyruvate carboxylation rate ($V_{PC}$) was $0.069 \pm 0.004$ μmol/g/min, i.e., $25 \pm 1$% of the glial TCA cycle rate. These results support a role of glial cells as active partners of neurons during synaptic transmission beyond glycolytic metabolism.

**Keywords: glucose metabolism, neurotransmission, mathematical modeling, NMR spectroscopy, neurotransmitter metabolism**

## INTRODUCTION

Cerebral function depends on coordinated interaction of distinct cell types, namely neurons and glial cells, and relies on high metabolic activity that is supported by continuous and adequate supply of glucose and oxygen from the blood stream (Siesjo, 1978). Regulation of neuronal-glial cooperation at metabolic level involves the mechanism of deactivation of the major excitatory neurotransmitter, glutamate, through glial uptake and conversion to electrophysiologically inactive glutamine, which is then transported back to the neuron to replenish the neurotransmitter pool of glutamate (see revision by Zwingmann and Leibfritz, 2003). The maintenance of this exchange of glutamate and glutamine between neurons and glia requires energy provided by glucose oxidation in glycolysis and tricarboxylic acid (TCA) cycle (e.g., Sibson et al., 1998).

Although brain activity relies on blood glucose, it is not excluded the possibility of lactate exchange between metabolic compartments. In fact, a putative lactate shuttle is thought to exist from astrocytes to neurons (Magistretti et al., 1999). According to this hypothesis, most glucose is oxidized to lactate in astrocytes and the resulting adenosine-5′-triphosphate (ATP) suffices to maintain glutamate clearance from the synaptic cleft and conversion to glutamine. The produced lactate is transferred to neurons for oxidative degradation (Pellerin and Magistretti, 1994; Magistretti et al., 1999). Based on this hypothesis, glial metabolism has been thought to be mostly glycolytic (Sibson et al., 1998; Shulman et al., 2003), which is controversial (e.g., Dienel and Hertz, 2001; Gjedde and Marrett, 2001; Simpson et al., 2007; Mangia et al., 2009). Furthermore, astrocytic uptake of glutamate could also be fueled by ATP of mitochondrial origin (Dienel and Hertz, 2001) and, in fact, the glial TCA cycle was found to account for 30% of total TCA cycle activity in the conscious rat brain (Oz et al., 2004). A substantial fraction of mitochondrial oxidation in astrocytes occurs through pyruvate carboxylase and was suggested to increase with cerebral activity (Sibson et al., 1998; Choi et al., 2002; Oz et al., 2004).

The compartmentalization of these metabolic pathways and inter-compartmental interactions have been studied by non-invasive $^{13}$C nuclear magnetic resonance (NMR). Dynamic

**Abbreviations:** ATP, Adenosine-5′-triphosphate; FE, fractional enrichment; NMR, nuclear magnetic resonance; PCA, perchloric acid; TCA, tricarboxylic acid.

*in vivo* $^{13}$C NMR spectroscopy combined with the infusion of $^{13}$C-enriched substrates and followed by appropriate mathematical modeling was proved to be a powerful tool for studying the compartmentalized cerebral metabolism. Although brain cells have the ability of using several substrates, glucose is well established as the main fuel for cerebral metabolism (Siesjo, 1978). The most determined metabolic rates upon infusion of $^{13}$C-enriched glucose include glucose utilization ($CMR_{glc}$), neuronal, and glial TCA cycles ($V_{TCA}$), the malate–aspartate shuttle activity ($V_x$), apparent neurotransmission flux ($V_{NT}$), i.e., glutamate–glutamine cycle, and glial anaplerotic pyruvate carboxylation ($V_{PC}$) (e.g., Sibson et al., 1998; Gruetter et al., 2001; Oz et al., 2004; Patel et al., 2005). However, strong debate is continuously generated on the relative values for these metabolic fluxes and how should they be properly determined (Shestov et al., 2007; Uffmann and Gruetter, 2007; Shen et al., 2009). Many assumptions are generally used for *in vivo* determination of metabolic fluxes and concern has been raised on the reliability of estimated fluxes from experiments using $^{13}$C-enriched glucose as metabolic tracer (Shestov et al., 2007; Shen et al., 2009).

We tested the hypothesis that high sensitivity and resolution achieved in $^{13}$C NMR spectra at 14.1 T leads to increased reliability in detected $^{13}$C enrichment time courses and thus allows us to determine accurate metabolic fluxes. In fact, the present data was acquired with high temporal resolution, during approximately 6 h and with low noise level, which are conditions required for accurate flux estimation (Shestov et al., 2007). In addition, although most mathematical models were designed with many unknown metabolic pools, namely for TCA cycle intermediates, a simplification has been proposed and resulted in a mathematical model where flux estimation is mostly dependent on $^{13}$C enrichment of measured metabolites (Uffmann and Gruetter, 2007). The comparison between these two approaches was now performed. For the first time we show experimental evidence supporting that TCA cycle intermediates are not required in mathematical models of cerebral metabolism, as previously suggested by mathematical simulations (Uffmann and Gruetter, 2007).

In this study, metabolic fluxes were determined with higher precision than in previous $^{13}$C NMR studies in the brain of rodents (e.g., Choi et al., 2002; Patel et al., 2005) or humans (e.g., Gruetter et al., 2001), as depicted by an average associated error of 8%. We identified substantial pyruvate carboxylation and glial TCA cycle rates that together accounted for more than half of neuronal $V_{TCA}$, suggesting high glial oxidative metabolism.

## MATERIALS AND METHODS

### ANIMALS

All experimental procedures involving animals were approved by the local ethics committee. Male Sprague-Dawley rats ($276 \pm 11$ g, $n = 5$, obtained from Charles River Laboratoires, France) were prepared as previously described (Duarte et al., 2009a). Briefly, after fasting for 6 h, rats were anesthetized using 2% isoflurane (Attane, Minrad, NY, USA) in 30% oxygen in air, and then intubated with an endotracheal catheter and ventilated with a pressure-driven ventilator (MRI-1, CWE incorporated, PA, USA). Catheters were inserted into a femoral artery for monitoring blood gases, glucose, lactate, and arterial blood pressure, and into a femoral vein for infusion of saline solutions containing α-chloralose (Acros Organics, Geel, Belgium) or [1,6-$^{13}$C]glucose (Isotec, Sigma-Aldrich, Basel, Switzerland).

Animals were immobilized in a homebuilt holder with a bite bar and two ear inserts to minimize potential motion. Body temperature was maintained between 37.0 and 37.5°C with a warm water circulation system based on the feedback obtained from a homebuilt rectal temperature probe. Arterial blood pressure, heart rate, and respiratory rate were continuously monitored with an animal monitoring system (SA Instruments, NY, USA). Before inserting the animal in the bore of the magnet, anesthesia was switched to α-chloralose (intravenous bolus of 80 mg/kg and continuous infusion rate of 28 mg/kg/h). Arterial pH and pressures of $O_2$ and $CO_2$ were measured using a blood gas analyzer (AVL Compact 3, Diamond Diagnostics, MA, USA). Plasma glucose and lactate concentrations were quantified with the glucose or lactate oxidase methods, respectively, using two multi-assay analyzers (GW7 Micro-Stat, Analox Instruments, London, UK).

The glucose infusion procedure was adapted from the protocol described by Henry et al. (2003a). Briefly, a bolus of 99.9% enriched [1,6-$^{13}$C]glucose (1.1 M in saline solution) was given at a 5-min exponential decay based on the measured basal glycemia and aiming at 70% plasma fractional enrichment (FE). After the bolus, 70% enriched [1,6-$^{13}$C]glucose (1.1 M in saline solution) was infused at a rate equivalent to the whole body glucose disposal rate of 33.2 mg/kg/min (Jucker et al., 2002) and adjusted based on concomitantly measured arterial plasma glucose concentrations. Plasma samples were stored at −80°C for determination of substrate FE. Arterial pH and blood gases were maintained within the normal physiological range by adjusting respiratory rate and volume.

### *IN VIVO* NMR SPECTROSCOPY

All *in vivo* NMR experiments were carried out in a DirectDrive spectrometer (Varian, Palo Alto, CA, USA) interfaced to a 14.1 T magnet with a 26-cm horizontal bore (Magnex Scientific, Abingdon, UK), using a homebuilt coil consisting of a $^{1}$H quadrature surface coil and a $^{13}$C linearly polarized surface coil. The rat brain was positioned in the isocenter of the magnet and fast-spin-echo images with repetition time of 5 s, echo time of 52 ms and echo train length of eight allowed to identify anatomical landmarks, which were used to place the volume of interest (VOI) of 320 μL in the brain. Shimming was performed with FAST(EST)MAP (Gruetter and Tkác, 2000). Localized $^{1}$H NMR spectra were acquired using SPECIAL (Mlynárik et al., 2006) with echo time of 2.8 ms and repetition time of 4 s. $^{13}$C NMR spectra were acquired using semi-adiabatic distortionless enhancement by polarization transfer (DEPT) combined with 3D-ISIS $^{1}$H localization (Henry et al., 2003a).

Spectral analysis was carried out using LCModel (Stephen Provencher Inc., Oakville, ON, Canada) for both $^{1}$H (Mlynárik et al., 2006) and $^{13}$C NMR spectra (Henry et al., 2003b). Simulation of basis spectra for the observable isotopomers was performed in Matlab (The MathWorks, Natick, MA, USA) as described by Henry et al. (2003b). The scaling of dynamically measured $^{13}$C concentrations was based on the FE of glutamate C3, which was determined through the multiplicity of glutamate C4, and the total

glutamate concentration obtained from $^{1}$H NMR spectra. In other words, FE of glutamate C3 was determined from the C4 resonance in $^{13}$C spectra from the last 20 min, assuming steady-state for C4 enrichment and FE(C3) = C4D34/(C4S + C4D34). Then, relative intensities in $^{13}$C NMR spectra were used to scale $^{13}$C concentration for all carbon resonances through all time courses. Additionally, *in vitro* $^{13}$C NMR spectra from brain extracts and standard solutions including the metabolites of interest allowed correcting for the relative differences in signal enhancement by polarization transfer in DEPT.

### *IN VITRO* NMR SPECTROSCOPY

After each experiment, rats were sacrificed using a focused microwave fixation device (Gerling Applied Engineering, Inc., Modesto, CA, USA) at 4 kW for 2 s. Brain tissue excluding cerebellum was immediately stored at −80°C until extraction. Water-soluble metabolites from brain and plasma samples were extracted with 7% (v/v) perchloric acid (PCA) as previously described (Duarte et al., 2007) and dried with a sample concentrator (Speed-Vac DNA 120, Thermo Fisher Scientific, Wohlen, Switzerland). The dried extracts were dissolved in $^{2}H_2O$ (99.9% $^{2}$H, Sigma-Aldrich) and 1.2 mmol sodium fumarate (Sigma-Aldrich) was added as internal standard for quantification by $^{1}$H NMR spectroscopy. $^{1}$H and $^{13}$C NMR spectra were acquired on a 14.1 T DRX-600 spectrometer equipped with a 5-mm cryoprobe (Bruker BioSpin SA, Fallanden, Switzerland) as previously described (Duarte et al., 2007). Peak areas were quantified by curve fitting.

### DETERMINATION OF METABOLIC FLUXES

Kinetic modeling of [1,6-$^{13}$C]glucose metabolism was performed with basis on the mathematical model of compartmentalized cerebral metabolism described by Gruetter et al. (2001). **Figure 1** depicts metabolic pools and fluxes defined in our model, which is detailed in Section "Appendix." An alternative model was designed to eliminate the non-measurable $^{13}$C enrichment of TCA cycle intermediates (Uffmann and Gruetter, 2007).

Each model was fitted to the $^{13}$C enrichment curves over time using the Levenberg–Marquardt algorithm for non-linear regression, coupled to a Runge–Kutta method for non-stiff systems to obtain numerical solutions of the ordinary differential equations (see Appendix). Significance of the fitted parameters (fluxes) was inferred from $t$-statistics. $F$-statistics was used for assessment of fit quality and for inter-model comparison. Reliability of determined fluxes was evaluated by Monte-Carlo analysis, in which Gaussian noise with the same variance of fit residuals was added to the best fit and initial conditions were randomly generated within confidence interval of the obtained value. Typically, 500 simulated datasets were created for each individual analysis. All numerical procedures were performed in Matlab.

The estimated metabolic fluxes are shown as mean ± SD, being the SD resulting from Monte-Carlo simulations. Other results are shown as mean ± SEM of $n = 5$ experiments.

## RESULTS

The specific protocol of $^{13}$C-enriched glucose infusion raised plasma glucose from 100 to 350 mg/dL in 5 min and then remained constant (**Figure 2A**), leading to a step function in plasma glucose FE of ∼70% (**Figure 2B**). Concentration of lactate in plasma varied during the experiment as consequence of the variable glucose infusion rate that aimed at a stable plasma glucose level (**Figure 2A**). FE of lactate increased at the onset of [1,6-$^{13}$C]glucose and was maintained constant over time (**Figure 2B**), and may contribute to brain metabolism. For example, at the end of the experiment, the FE of plasma glucose and lactate were 0.67 ± 0.01 and 0.50 ± 0.01, respectively. FE in plasma alanine and acetate increased over the experimental time course and seemed to reach a steady-state after 300 min, respectively achieving a FE of 0.45 ± 0.02 and 0.33 ± 0.01 (**Figure 2C**). Therefore, the influx of $^{13}$C labeling from extra-cerebral lactate and acetate was included in the model (see Appendix). Plasma alanine was considered to have minor contribution to brain metabolism since it exists at only 11.2 ± 3.2% of lactate concentration (quantified in PCA extracts of plasma samples by *in vitro* NMR spectroscopy). This is further supported by the relative low rate of alanine transport into the brain and contribution to metabolism (Bröer et al., 2007).

The *in vivo* spectral quality achieved at 14.1 T can be appreciated from **Figure 3**. A major improvement was the increased sensitivity relative to lower fields and the full separation of the carbon positions of glutamate and glutamine C3 which was not possible at, for example, 9.4 T (Henry et al., 2003b). The $^{13}$C resonances of glucose, glutamate, glutamine, and aspartate were determined with a temporal resolution of 5.3 min (**Figures 3** and **4**). Total concentration of these amino acids was determined *in vivo* and found to be 8.5 ± 0.4 μmol/g for glutamate, 5.1 ± 0.5 μmol/g for glutamine, and 2.4 ± 0.3 μmol/g for aspartate.

In brain extracts, prepared at the end of the experiment, FE was 0.70 ± 0.02 for glucose, 0.53 ± 0.02 for lactate, and 0.54 ± 0.01 for alanine. Therefore, a significant dilution flux $V_{out}$ must occur, leading to different FE in brain glucose and the end products of glycolysis, namely lactate. Lactate homeostasis resides in a balance between production, consumption and exchange between brain parenchyma, and extra-cerebral lactate equivalents. Plasma lactate was labeled at a different enrichment than that of plasma glucose (**Figure 2**), thus contributing to brain lactate through $V_{in}$. However, the redundancy between contributions of [1,6-$^{13}$C]glucose and [3-$^{13}$C]lactate enriched at different levels to metabolism in mitochondria leads to a high correlation between $V_{out}$, glucose transport ($T_{max}$), and consumption ($CMR_{glc}$) (**Figure 5**). Therefore, glucose transport was determined from the experimental data with a dynamic version of the reversible Michaelis–Menten model described by Duarte et al. (2009b) and transport parameters used to simulate glucose transport that feeds the pyruvate pool: $T_{max} = 0.91 \pm 0.03$ μmol/g/min, $CMR_{glc} = 0.50 \pm 0.02$ μmol/g/min, and $K_t = 0.32 \pm 0.10$ mM. The constraint of parameters directly involved in glucose homeostasis was devoid of significant effects on the remaining metabolic fluxes, with the obvious exception of $V_{out}$.

The compartmentalized model of brain metabolism previously proposed (Gruetter et al., 2001) was adapted to include a non-zero concentration of aspartate in the glial compartment and a dilution factor at the level of glial acetyl-CoA (see Appendix). Non-linear regression of the model to the determined $^{13}$C enrichment curves is shown in **Figure 4**. Following the suggestion that TCA cycle intermediates can be excluded from the mathematical model, at least for the non-compartmentalized case (Uffmann and

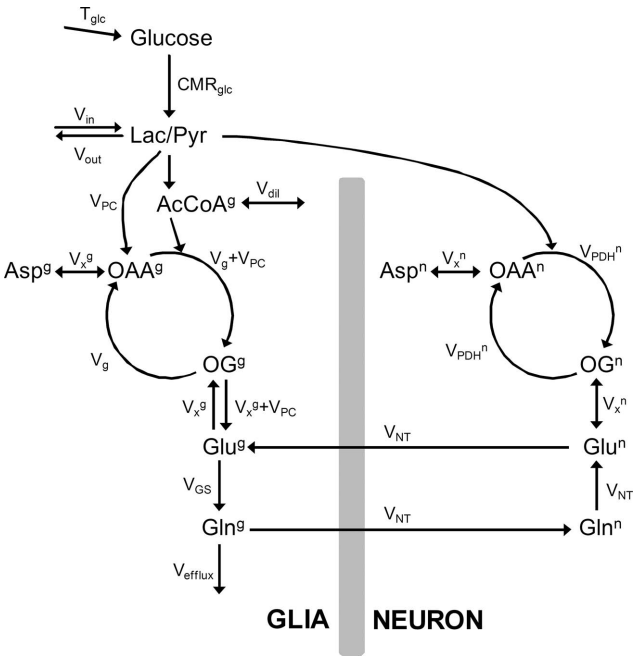


**FIGURE 1 | Model of compartmentalized brain metabolism adapted from Gruetter et al. (2001).** Glucose transport is here represented by $T_{glc}$. $CMR_{glc}$ is the cerebral metabolic rate of glucose. Pyruvate (Pyr) originated from glucose consumption is in fast equilibrium with lactate (Lac) that is exchanged between neurons and glia and is diluted with extra-cerebral lactate through $V_{out}/V_{in}$. $V^n_{PDH}$ is the neuronal TCA cycle, $V_g + V_{PC}$ is the total glial TCA cycle, $V_{PC}$ is the rate of pyruvate carboxylase. In the glial compartment, the dilution of label at the level of acetyl-CoA (AcCoA) by glial specific substrates is accounted by $V_{dil}$. TCA cycle intermediates oxaloacetate (OAA) and 2-oxoglutarate (OG) exchange with aminoacids through the exchange flux $V_X$. The apparent glutamatergic neurotransmission (i.e., glutamate–glutamine cycle) is $V_{NT}$ and glutamine synthetase rate is $V_{GS}$. Finally, efflux of labeling from the metabolic system occurs through the rate of glial glutamine loss $V_{efflux}$. The superscripts g and n distinguish metabolic pools or fluxes in the glial and neuronal compartments, respectively.

Gruetter, 2007), we further tested the fit of such model (derived in Appendix) with successful results. In any of the cases, the non-linear regressions were performed without imposing any constraint to the eight fluxes of intermediary metabolism that were estimated. Precision of the estimated fluxes was determined by Monte-Carlo simulations and the resulting probability was fitted with a gamma function that, for all estimated fluxes, approached a Gaussian distribution. For the sake of comparison, estimated fluxes with both models are shown in **Table 1**. As the increasing number of experimental $^{13}$C enrichment time courses used in the fitting process may increase the accuracy of estimated fluxes, as suggested by numerical simulations (Shestov et al., 2007), we fitted both models providing or not the aspartate C2 and C3 turnover curves (**Table 1**). Although increased precision was found to be associated with the number of fitted $^{13}$C enrichment curves, estimated fluxes did not diverge significantly.

For the most complete model, i.e., including TCA cycle intermediates and fitted to $^{13}$C enrichment curves of glutamate, glutamine, and aspartate, the TCA cycle $V_{TCA}$ was $0.45 \pm 0.01$ μmol/g/min and $0.28 \pm 0.02$ μmol/g/min the neuronal and glial compartments, respectively. Notably, the flux though the malate–aspartate shuttle $V_x$ was in the same order of $V_{TCA}$. Pyruvate carboxylation $V_{PC}$ was $0.069 \pm 0.004$ μmol/g/min, accounting for specific labeling of glutamate and glutamine C2. The neurotransmission flux $V_{NT}$ of $0.11 \pm 0.01$ μmol/g/min is, in our model, the responsible for labeling exchange between the two compartments. These fluxes were not statistically different between the different analyses (**Table 1**).

## DISCUSSION

Compartmentalized brain energy metabolism was determined following infusion of [1,6-$^{13}$C]glucose and direct detection of $^{13}$C enrichment of brain metabolites by high resolution $^{13}$C NMR spectroscopy at 14.1 T. High sensitivity was achieved in this study and permitted to quantify $^{13}$C enrichment curves of brain amino acid carbons with high reproducibility and to reliably determine cerebral metabolic fluxes, as indicated by the mean error of 8% associated to the determined fluxes (**Table 1**). For the first time to our knowledge, we used $^{13}$C turnover curves determined *in vivo* in the rat brain for all aliphatic carbons of glutamate, glutamine, and aspartate for metabolic modeling, similarly to what was performed for the human brain (Gruetter et al., 2001). This, together with the high temporal resolution and long time course of the detected $^{13}$C enrichment, increased the level of precision of the measured metabolic fluxes (Shestov et al., 2007). For the determined metabolic fluxes, although similar results were obtained in the absence or inclusion of aspartate $^{13}$C enrichment curves in the fitting process, precision generally increased with the number of used turnover curves, especially

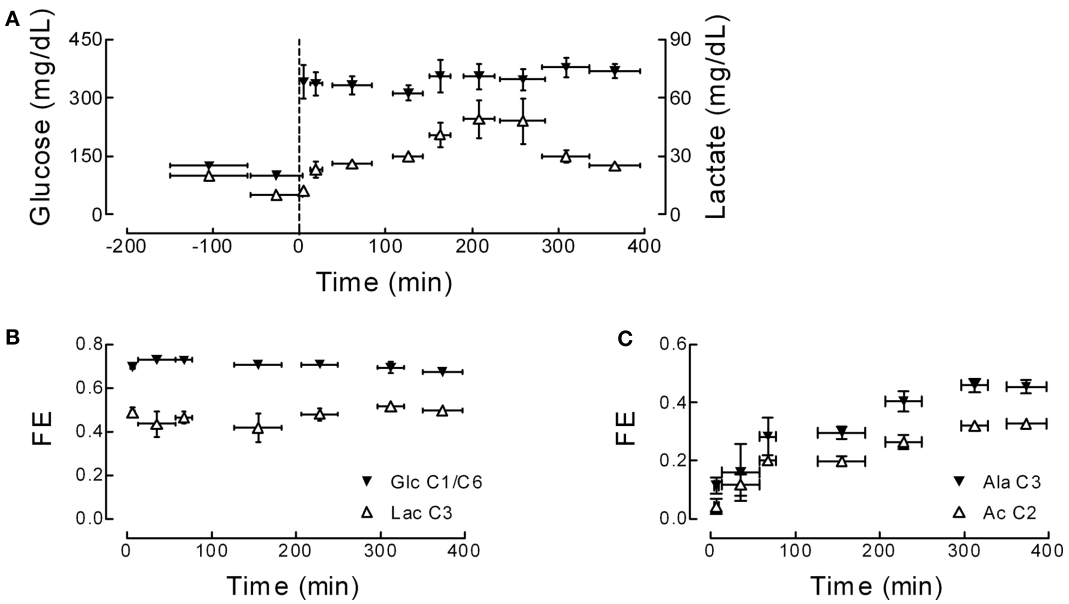


**FIGURE 2 | Concentration and fractional enrichment (FE) of plasma glucose, lactate, alanine, and acetate upon infusion of [1,6-$^{13}$C]glucose. (A)** Shows glucose (filled symbols) and lactate (open symbols) concentration determined during the entire time course. **(B)** Depicts FE of glucose and lactate determined by *in vitro* $^{1}$H NMR spectroscopy. FE of alternative brain substrates alanine and acetate were determined in $^{1}$H NMR spectra of plasma samples **(C)**.

when TCA cycle intermediates are absent from the model (see **Table 1**).

Uffmann and Gruetter (2007) previously demonstrated by means of numerical simulations that the unknown *in vivo* $^{13}$C enrichment time courses of TCA cycle intermediates can be neglected using a single compartment model of brain metabolism. We now extended that model to include the two main cerebral metabolic compartments (glial and neuronal compartments) and found similar results in the absence or presence of TCA cycle intermediates in the mathematical model. In fact, similar metabolic fluxes were estimated with the two approaches and identical best fit curves were obtained. However, without the intermediates, increased correlation between the estimated fluxes was observed (**Figure 5**). This is caused by the fact that metabolic fluxes are directly combined in products and quotients in the derived equations.

Recent publications restricted the analysis of cerebral intermediary metabolism by *in vivo* $^{13}$C NMR spectroscopy to resonances C4 and C3 and disregarded the C2 of glutamate and glutamine, which may be principally due to low resolution of acquired $^{13}$C NMR spectra or to the use of indirect detection of $^{13}$C enrichment in $^{1}$H NMR spectra (de Graaf et al., 2003; Patel et al., 2010; van Eijsden et al., 2010; Xin et al., 2010). Indirect $^{13}$C detection has the great advantage of higher sensitivity but the drawback of lower spectral resolution characteristic of $^{1}$H NMR spectroscopy even at 14.1 T (Xin et al., 2010). Our results show that, with increased sensitivity at high magnetic field strengths, direct $^{13}$C detection may be preferred. We achieved good time resolution for aliphatic carbons of glutamate and glutamine (the most concentrated metabolites appearing in the $^{13}$C spectra of the brain) with high reproducibility between all animals studied. The data further suggested that we could reduce the time span of C4 enrichment curves of these amino acids to 3 min without losing the consistency of the $^{13}$C time course measurement (data not shown). Conversely, the $^{13}$C enrichment curves could be acquired from a volume of interest smaller than 320 μL (used in this study). In our experimental conditions, we determined the turnover curves for all aliphatic carbons of glutamate, glutamine, and aspartate and provided them for the non-linear fit of the mathematical model (**Figure 4**).

The simultaneous determination of $^{13}$C-enriched glucose concentrations in plasma and brain allows measuring glucose transport. Notably, high correlation was found between glucose transport ($T_{max}$), consumption ($CMR_{glc}$), and label exchange before mitochondrial oxidation ($V_{out}$). Therefore, glucose transport was analyzed as described by Duarte et al. (2009b) and the obtained parameters were used to simulate brain glucose enrichment and concentration as input for the metabolic model. However, by simulating $T_{max}$ and $CMR_{glc}$, correlation between $V_{out}$ and other fluxes increased. $V_{out}$, along with $V_{in}$, represent metabolic exchange with other metabolites fueling brain metabolism, such as free amino acids (e.g., Bröer et al., 2007; Boumezbeur et al., 2010), and interaction of glycolysis with other brain pathways like the pentose phosphate shunt (e.g., Dusick et al., 2007). In fact, the brain is capable of lactate uptake and metabolism (e.g., Dienel and Cruz, 2009; Gallagher et al., 2009; Boumezbeur et al., 2010). Exchange between extra-cerebral lactate with pyruvate is modeled by $V_{in}$ and $V_{out}$ and a net gain or loss of lactate concentration is taken into account by the ratio of $V_{in}$ to $V_{out}$. FE of brain lactate was significantly lower than that of the precursor glucose. Assuming that lactate is in fast exchange with the direct end product of glycolysis, pyruvate, and thus achieves similar FE, there would be a significant diversion of labeling between glucose entry in the brain

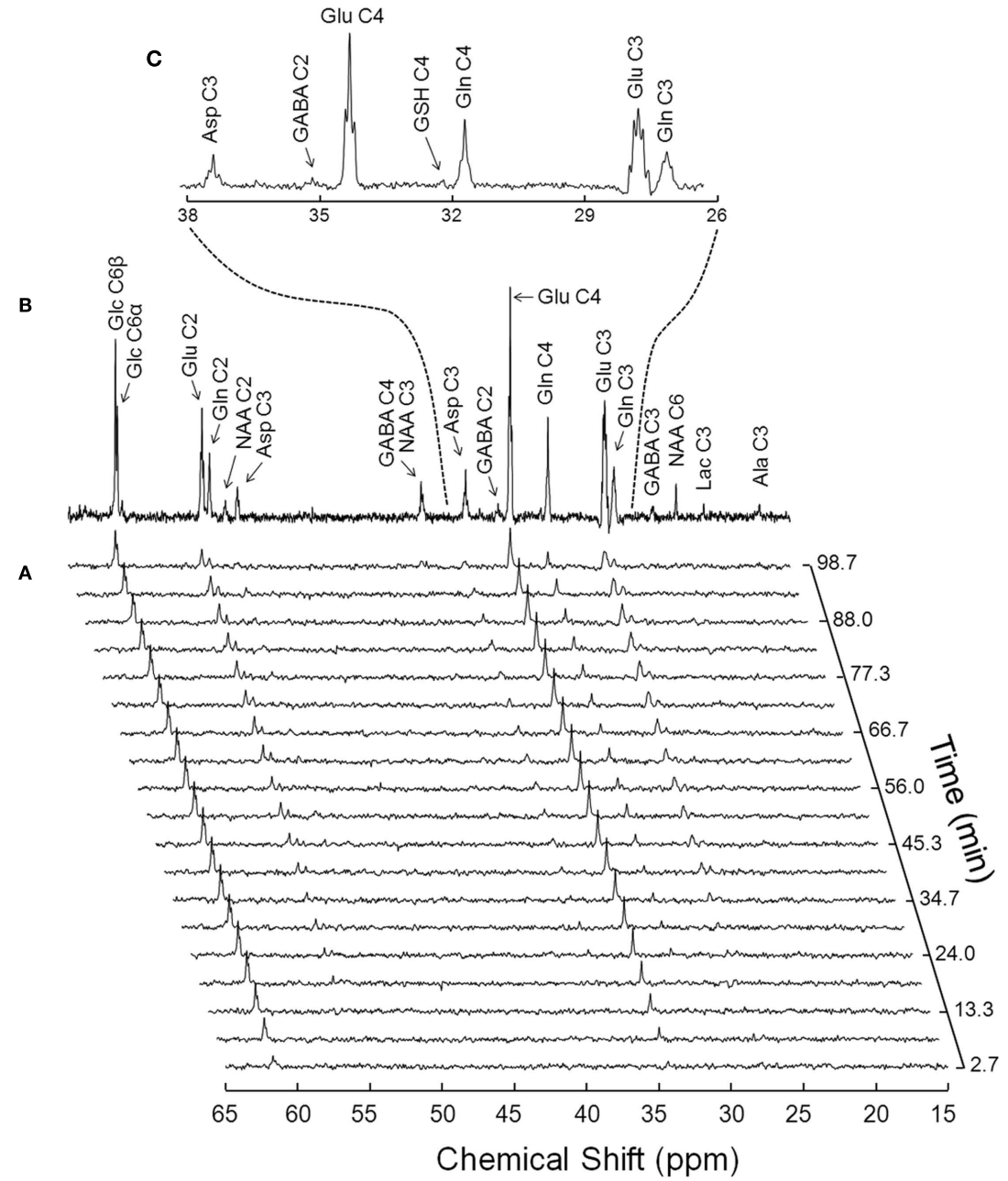


**FIGURE 3 | Typical *in vivo* $^{13}$C NMR spectra acquired at 14.1 T from a 320-μL volume in the rat brain upon infusion of [1,6-$^{13}$C]glucose.** **(A)** Shows the initial 100 min of a time course of $^{13}$C enrichment of brain metabolites from plasma [1,6-$^{13}$C]glucose, with a temporal resolution of 5.3 min (128 scans with TR of 2.5 s). The spectrum in **(B)** was acquired for 1.8 h, starting 3.5 h after the onset of [1,6-$^{13}$C]glucose infusion. **(C)** Depicts the expansion of **(B)** from 26 to 38 ppm, where are visible the multiplets originated by the different isotopomers of glutamine (Gln), glutamate (Glu), and aspartate (Asp). For resolution enhancement, Lorentzian–Gaussian apodization was applied before Fourrier transformation [lb = 7, sb = 0.12, and sbs = 0.02 for **(A)**; sb = 0.12 and sbs = 0.02 for **(B,C)**].

and oxidation in the mitochondrial TCA cycle. In fact, a significant $V_{out}$ was determined and, additionally, it was different from $V_{in}$ that represents lactate utilization from extra-cerebral sources (note that plasma lactate was also enriched). Since $V_{out} > V_{in}$, not all glucose consumption rate ($CMR_{glc}$) follows complete oxidation, i.e. $CMR_{glc(ox)}$. Our results indicate that only 78 ± 4% of the total glucose phosphorylation is oxidized in the TCA cycle, which is comparable to previous findings (discussed in Siesjo, 1978; Dienel and Hertz, 2001).

Different relative FE was observed in carbons of glutamate relative to glutamine. For example, at the end of the experiment, while glutamate C2 enrichment approaches that of C3

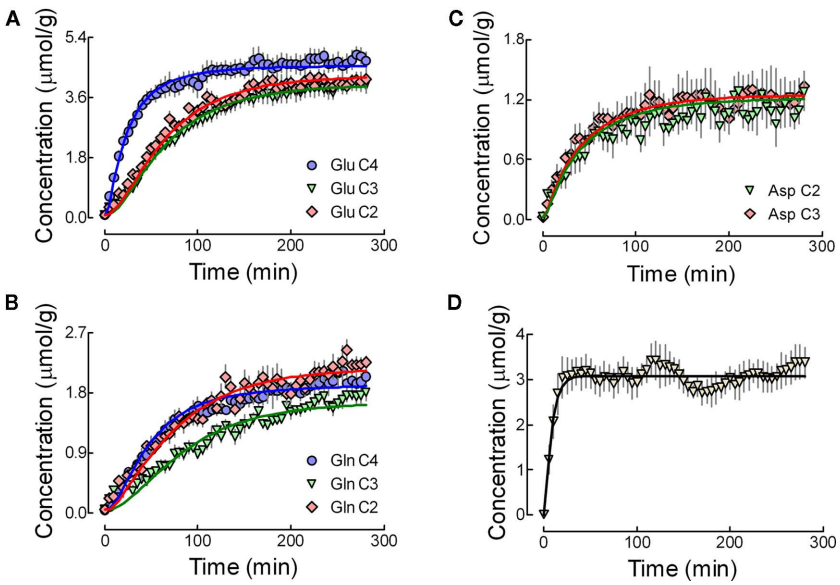


**FIGURE 4 | Concentration of enriched glutamate (A), glutamine (B), and aspartate (C) carbons detected *in vivo* during infusion of [1,6-$^{13}$C]glucose.** For glutamate and glutamine, blue, green, and red lines represent best fit to the $^{13}$C enrichment curves for C4, C3, and C2, respectively. For aspartate, green and red lines depict C2 and C3. Exact overlap was observed for the best fit curves with both metabolic models, i.e., with and without the inclusion of TCA cycle intermediates. This particular fits were performed with the inclusion of aspartate resonances. Although some experiments were conducted over a longer period (**Figure 2**), the data used for flux estimation was averaged for 280 min. **(D)** Shows the concentration of glucose C6 determined *in vivo* and the fit result of the dynamic reversible Michaelis–Menten model described in Duarte et al. (2009b).

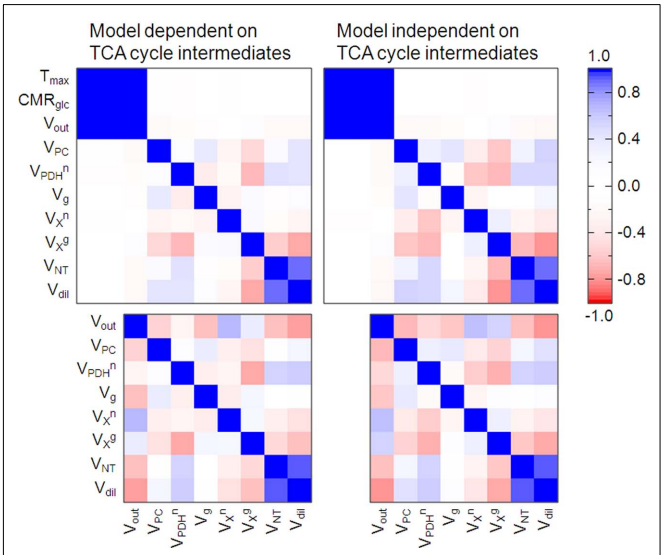


**FIGURE 5 | Correlation matrices showing the covariances between estimated metabolic fluxes.** Metabolic modeling was performed with all measurable $^{13}$C enrichment curves for glutamate, glutamine, and aspartate either including (left plots) or excluding (right plots) TCA cycle intermediate pools. Due to high correlation found between $T_{max}$, $CMR_{glc}$, and $V_{out}$, glucose transport kinetics was then determined as described in Duarte et al. (2009b) and simulated in the present model (bottom matrices).

(**Figure 4A**), glutamine C2 is close to C4 and different from that of C3 (**Figure 4B**). This would only be possible if, in addition to the glial $V_{PC}$ labeling C2 of glutamate and glutamine, the TCA cycle precursor pools in glial and neuronal compartments display different FE. This is consistent with alternative glial specific substrates fueling brain metabolism, namely acetate (Badar-Goffer et al., 1990; Cerdán et al., 1990), fatty acids (Ebert et al., 2003), and ketone bodies (Künnecke et al., 1993), which are oxidized to glial acetyl-CoA. Therefore, a dilution factor was introduced at the level of glial acetyl-CoA ($V_{dil}$). $V_{dil}$ not only acts as dilution factor for glial acetyl-CoA but can also incorporate $^{13}$C label from blood-born acetate (**Figure 2C**, which was considerable at the end of the experiment (FE = 0.33 ± 0.01). This dilution factor also accounts for eventual glial specific metabolic processes that deviate $^{13}$C labeling from oxidation in the TCA cycle, such as glycogen synthesis (Gruetter, 2003). $V_{dil}$ was thus found to be slightly higher but not substantially different from the acetate consumption rate determined in the rat brain upon with infusions of $^{13}$C enriched acetate (Deelchand et al., 2009). This glial labeling dilution of the acetyl-CoA pool through $V_{dil}$ was positively correlated to the apparent neurotransmission $V_{NT}$ as they are both responsible for the observed difference in C4 labeling between glutamate and glutamine.

One should note that, since glutamine and glutamate are mostly located in glial cells and neurons, respectively, $V_{dil}$ also accounts for the $^{13}$C labeling dilution between the two amino acids. Because part of glutamine may be undetected in *in vivo* $^{1}$H NMR spectra (e.g., Hancu and Port, 2011), we determined total glutamine relative to that of glutamate using resonance intensities and FEs from the $^{13}$C NMR spectra. Therefore, a total glutamine concentration different from 5.1 ± 0.5 μmol/g (measured in this study), may lead to a modification of $V_{dil}$.

**Table 1 | Cerebral metabolic fluxes (in μmol/g/min) determined either including or excluding TCA cycle intermediates.**

| Curves fitted | With TCA cycle intermediates | | Without TCA cycle intermediates | |
|---|---|---|---|---|
| | Glu + Gln | Glu + Gln + Asp | Glu + Gln | Glu + Gln + Asp |
| **DETERMINED FLUXES** | | | | |
| $V_{out}$ | 0.36 ± 0.05 | 0.42 ± 0.04 | 0.37 ± 0.06 | 0.41 ± 0.05 |
| $V_{PC}$ | 0.070 ± 0.004 | 0.069 ± 0.004 | 0.069 ± 0.005 | 0.067 ± 0.004 |
| $V^n_{PDH}$ | 0.44 ± 0.01 | 0.45 ± 0.01 | 0.46 ± 0.02 | 0.46 ± 0.01 |
| $V_g$ | 0.23 ± 0.02 | 0.21 ± 0.02 | 0.23 ± 0.03 | 0.21 ± 0.02 |
| $V^n_X$ | 0.76 ± 0.07 | 0.91 ± 0.09 | 0.83 ± 0.11 | 0.99 ± 0.12 |
| $V^g_X$ | 0.17 ± 0.06 | 0.16 ± 0.05 | 0.23 ± 0.12 | 0.25 ± 0.16 |
| $V_{NT}$ | 0.12 ± 0.01 | 0.11 ± 0.01 | 0.11 ± 0.01 | 0.10 ± 0.01 |
| $V_{dil}$ | 0.76 ± 0.15 | 0.66 ± 0.10 | 0.64 ± 0.13 | 0.55 ± 0.08 |
| **CALCULATED FLUXES** | | | | |
| $V^g_{TCA}$ | 0.30 ± 0.02 | 0.28 ± 0.02 | 0.30 ± 0.03 | 0.27 ± 0.02 |
| $V_{in}$ | 0.19 ± 0.05 | 0.22 ± 0.05 | 0.21 ± 0.07 | 0.24 ± 0.05 |
| $V_{GS}$ | 0.19 ± 0.01 | 0.18 ± 0.01 | 0.18 ± 0.01 | 0.17 ± 0.01 |
| $CMR_{glc(ox)}$ | 0.41 ± 0.02 | 0.39 ± 0.02 | 0.42 ± 0.04 | 0.40 ± 0.02 |

*Determinations were made with $^{13}$C enrichment curves from glutamine (Gln), glutamate (Glu), and eventually aspartate (Asp). Estimated values are presented with two significant digits and the associated SD was determined by Monte-Carlo analysis with at least 500 simulations. Calculated fluxes are defined in the Section "Appendix."*

The neuronal and glial $V_{TCA}$ were 0.45 ± 0.01 and 0.28 ± 0.02 μmol/g/min, respectively. This means that glial $V_{TCA}$ accounts for 38 ± 3% of total mitochondrial oxidative metabolism, from which 25 ± 1% is $V_{PC}$. $V_{PC}$ is further increased upon higher cerebral activity in the conscious rat (Oz et al., 2004) and reduced under isoelectricity (Sibson et al., 1998; Choi et al., 2002). This substantial pyruvate carboxylation flux supports the active role of glial cells in their metabolic relationship with neurons, especially during synaptic transmission. In fact, in cultured astrocytes, extracellular potassium was suggested to stimulate bicarbonate influx (Brookes and Turner, 1994), which can induce anaplerosis (Gamberino et al., 1997), and to increase glutamine content (Brookes and Turner, 1993). In our model, $V_{GS}$ results from the addition of $V_{PC}$ to $V_{NT}$ and thus depicts this coupling of anaplerosis to glutamine synthesis, both occurring in the glial compartment. To maintain mass balance in the glutamine–glutamate cycle, exit of labeling from the cycle was modeled as $V_{efflux}$, representing other fates of glutamate and glutamine (McKenna, 2007). It is proposed that astrocytic glycolysis sustains glutamatergic neurotransmission and the resulting lactate is shuttled to neurons for oxidative metabolism (Pellerin and Magistretti, 1994; Magistretti et al., 1999). This hypothesis considers that astrocytic metabolism is mainly glycolytic, which would be sufficient to meet the energetic requirements of glutamate uptake and glutamine synthesis in the neurotransmission process (Magistretti et al., 1999). However, clearance of glutamate could be fueled by mitochondrial oxidative phosphorylation in astrocytes (Dienel and Hertz, 2001). In accordance, the present results suggest that a substantial part of mitochondrial oxidation of glycolytic pyruvate takes place in the glial compartment, as observed in the conscious rat (Oz et al., 2004).

The exchange between amino acids in the cytosol and the mitochondrial matrix, where the TCA cycle takes place, is mediated by the malate–aspartate shuttle and responsible for most labeling exchange between glutamate or aspartate and their oxo-acids 2-oxoglutarate and oxaloacetate, represented by $V_x$ (Gruetter et al., 2001). $V_x$ has frequently been assumed to be much larger than $V_{TCA}$ (e.g., Hyder et al., 1996, 1997; Sibson et al., 1998), i.e., $V_{TCA}/V_x = 0$, which allows simplification of the mathematical models but may lead to underestimation of TCA cycle fluxes (see Uffmann and Gruetter, 2007). This assumption implies that $^{13}$C enrichment of glutamate and aspartate resembles that of OG and OAA, respectively, which may not be accurate (Gruetter et al., 2001). Experimental evidence shows that this flux could be either in the range of the TCA cycle flux (e.g., Gruetter et al., 2001; Oz et al., 2004) or effectively larger (e.g., de Graaf et al., 2004; Yang et al., 2009). In the rat brain under α-chloralose, we determined $^{13}$C enrichment curves with increased sensitivity and estimated a finite $V_x$ that is on the same order of $V_{TCA}$ in both neurons and glia. Although from all estimated fluxes, glial $V_x$ was the poorest estimated, i.e., with larger relative SD, all numerical simulations resulted in a $V^g_X$ on the order of $V^g_{TCA}$. To our knowledge this is the first time that $V_x$ is simultaneously determined in neurons and glia. Half of the total $V_{TCA}$, that represents oxidative glucose consumption $CMR_{glc(ox)}$, was found to be 0.39 ± 0.02 μmol/g/min (see **Table 1**), in agreement to other determinations by $^{13}$C NMR (Henry et al., 2002), or to measurements of $CMR_{O2}$ by $^{17}$O NMR spectroscopy (Zhu et al., 2002) and $CMR_{glc}$ by autoradiography (Ueki et al., 1992; Nakao et al., 2001) in rats under α-chloralose anesthesia.

The neurotransmission flux $V_{NT}$ represents the flow of $^{13}$C labeling in the glutamate–glutamine cycle and was now determined to be 0.11 ± 0.01 μmol/g/min (see **Table 1**) that is similar to that reported by (Sibson et al., 1998) for the rat brain under α-chloralose anesthesia. It should however be noted that in the present work, $V_{NT}$ was determined with higher precision

as suggested by an SD below 10%. The use of the C2 turnover curves of both glutamate and glutamine greatly contributed to the precision in the estimation of $V_{NT}$ by receiving direct $^{13}$C labeling input through pyruvate carboxylation that occurs in the glial compartment. A positive correlation was observed between $V_{NT}$ and the dilution of glial acetyl-CoA $V_{dil}$ (Shen et al., 2009), which resides in the fact that $V_{dil}$ creates a difference between the FEs of glutamine and glutamate while $V_{NT}$ is responsible for its dissipation.

*In vitro* studies suggest the existence of high fumarase activity randomizing $^{13}$C labeling from oxaloacetate (Sonnewald et al., 1993; Merle et al., 1996). Direct injection of [1-$^{14}$C]pyruvate in the neocortex of mice labels glutamate and glutamine, which would only occur with pyruvate carboxylation and a notable rate through fumarase (Nguyen et al., 2007). In an alternative model, flux through fumarase ($V_{fum}$) allowing labeling exchange between OAA C3 and C2 was included. $V_{fum}$ was detected but poorly determined, i.e., presented high relative SD, and was not significantly different from zero, as in a previous *in vivo* study (Oz et al., 2004). This is likely due to the high correlation of $V_{fum}$ to $V_{PC}$ that alone accounts for the difference in C2 and C3 enrichment of glutamate and glutamine. The fact that aspartate, which is in exchange with OAA, is mostly located in neurons (discussed in Gruetter et al., 2001), makes it insensitive to this flux. In accordance to the primary location of aspartate to neurons, NMR spectroscopy of brain extracts at the end of the experiment revealed similar FE for C3 and C2 of aspartate in our study ($0.52 \pm 0.02$ and $0.52 \pm 0.01$, respectively). However, the significant difference between $^{13}$C enrichment of carbons C2 and C3 of glutamate and glutamine at steady-state is in agreement with low $V_{fum}$ compared to $V_{PC}$.

Pyruvate recycling was suggested to occur in the brain (e.g., Cerdán et al., 1990; Sonnewald et al., 1996; Waagepetersen et al., 2002; Serres et al., 2007; Scafidi et al., 2010). This process would lead to enrichment of pyruvate C2 and consequently lactate C2 and, in fact, FE of lactate C2 in brain extracts at the end of the experiment was $0.029 \pm 0.001$. Although significant compared to the natural abundance of 0.011 ($P < 0.01$ with one-sample $t$ test), it was much lower than the enrichment of C3 and therefore negligible. This pathway was suggested to be mainly used for complete oxidation of glutamate or glutamine in the TCA cycle and to occur in cultured astrocytes but not in neurons and in co-cultures of both (Sonnewald et al., 1996; Waagepetersen et al., 2002). This is in agreement with the lack of evidence for substantial pyruvate recycling *in vivo*. In addition, high glucose concentration may lead to reduction of the pyruvate recycling flux (discussed in Waagepetersen et al., 2002) and some C2 enrichment observed *in vivo* may be of systemic origin due to scrambling of $^{13}$C labeling in tissues such as the liver (discussed in Serres et al., 2007).

## CONCLUSION

The present work experimentally demonstrates that reliable determination of $^{13}$C enrichment curves with high temporal resolution increases the precision of estimated metabolic fluxes. Additionally, precision increases with the number of experimentally measured turnover curves. Furthermore, we provide experimental evidence that non-measurable $^{13}$C enrichment of TCA cycle intermediates is not required for flux estimation, but increased correlation between the resulting fluxes must be expected. We found a substantial glial oxidative metabolism, part being driven through pyruvate carboxylase, which corresponds to more than half of the neuronal TCA cycle rate. This is consistent with the active role of astrocytes in the support of glutamatergic neurotransmission.

## ACKNOWLEDGMENTS

This work was supported by Swiss National Science Foundation (grant 131087) and by Centre d'Imagerie BioMédicale (CIBM) of the UNIL, UNIGE, HUG, CHUV, EPFL, and the Leenaards and Jeantet Foundations.

## REFERENCES

Badar-Goffer, R. S., Bachelard, H. S., and Morris, P. G. (1990). Cerebral metabolism of acetate and glucose studied by 13C-n.m.r. spectroscopy – a technique for investigating metabolic compartmentation in the brain. *Biochem. J.* 266, 133–139.

Boumezbeur, F., Petersen, K. F., Cline, G. W., Mason, G. F., Behar, K. L., Shulman, G. I., and Rothman, D. L. (2010). The contribution of blood lactate to brain energy metabolism in humans measured by dynamic 13C nuclear magnetic resonance spectroscopy. *J. Neurosci.* 30, 13983–13991.

Bröer, S., Bröer, A., Hansen, J. T., Bubb, W. A., Balcar, V. J., Nasrallah, F. A., Garner, B., and Rae, C. (2007). Alanine metabolism, transport, and cycling in the brain. *J. Neurochem.* 102, 1758–1770.

Brookes, N., and Turner, R. J. (1993). Extracellular potassium regulates the glutamine content of astrocytes: mediation by intracellular pH. *Neurosci. Lett.* 160, 73–76.

Brookes, N., and Turner, R. J. (1994). K(()-induced alkalinization in mouse cerebral astrocytes mediated by reversal of electrogenic Na(()-HCO3- cotransport. *Am. J. Physiol.* 267, C1633–C1640.

Cerdán, S., Künnecke, B., and Seelig, J. (1990). Cerebral metabolism of [1,2-13C2]acetate as detected by in vivo and in vitro 13C NMR. *J. Biol. Chem.* 265, 12916–12926.

Choi, I. Y., Lei, H., and Gruetter, R. (2002). Effect of deep pentobarbital anesthesia on neurotransmitter metabolism in vivo: on the correlation of total glucose consumption with glutamatergic action. *J. Cereb. Blood Flow Metab.* 22, 1343–1351.

de Graaf, R. A., Brown, P. B., Mason, G. F., Rothman, D. L., and Behar, K. L. (2003). Detection of [1,6-13C2]-glucose metabolism in rat brain by in vivo 1H-[13C]-NMR spectroscopy. *Magn. Reson. Med.* 49, 37–46.

de Graaf, R. A., Mason, G. F., Patel, A. B., Rothman, D. L., and Behar, K. L. (2004). Regional glucose metabolism and glutamatergic neurotransmission in rat brain in vivo. *Proc. Natl. Acad. Sci. U.S.A.* 101, 12700–12705.

Deelchand, D. K., Shestov, A. A., Koski, D. M., Ugurbil, K., and Henry, P. G. (2009). Acetate transport and utilization in the rat brain. *J. Neurochem.* 109, 46–54.

Dienel, G. A., and Cruz, N. F. (2009). Exchange-mediated dilution of brain lactate specific activity: implications for the origin of glutamate dilution and the contributions of glutamine dilution and other pathways. *J. Neurochem.* 109(Suppl. 1), 30–37.

Dienel, G. A., and Hertz, L. (2001). Glucose and lactate metabolism during brain activation. *J. Neurosci. Res.* 66, 824–838.

Duarte, J. M. N., Carvalho, R. A., Cunha, R. A., and Gruetter, R. (2009a). Caffeine consumption attenuates neurochemical modifications in the hippocampus of streptozotocin-induced diabetic rats. *J. Neurochem.* 111, 368–379.

Duarte, J. M. N., Morgenthaler, F. D., Lei, H., Poitry-Yamate, C., and Gruetter, R. (2009b). Steady-state brain glucose transport kinetics re-evaluated with a four-state conformational model. *Front. Neuroenergetics* 1:6. doi: 10.3389/neuro.14.006.2009

Duarte, J. M. N., Cunha, R. A., and Carvalho, R. A. (2007). Different metabolism of glutamatergic and GABAergic compartments in superfused hippocampal slices characterized by nuclear magnetic resonance spectroscopy. *Neuroscience* 144, 1305–1313.

Dusick, J. R., Glenn, T. C., Lee, W. N., Vespa, P. M., Kelly, D. F., Lee, S. M., Hovda, D. A., and Martin, N. A. (2007). Increased pentose phosphate pathway flux after clinical traumatic brain injury: a [1,2-13C2]glucose labeling study in humans. *J. Cereb. Blood Flow Metab.* 27, 1593–1602.

Ebert, D., Haller, R. G., and Walton, M. E. (2003). Energy contribution of octanoate to intact rat brain metabolism measured by 13C nuclear magnetic resonance spectroscopy. *J. Neurosci.* 23, 5928–5935.

Gallagher, C. N., Carpenter, K. L., Grice, P., Howe, D. J., Mason, A., Timofeev, I., Menon, D. K., Kirkpatrick, P. J., Pickard, J. D., Sutherland, G. R., and Hutchinson, P. J. (2009). The human brain utilizes lactate via the tricarboxylic acid cycle: a 13C-labelled microdialysis and high-resolution nuclear magnetic resonance study. *Brain* 132, 2839–2849.

Gamberino, W. C., Berkich, D. A., Lynch, C. J., Xu, B., and LaNoue, K. F. (1997). Role of pyruvate carboxylase in facilitation of synthesis of glutamate and glutamine in cultured astrocytes. *J. Neurochem.* 69, 2312–2325.

Gjedde, A., and Marrett, S. (2001). Glycolysis in neurons, not astrocytes, delays oxidative metabolism of human visual cortex during sustained checkerboard stimulation in vivo. *J. Cereb. Blood Flow Metab.* 21, 1384–1392.

Gruetter, R. (2003). Glycogen: the forgotten cerebral energy store. *J. Neurosci. Res.* 74, 179–183.

Gruetter, R., Seaquist, E. R., and Ugurbil, K. (2001). A mathematical model of compartmentalized neurotransmitter metabolism in the human brain. *Am. J. Physiol. Endocrinol. Metab.* 281, E100–E112.

Gruetter, R., and Tkác, I. (2000). Field mapping without reference scan using asymmetric echo-planar techniques. *Magn. Reson. Med.* 43, 319–323.

Hancu, I., and Port, J. (2011). The case of the missing glutamine. *NMR. Biomed.* doi: 10.1002/nbm.1620. [Epub ahead of print].

Henry, P. G., Lebon, V., Vaufrey, F., Brouillet, E., Hantraye, P., and Bloch, G. (2002). Decreased TCA cycle rate in the rat brain after acute 3-NP treatment measured by in vivo 1H-13C NMR spectroscopy. *J. Neurochem.* 82, 857–866.

Henry, P. G., Tkác, I., and Gruetter, R. (2003a). 1H-localized broadband 13C NMR spectroscopy of the rat brain in vivo at 9.4 T. *Magn. Reson. Med.* 50, 684–692.

Henry, P. G., Oz, G., Provencher, S., and Gruetter, R. (2003b). Toward dynamic isotopomer analysis in the rat brain in vivo: automatic quantitation of 13C NMR spectra using LCModel. *NMR. Biomed.* 16, 400–412.

Hyder, F., Chase, J. R., Behar, K. L., Mason, G. F., Siddeek, M., Rothman, D. L., and Shulman, R. G. (1996). Increased tricarboxylic acid cycle flux in rat brain during forepaw stimulation detected with 1H[13C]NMR. *Proc. Natl. Acad. Sci. U.S.A.* 93, 7612–7617.

Hyder, F., Rothman, D. L., Mason, G. F., Rangarajan, A., Behar, K. L., and Shulman, R. G. (1997). Oxidative glucose metabolism in rat brain during single forepaw stimulation: a spatially localized 1H[13C] nuclear magnetic resonance study. *J. Cereb. Blood Flow Metab.* 17, 1040–1047.

Jucker, B. M., Schaeffer, T. R., Haimbach, R. E., McIntosh, T. S., Chun, D., Mayer, M., Ohlstein, D. H., Davis, H. M., Smith, S. A., Cobitz, A. R., and Sarkar, S. K. (2002). Normalization of skeletal muscle glycogen synthesis and glycolysis in rosiglitazone-treated Zucker fatty rats: an in vivo nuclear magnetic resonance study. *Diabetes* 51, 2066–2073.

Künnecke, B., Cerdán, S., and Seelig, J. (1993). Cerebral metabolism of [1,2-13C2]glucose and [U-13C4]3-hydroxybutyrate in rat brain as detected by 13C NMR spectroscopy. *NMR Biomed.* 6, 264–277.

Magistretti, P. J., Pellerin, L., Rothman, D. L., and Shulman, R. G. (1999). Energy on demand. *Science* 283, 496–497.

Mangia, S., Simpson, I. A., Vannucci, S. J., and Carruthers, A. (2009). The in vivo neuron-to-astrocyte lactate shuttle in human brain: evidence from modeling of measured lactate levels during visual stimulation. *J. Neurochem.* 109, 55–62.

McKenna, M. C. (2007). The glutamate-glutamine cycle is not stoichiometric: fates of glutamate in brain. *J. Neurosci. Res.* 85, 3347–3358.

Merle, M., Martin, M., Villégier, A., and Canioni, P. (1996). Mathematical modelling of the citric acid cycle for the analysis of glutamine isotopomers from cerebellar astrocytes incubated with [1-13C]glucose. *Eur. J. Biochem.* 239, 742–751.

Mintun, M. A., Vlassenko, A. G., Rundle, M. M., and Raichle, M. E. (2004). Increased lactate/pyruvate ratio augments blood flow in physiologically activated human brain. *Proc. Natl. Acad. Sci. U.S.A.* 101, 659–664.

Mlynárik, V., Gambarota, G., Frenkel, H., and Gruetter, R. (2006). Localized short-echo-time proton MR spectroscopy with full signal-intensity acquisition. *Magn. Reson. Med.* 56, 965–970.

Nakao, Y., Itoh, Y., Kuang, T. Y., Cook, M., Jehle, J., and Sokoloff, L. (2001). Effects of anesthesia on functional activation of cerebral blood flow and metabolism. *Proc. Natl. Acad. Sci. U.S.A.* 98, 7593–7598.

Nguyen, N. H., Morland, C., Gonzalez, S. V., Rise, F., Storm-Mathisen, J., Gundersen, V., and Hassel, B. (2007). Propionate increases neuronal histone acetylation, but is metabolized oxidatively by glia. Relevance for propionic acidemia. *J. Neurochem.* 101, 806–814.

Oz, G., Berkich, D. A., Henry, P. G., Xu, Y., LaNoue, K., Hutson, S. M., and Gruetter, R. (2004). Neuroglial metabolism in the awake rat brain: CO2 fixation increases with brain activity. *J. Neurosci.* 24, 11273–11279.

Patel, A. B., de Graaf, R. A., Mason, G. F., Rothman, D. L., Shulman, R. G., and Behar, K. L. (2005). The contribution of GABA to glutamate/glutamine cycling and energy metabolism in the rat cortex in vivo. *Proc. Natl. Acad. Sci. U.S.A.* 102, 5588–5593.

Patel, A. B., de Graaf, R. A., Rothman, D. L., Behar, K. L., and Mason, G. F. (2010). Evaluation of cerebral acetate transport and metabolic rates in the rat brain in vivo using 1H-[13C]-NMR. *J. Cereb. Blood Flow Metab.* 30, 1200–1213.

Pellerin, L., and Magistretti, P. J. (1994). Glutamate uptake into astrocytes stimulates aerobic glycolysis: a mechanism coupling neuronal activity to glucose utilization. *Proc. Natl. Acad. Sci. U.S.A.* 91, 10625–10629.

Scafidi, S., Fiskum, G., Lindauer, S. L., Bamford, P., Shi, D., Hopkins, I., and McKenna, M. C. (2010). Metabolism of acetyl-L-carnitine for energy and neurotransmitter synthesis in the immature rat brain. *J. Neurochem.* 114, 820–831.

Serres, S., Bezancon, E., Franconi, J. M., and Merle, M. (2007). Brain pyruvate recycling and peripheral metabolism: an NMR analysis ex vivo of acetate and glucose metabolism in the rat. *J. Neurochem.* 101, 1428–1440.

Shen, J., Rothman, D. L., Behar, K. L., and Xu, S. (2009). Determination of the glutamate-glutamine cycling flux using two-compartment dynamic metabolic modeling is sensitive to astroglial dilution. *J. Cereb. Blood Flow Metab.* 29, 108–118.

Shestov, A. A., Valette, J., Ugurbil, K., and Henry, P. G. (2007). On the reliability of 13C metabolic modeling with two-compartment neuronal-glial models. *J. Neurosci. Res.* 85, 3294–3303.

Shulman, R. G., Hyder, F., and Rothman, D. L. (2003). Cerebral metabolism and consciousness. *C. R. Biol.* 326, 253–273.

Sibson, N. R., Dhankhar, A., Mason, G. F., Rothman, D. L., Behar, K. L., and Shulman, R. G. (1998). Stoichiometric coupling of brain glucose metabolism and glutamatergic neuronal activity. *Proc. Natl. Acad. Sci. U.S.A.* 95, 316–321.

Siesjo, B. K. (1978). *Brain Energy Metabolism*. New York: Wiley, 101–130.

Simpson, I. A., Carruthers, A., and Vannucci, S. J. (2007). Supply and demand in cerebral energy metabolism: the role of nutrient transporters. *J. Cereb. Blood Flow Metab.* 27, 1766–1791.

Sonnewald, U., Westergaard, N., Hassel, B., Müller, T. B., Unsgård, G., Fonnum, F., Hertz, L., Schousboe, A., and Petersen, S. B. (1993). NMR spectroscopic studies of 13C acetate and 13C glucose metabolism in neocortical astrocytes: evidence for mitochondrial heterogeneity. *Dev. Neurosci.* 15, 351–358.

Sonnewald, U., Westergaard, N., Jones, P., Taylor, A., Bachelard, H. S., and Schousboe, A. (1996). Metabolism of [U-13C5] glutamine in cultured astrocytes studied by NMR spectroscopy: first evidence of astrocytic pyruvate recycling. *J. Neurochem.* 67, 2566–2572.

Ueki, M., Mies, G., and Hossmann, K. A. (1992). Effect of alpha-chloralose, halothane, pentobarbital and nitrous oxide anesthesia on metabolic coupling in somatosensory cortex of rat. *Acta Anaesthesiol. Scand.* 36, 318–322.

Uffmann, K., and Gruetter, R. (2007). Mathematical modeling of 13C label incorporation of the TCA cycle: the concept of composite precursor function. *J. Neurosci. Res.* 85, 3304–3317.

van Eijsden, P., Behar, K. L., Mason, G. F., Braun, K. P., and de Graaf, R. A. (2010). In vivo neurochemical profiling of rat brain by 1H-[13C] NMR spectroscopy: cerebral energetics and glutamatergic/GABAergic

neurotransmission. *J. Neurochem.* 112, 24–33.

Waagepetersen, H. S., Qu, H., Hertz, L., Sonnewald, U., and Schousboe, A. (2002). Demonstration of pyruvate recycling in primary cultures of neocortical astrocytes but not in neurons. *Neurochem. Res.* 27, 1431–1437.

Xin, L., Mlynárik, V., Lanz, B., Frenkel, H., and Gruetter, R. (2010). 1H-[13C] NMR spectroscopy of the rat brain during infusion of [2-13C] acetate at 14.1 T. *Magn. Reson. Med.* 64, 334–340.

Yang, J., Xu, S., and Shen, J. (2009). Fast isotopic exchange between mitochondria and cytosol in brain revealed by relayed 13C magnetization transfer spectroscopy. *J. Cereb. Blood Flow Metab.* 29, 661–669.

Zhu, X. H., Zhang, Y., Tian, R. X., Lei, H., Zhang, N., Zhang, X., Merkle, H., Ugurbil, K., and Chen, W. (2002). Development of 17O NMR approach for fast imaging of cerebral metabolic rate of oxygen in rat brain at high field. *Proc. Natl. Acad. Sci. U.S.A.* 99, 13194–13199.

Zwingmann, C., and Leibfritz, D. (2003). Regulation of glial metabolism studied by 13C-NMR. *NMR Biomed.* 16, 370–399.

**Conflict of Interest Statement:** The authors declare that the research was conducted in the absence of any commercial or financial relationships that could be construed as a potential conflict of interest.

*Received: 01 April 2011; accepted: 17 May 2011; published online: 06 June 2011.*

*Citation: Duarte JMN, Lanz B and Gruetter R (2011) Compartmentalized cerebral metabolism of [1,6-$^{13}$C]glucose determined by in vivo $^{13}$C NMR spectroscopy at 14.1 T. Front. Neuroenerg.* ***3****:3. doi: 10.3389/fnene.2011.00003*

## APPENDIX

### KINETIC MODEL OF [1,6-$^{13}$C]GLUCOSE METABOLISM

The mathematical model of compartmentalized cerebral metabolism was adapted from Gruetter et al. (2001) and this publication should be consulted for an exhaustive description of the model. In **Figure 1** are depicted the metabolic pools and fluxes in glia and neurons used to define the model.

Metabolic but not isotopic steady-state was assumed over the time course of [1,6-$^{13}$C]glucose infusion. Metabolite concentrations determined *in vivo* (all in μmol/g) were $8.5 \pm 0.4$ for glutamate, $5.1 \pm 0.5$ for glutamine, and $2.4 \pm 0.3$ for aspartate. The remaining concentrations required for the model were assumed. Acetyl-CoA and TCA cycle intermediates were considered to be 0.1 μmol/g in both compartments. Pyruvate was assumed to occur at 10% of lactate concentration (e.g., Mintun et al., 2004) that was measured as $0.7 \pm 0.1$ μmol/g. Neurons were assumed to retain 90% of total glutamate and aspartate pools, while glial cells contain 90% of total observed glutamine concentration. Due to fast exchange between the two compartments, a single virtual pool of pyruvate was considered to be shared by neurons and glia. This also implies that isotopic enrichment in pyruvate is equivalent to lactate, which is detectable.

At metabolic steady-state, the fraction of glucose oxidation entering the TCA cycle is $(V_{\mathrm{TCA}}^{\mathrm{n}} + V_{\mathrm{TCA}}^{\mathrm{g}} + V_{\mathrm{PC}})/2$ that we call $\mathrm{CMR_{glc(ox)}}$. Similarly, total glucose consumption ($\mathrm{CMR_{glc}}$) is $\mathrm{CMR_{glc(ox)}} + (V_{\mathrm{out}} - V_{\mathrm{in}})/2$. When the outflow ($V_{\mathrm{out}}$) of labeling at the level of lactate equals the inflow ($V_{\mathrm{in}}$) from extra-cerebral lactate, the total glucose consumption is used for oxidation in the TCA cycle.

The TCA cycle was considered equivalent to the flux through pyruvate dehydrogenase. While in the neuron $V_{\mathrm{TCA}}^{\mathrm{n}}$ equals $V_{\mathrm{PDH}}^{\mathrm{n}}$, in the glia $V_{\mathrm{TCA}}^{\mathrm{g}}$ is $V_{\mathrm{g}} + V_{\mathrm{PC}}$, corresponding to the total oxidation of one molecule of pyruvate.

The flux through neuronal glutaminase is $V_{\mathrm{NT}}$. In the glia, glutaminase was neglected because the net flux of $^{13}$C follows the direction of the apparent neurotransmission cycle $V_{\mathrm{NT}}$. The net loss of $^{13}$C labeling was modeled as $V_{\mathrm{efflux}}$ and mass conservation sets it equivalent to the anaplerotic flux through pyruvate carboxylase $V_{\mathrm{PC}}$. Thus $V_{\mathrm{GS}} = V_{\mathrm{NT}} + V_{\mathrm{PC}}$.

Glucose transport across the BBB was defined using a reversible Michaelis–Menten kinetics as previously described for the rat brain (Duarte et al., 2009b). Therefore, brain glucose ($\mathrm{G_{brain}}$) is given by the following expression:

$$\frac{\mathrm{dG_{brain}}}{\mathrm{dt}} = T_{\max}\frac{\mathrm{G_{plasma}}(t) - \mathrm{G_{brain}}(t)/V_{\mathrm{d}}}{K_{\mathrm{t}} + \mathrm{G_{brain}}(t)/V_{\mathrm{d}} + \mathrm{G_{plasma}}(t)} - \mathrm{CMR_{glc}}$$

where $T_{\max}$ is the apparent maximal transport rate, $K_{\mathrm{t}}$ is the apparent Michaelis constant for glucose transport, $\mathrm{CMR_{glc}}$ is the cerebral metabolic rate of glucose consumption, and $V_{\mathrm{d}}$ is the physical volume for glucose distribution in the brain (0.77 mL/g, as in Duarte et al., 2009b). Similarly, for $^{13}$C-enriched carbons of glucose, transport is defined by

$$\frac{\mathrm{d}^{13}\mathrm{G_{brain}}}{\mathrm{dt}} = T_{\max}\frac{^{13}\mathrm{G_{plasma}}(t) - {}^{13}\mathrm{G_{brain}}(t)/V_{\mathrm{d}}}{K_{\mathrm{t}} + \mathrm{G_{brain}}(t)/V_{\mathrm{d}} + \mathrm{G_{plasma}}(t)} - \mathrm{CMR_{glc}}\frac{^{13}\mathrm{G_{brain}}(t)}{\mathrm{G_{brain}}(t)}.$$

Although brain glucose can divert to other pathways, it is consumed mainly through glycolysis and the $^{13}$C enrichment in C1 and C6 originates the C3 of pyruvate. Pyruvate was considered to be in fast equilibrium with lactate that is exchanged between compartments and thus a single pyruvate pool was assumed in the model (**Figure 1**). Brain pyruvate enrichment is defined as follows:

$$\frac{\mathrm{d}^{13}\mathrm{Pyr_3}}{\mathrm{dt}} = \mathrm{CMR_{glc}}\left(\frac{^{13}\mathrm{Glc_1}(t) + {}^{13}\mathrm{Glc_6}(t)}{\mathrm{Glc}(t)}\right) + V_{\mathrm{in}}\frac{^{13}\mathrm{Lac_3}(t)}{\mathrm{Lac}(t)} - \left(V_{\mathrm{out}} + V_{\mathrm{TCA}}^{\mathrm{n}} + V_{\mathrm{TCA}}^{\mathrm{g}} + V_{\mathrm{PC}}\right)\frac{^{13}\mathrm{Pyr_3}(t)}{\mathrm{Pyr}}$$

Note that, in the model, total concentration of extra-cerebral lactate (Lac) may vary over time in accordance to the observed plasma lactate levels (**Figure 2**). Transport of lactate into the brain was simulated with a reversible Michaelis–Menten kinetics as described by Boumezbeur et al. (2010) leading to enrichment of $^{13}$Lac from plasma lactate. Therefore, alteration of plasma lactate levels is reflected in brain lactate concentration. However, total concentration of pyruvate remains invariable because $V_{\mathrm{in}}$ is constant under the assumption of metabolic steady-state.

In peripheral tissues, metabolism of [1,6-$^{13}$C]glucose produces [3-$^{13}$C]lactate that is released to the blood stream. Incorporation of $^{13}$C from blood-born lactate ($\mathrm{Lac_3}$) into brain metabolism may occur (e.g., Dienel and Cruz, 2009; Gallagher et al., 2009; Boumezbeur et al., 2010) and is accounted by $V_{\mathrm{in}}$ in the equations of brain pyruvate. In addition, $V_{\mathrm{out}}$ represents $^{13}$C labeling dilution from the glycolysis, either by lactate release from brain parenchyma or by glucose utilization in alternative pathways.

Since scrambling of blood $^{13}$C glucose and lactate enrichment may occur during peripheral metabolism and enrich carbons other than glucose C1 and C6 and lactate C3. These carbons are metabolized and lead to enrichment of pyruvate C2 that, by pyruvate carboxylation, contributes to direct enrichment of oxaloacetate C2. The following expression was defined but, in the absence of substantial enrichment of glucose C2 or C5 and lactate C2, it leads to simple dilution of oxaloacetate C2 while C3 is enriched in the glial compartment.

$$\frac{\mathrm{d}^{13}\mathrm{Pyr_2}}{\mathrm{dt}} = \mathrm{CMR_{glc}}\left(\frac{^{13}\mathrm{Glc_2}(t) + {}^{13}\mathrm{Glc_5}(t)}{\mathrm{Glc}(t)}\right) + V_{\mathrm{in}}\frac{^{13}\mathrm{Lac_2}(t)}{\mathrm{Lac}(t)} - \left(V_{\mathrm{out}} + V_{\mathrm{TCA}}^{\mathrm{n}} + V_{\mathrm{TCA}}^{\mathrm{g}} + V_{\mathrm{PC}}\right)\frac{^{13}\mathrm{Pyr_2}(t)}{\mathrm{Pyr}}.$$

***Neuronal compartment***

In the neuronal compartment, the concentration of $^{13}$C-enriched TCA cycle intermediates is given by:

$$\frac{d^{13}OG_4^n}{dt} = V_{PDH}^n \frac{^{13}Pyr_3(t)}{Pyr} - \left(V_{PDH}^n + V_x^n\right)\frac{^{13}OG_4^n(t)}{OG^n} + V_x^n \frac{^{13}Glu_4^n(t)}{Glu^n}$$

$$\frac{d^{13}OG_3^n}{dt} = V_{PDH}^n \frac{^{13}OAA_2^n(t)}{OAA^n} - \left(V_{PDH}^n + V_x^n\right)\frac{^{13}OG_3^n(t)}{OG^n} + V_x^n \frac{^{13}Glu_3^n(t)}{Glu^n}$$

$$\frac{d^{13}OG_2^n}{dt} = V_{PDH}^n \frac{^{13}OAA_3^n(t)}{OAA^n} - \left(V_{PDH}^n + V_x^n\right)\frac{^{13}OG_2^n(t)}{OG^n} + V_x^n \frac{^{13}Glu_2^n(t)}{Glu^n}$$

$$\frac{d^{13}OAA_2^n}{dt} = \frac{V_{PDH}^n}{2}\left(\frac{^{13}OG_4^n(t) + {}^{13}OG_3^n(t)}{OG^n}\right) - \left(V_{PDH}^n + V_x^n\right)\frac{^{13}OAA_2^n(t)}{OAA^n} + V_x^n \frac{^{13}Asp_2^n(t)}{Asp^n}$$

$$\frac{d^{13}OAA_3^n}{dt} = \frac{V_{PDH}^n}{2}\left(\frac{^{13}OG_4^n(t) + {}^{13}OG_3^n(t)}{OG^n}\right) - \left(V_{PDH}^n + V_x^n\right)\frac{^{13}OAA_3^n(t)}{OAA^n} + V_x^n \frac{^{13}Asp_3^n(t)}{Asp^n}$$

In the neurons, $^{13}$C glutamate, glutamine, and aspartate concentrations are given by the following expressions, where i can refer to any carbon position.

$$\frac{d^{13}Glu_i^n}{dt} = V_x^n \frac{^{13}OG_i^n(t)}{OG^n} - \left(V_{NT} + V_x^n\right)\frac{^{13}Glu_i^n(t)}{Glu^n} + V_{NT}\frac{^{13}Gln_i^n(t)}{Gln^n}$$

$$\frac{d^{13}Gln_i^n}{dt} = V_{NT}\left(\frac{^{13}Gln_i^g(t)}{Gln^g} - \frac{^{13}Gln_i^n(t)}{Gln^n}\right)$$

$$\frac{d^{13}Asp_i^n}{dt} = V_x^n\left(\frac{^{13}OAA_i^n(t)}{OAA^n} - \frac{^{13}Asp_i^n(t)}{Asp^n}\right)$$

***Glial compartment***

The glia comprises the additional fluxes through pyruvate carboxylase ($V_{PC}$) and glutamine synthesis ($V_{GS}$) (see Gruetter et al., 2001). In the glial compartment, a dilution factor was introduced at the level of acetyl-CoA ($V_{dil}$), accounting for possible $^{13}$C label dilution by *in vivo* metabolism of acetate (Badar-Goffer et al., 1990; Cerdán et al., 1990; Deelchand et al., 2009), fatty acids (Ebert et al., 2003), or ketone bodies (Künnecke et al., 1993).

$$\frac{d^{13}AcCoA_2^g}{dt} = \left(V_g + V_{PC}\right)\frac{^{13}Pyr_3(t)}{Pyr} + V_{dil}\frac{^{13}Ac_2(t)}{Ac(t)} - \left(V_{dil} + V_g + V_{PC}\right)\frac{^{13}AcCoA_2^g(t)}{AcCoA^g}$$

Extra-cerebral acetate may contribute to brain metabolism and therefore $^{13}$Ac represents blood-born $^{13}$C acetate (**Figure 2C**). Transport of acetate into the brain was simulated as described by Deelchand et al. (2009) leading to enrichment of $^{13}$Ac from plasma acetate.

Concentration of $^{13}$C in carbons of glial TCA cycle intermediary metabolic pools is defined as follows:

$$\frac{d^{13}OG_4^g}{dt} = \left(V_g + V_{PC}\right)\frac{^{13}AcCoA_2^g(t)}{AcCoA^g} + V_x^g\frac{^{13}Glu_4^g(t)}{Glu^g} - \left(V_g + V_x^g + V_{PC}\right)\frac{^{13}OG_4^g(t)}{OG^g}$$

$$\frac{d^{13}OG_3^g}{dt} = \left(V_g + V_{PC}\right)\frac{^{13}OAA_2^g(t)}{OAA^g} + V_x^g\frac{^{13}Glu_3^g(t)}{Glu^g} - \left(V_g + V_x^g + V_{PC}\right)\frac{^{13}OG_3^g(t)}{OG^g}$$

$$\frac{d^{13}OG_2^g}{dt} = \left(V_g + V_{PC}\right)\frac{^{13}OAA_3^g(t)}{OAA^g} + V_x^g\frac{^{13}Glu_2^g(t)}{Glu^g} - \left(V_g + V_x^g + V_{PC}\right)\frac{^{13}OG_2^g(t)}{OG^g}$$

$$\frac{d^{13}OAA_2^g}{dt} = \frac{V_g}{2}\left(\frac{^{13}OG_4^g(t) + {}^{13}OG_3^g(t)}{OG^g}\right) + V_x^g\frac{^{13}Asp_2^g(t)}{Asp^g} + V_{PC}\frac{^{13}Pyr_2(t)}{Pyr} - \left(V_g + V_{PC} + V_x^g\right)\frac{^{13}OAA_2^g(t)}{OAA^g}$$

$$\frac{d^{13}OAA_3^g}{dt} = \frac{V_g}{2}\left(\frac{^{13}OG_4^g(t) + {}^{13}OG_3^g(t)}{OG^g}\right) + V_x^g\frac{^{13}Asp_3^g(t)}{Asp^g} + V_{PC}\frac{^{13}Pyr_3(t)}{Pyr} - \left(V_g + V_{PC} + V_x^g\right)\frac{^{13}OAA_3^g(t)}{OAA^g}$$

Concentration of $^{13}$C in carbons of glial glutamate, glutamine, and aspartate is defined by the equations below, where i can refer to any carbon position.

$$\frac{d^{13}Glu_i^g}{dt} = \left(V_x^g + V_{PC}\right)\frac{^{13}OG_i^g(t)}{OG^g} - \left(V_{GS} + V_x^g\right)\frac{^{13}Glu_i^g(t)}{Glu^g} + V_{NT}\frac{^{13}Glu_i^n(t)}{Glu^n}$$

$$\frac{d^{13}Gln_i^g}{dt} = V_{GS}\frac{^{13}Glu_i^g(t)}{Glu^g} - \left(V_{NT} + V_{efflux}\right)\frac{^{13}Gln_i^g(t)}{Gln^g}$$

$$\frac{d^{13}Asp_i^g}{dt} = V_x^g\left(\frac{^{13}OAA_i^g(t)}{OAA^g} - \frac{^{13}Asp_i^g(t)}{Asp^g}\right)$$

#### REMOVING TCA CYCLE INTERMEDIATES FROM THE MODEL

Simplification of the mathematical model of cerebral metabolism was used to remove TCA cycle intermediates from mathematical expressions, as previously suggested by simulations (Uffmann and Gruetter, 2007).

For the sake of example, the combination of equations for neuronal glutamate C4 ($\frac{d^{13}Glu_4^n}{dt}$) and 2-oxoglutarate C4 ($\frac{d^{13}OG_4^n}{dt}$) can be used to eliminate terms with $\frac{^{13}OG_4^n(t)}{OG^n}$, leading to the following expression:

$$\frac{d^{13}Glu_4^n}{dt} + \frac{V_x^n}{V_{PDH}^n + V_x^n}\frac{d^{13}OG_4^n}{dt} = \frac{V_x^n V_{PDH}^n}{V_{PDH}^n + V_x^n}\frac{^{13}Pyr_3(t)}{Pyr} - \left(\frac{V_x^n V_{PDH}^n}{V_{PDH}^n + V_x^n} + V_{NT}\right)\frac{^{13}Glu_4^n(t)}{Glu^n} + V_{NT}\frac{^{13}Gln_4^n(t)}{Gln^n}.$$

Because the concentration of glutamate is much larger than that of the TCA cycle intermediates, the increase in concentration of glutamate enriched carbons is much larger at metabolic steady-state, i.e., $\frac{d^{13}Glu_4^n}{dt} >> \frac{d^{13}OG_4^n}{dt}$. Therefore, the expression can be approximated to

$$\frac{d^{13}Glu_4^n}{dt} = \frac{V_x^n V_{PDH}^n}{V_{PDH}^n + V_x^n}\frac{^{13}Pyr_3(t)}{Pyr} - \left(\frac{V_x^n V_{PDH}^n}{V_{PDH}^n + V_x^n} + V_{NT}\right) \times \frac{^{13}Glu_4^n(t)}{Glu^n} + V_{NT}\frac{^{13}Gln_4^n(t)}{Gln^n}.$$

Applying the same procedure to neuronal glutamate C3 ($Glu_3^n$), we obtain the following expression:

$$\frac{d^{13}Glu_3^n}{dt} = \frac{V_x^n V_{PDH}^n}{V_{PDH}^n + V_x^n}\frac{^{13}OAA_2^n(t)}{OAA^n} - \left(\frac{V_x^n V_{PDH}^n}{V_{PDH}^n + V_x^n} + V_{NT}\right) \times \frac{^{13}Glu_3^n(t)}{Glu^n} + V_{NT}\frac{^{13}Gln_3^n(t)}{Gln^n}.$$

From this expression, the term with oxaloacetate (OAA) can be removed by intermediary of the respective differential equation of aspartate, originating the expression:

$$\frac{d^{13}Glu_3^n}{dt} = \frac{V_{PDH}^n}{V_{PDH}^n + V_x^n}\left(\frac{d^{13}Asp_2^n}{dt} + V_x^n\frac{^{13}Asp_2^n(t)}{Asp^n}\right) - \left(\frac{V_x^n V_{PDH}^n}{V_{PDH}^n + V_x^n} + V_{NT}\right)\frac{^{13}Glu_3^n(t)}{Glu^n} + V_{NT}\frac{^{13}Gln_3^n(t)}{Gln^n}$$

With the same treatment for $Glu_2^n$ originates the expression:

$$\frac{d^{13}Glu_2^n}{dt} = \frac{V_{PDH}^n}{V_{PDH}^n + V_x^n}\left(\frac{d^{13}Asp_3^n}{dt} + V_x^n\frac{^{13}Asp_3^n(t)}{Asp^n}\right) - \left(\frac{V_x^n V_{PDH}^n}{V_{PDH}^n + V_x^n} + V_{NT}\right)\frac{^{13}Glu_2^n(t)}{Glu^n} + V_{NT}\frac{^{13}Gln_2^n(t)}{Gln^n}$$

The same can be applied to equations of aspartate and we obtain the following expression where i can be any aliphatic carbon of aspartate.

$$\frac{d^{13}Asp_i^n}{dt} = \frac{V_{PDH}^n}{2\left(V_{PDH}^n + V_x^n\right)}\left(\frac{d^{13}Glu_4^n}{dt} + \frac{d^{13}Glu_3^n}{dt} + \left(V_{NT} + V_x^n\right)\frac{^{13}Glu_4^n(t) + ^{13}Glu_3^n(t)}{Glu^n} - V_{NT}\frac{^{13}Gln_4^n(t) + ^{13}Gln_3^n(t)}{Gln^n}\right) - \frac{V_x^n V_{PDH}^n}{V_{PDH}^n + V_x^n}\frac{^{13}Asp_i^n(t)}{Asp^n}$$

A similar approach in the glial compartment will originate the following equations for carbons of glutamate:

$$\frac{d^{13}Glu_4^g}{dt} = \frac{\left(V_x^g + V_{PC}\right)\left(V_g + V_{PC}\right)}{V_g + V_x^g + V_{PC}}\frac{^{13}AcCoA_2^g(t)}{AcCoA^g} + V_{NT}\frac{^{13}Glu_4^n(t)}{Glu^n} - \frac{V_{GS}\left(V_g + V_x^g + V_{PC}\right) + V_x^g V_g}{V_g + V_x^g + V_{PC}}\frac{^{13}Glu_4^g(t)}{Glu^g}$$

$$\frac{d^{13}Glu_3^g}{dt} = \frac{\left(V_x^g + V_{PC}\right)\left(V_g + V_{PC}\right)}{V_x^g\left(V_g + V_x^g + V_{PC}\right)}\frac{d^{13}Asp_2^g}{dt} + \frac{\left(V_x^g + V_{PC}\right)\left(V_g + V_{PC}\right)}{V_g + V_x^g + V_{PC}}\frac{^{13}Asp_2^g(t)}{Asp^g} - \frac{V_{GS}\left(V_g + V_x^g + V_{PC}\right) + V_x^g V_g}{V_g + V_x^g + V_{PC}}\frac{^{13}Glu_3^g(t)}{Glu^g} + V_{NT}\frac{^{13}Glu_3^n(t)}{Glu^n}$$

$$\frac{d^{13}Glu_2^g}{dt} = \frac{\left(V_x^g + V_{PC}\right)\left(V_g + V_{PC}\right)}{V_x^g\left(V_g + V_x^g + V_{PC}\right)}\frac{d^{13}Asp_3^g}{dt} + \frac{\left(V_x^g + V_{PC}\right)\left(V_g + V_{PC}\right)}{V_g + V_x^g + V_{PC}}\frac{^{13}Asp_3^g(t)}{Asp^g} - \frac{V_{GS}\left(V_g + V_x^g + V_{PC}\right) + V_x^g V_g}{V_g + V_x^g + V_{PC}}\frac{^{13}Glu_2^g(t)}{Glu^g} + V_{NT}\frac{^{13}Glu_2^n(t)}{Glu^n}$$

For the concentration of $^{13}$C in carbons of glial aspartate, the following equation is obtained, where i can be either the position 2 or 3 in carbons of aspartate and pyruvate. Note that $^{13}Pyr_2$ and $^{13}Pyr_3$ will respectively label $^{13}OAA_2$ and $^{13}OAA_3$, and consequently $^{13}Asp_2$ and $^{13}Asp_3$.

$$\frac{d^{13}Asp_i^g}{dt} = \frac{V_x^g V_g}{2\left(V_g + V_{PC} + V_x^g\right)\left(V_x^g + V_{PC}\right)}\left(\frac{d^{13}Glu_4^g}{dt} + \frac{d^{13}Glu_3^g}{dt}\right) + \frac{V_x^g V_g}{2\left(V_g + V_{PC} + V_x^g\right)\left(V_x^g + V_{PC}\right)}\left[\left(V_{GS} + V_x^g\right)\left(\frac{^{13}Glu_4^g(t) + ^{13}Glu_3^g(t)}{Glu^g}\right) - V_{NT}\left(\frac{^{13}Glu_4^n(t) + ^{13}Glu_3^n(t)}{Glu^n}\right)\right] - \frac{V_x^g\left(V_g + V_{PC}\right)}{V_g + V_{PC} + V_x^g}\frac{^{13}Asp_i^g(t)}{Asp^g} + \frac{V_x^g V_{PC}}{V_g + V_{PC} + V_x^g}\frac{^{13}Pyr_i(t)}{Pyr}$$

frontiers in
NEUROENERGETICS

REVIEW ARTICLE
published: 28 January 2013
doi: 10.3389/fnene.2013.00001

# Modeling the glutamate–glutamine neurotransmitter cycle

***Jun Shen****

*Molecular Imaging Branch, National Institute of Mental Health, Bethesda, MD, USA*

***Edited by:***
*Sebastian Cerdan, Instituto de Investigaciones Biomedicas Alberto Sols, Spain*

***Reviewed by:***
*Sebastian Cerdan, Instituto de Investigaciones Biomedicas Alberto Sols, Spain*
*Kevin L. Behar, Yale University, USA*

***Correspondence:**
*Jun Shen, Molecular Imaging Branch, National Institute of Mental Health, Bldg 10, Rm 2D51A, 9000 Rockville Pike, Bethesda, MD 20892, USA.*
*e-mail: shenj@intra.nimh.nih.gov*

Glutamate is the principal excitatory neurotransmitter in brain. Although it is rapidly synthesized from glucose in neural tissues the biochemical processes for replenishing the neurotransmitter glutamate after glutamate release involve the glutamate–glutamine cycle. Numerous *in vivo* $^{13}C$ magnetic resonance spectroscopy (MRS) experiments since 1994 by different laboratories have consistently concluded: (1) the glutamate–glutamine cycle is a major metabolic pathway with a flux rate substantially greater than those suggested by early studies of cell cultures and brain slices; (2) the glutamate–glutamine cycle is coupled to a large portion of the total energy demand of brain function. The dual roles of glutamate as the principal neurotransmitter in the CNS and as a key metabolite linking carbon and nitrogen metabolism make it possible to probe glutamate neurotransmitter cycling using MRS by measuring the labeling kinetics of glutamate and glutamine. At the same time, comparing to non-amino acid neurotransmitters, the added complexity makes it more challenging to quantitatively separate neurotransmission events from metabolism. Over the past few years our understanding of the neuronal-astroglial two-compartment metabolic model of the glutamate–glutamine cycle has been greatly advanced. In particular, the importance of isotopic dilution of glutamine in determining the glutamate–glutamine cycling rate using [1−$^{13}C$] or [1,6-$^{13}C_2$] glucose has been demonstrated and reproduced by different laboratories. In this article, recent developments in the two-compartment modeling of the glutamate–glutamine cycle are reviewed. In particular, the effects of isotopic dilution of glutamine on various labeling strategies for determining the glutamate–glutamine cycling rate are analyzed. Experimental strategies for measuring the glutamate–glutamine cycling flux that are insensitive to isotopic dilution of glutamine are also suggested.

**Keywords: glutamate, glutamine, magnetic resonance spectroscopy, glucose metabolism, CNS, metabolic modeling, acetate**

## INTRODUCTION

Glutamate is the principal excitatory neurotransmitter in brain. At low concentrations it excites virtually all neurons in the CNS. Excessive activation of glutamate receptors by glutamate can result in a number of pathological conditions and can lead to cell death. As a zwitterionic molecule glutamate cannot diffuse across cell membranes. It is well understood that glutamate uptake plays important roles in regulating the extracellular concentration of glutamate in the brain. Both *in vivo* and *in vitro* studies have indicated that glutamate released by neurons is rapidly taken up by astroglial cells, via high-affinity $Na^+$-dependent glutamate transporters. Evidence from studies using antisense mRNA to selectively knock down neuronal and astroglial transporters, as well as direct measurements of glutamate-gated ionic currents, support the hypothesis that almost all released glutamate is taken up by astroglia in the cerebral cortex (Rothstein, 1996; Bergles et al., 1999). Subsequently, glutamate is either converted into glutamine by glutamine synthetase, which is exclusively localized in glial cells (Martinez-Hernandez et al., 1977), or oxidized by assimilation into the Krebs cycle located in the mitochondria of astroglial cells. Although glutamate is rapidly synthesized from glucose in neural tissues the biochemical processes for replenishing the neurotransmitter glutamate after glutamate release involve the glutamate–glutamine cycle (Cerdán et al., 1990; Erecińska and Silver, 1990). Glutamine, formed by amidization of glutamate, is readily discharged from astroglial cells by facilitated diffusion via $Na^+$ and $H^+$-coupled, electroneutral systems-N transporters. Glutamine readily enters nerve terminals mainly by electrogenic systems-A transporters (Chaudhry et al., 2002). There glutaminase converts it back into glutamate which can be again used for neuronal transmission or assimilated into the neuronal Krebs cycle.

The existence of this glutamate–glutamine cycle was initially proposed based on the multiple findings: (1) isolated nerve terminals contain the majority of tissue content of glutaminase but no glutamine synthetase, the latter is found to be exclusively located in glial cells (Martinez-Hernandez et al., 1977; Hertz, 1979); (2) biochemical and autoradiographic studies clearly demonstrated that glutamate is selectively accumulated by glial cells and rapidly converted into glutamine; (3) by comparison, glutamine preferentially enters neurons where it is converted in large proportions into glutamate (Duce et al., 1983). The glutamate–glutamine cycling pathway between neurons and astroglia has been studied extensively *in vivo*, in cell culture, and in brain slices using isotope tracers (e.g., Shank et al., 1993; Lapidot and Gopher, 1994). Despite the large amount of

evidence for its existence, early kinetic studies considered that the glutamate–glutamine cycling flux is small and makes only a minor contribution to brain energy metabolism. Consistent with this early notion, the fraction of glutamate participating in the glutamate–glutamine cycle was considered small, leading to the conceptualization of a neurotransmitter glutamate pool and a separate metabolic glutamate pool (Erecińska and Silver, 1990). This compartmentalization of neuronal glutamate is supported by the experimental findings of a low rate of label incorporation in cell cultures and in non-electrically stimulated brain slices from various labeled precursors (e.g., Badar-Goffer et al., 1992).

The initial detection of glucose metabolism using *in vivo* $^{13}$C magnetic resonance spectroscopy (MRS) found rapid and significant labeling of glutamine (Gruetter et al., 1994), which is predominantly located in the astroglial cells. This *in vivo* evidence suggests rapid transfer of $^{13}$C labels from the predominantly neuronal glutamate compartment to the predominantly astroglial glutamine compartment. Subsequent studies on human and animal brains using refined MRS techniques and various $^{13}$C-labeled substrates have consistently contradicted the concept of a small, metabolically inactive neurotransmitter glutamate pool (for a recent review, see, for example, Rothman et al., 2011). Using [1-$^{13}$C] glucose or [1,6-$^{13}C_2$] glucose infusion, which predominantly labels neuronal glutamate due to the high energy demand by neurons, rapid and significant labeling of glutamine C2–C4 has been consistently reproduced by all studies employing either direct $^{13}$C detection or the more sensitive indirect proton detection. Using [2-$^{13}$C] glucose or [2,5-$^{13}C_2$] glucose and direct $^{13}$C detection of carboxyl/amide carbons the similar labeling of glutamine C5 was also found (Li et al., 2009). The findings of rapid labeling of glutamine by $^{13}$C-labeled glucose that is predominantly metabolized in the neuronal compartment are corroborated by $^{15}$N MRS studies of $^{15}NH_3$ labeling of glutamine in a hyperammonemia model (Shen et al., 1998). Preferential labeling of the predominantly astroglial glutamine can be achieved by utilizing either the glia-specific anaplerotic pathway or the preference for acetate by glial cells. Using [2-$^{13}$C] glucose or [2,5-$^{13}C_2$] glucose infusion, rapid transfer of $^{13}$C labels from glutamine C3 and C2 to glutamate C3 and C2 was observed (Sibson et al., 2001). Similarly, when the glia-specific substrate acetate is infused glutamine is labeled first followed by glutamate reflecting the transfer of $^{13}$C labels from astroglia to neurons (Lebon et al., 2002; Deelchand et al., 2009). The numerous *in vivo* $^{13}$C- and $^{15}$N MRS studies since 1994 by different laboratories have consistently concluded: (1) glutamate–glutamine cycling is a major metabolic pathway with a flux rate substantially greater than those suggested by early studies of cell cultures and brain slices; (2) the glutamate–glutamine cycle is coupled to a large portion of the total energy demand of brain function (Rothman et al., 2011).

Extracting quantitative flux rates from any metabolic study requires modeling, which, historically, has led to controversial results with few exceptions. The dual roles of glutamate as the principal neurotransmitter in the CNS and as a key metabolite linking carbon and nitrogen metabolism make it possible to probe glutamate neurotransmitter cycling using MRS by measuring the labeling kinetics of glutamate and glutamine. At the same time, comparing to non-amino acid neurotransmitters, the added complexity makes it more challenging to quantitatively separate neurotransmission events from metabolism. Although the findings from *in vivo* MRS studies are in agreement that the glutamate–glutamine cycle is a major metabolic pathway flux reflecting presynaptic glutamate release, significantly different cycling rates have been reported by different laboratories for the same or similar physiological conditions (Gruetter et al., 2001; Shen and Rothman, 2002; Shestov et al., 2007; Rothman et al., 2011). Since the MRS measures total glutamate and glutamine the absolute rates of $^{13}$C labeling kinetics depend on the rate of the exchange of TCA cycle intermediates across the inner mitochondrial membrane ($V_x$). Evidence for both a fast exchange (i.e., $V_x \gg V_{TCA}$; Mason et al., 1995; de Graaf et al., 2004; Patel et al., 2004; Yang et al., 2009) and a slow exchange (i.e., $V_x \approx V_{TCA}$; Gruetter et al., 2001; Berkich et al., 2005) has been presented in the literature. Part of the controversy surrounding the magnitude of $V_{cyc}$ can be traced to whether $V_x \gg V_{TCA}$ or $V_x \approx V_{TCA}$ is used in the two-compartment model.

In addition to the $V_x$ issues, a recent study claimed that, with the signal-to-noise ratio achievable by *in vivo* MRS, it is very difficult, if possible, to quantitatively determine the glutamate–glutamine cycling rate at a useful precision (Shestov et al., 2007). Over the past few years our understanding of the neuronal-astroglial two-compartment metabolic model of the glutamate–glutamine cycle has been greatly advanced. In particular, the importance of isotopic dilution of glutamine in determining the glutamate–glutamine cycling rate using the glutamate-to-glutamine label transfer has been demonstrated (Shen et al., 2009) and reproduced (Duarte et al., 2011; Shestov et al., 2012). Recent publications from different laboratories have shown a clear consensus that glutamate–glutamine cycling rate can be determined using *in vivo* MRS with high precision (Boumezbeur et al., 2010a; Duarte et al., 2011; Rothman et al., 2011; Shestov et al., 2012). Most recently, by analyzing $^{13}$C MRS experiments performed by several laboratories in both rats and humans which measure both neuronal energy consumption and glutamate–glutamine cycling, the Yale group has shown that different studies (both human and animal studies) are highly consistent in terms of the relationship between neuronal energy consumption and the rate of the glutamate–glutamine cycle, which shows that ∼80% of the resting energy consumption in the awake brain is coupled to neuronal activity (Hyder and Rothman, 2012). In this article, we first give an overview of the two-compartment glutamate–glutamine cycle model. To highlight the main features and implications of the glutamate–glutamine cycle, a simplified two-compartment model that captures the major $^{13}$C label flows is analyzed in detail. Recent developments in two-compartment modeling of the glutamate–glutamine cycle are reviewed. In particular, the effects of isotopic dilution of glutamine on various labeling strategies for determining the glutamate–glutamine cycle are analyzed in detail. Experimental strategies for measuring the absolute rate of the glutamate–glutamine cycling flux that are insensitive to isotopic dilution of glutamine are also suggested.

## THE TWO-COMPARTMENT MODEL OF THE GLUTAMATE–GLUTAMINE CYCLE

Important metabolic couplings exist among various cells through the use of common substrates and the exchange of several metabolic intermediates such as glutamate, glutamine, and γ-aminobutyric acid (GABA) (Erecińska and Silver, 1990; Cerdán et al., 2006). Because glutamate also acts as the major excitatory neurotransmitter in the CNS, the neurotransmission of glutamate is intimately related to the metabolism of glutamate and glutamine. To quantitatively model glutamate metabolism and its neurotransmission in the CNS, Sibson et al. (1997) proposed a quantitative two-compartment model describing the glutamate–glutamine cycle between neurons and astroglia (**Figure 1**). In this model, glutamate released by glutamatergic neurons into the synaptic cleft is taken up by surrounding astroglia and converted into its inactive form glutamine by the glia-specific glutamine synthetase. The abundant expression of high capacity glutamate transporters on glial cell membrane ensures that the extracellular glutamate concentration is kept very low in normal brain to avoid excitotoxicity. To replenish the neuronal carbon lost to astroglia, resulting from synaptic glutamate release, glutamine is released by astroglia and recycled back to neurons where it is hydrolyzed into glutamate by glutaminase. The model shown in **Figure 1** imposes mass balance constraints for all carbon and nitrogen fluxes across the blood–brain barrier and between neurons and astroglia at metabolic steady state. At metabolic steady state, the rate of glutamate release by nerve terminals, the subsequent uptake and glutamine synthesis by and in astroglial cells, as well as glutamine uptake and conversion into glutamate in neurons are equal ($V_{cycle}$). The rate of glutamine synthesis ($V_{gln}$) is the sum of the rate of anaplerotic de novo glutamine synthesis in the astroglia ($V_{ana}$), the glial-specific process in which $CO_2$ and pyruvate derived from glucose are converted into oxaloacetate by pyruvate carboxylase (Berl et al., 1963), and the rate of the glutamate–glutamine cycle between neurons and astroglia:

$$V_{Gln} = V_{cyc} + V_{ana} \quad (1)$$

In addition, the Sibson et al. model connects Vana to the net uptake of anaplerotic precursors from the blood. At the metabolic steady state, glutamine efflux ($V_{efflux}$) is balanced by glutamine de novo synthesis via anaplerosis ($V_{ana}$):

$$V_{ana} = V_{efflux} \quad (2)$$

Following $CO_2$ fixation, oxaloacetate is converted into glutamate either by ammonia fixation ($V_{NH3}$) or transamination. Glial glutamate is subsequently converted to glutamine by glutamine synthetase.

The above model describes the same glutamate–glutamine cycle proposed decades ago (Hertz, 1979; Erecińska and Silver, 1990). The key difference lies in the interpretation of the rapid glutamine labeling observed using *in vivo* MRS. To illustrate the labeling of glutamate and glutamine, a different illustration of the glutamate–glutamine cycle is shown in **Figure 2**, where the coupling between the glutamate–glutamine cycle and energy metabolism is explicitly shown.

In **Figure 2**, with infusion of $^{13}C$-labeled glucose $^{13}C$ labels are mainly incorporated into neuronal glutamate first, accompanying the intensive metabolic activities in neurons. Although

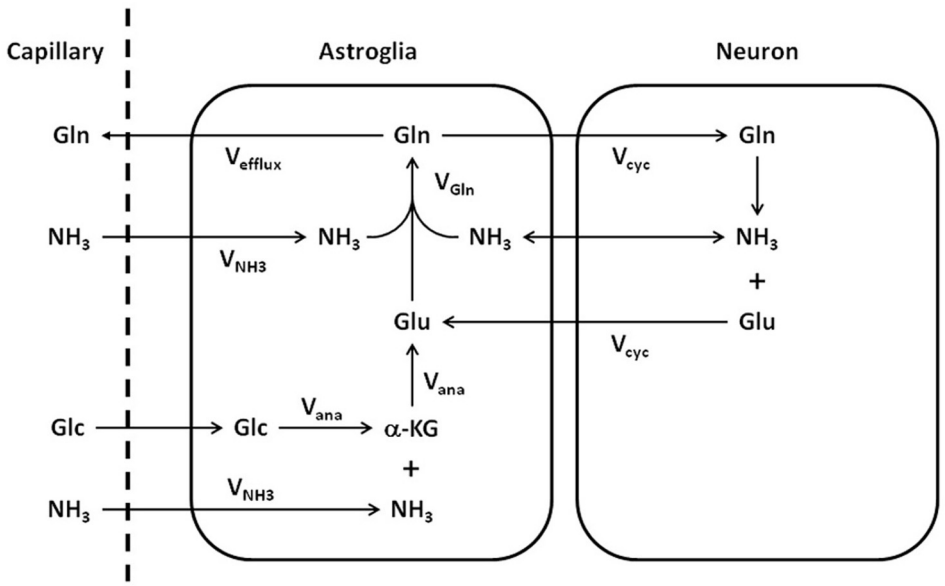


**FIGURE 1 | Schematic representation of the glutamate–glutamine cycle between neurons and astroglia and the ammonia detoxification pathway (adapted from Sibson et al., 1997).** Released neurotransmitter glutamate (Glu) is transported from the synaptic cleft to surrounding astroglial end processes. Once in the astroglia, glutamate is converted to glutamine (Gln) by glutamine synthetase. Glutamine is released by the astroglia, transported into the neurons, and converted to glutamate by glutaminase, which completes the cycle. The net rate of glutamine synthesis reflects both glutamate–glutamine neurotransmitter cycling ($V_{cyc}$) and anaplerosis ($V_{ana}$). $NH_3$, ammonia; $V_{NH3}$, ammonia fixation; $V_{gln}$, glutamine synthesis; Glc, glucose; α-KG, α-ketoglutarate.

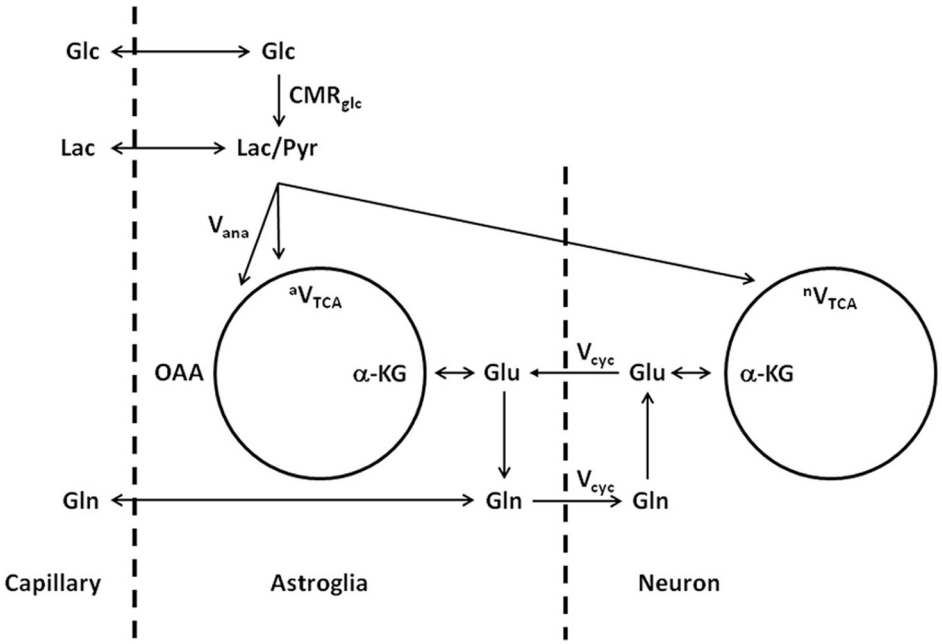


**FIGURE 2 | Schematic illustration of the glutamate–glutamine cycle between neurons and astroglia and glucose metabolism (adapted from Shen et al., 1999).** Released neurotransmitter glutamate is transported from the synaptic cleft by surrounding astroglial end processes. In astroglia, glutamate is converted into glutamine by glutamine synthetase. Glutamine is then released by the astroglia, transported into the neurons, and converted back into glutamate by glutaminase, which completes the cycle. Glc, glucose; Pyr/Lac, pyruvate/lactate; OAA, oxaloacetate; α-KG, α-ketoglutarate; Glu, glutamate; Gln, glutamine; CMRglc, cerebral metabolic rate of glucose utilization; $V_{ana}$, anaplerotic flux for de novo synthesis of oxaloacetate; $^{a}V_{TCA}$, astroglial tricarboxylic acid cycle flux; $V_{cyc}$, glutamate–glutamine cycling flux; $^{n}V_{TCA}$, neuronal tricarboxylic acid cycle flux.

seldom emphasized in the literature, it is important to point out that the labeling of glutamate and glutamine is on a very slow time scale when compared to the rapid vesicular release of glutamate and its uptake by astroglia. Experimentally, the *in vivo* turnover time constant of glutamate and glutamine is roughly one hour at resting state in the human brain. At this time scale, there is essentially no distinction between neurotransmitter pool and metabolic pool of glutamate as far as the labeling of the glutamate and glutamine are concerned. It is not surprising that, using *in vivo* microdialysis and mass spectrometry to determine the labeling of extracellular glutamate and glutamine, neuronal glutamate (through glutamate–glutamine cycling) was found to be the precursor for 80–90% of astroglial glutamine synthesis (Kanamori et al., 2003). Therefore, on the time scale of glutamate and glutamine turnover the experimental observation of rapid labeling of glutamine, which is predominantly located in astroglial cells, lead to the logical conclusion that neuronal glutamate is the main metabolic precursor of astroglial glutamine via the glutamate–glutamine cycling flux. In a subsequent analysis of energy cost associated with the glutamate–glutamine cycle Sibson et al. (1998) noticed that glutamate uptake into astroglial cells and its subsequent conversion to glutamine there costs two ATPs. This energy cost is matched by the number of ATPs produced by astroglial glycolysis. By extending the Magistretti hypothesis (Pellerin and Magistretti, 1994) that atroglial glycolysis is coupled to glucose oxidative in neurons Sibson et al. proposed that, although the glutamate–glutamine cycling uses two ATPs in the astrocytic portion of the cycle, the full cycle itself is coupled to the production of a 36 ATPs per glutamate release which are thought to be mostly used for other activities in the brain.

The identification of neuronal glutamate as the main metabolic precursor of astroglial glutamine via the glutamate–glutamine cycling flux leads to a simplified (while conceptually clearer) model of the glutamate–glutamine cycle (see **Figure 3**), which captures the main feature of intercompartmental trafficking of glutamate and glutamine molecules (Shen et al., 2009). Note that in **Figure 3**, the astroglial dilution flux, which will be elaborated later, was explicitly added at the level of glutamine. This simplified model represents the dominant metabolic relationship between neuronal glutamate and astroglial glutamine in the brain. That is, when [1-$^{13}$C] or [1,6-$^{13}C_2$] glucose infusion is used to introduce exogenous $^{13}$C labels into the brain, most labels flow from pyruvate C3 to neuronal glutamate C4 and then to astroglial glutamine C4. To better illustrate the conceptual aspects of modeling of the glutamate–glutamine cycle this simplified model will be repeatedly referred to.

## *In vivo* MRS METHODS

Both $^{13}$C and $^{15}$N MRS methods have been developed and used to determine the glutamate–glutamine cycling rate. $^{13}$C MRS methods have been applied to both human subjects and animals while $^{15}$N MRS methods are limited to animal models of hyperammonemia. Only the $^{13}$C MRS methods are summarized here. **Table 1** lists various $^{13}$C-related MRS techniques for studying

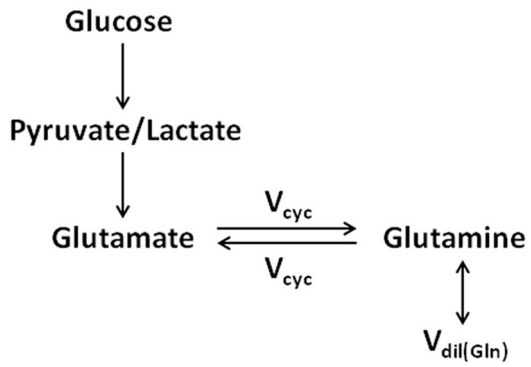


**FIGURE 3 | The simplified two-compartment model in which all $^{13}C$ labels flow from pyruvate/lactate to neuronal glutamate, which is in exchange with astroglial glutamine (adapted from Shen et al., 2009).** This simplified model represents the dominant metabolic pathways for the cycling of $^{13}C$ labels when [1-$^{13}C$] or [1,6-$^{13}C_2$] glucose infusion is used to introduce exogenous $^{13}C$ labels into the brain. As captured by the simplified model, most $^{13}C$ labels flow from pyruvate C3 to neuronal glutamate C4 and then to astroglial glutamine C4. The astroglial dilution flux was explicitly added at the level of glutamine.

**Table 1 | Heteronuclear MRS methods for studying the glutamate–glutamine cycle using infusion of $^{13}C$-labeled substrates.**

| | |
|---|---|
| $^{13}C\{^1H\}$ | Detect aliphatic carbons such as glutamate C4 and glutamine C4; use either carbon excitation or proton excitation and subsequent proton-to-carbon polarization transfer; need high power coherent proton decoupling (de Graaf et al., 2011)<br>Detect carboxylic carbons such as glutamate C5 and glutamine C5; use carbon excitation; can use low power stochastic proton decoupling (Li et al., 2009) |
| $^1H\{^{13}C\}$ | Detect aliphatic protons such as glutamate H4 and glutamine H4; use proton excitation and proton detection; need high power coherent carbon decoupling (de Graaf et al., 2011) |

the CNS, especially the glutamate–glutamine cycle. They fall into two main categories based on the choice of observed nucleus ($^{13}C$ or $^1H$). Generally, $^{13}C$ detection affords more spectral information. In the aliphatic (carboxyl/amide) spectral region, glutamate and glutamine C2–C4 (C1 and C5) carbons can be measured. Proton detection methods (POCE) have higher sensitivity at the expense of more spectral overlap. $^1H\{^{13}C\}$ methods that incorporate proton editing are yet to be fully developed.

## LABELING STRATEGIES

Accompanying the advancement of *in vivo* MRS technology many methods have been developed for labeling glutamate and glutamine by administering $^{13}C$-labeled exogenous substrates (e.g., Sibson et al., 1997, 2001; Blüml et al., 2002; Lebon et al., 2002; Deelchand et al., 2009). The most commonly used substrate is D-glucose, which is the primary source of energy for brain metabolism and function under normal physiological conditions. As shown by **Figure 3**, with infusion of [1-$^{13}C$] or [1,6-$^{13}C_2$] glucose $^{13}C$ labels are mainly incorporated into neuronal glutamate C4 first. Since neuronal glutamate is the main metabolic precursor of astroglial glutamine via the glutamate–glutamine cycling flux, $^{13}C$ label incorporation into glutamine C4 occurs mainly via the glutamate–glutamine cycling pathway ($V_{cyc}$). The simplified model shown in **Figure 3** excludes the contribution to the labeling of glutamine C4 via the internal TCA cycle of the astroglial cells, assumed to be small. Subsequent turns of the TCA cycles move the $^{13}C$ labels into C3, C2, C1 of glutamate and glutamine, and eventually carbon dioxide. $^{13}C$ labels on the C3 and C2 carbons of glutamate and glutamine can be readily detected in the aliphatic carbon region of the spectra and their labeling kinetics may be used to improve the determination of the glutamate–glutamine cycling rate. Since the exact contribution to the labeling of glutamine C4 by oxidative metabolism in astroglial cells is difficult to measure by the use of [1-$^{13}C$] or [1,6-$^{13}C_2$] glucose alone, alternative labeling strategies for *in vivo* $^{13}C$ MRS have been developed and applied to measuring the glutamate–glutamine cycling rate.

In addition to the main pathway of $^{13}C$ label flow depicted by the simplified model of **Figure 3**, the astroglial anaplerotic pathway ($V_{ana}$) was explicitly shown in **Figures 1** and **2**. The primarily astroglial anaplerotic pathway in the CNS offers an alternative route, albeit less effective than $V_{cyc}$, of incorporating $^{13}C$ labels into glutamate and glutamine. By the action of the astroglial enzyme pyruvate carboxylase (Patel, 1974) $^{13}C$ labels originated from [1-$^{13}C$] or [1,6-$^{13}C_2$] glucose labels pyruvate C3. Through $CO_2$ (either $^{13}CO_2$ or $^{12}CO_2$) fixation the astroglial anaplerotic pathway generates the TCA cycle intermediate [3-$^{13}C$] or [3,4-$^{13}C_2$] OAA, which through the first turn of the TCA cycle, labels C2 of α-ketoglutarate, followed by C2 of glutamate and glutamine. Label scrambling at fumarate due to potential backward flux from OAA to fumarate will label glutamate and glutamine C3 in the first turn of the TCA cycle as well (Merle et al., 1996; Brekke et al., 2012). Depending on if the acetylCoA that condenses with OAA generated by $CO_2$ fixation is labeled or not by the infused [1-$^{13}C$] or [1,6-$^{13}C_2$] glucose, then either [2-$^{13}C$] glutamine or [2,4-$^{13}C_2$] glutamine is produced during the first turn of the astroglial TCA cycle. Unfortunately, the weak glutamine $^{13}C$ NMR signal contributed by astroglial anaplerosis is strongly masked by the much larger contribution from neuronal oxidative metabolism and the main route of $^{13}C$ label incorporation into glutamine via the glutamate–glutamine cycle ($V_{cyc}$).

The strong interference from the heavy $^{13}C$ traffic coming from neurons, fortunately, can be more or less eliminated by choosing [2-$^{13}C$] or [2,5-$^{13}C_2$] glucose instead of [1-$^{13}C$] or [1,6-$^{13}C_2$] glucose (Badar-Goffer et al., 1992). The primary route of $^{13}C$ labeling from [2-$^{13}C$] or [2,5-$^{13}C_2$] glucose leads to labeling of pyruvate C2 followed by glutamate and glutamine C5 after the first turn of the TCA cycles. Parenthetically, this fact also prompted the development of carboxyl/amide carbon MRS with low power stochastic proton decoupling (Li et al., 2009). Without the anaplerotic pathway only natural abundance (1.1%) $^{13}C$ signals are expected in the aliphatic carbon spectral region, with the possible exception of minor contributions that may arise from isotopic impurity of the infused glucose, label scrambling via hepatic gluconeogenesis, the pentose phosphate shunt and pyruvate recycling (Cerdán et al., 1990). The major

contribution to the aliphatic $^{13}C$ signals therefore comes from the astroglial anaplerotic pathway. Through $CO_2$ (either $^{13}CO_2$ or $^{12}CO_2$) fixation catalyzed by the astroglial enzyme pyruvate carboxylase the astroglial anaplerotic pathway generates the TCA cycle intermediate [2-$^{13}C$] or [2,4-$^{13}C_2$] OAA. As a result, the $^{13}C$ labeling via the astroglial anaplerotic pathway labels C3 of astroglial glutamate (and glutamine) during the first turn of the astroglial TCA cycle. Since the heavy $^{13}C$ traffic generated inside neurons labels carboxyl/amide carbons the kinetics of $^{13}C$ label flow from astroglial glutamine C3 to neuronal glutamate C3 could be measured if sensitivity of the method is sufficient. An independent measurement of the more elusive astroglial TCA cycle rate could also be achieved (Sibson et al., 2001).

The sensitivity of the above approach is ultimately limited by the much smaller $V_{ana}$. It is expected that with high magnetic field strength and indirect detection of glutamine and glutamate H3 (with the aid of selective $^{1}H$ and/or $^{13}C$ editing to separate glutamate and glutamine H3 signals) further improvements in the determination of the astroglial TCA cycle rate may be possible. Nevertheless, at metabolic and isotopic steady state, the $V_{cyc}$/neuronal $V_{TCA}$ ($V_{cyc}/^{n}V_{TCA}$) ratio can be reliably measured. This is because the steady state signal of glutamate C3, in this case, results from a balance among the fluxes which feed label from astroglial glutamine C3 via the glutamate–glutamine cycle and outgoing fluxes to the astroglial glutamine C3 and label scrambling to other carbon positions by the neuronal TCA cycle.

A similar measurement of $^{13}C$ label flow from astroglial glutamine to neuronal glutamate can be made by taking advantage of the glial specific substrate acetate (Muir et al., 1986; Waniewski and Martin, 1998). Prolonged incubation of neuron culture with $^{13}C$-labeled acetate showed no enrichment of $^{13}C$ labels in glutamate, glutamine, or GABA (Sonnewald et al., 1993). Exogenous [2-$^{13}C$] acetate is metabolized via astroglial acetate-CoA ligase and TCA cycle, and subsequently produces [4-$^{13}C$] glutamine. Then, $^{13}C$ labels enter neuronal compartments via the glutamate–glutamine cycling flux to produce [4-$^{13}C$] glutamate. Because of the high specificity of acetate metabolism [2-$^{13}C$] acetate has been used *in vivo* to quantitatively characterize astroglial metabolism in the human brain (Blüml et al., 2002; Lebon et al., 2002). When [1-$^{13}C$] acetate, instead of [2-$^{13}C$] acetate, is administered, the primary route of intercompartmental $^{13}C$ label transfer is from astroglial glutamine C5 to neuronal glutamate C5. Unlike the avid utilization of glucose by brain, the rate of $^{13}C$ label transfer from acetate to glutamine and glutamate is significantly slower, making direct measurement of the absolute rate of metabolic fluxes by *in vivo* MRS more challenging, especially on human subjects. Again, similar to the strategy adopted for probing $^{13}C$ label flow from astroglial glutamine to neuronal glutamate using [2-$^{13}C$] or [2,5-$^{13}C_2$] glucose, the $V_{cyc}/^{n}V_{TCA}$ flux ratio can be measured at metabolic and isotopic steady state during [2-$^{13}C$] acetate infusion (Lebon et al., 2002). This is because the steady state signal of glutamate C4 reflects a balance among the fluxes that feed label from astroglial glutamine C4 via the glutamate–glutamine cycle and the outgoing fluxes to the astroglial glutamine C4 and label shift to C3 by the neuronal TCA cycle. A detailed mathematical treatment is given in the section "Effects of glutamine isotopic dilution on the determination of the glutamate–glutamine cycling rate."

Like acetate, monocarboxylic acids such as β-hydroxybutyrate (bHB) and lactate readily cross the blood brain barrier via the monocarboxylate transporters and are utilized as fuels. Both $^{13}C$-labeled bHB and lactate have been used to assess $^{13}C$ label incorporation into brain glutamate and glutamine (Kunnecke et al., 1993; Pan et al., 2002; Tyson et al., 2003; Boumezbeur et al., 2010b; Jiang et al., 2011; Xiang and Shen, 2011a). Tissue culture studies of neonatal and embryonic mouse cortex (Lopes-Cardozo et al., 1986) have reported that the majority of the bHB consumed in neurons is oxidized, whereas in astroglial cells it is only 20%. Thus, bHB oxidation should be more indicative of neuronal metabolism than astroglial metabolism. But unlike the high compartmental specificity associated with acetate, oxidation of bHB by both neuronal and astroglial TCA cycles has to be modeled in metabolic pathway analysis. The situation is similar for the case of $^{13}C$-labeled lactate infusion. Similar to glucose, oxidation of lactate by both neuronal and astroglial TCA cycles needs to be modeled although the majority of plasma lactate is metabolized in neurons (Boumezbeur et al., 2010b).

## DIFFERENTIAL EQUATIONS OF THE GLUTAMATE–GLUTAMINE CYCLE

The $^{13}C$ labeling dynamics implied in the two-compartment model depicted in **Figures 2** and **3** can be described explicitly using coupled linear differential equations, following standard theory of chemical kinetics. That is, the rate of change in concentration equals the sum of total incoming fluxes minus the sum of total outgoing fluxes. Here we use the *in vivo* time courses of the [4-$^{13}C$] glutamate and [4-$^{13}C$] glutamine concentrations measured during infusion of [1-$^{13}C$] or [1,6-$^{13}C_2$] glucose as a simple illustration. The two-compartment metabolic model is shown in **Figure 2**. As described by the equations below, $^{13}C$ label enters the [4-$^{13}C$] glutamine pool from both neuronal [4-$^{13}C$] glutamate, which is taken up by astroglia, and directly from the astroglial TCA cycle coupled to the anaplerotic pathway.

### ASTROGLIAL COMPARTMENT

Based on metabolic steady-state considerations, the only net pathways of glutamine synthesis ($V_{Gln}$) are the glutamate–glutamine cycle ($V_{cyc}$) and de novo glutamine synthesis by the anaplerotic pathway ($V_{ana}$) (Equation 1). The enrichment of the astroglial [4-$^{13}C$] glutamate pool can be calculated using the standard small pool assumption that the pool size is small enough to be approximated as instantaneously reaching isotopic steady state with the isotopic fluxes passing through the pool. Experimental evidence for this assumption of a relatively small glutamate pool in astrocytes comes from glutamate immunocytochemistry (Ottersen et al., 1992), studies showing that the enrichment in glutamine from infused $^{13}N$ and $^{15}N$ ammonia is several times greater than that of glutamate (Cooper et al., 1979), and estimates based on *in vivo* $^{13}C$ MRS (Lebon et al., 2002). The reversal of the normal product-precursor relationship during ammonia fixation is seen as evidence that the astroglial glutamate pool is much smaller than the glutamine pool and undergoes rapid isotopic turnover. The steady state equation for the concentration

of astroglial [4-$^{13}$C]-glutamate ([$^{a}$Glu4*]) is given by Shen et al. (1999):

$$d[^{a}Glu4^{*}]/dt = {}^{a}V_{TCA}[Lac3^{*}]/[Lac] + V_{cyc}[^{n}Glu4^{*}]/[^{n}Glu] - (V_{cyc} + V_{ana})[^{a}Glu4^{*}]/[^{a}Glu] - ({}^{a}V_{TCA} - V_{ana})[^{a}Glu4^{*}]/[^{a}Glu] = 0 \quad (3)$$

where $^{a}V_{TCA}$ is the astroglial tricarboxylic acid cycle flux, $V_{cyc}$ is the glutamate–glutamine cycle flux, and $V_{ana}$ is the anaplerotic flux. [Lac3*]/[Lac] denotes the fractional enrichment of the label feeding flux at pyruvate dehydrogenase in astrocytes (The exchange between lactate and pyruvate catalyzed by lactate dehydrogenase is much faster than the rate of the pyruvate dehydrogenase reaction.). [$^{n}$Glu4*]/[$^{n}$Glu] denotes the fractional enrichment of the neuronal glutamate pool. The labeling of astroglial [4-$^{13}$C] glutamine is described by

$$d[^{a}Gln4^{*}]/dt = V_{Gln}[^{a}Glu4^{*}]/[^{a}Glu] - V_{cyc}[^{a}Gln4^{*}]/[^{a}Gln] - (V_{efflux} + V_{dil(Gln)})[^{a}Gln4^{*}]/[^{a}Gln] \quad (4)$$

where $V_{Gln}$ is the total glutamine synthesis rate, $V_{efflux}$ is the net glutamine efflux rate, and $V_{dil(Gln)}$ is the flux term that accounts for the additional isotopic dilution of glutamine observed experimentally (vide infra).

### NEURONAL COMPARTMENT

The labeling of the neuronal [4-$^{13}$C] glutamine pool can be described by the same small pool isotopic steady-state assumption:

$$d[^{n}Gln4^{*}]/dt = V_{cyc}([^{a}Gln4^{*}]/[^{a}Gln] - [^{n}Gln4^{*}]/[^{n}Gln]) = 0 \quad (5)$$

The $^{13}$C labeling kinetics of the neuronal glutamate pool is given by

$$d[^{n}Glu4^{*}]/dt = {}^{n}V_{TCA}[Lac3^{*}]/[Lac] + V_{cyc}[^{n}Gln4^{*}]/[^{n}Gln] - (V_{cyc} + {}^{n}V_{TCA})[^{n}Glu4^{*}]/[^{n}Glu] \quad (6)$$

where $^{n}V_{TCA}$ is the neuronal tricarboxylic acid cycle flux. If the input plasma glucose concentration and [1-$^{13}$C] or [1,6-$^{13}C_2$] glucose fractional enrichment time courses can be described using simple analytical functions the coupled differential equations (3–6) can be solved exactly using either inverse Laplace transform or eigen value decomposition. Since the real arterial input function is time-varying and coupled to glucose transport kinetics numerical, iterative methods are used in practice to derive $V_{cyc}$ by minimizing the least-square difference between the calculated and measured values for [Glu4*] and [Gln4*]. The time courses of glutamate and glutamine C3 (and C2) measured during infusion of [1-$^{13}$C] or [1,6-$^{13}C_2$] glucose can be described mathematically using the same principle. Similarly, the time courses of $^{13}$C-labeled glutamate and glutamine measured using other labeling strategies can also be modeled to extract metabolic fluxes of interest.

Instead of attempting to summarize the full sets of differential equations applicable to individual labeling strategies we examine the differential equations for the simplified two-compartment model depicted in **Figure 3**, which captures the main features of the full two-compartment model shown in **Figure 2**. In particular, the effects of isotopic dilution of glutamine on various labeling strategies for determining the glutamate–glutamine cycling rate are illustrated using the simplified two-compartment model.

## ORIGINS OF GLUTAMINE ISOTOPIC DILUTION

Although the complete TCA cycle is known to occur exclusively in mitochondria many enzymes involved in the TCA cycle in brain (e.g., malate dehydrogenase, aconitase, and isocitrate dehydrogenase) are found in the cytosol of neurons and astrocytes as well (Koen and Goodman, 1969; Siesjo, 1978; Rodrigues and Cerdán, 2006). Only brain pyruvate dehydrogenase, citrate synthase, fumarase, succinate dehydrogenase and succinate thiokinase are exclusively mitochondrial (e.g., Siesjo, 1978; Akiba et al., 1984; Lai et al., 1989; Rodrigues and Cerdán, 2006). Many TCA cycle intermediates outside the mitochondria are in exchange with their mitochondrial counterparts via various transporters and channels. In terms of metabolic modeling the above processes contribute to "isotopic dilution" because a net loss of $^{13}$C labels occurs via exchange with unlabeled cytosolic pools which are connected to non-TCA cycle pathways. In addition, the net oxidation of (unlabeled) non-glucose fuels in brain is significant despite that glucose is the major source of carbon oxidized in the TCA cycles of brain cells under normal physiological conditions. As described in "Labeling strategies" the contributions of several non-glucose fuels to brain metabolism have been probed by administering the fuel source labeled with $^{13}$C. Despite the inflows of unlabeled substrates, the TCA cycle rate can still be correctly determined by incorporating isotopic dilution pathways in the metabolic models. The experimentally determined fractional enrichment of glutamate C4 was smaller than that expected with [1-$^{13}$C] or [1,6-$^{13}C_2$] glucose being the sole carbon source for glutamate. This dilution includes contributions from the influx of unlabeled substrates from blood and cytosol, including lactate, pyruvate, ketone bodies, free amino acids, as well as amino acids produced by protein degradation. On the basis of a quantitative analysis of various carbon flows into brain reported in the literature, lactate was considered to be the major contribution to this dilution under normal physiologic conditions (Mason et al., 1995). Hence, $V_{dil(Lac)}$ has been used to represent the lumped effect of these dilution fluxes.

In addition to the isotopic dilution effect observed at glutamate, astroglial dilution flux accounts for an additional 26% of label dilution at glutamine C4 (Shen et al., 1999). A detailed analysis of glutamate and glutamine dilutions has been given by Dienel and Cruz (2009). There are several potential sources of this dilution although it is unclear if any single source dominates. Astroglial glutamine is in exchange with unlabeled glutamine in blood across the blood–brain barrier ($V_{efflux}$, see **Figure 1**), primarily mediated by N-system transporters (Bröer and Brookes, 2001). Oxidation of short- and medium-chain free fatty acids

(e.g., acetate and bHB) occur significantly in the astroglia with acetate regarded as an astroglial specific substrate. $^{14}$C-acetate (Cruz et al., 2005) and $^{13}$C-octanoate (Ebert et al., 2003) studies showed that these endogenous free fatty acids at basal blood levels contribute significantly to astroglial oxidation (see **Table 2**). For example, Cruz et al. (2005) found that, depending on brain region and level of activity, acetate utilization may provide 28–115% of total astroglial oxidation. Oxidation of these free fatty acids undoubtably generates unlabeled acetyl-CoA leading to additional label dilution at glutamine C4. Branched chain amino acids readily cross the blood–brain barrier and can act as a fuel source in the brain (Hutson et al., 2005). [U-$^{14}$C] leucine injected systemically was found to label brain glutamine, glutamate, and aspartate in early neurochemical research (Patel and Balázs, 1970). Therefore, branched chain amino acids metabolized to acetyl-CoA or glutamate also contribute to isotopic dilution of glutamine C4. As a result of the additional isotopic dilution in astroglial cells, the fractional enrichment of glutamine C4 is significantly lower than glutamate C4 at all times during [1-$^{13}$C] or [1,6-$^{13}C_2$] glucose infusion, including the isotopic steady state. Similar to the case of $V_{dil(Lac)}$, we use a single flux term $V_{dil(Gln)}$ to represent the lumped glutamine dilution fluxes, including dilutions at both glutamine and acetyl-CoA levels.

## EFFECTS OF GLUTAMINE ISOTOPIC DILUTION ON THE DETERMINATION OF THE GLUTAMATE–GLUTAMINE CYCLING RATE

The extraction of $V_{cyc}$ requires metabolic modeling by least square minimization. In least square minimization, the cost function is proportional to $\chi^2$ when error per data point has the same noise level (von Mises, 1964). In metabolic modeling fluxes are determined by minimizing $\chi^2$. Generally, the terms in $\chi^2$ are not all statistically independent. For non-linear systems, such as the two-compartment model of the glutamate–glutamine cycle the analytical derivation of the probability density function for different $\chi^2$ at its minimum is very difficult. Even for the simplified two-compartment model analytical derivation of the probability density function for $V_{cyc}$ remains a daunting task. Instead, Monte Carlo simulation can be used to accurately assess the reliability of $V_{cyc}$. Using the Monte Carlo method, turnover data sets drawn from the predefined metabolic model are numerically synthesized. Subsequently, the synthesized data are used to determine both the probability density function of the $\chi^2$-statistic, and the reproducibility of metabolic fluxes extracted using the fitting procedure. To ensure that the optimization method of choice works properly for metabolic modeling statistical analysis of $\chi^2$ data can be performed. When the number of noise realizations is sufficiently large, the $\chi^2$-statistic should be normally distributed with a mean value of $N$–$n$ and a standard deviation of sqrt[2($N$–$n$)] for a small set of metabolic fluxes. Here $N$ is the total number of data points in the turnover curves and $n$ the number of free metabolic fluxes to be derived from the fit (von Mises, 1964). Therefore, the mean and standard deviation of $\chi^2$ are indicators of the goodness-of-fit in Monte Carlo analysis. When metabolic fluxes are derived based on local instead of global minima, significant deviations from the theoretical $\chi^2$-statistic are expected.

**Table 2 | $^{13}$C labeling strategies for studying the glutamate–glutamine cycle***

| | |
|---|---|
| **GLUCOSE** | |
| [1-$^{13}$C] or [1,6-$^{13}C_2$] glucose | Primary route of label transfer: glutamate C4 → glutamine C4<br>Anaplerotic pathway: glutamine C2 → glutamate C2 |
| [2-$^{13}$C] or [2,5-$^{13}C_2$] glucose | Primary route of label transfer: glutamate C5 → glutamine C5<br>Anaplerotic pathway: glutamine C3 → glutamate C3 |
| **ACETATE**** | |
| [2-$^{13}$C]acetate | Primary route of label transfer: glutamine C4 → glutamate C4 |
| [1-$^{13}$C]acetate | Primary route of label transfer: glutamine C5 → glutamate C5 |
| **bHB AND LACTATE** | |
| [2,4-$^{13}C_2$]bHB, [3-$^{13}$C] lactate | Primary route of label transfer: glutamate C4 → glutamine C4 |
| [1,3-$^{13}C_2$]bHB, [ 2-$^{13}$C] lactate | Primary route of label transfer: glutamate C5 → glutamine C5 |

*For simplicity, only intercompartmental label transfer during the first turn of the TCA cycles is shown.

**Isotope labels originating from $^{13}$C-ethanol enter the brain after being converted into acetate in the liver. The labeling pathway for $^{13}$C-labeled ethanol is the same as that of acetate (Xiang and Shen, 2011b).

### [1-$^{13}$C] OR [1,6-$^{13}C_2$] GLUCOSE INFUSION

The effects of glutamine isotopic dilution on determination of the glutamate–glutamine cycling rate depend on specific labeling strategies. For studies utilizing infusion of [1-$^{13}$C] or [1,6-$^{13}C_2$] glucose, which produce the maximum MRS signal-to-noise ratio with direct or indirect detection of aliphatic carbons, explicit incorporation of the glutamine isotopic dilution flux into the two-compartment glutamate–glutamine cycling model is critical. Without the astroglial glutamine dilution flux, the isotopic steady state fractional enrichment of the downstream glutamine C4 would have been the same as that of glutamate C4. The experimentally measured glutamine C4 turnover curve results from a balance between incoming $^{13}$C labeled flux entering the glutamine pool (e.g., the glutamate–glutamine cycling flux) and outgoing $^{13}$C labeled flux leaving the glutamine pool (e.g., glutamate–glutamine cycling flux and the astroglial dilution flux). The effects of glutamine isotopic dilution on determination of the glutamate–glutamine cycling rate are best illustrated using the simplified two-compartment model depicted in **Figure 3**, which represents the dominant metabolic pathway for the trafficking of $^{13}$C labels in brain between neurons and astroglia. For this simplified model, the differential equations (4–6) describing the kinetics of $^{13}$C label incorporation into glutamine C4 are simplified into:

$$d[^aGln4^*]/dt = V_{cyc}[^nGlu4^*]/[^nGlu] - V_{cyc}[^aGln4^*]/[^aGln] - V_{dil(Gln)}[^aGln4^*]/[^aGln] \quad (7)$$

Note that the above Equation (7) is very similar to the full differential equation describing the labeling of astroglial glutamine C4 (Equation 4). To arrive at Equation (7), the term

$V_{efflux}([^aGlu4^*]/[^aGlu] - [^aGln4^*]/[^aGln])$ in Equation (4) was omitted. Since the astroglial glutamate pool size is much smaller than the astroglial glutamine pool size, approximately, we have $[^aGlu4^*]/[^aGlu] \approx [^aGln4^*]/[^aGln]$, which reduces Equation (4) to Equation (7). Here we have again applied the standard small pool approximation although a more accurate description of the fractional enrichment of the astroglial glutamate pool is given by Equation (3). Note that the incoming astroglial dilution flux involves $^{12}C$-labeled Gln C4, which does not enter into Equation (7).

At isotopic steady state, the following is obtained from Equation (7):

$$[^aGln4^*]/[^aGln] = ([^nGlu4^*]/[^nGlu])V_{cyc}/(V_{cyc} + V_{dil(Gln)}) \quad (8)$$

Note that, if $V_{dil(Gln)}$ is incorrectly set to zero, the fractional enrichment of the down-stream glutamine C4 approaches that of the upstream glutamate C4 after the initial glucose infusion period, progressively losing sensitivity to the label-feeding flux ($V_{cyc}$) over time and causing an overall reduced sensitivity to $V_{cyc}$. At isotopic steady state, the fractional enrichments of glutamine C4 and glutamate C4 become identical if $V_{dil(Gln)} = 0$. That is, at isotopic steady state the glutamine C4 curve is independent of $V_{cyc}$. In contrast, when the $V_{dil(Gln)}$ term is included in the differential equation (7) indicates that the whole glutamine C4 turnover curve is sensitive to $V_{cyc}$. This sensitivity is not lost at isotopic steady state. Unless $V_{cyc} >> V_{dil(Gln)}$, the fractional enrichment of glutamate C4 will always be larger than the fractional enrichment of glutamine C4 when [1-$^{13}$C] or [1,6-$^{13}C_2$] glucose is infused. As shown by Equations (7) and (8), $V_{dil(Gln)}$ and $V_{cyc}$ have different effects on the turnover of glutamine C4, allowing the two fluxes to be separately determined.

The above analysis was validated by the use of the full two-compartment model shown in **Figure 2**, the corresponding full differential equations (3–6), and Monte Carlo simulation (Shen et al., 2009). Specifically, glutamate C4 and glutamine C4 turnover curves (see **Figure 4A**) were generated by solving the differential equations (3–6) describing the full two-compartment model with the mean metabolic fluxes obtained from Shen et al. (1999). The total infusion time is 160 min with 32 data points per curve. Gaussian white noise with standard deviation $\sigma = 0.1\,\mu$mol/g was added to assess the accuracy and reproducibility of $V_{cyc}$. [1-$^{13}$C] or [1,6-$^{13}C_2$] glucose infusion was assumed. At the end point of glucose infusion the fractional enrichment of glutamine C4 is 26% lower than that of glutamate C4 as observed experimentally (Shen et al., 1999). This data set was fitted with the two-compartment model with suitable constraints using the simulated annealing method which is well-known for its robustness in determining global minimum in a multidimensional error space. Metabolic fluxes were determined by minimizing the summed square cost function which is proportional to $\chi^2$. The above procedure was repeated 100 times with the same noise variance but with different noise realizations. A probability density function for $V_{cyc}$ is shown in **Figure 4B**. For the data set shown in **Figure 4A** the mean $\chi^2$ obtained with 100 noise realizations is 60.8 with a standard deviation of 11.2. Comparison with the theoretical mean $\chi^2$ of $32 \times 2 - 4 = 60$ and standard

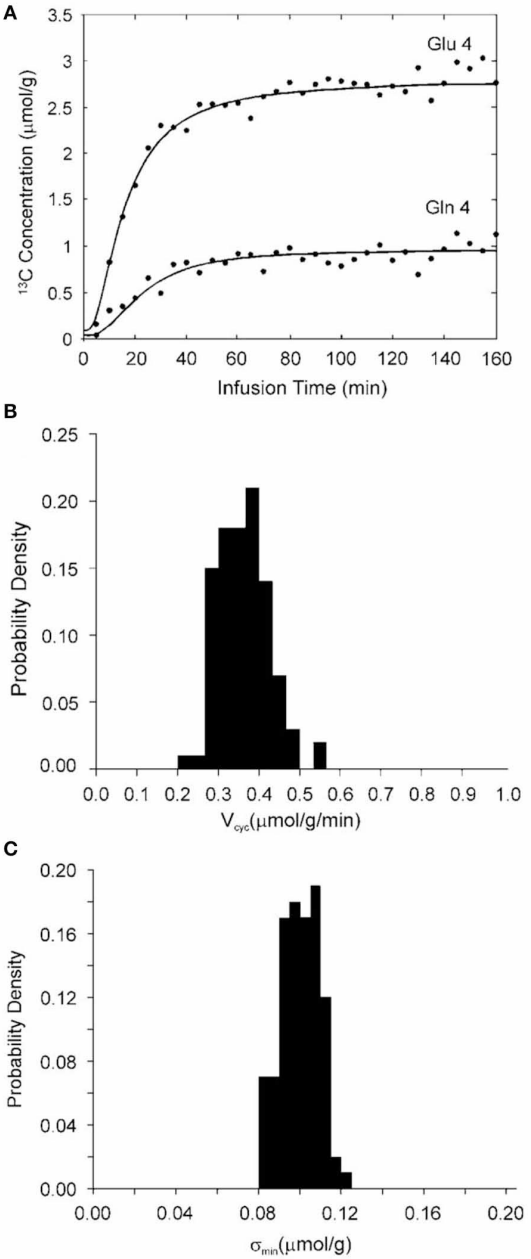


**FIGURE 4 | (A)** Synthetic glutamate C4 and glutamine C4 turnover curves (lines) generated by solving the four coupled differential equations describing the model in **Figure 2** with [1-$^{13}$C] or [1,6-$^{13}C_2$] glucose infusion, the mean metabolic fluxes, and adding normally distributed noise (dots). The astroglial dilution is revealed in **(A)** by comparing the fractional enrichments of glutamate and glutamine C4. At the end point of glucose infusion, the concentration of glutamine and glutamate with $^{13}$C labels at C4 is 0.96 and 2.75 μmol/g, respectively. The end point fractional enrichment of glutamine C4 is 26% lower than that of glutamate C4 as observed experimentally (Shen et al., 1999). **(B)** An example of the probability density function for $V_{cyc}$ with constraints $^aV_{TCA} \leq 0.1$, $V_{dil(Lac)} = 0.05$, and $V_{dil(Gln)} = 0.14\,\mu$mol/g/min. **(C)** The corresponding probability density function of the "noise level" after fitting ($\sigma_{min}$). The mean $\chi^2$ obtained is 60.8 with a standard deviation of 11.2. $\sigma_{min}$ averaged over the 100 Monte Carlo data sets is 0.098 μmol/g with a standard deviation of 0.009 μmol/g. (This image is reproduced from Shen et al., 2009).

deviation of 11.0 (the theoretical values are obtained when the number of noise realizations approaches infinity) indicates that global minima were found using the simulated annealing method. The $\chi^2$ data were also used to calculate the noise level after minimization by simulated annealing ($\sigma_{min}$). In the above case, $\sigma_{min}$ averaged across the 100 simulations is 0.098 μmol/g with a standard deviation of 0.009 μmol/g. The corresponding probability density function of $\sigma_{min}$ is shown in **Figure 4C**. Because poor data fitting caused by false minima was avoided by the use of simulated annealing the average $\sigma_{min}$ is expected to be slightly less than the added noise level ($\sigma$) with a relative standard deviation of slightly less than 10%. This is exactly what was found. This result also confirmed that the constraints imposed on the metabolic fluxes did not alter the quality of the fit.

The importance of the glutamine dilution flux in the accuracy and precision of determining $V_{cyc}$ was also assessed using numerical Monte Carlo simulations with $V_{dil(Gln)}$ forced to zero. When $V_{dil(Gln)}$ is set to zero the $^{13}$C-labeled glutamine concentration predicted by the model shown in **Figure 2** is higher than that shown in **Figure 4A**. To match the concentration of $^{13}$C-labeled glutamine in **Figure 4A** and the $^{13}$C-labeled glutamine concentration with $V_{dil(Gln)} = 0$, the total glutamine concentration needs to be reduced to 2.8 mmol/L in the Monte Carlo simulations because the actual $^{13}$C fractional enrichment of glutamine C4 is lower than that of glutamate C4. For a noise level of $\sigma = 0.2$ μmol/g, a relative standard deviation of 438% was calculated for $V_{cyc}$, indicating this flux cannot be reliably determined under the simulated condition [$V_{dil(Gln)} = 0$] using the two-compartment model shown in **Figure 2**. At the noise level of $\sigma = 0.1$ μmol/g the relative standard deviation of the calculated $V_{cyc}$ is 66%. When $^aV_{TCA}$ was constrained not to exceed 0.1 μmol/g/min and simultaneously $V_{efflux}$ was forced to $0.2*V_{Gln}$ a large reduction in the uncertainty of $V_{cyc}$ was found. In all cases investigated using numerical Monte Carlo simulations a smaller standard deviation was found when the $V_{dil(Gln)}$ term was included in the modeling.

### [2-$^{13}$C] OR [2,5-$^{13}C_2$] GLUCOSE INFUSION

The effects of glutamine isotopic dilution on determination of the glutamate–glutamine cycling rate using [2-$^{13}$C] or [2,5-$^{13}C_2$] glucose infusion are expected to be quite different. Glucose labeled at [2-$^{13}$C] or [2,5-$^{13}C_2$] is metabolized through glycolysis to [2−$^{13}$C] pyruvate, which enters the TCA cycle through one of two different pathways. Entry of [2-$^{13}$C] pyruvate through pyruvate dehydrogenase leads to labeling of glutamate (and glutamine) at C5, whereas entry through pyruvate carboxylase (anaplerosis) leads to labeling of glutamate (and glutamine) at C3 in the first turn of the TCA cycle followed by C2 and C1 in subsequent turns. Similar to [1-$^{13}$C] or [1,6-$^{13}C_2$] glucose infusion, potential label scrambling at fumarate during [2-$^{13}$C] or [2,5-$^{13}C_2$] glucose infusion labels glutamate and glutamine C2 in the first turn of the TCA cycle (see the "Labeling strategies" section). Half of the $^{13}$C labels on glutamate C3 move to glutamate C2 due to symmetric label scrambling of the TCA cycle. $^{13}$C-labeled glutamate C3 is also in exchange with $^{13}$C-labeled glutamine C3 via the glutamate–glutamine cycle. Using the simplified model shown in **Figure 3** the following differential equation describes the kinetics of $^{13}$C-labeled glutamate C3:

$$d[^nGlu3^*]/dt = -0.5^nV_{TCA}[^nGlu3^*]/[^nGlu] + V_{cyc}([^aGln3^*]/[^aGln] - [^nGlu3^*]/[^nGlu]) \quad (9)$$

At metabolic and isotopic steady state, Equation (9) becomes:

$$V_{cyc}/^nV_{TCA} = 0.5^*([^nGlu3^*]/[^nGlu])/([^aGln3^*]/[^aGln] - [^nGlu3^*]/[^nGlu]) \quad (10)$$

by setting $d[^nGlu3^*]/dt$ to zero. Equation (10) is identical to Equation (4) in Sibson et al. (2001) if a small correction term ($[^nGlu4^*]/[^nGlu]$) is ignored. Equation (4) in Sibson et al. (2001) was derived using the full two-compartment model (**Figure 2**). Note that, because Equation (9) describes the kinetics of a predominantly neuronal signal ($[^nGlu3^*]$), the astroglial $V_{dil(Gln)}$ term does not appear in Equations (9) or (10).

To describe the labeling kinetics of glutamine C3 the main label-feeding flux via the astroglial anaplerotic pathway needs to be incorporated. The following equation is then obtained:

$$d[^aGln3^*]/dt = V_{ana}[Lac2^*]/[Lac] + V_{cyc}([^nGlu3^*]/[^nGlu] - [^aGln3^*]/[^aGln]) - V_{dil(Gln)}[^aGln3^*]/[^aGln] \quad (11)$$

Equation (11) is analogous to Equation (7) for [1-$^{13}$C] or [1,6-$^{13}C_2$] glucose infusion. At metabolic and isotopic steady state Equation (11) is reduced to:

$$V_{dil(Gln)}/V_{cyc} = (V_{ana}/V_{cyc}) \times ([Lac2^*]/[Lac])/([^aGln3^*]/[^aGln]) + ([^nGlu3^*]/[^nGlu])/([^aGln3^*]/[^aGln]) - 1 \quad (12)$$

The most interesting conclusion of the above analysis of the effects of astroglial isotopic dilution of glutamine on determining $V_{cyc}$ using [2-$^{13}$C] or [2,5-$^{13}C_2$] glucose infusion is that $V_{cyc}$ (or $V_{cyc}/^nV_{TCA}$ if only steady state fractional enrichments of glutamate and glutamine C3 are measured) is insensitive to astroglial isotopic dilution of glutamine. As described in "Labeling strategies," the sensitivity of the [2-$^{13}$C] or [2,5-$^{13}C_2$] glucose infusion with detection of aliphatic carbons is limited because of the small $V_{ana}$ flux. Dynamic studies necessary for determining the absolute $V_{cyc}$ flux may be attempted by boosting sensitivity with high magnetic fields and indirect proton detection (with $^{13}$C or proton editing to separate spectral overlap between glutamate H3 and glutamine H3). An alternative experimental strategy also exists. Recent MRS data of human brain acquired during [2-$^{13}$C] glucose infusion have shown that the sensitivity of carboxyl/amide carbon detection is sufficient for the reliable measurement of glutamate turnover at 3 Tesla (Li et al., 2009). This would allow determination of the absolute, predominantly neuronal TCA cycle rate. Since the recycle delay of the carboxyl/amide carbon MRS experiment is relatively long, interleaved detection of the aliphatic

glutamate C3 and glutamine C3 signals can be performed in principle. Then, by adding all the time course data of glutamate C3 and glutamine C3, the $V_{cyc}/^nV_{TCA}$ ratio can be simultaneously measured [by utilizing the integrated form of Equation (9)]. By combining data from carboxyl/amide and aliphatic spectral regions, $V_{cyc}$ can be determined independent of $V_{dil(Gln)}$, in contrast to the case of [1-$^{13}$C] or [1,6-$^{13}C_2$] glucose infusion.

### [2-$^{13}$C] ACETATE INFUSION

The insensitivity to astroglial glutamine dilution flux $V_{dil(Gln)}$ in the determination of $V_{cyc}$ by the use of [2-$^{13}$C] or [2,5-$^{13}C_2$] glucose infusion is a direct result of extracting $V_{cyc}$ from signals (d[$^n$Glu3*]/dt) of the neuronal compartment (see Equation 9). In [2-$^{13}$C] or [2,5-$^{13}C_2$] glucose infusion experiments the flux causing the increased labeling of glutamate C3 signal comes from glutamine C3 predominantly located in the astroglia. A similar scenario can be generated by the use of [2-$^{13}$C] acetate infusion. During [2-$^{13}$C] acetate infusion, $^{13}$C label from [4-$^{13}$C] glutamine enters neuronal compartments via the glutamate–glutamine cycle to produce [4-$^{13}$C] glutamate. Here the glutamate C4 plays the same role as that of glutamate C3 during [2-$^{13}$C] or [2,5-$^{13}C_2$] glucose infusion. The corresponding differential equation describing the labeling kinetics of glutamate C4 is:

$$d[^nGlu4^*]/dt = -{}^nV_{TCA}[^nGlu4^*]/[^nGlu] + V_{cyc}([^aGln4^*]/[^aGln] - [^nGlu4^*]/[^nGlu]) \quad (13)$$

for the simplified two-compartment model shown in **Figure 3**. Essentially the same equation is obtained when the full two-compartment model (**Figure 2**) was used (Lebon et al., 2002). Similar to Equation (9), $V_{cyc}$, in principle, can be determined from the $^{13}$C MRS turnover data. The sensitivity of the acetate infusion experiment, however, is only a fraction of that of the corresponding [1-$^{13}$C] or [1,6-$^{13}C_2$] glucose infusion experiment. As an alternative to dynamic studies, the $V_{cyc}/^nV_{TCA}$ flux ratio can be determined from spectra acquired at the metabolic and isotopic steady state where d[$^n$Glu4*]/dt = 0:

$$V_{cyc}/^nV_{TCA} = ([^nGlu4^*]/[^nGlu])/([^aGln4^*]/[^aGln] - [^nGlu4^*]/[^nGlu]) \quad (14)$$

Note that, as expected, the astroglial glutamine dilution flux $V_{dil(Gln)}$ does not appear in either Equations (13) or (14). Therefore, $V_{cyc}$ determined in this manner is also insensitive to $V_{dil(Gln)}$.

As well-known in statistics, over-parameterization or over-fitting of a model leads to increased uncertainty. A familiar example is spectral fitting in quantification of crowded proton MRS spectra. When the spectral model is over-parameterized, erroneous concentration and increased uncertainty are easily obtained. In the case of [2-$^{13}$C] or [2,5-$^{13}C_2$] glucose and [2-$^{13}$C] acetate infusion experiments described here, the addition of flux terms [e.g., $V_{dil(Gln)}$] to which the data are insensitive (Shestov et al., 2012) can lead to increased uncertainly in $V_{cyc}$.

To extract the absolute flux of the glutamate–glutamine cycle an independent or simultaneous measurement of $V_{TCA}$ needs to be performed. In a recent study, difference in brain mitochondrial metabolism of young and old healthy human subjects was studied by infusing [1-$^{13}$C] glucose in one experiment and [2-$^{13}$C] acetate to the same subject in a separate experiment (Boumezbeur et al., 2010a). For [2-$^{13}$C] acetate infusion experiments, it is possible to infuse [2-$^{13}$C] acetate and [2-$^{13}$C] (or [2,5-$^{13}C_2$]) glucose simultaneously and measure $V_{TCA}$ in the carboxyl/amide spectral region and measure the $V_{cyc}/^nV_{TCA}$ flux ratio in the aliphatic spectral region as outlined for the case of [2-$^{13}$C] or [2,5-$^{13}C_2$] glucose infusion.

*In vivo* double-labeling experiments have been performed recently on both animals (Deelchand et al., 2009; Xiang and Shen, 2011a) and human subjects (Li et al., 2012). Since carboxyl/amide carbons are located at the end of the carbon skeleton of amino acids they can form either a singlet if its neighbor carbon is $^{12}$C, or a doublet if its neighbor carbon is $^{13}$C, leading to natural simplification of their isotopomer patterns (Xiang and Shen, 2011a). When $^{13}$C-labeled glucose is administered the glutamate and glutamine C4-C5 moieties are labeled by glucose C1-C2 and/or C5-C6, regardless of the number of the turns of the TCA cycle. Consequently, when the input is [1,2-$^{13}C_2$] acetyl-CoA, glutamate C5 and glutamine C5 can only form doublet signals. Vice versa, when the input is [2-$^{13}$C] acetyl-CoA glutamate C5 and glutamine C5 can only form singlet signals. This unique feature of the carboxyl/amide carbons makes it possible to simultaneously and unambiguously detect the labeling of glutamate and glutamine by two substrates with the second substrate (e.g., acetate) producing singlets only. Because of the large one-bond $^{13}$C-$^{13}$C homonuclear J coupling between a carboxyl/amide carbon and an aliphatic carbon (~50 Hz), the singlet and doublet signals of the same carboxyl/amide carbon can be well distinguished. It is readily conceivable that one may use the glutamate C5 doublet generated from uniformly labeled glucose to measure the absolute flux of $V_{TCA}$ and the glutamate C5 and glutamine C5 singlets generated from [1-$^{13}$C] acetate to measure the $V_{cyc}/^nV_{TCA}$ flux ratio. $V_{cyc}$ measured in this manner is expected to be insensitive to the astroglial glutamine dilution flux based on the above analysis.

## CONCLUSION

*In vivo* $^{13}$C MRS has evolved into a major non-invasive tool for assessing glutamatergic function in both human subjects and animal models. Recent development of $^{13}$C MRS techniques has been spurred by renewed interest in the glutamate–glutamine cycle proposed decades ago. Like all metabolic models the two-compartment glutamate–glutamine cycling model has generated controversy. While the dual roles of glutamate as primary excitatory neurotransmitter in the CNS and as a key metabolite linking carbon and nitrogen metabolism make it possible to probe glutamate neurotransmitter cycling using MRS this dual role also requires one to separate neurotransmission events from metabolism. In spite of the on-going controversies, the *in vivo* MRS community has made major contributions to our understanding of brain energy consumption and the relationship between neuroenergetics and neurotransmission. Over the past few years our understanding of the neuronal-astroglial two-compartment metabolic model of the glutamate–glutamine cycle has been further advanced. In particular, the

importance of isotopic dilution of glutamine in determining the glutamate–glutamine cycling rate using [1-$^{13}$C] or [1,6-$^{13}C_2$] glucose has been demonstrated and reproduced. It is hoped that the analysis of the astroglial dilution effects and $V_{dil(Gln)}$-insensitive experimental methods for absolute quantification of the glutamate–glutamine cycling rate discussed here will further advance the field. With the increasing availability of high-field MR magnets (7 Tesla or higher) and further developments of MRS techniques characterization of glutamatergic function by *in vivo* $^{13}$C MRS has the potential to significantly impact both basic and clinical research in neurological and psychiatric disorders.

## ACKNOWLEDGMENTS

This work is supported by the Intramural Research Program of the National Institutes of Health, NIMH and conducted in the absence of any commercial or financial relationships that could be construed as a potential conflict of interest.

## REFERENCES

Akiba, T., Hiraga, K., and Tuboi, S. (1984). Intracellular distribution of fumarase in various animals. *J. Biochem.* 96, 189–195.

Badar-Goffer, R. S., Ben-Yoseph, O., Bachelard, H. S., and Morris, P. G. (1992). Neuronal-astroglial metabolism under depolarizing conditions. A 13C-n.m.r. study. *Biochem. J.* 282(Pt 1), 225–230.

Bergles, D. E., Diamond, J. S., and Jahr, C. E. (1999). Clearance of glutamate inside the synapse and beyond. *Curr. Opin. Neurobiol.* 9, 293–298.

Berkich, D. A., Xu, Y., LaNoue, K. F., Gruetter, R., and Hutson, S. M. (2005). Evaluation of brain mitochondrial glutamate and alpha-ketoglutarate transport under physiologic conditions. *J. Neurosci. Res.* 79, 106–113.

Berl, S., Takagaki, G., Clarke, D. D., and Waelsch, H. (1963). Carbon dioxide fixation in the brain, *J. Biol. Chem.* 237, 2570–2573.

Blüml, S., Moreno-Torres, A., Shic, F., Nguy, C. H., and Ross, B. D. (2002). Tricarboxylic acid cycle of glia in the *in vivo* human brain. *NMR Biomed.* 15, 1–5.

Boumezbeur, F., Mason, G. F., de Graaf, R. A., Behar, K. L., Cline, G. W., Shulman, G. I., et al. (2010a). Altered brain mitochondrial metabolism in healthy aging as assessed by *in vivo* magnetic resonance spectroscopy. *J. Cereb. Blood Flow Metab.* 30, 211–221.

Boumezbeur, F., Petersen, K. F., Cline, G. W., Mason, G. F., Behar, K. L., Shulman, G. I., et al. (2010b). The contribution of blood lactate to brain energy metabolism in humans measured by dynamic $^{13}$C nuclear magnetic resonance spectroscopy. *J. Neurosci.* 30, 13983–13991.

Brekke, E., Walls, A. B., Nørfeldt, L., Schousboe, A., Waagepetersen, H. S., and Sonnewald, U. (2012). Direct measurement of backflux between oxaloacetate and fumarate following pyruvate carboxylation. *Glia* 60, 147–158.

Bröer, S., and Brookes, N. (2001). Transfer of glutamine between astrocytes and neurons. *J. Neurochem.* 77, 705–719.

Cerdán, S., Künnecke, B., and Seelig, J. (1990). Cerebral metabolism of [1, 2-$^{13}C_2$] acetate as detected by invivo and *in vitro*13C NMR. *J. Biol. Chem.* 265, 12916–12926.

Cerdán, S., Rodrigues, T. B., Sierra, A., Benito, M., Fonseca, L. L., Fonseca, C. P., et al. (2006). The redox switch/redox coupling hypothesis. *Neurochem. Int.* 48, 523–530.

Chaudhry, F. A., Reimer, R. J., and Edwards, R. H. (2002). The glutamine commute: take the N line and transfer to the A. *J. Cell Biol.* 157, 349–355.

Cooper, A. J. L., McDonald, J. M., Gelbard, A. S., Gledhill, R. F., and Durry, T. E. (1979). The metabolic fate of 13N-labeled ammonia in rat brain. *J. Biol. Chem.* 254, 4982–4992.

Cruz, N. F., Lasater, A., Zielke, H. R., and Dienel, G. A. (2005). Activation of astrocytes in brain of conscious rats during acoustic stimulation: acetate utilization in working brain. *J. Neurochem.* 92, 934–947.

Deelchand, D. K., Nelson, C., Shestov, A. A., Uğurbil, K., and Henry, P. G. (2009). Simultaneous measurement of neuronal and astroglial metabolism in rat brain *in vivo* using co-infusion of [1,6-$^{13}C_2$]glucose and [1,2-$^{13}C_2$]acetate. *J. Magn. Reson.* 196, 157–163.

de Graaf, R. A., Mason, G. F., Patel, A. B., Rothman, D. L., and Behar, K. L. (2004). Regional glucose metabolism and glutamatergic neurotransmission in rat brain *in vivo*. *Proc. Natl. Acad. Sci. U.S.A.* 101, 12700–12705.

de Graaf, R. A., Rothman, D. L., and Behar, K. L. (2011). State of the art direct $^{13}$C and indirect $^{1}$H-[$^{13}$C] NMR spectroscopy *in vivo*. A practical guide. *NMR Biomed.* 24, 958–972.

Dienel, G. A., and Cruz, N. F. (2009). Exchange-mediated dilution of brain lactate specific activity: implications for the origin of glutamate dilution and the contributions of glutamine dilution and other pathways. *J. Neurochem.* 109(Suppl. 1), 30–37.

Duarte, J. M., Lanz, B., and Gruetter, R. (2011). Compartmentalized cerebral metabolism of [1, 6-13C]Glucose determined by *in vivo* 13C NMR spectroscopy at 14.1 T. *Front. Neuroenerg.* 3:3. doi: 10.3389/fnene.2011.00003

Duce, I. R., Donaldson, P. L., and Usherwood, P. N. (1983). Investigations into the mechanism of excitant amino acid cytotoxicity using a well-characterized glutamatergic system. *Brain Res.* 263, 77–87.

Ebert, D., Haller, R. G., and Walton, M. E. (2003). Energy contribution of octanoate to intact rat brain metabolism measured by $^{13}$C nuclear magnetic resonance spectroscopy. *J. Neurosci.* 23, 5928–5935.

Erecińska, M., and Silver, I. A. (1990). Metabolism and role of glutamate in mammalian brain. *Prog. Neurobiol.* 35, 245–296.

Gruetter, R., Novotny, E. J., Boulware, S. D., Mason, G. F., Rothman, D. L., Shulman, G. I., et al. (1994). Localized 13C NMR spectroscopy in the human brain of amino acid labeling from D-[1-$^{13}$C]glucose. *J. Neurochem.* 63, 1377–1385.

Gruetter, R., Seaquist, E. R., and Ugurbil, K. (2001). A mathematical model of compartmentalized neurotransmitter metabolism in the human brain. *Am. J. Physiol. Endocrinol. Metab.* 281, E100–E112.

Hertz, L. (1979). Functional interactions between neurons and astrocytes I. Turnover and metabolism of putative amino acid transmitters. *Prog. Neurobiol.* 13, 277–323.

Hutson, S. M., Sweatt, A. J., and Lanoue, K. F. (2005). Branched-chain amino acid metabolism: implications for establishing safe intakes. *J. Nutr.* 135(Suppl. 6), 1557S–1564S.

Hyder, F., and Rothman, D. L. (2012). Quantitative fMRI and oxidative neuroenergetics. *Neuroimage* 62, 985–994.

Jiang, L., Mason, G. F., Rothman, D. L., de Graaf, R. A., and Behar, K. L. (2011). Cortical substrate oxidation during hyperketonemia in the fasted anesthetized rat *in vivo*. *J. Cereb. Blood Flow Metab.* 31, 2313–2323.

Kanamori, K., Kondrat, R. W., and Ross, B. D. (2003). $^{13}$C enrichment of extracellular neurotransmitter glutamate in rat brain–combined mass spectrometry and NMR studies of neurotransmitter turnover and uptake into glia *in vivo*. *Cell. Mol. Biol. (Noisy-le-grand)* 49, 819–836.

Koen, A. L., and Goodman, M. (1969). Aconitate hydratase isozymes: subcellular location, tissue distribution and possible subunit structure. *Biochim. Biophys. Acta* 191, 698–701.

Kunnecke, B., Cerdan, S., and Seelig, J. (1993). Cerebral metabolism of [1, 2-13C, IGlucose and [U-13C]3-Hydroxybutyrate in rat brain as detected by 13C NMR spectroscopy. *NMR Biomed.* 6, 264–277.

Lapidot, A., and Gopher, A. (1994). Cerebral metabolic compartmentation. Estimation of glucose flux via pyruvate carboxylase/pyruvate dehydrogenase by 13C NMR isotopomer analysis of D-[U-13C]glucose metabolites. *J. Biol. Chem.* 269, 27198–27208.

Lai, J. C., Murthy, C. R., Cooper, A. J., Hertz, E., and Hertz, L. (1989). Differential effects of ammonia and beta-methylene-DL-aspartate on metabolism of glutamate and related amino acids by astrocytes and neurons in primary culture. *Neurochem. Res.* 14, 377–389.

Lebon, V., Petersen, K. F., Cline, G. W., Shen, J., Mason, G. F., Dufour, S., et al. (2002). Astroglial contribution to brain energy metabolism in humans revealed by $^{13}$C nuclear magnetic resonance spectroscopy: elucidation of the dominant pathway for neurotransmitter glutamate repletion and measurement of astrocytic oxidative metabolism. *J. Neurosci.* 22, 1523–1531.

Li, S., Zhang, Y., Ferraris Araneta, M., Xiang, Y., Johnson, C., Innis, R. B.,

et al. (2012). *In vivo* detection of $^{13}$C isotopomer turnover in the human brain by sequential infusion of $^{13}$C labeled substrates. *J. Magn. Reson.* 218, 16–21.

Li, S., Zhang, Y., Wang, S., Yang, J., Ferraris Araneta, M., Johnson, C., et al. (2009). *In vivo* $^{13}$C magnetic resonance spectroscopy of human brain on a clinical 3 T scanner using [2-$^{13}$C]glucose infusion and low-power stochastic decoupling. *Magn. Reson. Med.* 62, 565–573.

Lopes-Cardozo, M., Larsson, O. M., and Schousboe, A. (1986). Acetoacetate and glucose as lipid precursors and energy substrates in primary cultures of astrocytes and neurons from mouse cerebral cortex. *J. Neurochem.* 46, 773–778.

Martinez-Hernandez, A., Bell, K. P., and Norenberg, M. D. (1977). Glutamine synthetase: glial localization in brain. *Science* 195, 1356–1358.

Mason, G. F., Gruetter, R., Rothman, D. L., Behar, K. L., Shulman, R. G., and Novotny, E. J. (1995). Simultaneous determination of the rates of the TCA cycle, glucose utilization, alpha-ketoglutarate/glutamate exchange, and glutamine synthesis in human brain by NMR. *J. Cereb. Blood Flow Metab.* 15, 12–25.

Merle, M., Martin, M., Villégier, A., and Canioni, P. (1996). Mathematical modelling of the citric acid cycle for the analysis of glutamine isotopomers from cerebellar astrocytes incubated with [1-13C]glucose. *Eur. J. Biochem.* 239, 742–751.

Muir, D., Berl, S., and Clarke, D. D. (1986). Acetate and fluoroacetate as possible markers for glial metabolism *in vivo*. *Brain Res.* 380, 336–340.

Ottersen, O. P., Zhang, N., and Walberg, F. (1992). Metabolic compartmentation of glutamate and glutamine: morphological evidence obtained by quantitative immunocytochemistry in rat cerebellum. *Neuroscience* 46, 519–534.

Pan, J. W., de Graaf, R. A., Petersen, K. F., Shulman, G. I., Hetherington, H. P., and Rothman, D. L. (2002). [2, 4-$^{13}C_2$]-beta-Hydroxybutyrate metabolism in human brain. *J. Cereb. Blood Flow Metab.* 22, 890–898.

Patel, A. B., de Graaf, R. A., Mason, G. F., Kanamatsu, T., Rothman, D. L., Shulman, R. G., et al. (2004). Glutamatergic neurotransmission and neuronal glucose oxidation are coupled during intense neuronal activation. *J. Cereb. Blood Flow Metab.* 24, 972–985.

Patel, A. J., and Balázs, R. (1970). Manifestation of metabolic compartmentation during the maturation of the rat brain. *J. Neurochem.* 17, 955–971.

Patel, M. S. (1974). The relative significance of $CO_2$-fixing enzymes in the metabolism of rat brain. *J. Neurochem.* 22, 717–724.

Pellerin, L., and Magistretti, P. J. (1994). Glutamate uptake into astrocytes stimulates aerobic glycolysis: a mechanism coupling neuronal activity to glucose utilization. *Proc. Natl. Acad. Sci. U.S.A.* 91, 10625–10629.

Rodrigues, T. B., and Cerdan, S. (2006). "The cerebral tricarboxylic acid cycles," in *Handbook of Neurochemistry and Molecular Neurobiology,* eds A. Lajtha, G. E. Gibson, and G. A. Dienel (Berlin: Springer-Verlag), 63–91.

Rothman, D. L., De Feyter, H. M., de Graaf, R. A., Mason, G. F., and Behar, K. L. (2011). $^{13}$C MRS studies of neuroenergetics and neurotransmitter cycling in humans. *NMR Biomed.* 24, 943–957.

Rothstein, J. D. (1996). Excitotoxicity hypothesis. *Neurology* 47(4 Suppl. 2), S19–S25.

Shank, R. P., Leo, G. C., and Zielke, H. R. (1993). Cerebral metabolic compartmentation as revealed by nuclear magnetic resonance analysis of D-[1-$^{13}$C]glucose metabolism. *J. Neurochem.* 61, 315–323.

Shen, J., Petersen, K. F., Behar, K. L., Brown, P., Nixon, T. W., Mason, G. F., et al. (1999). Determination of the rate of the glutamate / glutamine cycle in the human brain by in vivo 13C NMR. *Proc. Natl. Acad. Sci. U.S.A.* 96, 8235–8240.

Shen, J., and Rothman, D. L. (2002). Magnetic resonance spectroscopic approaches to studying neuronal: astroglial interactions. *Biol. Psychiatry* 52, 694–700.

Shen, J., Rothman, D. L., Behar, K. L., and Xu, S. (2009). Determination of the glutamate-glutamine cycling flux using two-compartment dynamic metabolic modeling is sensitive to astroglial dilution. *J. Cereb. Blood Flow Metab.* 29, 108–118.

Shen, J., Sibson, N. R., Cline, G., Behar, K. L., Rothman, D. L., and Shulman, R. G. (1998). $^{15}$N-NMR spectroscopy studies of ammonia transport and glutamine synthesis in the hyperammonemic rat brain. *Dev. Neurosci.* 20, 434–443.

Shestov, A. A., Valette, J., Deelchand, D. K., Ugurbil, K., and Henry, P. G. (2012). Metabolic modeling of dynamic brain 13C NMR multiplet data: concepts and simulations with a two-compartment neuronal-astroglial model. *Neurochem. Res.* 37, 2388–2401.

Shestov, A. A., Valette, J., Ugurbil, K., and Henry, P. G. (2007). On the reliability of $^{13}$C metabolic modeling with two-compartment neuronal-astroglial models. *J. Neurosci. Res.* 85, 3294–3303.

Sibson, N. R., Dhankhar, A., Mason, G. F., Behar, K. L., Rothman, D. L., and Shulman, R. G. (1997). *In vivo* $^{13}$C NMR measurements of cerebral glutamine synthesis as evidence for glutamate-glutamine cycling. *Proc. Natl. Acad. Sci. U.S.A.* 94, 2699–2704.

Sibson, N. R., Dhankhar, A., Mason, G. F., Rothman, D. L., Behar, K. L., and Shulman, R. G. (1998). Stoichiometric coupling of brain glucose metabolism and glutamatergic neuronal activity. *Proc. Natl. Acad. Sci. U.S.A.* 95, 316–321.

Sibson, N. R., Mason, G. F., Shen, J., Cline, G. W., Herskovits, A. Z., Wall, J. E., et al. (2001). *In vivo* $^{13}$C NMR measurement of neurotransmitter glutamate cycling, anaplerosis and TCA cycle flux in rat brain during [2-$^{13}$C]glucose infusion. *J. Neurochem.* 76, 975–989.

Siesjo, B. K. (1978). *Brain Energy Metabolism.* Chichester: John Wiley and Sons.

Sonnewald, U., Westergaard, N., Schousboe, A., Svendsen, J. S., Unsgård, G., and Petersen, S. B. (1993). Direct demonstration by [$^{13}$C]NMR spectroscopy that glutamine from astrocytes is a precursor for GABA synthesis in neurons. *Neurochem. Int.* 22, 19–29.

Tyson, R. L., Gallagher, C., and Sutherland, G. R. (2003). $^{13}$C-Labeled substrates and the cerebral metabolic compartmentalization of acetate and lactate. *Brain Res.* 992, 43–52.

von Mises, R. (Ed.). (1964). *Mathematical Theory of Probability and Statistics.* New York, NY: Academic Press

Waniewski, R. A., and Martin, D. L. (1998). Preferential utilization of acetate by astrocytes is attributable to transport. *J. Neurosci.* 18, 5225–5233.

Xiang, Y., and Shen, J. (2011a). Simultaneous detection of cerebral metabolism of different substrates by *in vivo* $^{13}$C isotopomer MRS. *J. Neurosci. Methods* 198, 8–15.

Xiang, Y., and Shen, J. (2011b). *In vivo* detection of intermediate metabolic products of [1-13C]ethanol in the brain using 13C MRS. *NMR Biomed.* 24, 1054–1062.

Yang, J., Xu, S., and Shen, J. (2009). Fast isotopic exchange between mitochondria and cytosol in brain revealed by relayed $^{13}$C magnetization transfer spectroscopy. *J. Cereb. Blood Flow Metab.* 29, 661–669.

**Conflict of Interest Statement:** The author declares that the research was conducted in the absence of any commercial or financial relationships that could be construed as a potential conflict of interest.

*Received: 22 November 2012; paper pending published: 08 December 2012; accepted: 08 January 2013; published online: 28 January 2013.*

*Citation: Shen J (2013) Modeling the glutamate–glutamine neurotransmitter cycle. Front. Neuroenerg.* ***5****:1. doi: 10.3389/fnene.2013.00001*

frontiers in
NEUROENERGETICS

ORIGINAL RESEARCH ARTICLE
published: 31 May 2013
doi: 10.3389/fnene.2013.00005

# Glucose and lactate metabolism in the awake and stimulated rat: a $^{13}$C-NMR study

***Denys Sampol[1†], Eugène Ostrofet[1†], Marie-Lise Jobin[1], Gérard Raffard[1], Stéphane Sanchez[1], Véronique Bouchaud[1], Jean-Michel Franconi[1], Gilles Bonvento[2] and Anne-Karine Bouzier-Sore[1]****

[1] *Centre de Résonance Magnétique des Systèmes Biologiques, CNRS-Université Bordeaux Segalen UMR 5536, Bordeaux, France*
[2] *Commissariat à l'Energie Atomique et aux Energies Alternatives, Département des Sciences du Vivant, Institut d'Imagerie Biomédicale, Molecular Imaging Research Center and CNRS CEA URA 2210, Fontenay-aux-Roses, France*

***Edited by:***
*Sebastian Cerdan, Instituto de Investigaciones Biomedicas Alberto Sols, Spain*

***Reviewed by:***
*Luc Pellerin, University of Lausanne, Switzerland*
*Sebastian Cerdan, Instituto de Investigaciones Biomedicas Alberto Sols, Spain*
*Ursula Sonnewald, Norwegian University of Science and Technology, Norway*

***Correspondence:**
*Anne-Karine Bouzier-Sore, Centre de Résonance Magnétique des Systèmes Biologiques, CNRS-Université Bordeaux Segalen UMR 5536, 146 rue Léo-Saignat, case 93, 33076 Bordeaux, France*
*e-mail: akb@rmsb.u-bordeaux2.fr*
*† These authors have contributed equally to this work.*

Glucose is the major energetic substrate for the brain but evidence has accumulated during the last 20 years that lactate produced by astrocytes could be an additional substrate for neurons. However, little information exists about this lactate shuttle *in vivo* in activated and awake animals. We designed an experiment in which the cortical barrel field (S1BF) was unilaterally activated during infusion of both glucose and lactate (alternatively labeled with $^{13}$C) in rats. At the end of stimulation (1 h) both S1BF areas were removed and analyzed by HR-MAS NMR spectroscopy to compare glucose and lactate metabolism in the activated area vs. the non-activated one. In combination with microwave irradiation HR-MAS spectroscopy is a powerful technical approach to study brain lactate metabolism *in vivo*. Using *in vivo* $^{14}$C-2-deoxyglucose and autoradiography we confirmed that whisker stimulation was effective since we observed a 40% increase in glucose uptake in the activated S1BF area compared to the ipsilateral one. We first determined that lactate observed on spectra of biopsies did not arise from post-mortem metabolism. $^{1}$H-NMR data indicated that during brain activation there was an average 2.4-fold increase in lactate content in the activated area. When [1-$^{13}$C]glucose + lactate were infused $^{13}$C-NMR data showed an increase in $^{13}$C-labeled lactate during brain activation as well as an increase in lactate C3-specific enrichment. This result demonstrates that the increase in lactate observed on $^{1}$H-NMR spectra originates from newly synthesized lactate from the labeled precursor ([1-$^{13}$C]glucose). It also shows that this additional lactate does not arise from an increase in blood lactate uptake since it would otherwise be unlabeled. These results are in favor of intracerebral lactate production during brain activation *in vivo* which could be a supplementary fuel for neurons.

**Keywords: $^{13}$C NMR spectroscopy, lactate, brain metabolism, neurons, astrocytes**

## INTRODUCTION

Glucose is the main blood substrate to provide energy to the central nervous system. However, alternative substrates other than glucose can be used by the brain. As early as 1991, two groups observed that during photic stimulation, a lactate peak was transiently observed in the human visual cortex using localized $^{1}$H-NMR spectroscopy, and that it disappeared in the dark (Prichard et al., 1991; Sappey-Marinier et al., 1992). Both concluded that this phenomenon could be due to a transient increase in glycolysis over respiration during stimulation. However, a more detailed explanation was given in 1994 with the observation that when primary astrocytes in culture are exposed to glutamate, they increase their glucose consumption and produce a significant amount of lactate that is released in the medium (Pellerin and Magistretti, 1994). An astrocyte-neuron lactate shuttle (ANLS) was proposed, a concept that describes a coupling mechanism between neuronal activity and glucose utilization and involving activation of aerobic glycolysis in astrocytes and lactate consumption by neurons. Several articles collecting experimental evidence as well as theoretical arguments in favor or against this model have been written (Bouzier-Sore et al., 2002; Chih and Roberts, 2003; Hertz, 2004; Bonvento et al., 2005; Pellerin et al., 2007; Dienel, 2012; Pellerin and Magistretti, 2012). More recently, another molecular pathway involving soluble adenylyl cyclase was proposed to play a role in this metabolic coupling between neurons and astrocytes (Choi et al., 2012). Whatever the mechanism to couple astrocyte and neuron metabolism, brain lactate has become an issue for debate among scientists in the last 15 years (Pellerin et al., 1998; Schurr and Rigor, 1998; Magistretti and Pellerin, 1999; Chih et al., 2001; Dienel and Hertz, 2001).

$^{13}$C-NMR spectroscopy is a powerful method to analyze brain metabolism and to study metabolic interactions between neurons and astrocytes. The first studies using NMR spectroscopy were performed *in vitro*. Neurons were incubated with various $^{13}$C-labeled substrates. When incubated with [1-$^{13}$C]glucose, the latter was shown to be an efficient substrate for the neurons (Cruz et al., 2001) and surprisingly to a lesser extent than astrocytes in

**Abbreviations:** TCA, tricarboxylic acid; EG, ethylene glycol; NAA, N-acetyl-L-aspartate; POCE, proton-observed $^{13}$C-editing.

another study (Leo et al., 1993). When neurons were incubated with [3-$^{13}$C]lactate, the latter was also shown to be an efficient substrate (Schousboe et al., 1997; Waagepetersen et al., 1998a,b). $^{13}$C-pyruvate (Brand et al., 1992; Cruz et al., 2001), $^{13}$C-aspartate (Bakken et al., 1998), and $^{13}$C-alanine (Zwingmann et al., 2000) have also proved to be neuronal substrates. For each experiment, the $^{13}$C of the labeled substrate was incorporated into different metabolites and amino acids, indicating that the labeled substrate was metabolized. Therefore, no clear difference was evidenced at that time between glucose and lactate metabolism in neuronal cultures. It seems that whatever the substrate present in the medium, the cell has no choice other than to adapt and to metabolize it, a well-known phenomenon. In response to these studies, a competition experiment between glucose and lactate was performed (Bouzier-Sore et al., 2003, 2006). Both glucose and lactate, which were alternatively $^{13}$C-labeled, were added to the culture neuronal medium, a much more physiological condition since both molecules are present in brain tissue. The results clearly indicated that lactate was preferentially used for the neuronal oxidative metabolism compared to glucose. Moreover, when injected intravenously to anesthetized rats, [3-$^{13}$C]lactate was found to be metabolized only in neurons (Bouzier et al., 2000; Hassel and Brathe, 2000). However, *in vitro* experiments do not reflect what occurs *in vivo*, and the latter-mentioned *in vivo* studies were performed on anesthetized animals, a situation not entirely reflecting the metabolism occurring during brain activation.

We designed an experiment where $^{13}$C-labeled substrate was infused in awake rats in which unilateral whisker stimulation was performed. This stimulation leads to activation of a local brain area called the barrel field or S1BF region, which is located in the somatosensory cortex. This protocol has two major advantages. First, the S1BF is a brain area in which the neuronal anatomy and circuitry are widely documented (Giaume et al., 2009). Neurons are arranged in clusters called barrels. Each barrel is an element of a functional column that spreads from layers II and III to layer IV and receives inputs from its corresponding whisker on the contralateral side of the rat face: one right whisker activates one left barrel. Since we performed unilateral stimulation, the second advantage was to obtain an internal control for each rat, i.e., the right S1BF at rest.

Using $^{14}$C-2-deoxyglucose, we first checked that whisker stimulation could be observed in the corresponding S1BF area. Then, awake rats were infused with either a [1-$^{13}$C]glucose + lactate, or a glucose + [3-$^{13}$C]lactate solution during stimulation. After a rapid euthanasia (less than 1 s) using microwaves focused on the brain, both left (activated) and right (rest) S1BF areas were dissected and further analyzed by $^{1}$H- and $^{13}$C-NMR spectroscopy.

## MATERIALS AND METHODS

### ANIMALS AND INFUSION TECHNIQUES

The experimental protocols used in this study were approved by appropriate institutional review committees, met the guidelines of the appropriate governmental agency and were performed by persons having their own animal experiment accreditation (authorization n°33 10 003).

#### *Infusion protocol*

Female Wistar rats (200 ± 10 g) were used in all experiments ($n = 14$). Animals were slightly held on a Plexiglas support during stimulation. Therefore, before infusion, each animal was accustomed to the experimental set-up (at least 3 times, 1 h) to reduce the stress of contention. Once rats were lying quietly, they were prepared for infusion. Right whiskers were mechanically stimulated at a rate of 5 Hz for 1 h. Infusions were performed in the tail vein for 1 h during whisker stimulation to reach the isotopic steady state. Rats were infused with a solution containing either [1-$^{13}$C]glucose (750 mM, Cambridge isotope, 99% enrichment) + lactate (534 mM) or glucose (750 mM) + [3-$^{13}$C]lactate (534 mM, Cambridge isotope, 98% enrichment). Intravenous infusions were carried out using a syringe pump that allows a flux such as glucose and lactate concentrations in the blood to remain constant. The infusate flow was monitored to obtain a time-decreasing exponential from 15 to 1.23 mL/h during the first 25 min, after which the rate was kept unchanged. At the end of the experiment, a sample of blood was removed. Rats were rapidly euthanized by cerebral-focused microwaves (5 KW, 1 s, Sacron8000, Sairem), the only way to immediately stop all enzymatic activities. This method avoids post-mortem artifacts such as anaerobic lactate production.

S1BF areas (right non-activated and left-activated) were dissected out using a rat brain matrix that allows precise and reproducible sampling of small brain regions, dipped in liquid nitrogen and kept at –80°C for further NMR analyses. Both activated and non-activated S1BF areas were analyzed by HR-MAS NMR spectroscopy on a Bruker Advance 500 MHz, directly on biopsies or after perchloric acid extracts. HR-MAS, high resolution at magic angle spinning, allowed spectra to be obtained directly on biopsies (50 µg) or on small perchloric acid extracts (50 µl). Moreover, the use of cerebral-focused microwaves is a method of choice since no post-mortem metabolism occurs (spectra were compared and lactate was quantified after either microwave, funnel freezing or decapitation under sodium pentobarbital overdose euthanasia).

#### *Blood kinetics*

During the 60-min infusion, blood samples (200–300 µL, femoral artery) were periodically collected (at $t = 0$, 5, 10, 20, 30, and 60 min) to determine glucose and lactate concentrations as well as glucose- and lactate-specific $^{13}$C-enrichments. Experiments were performed both on awake ($n = 4$) and anesthetized animals (intraperitoneal injection of chloral hydrate, 8%, 0.5 ml/100 g of body weight, $n = 4$).

### MEASUREMENT OF CEREBRAL GLUCOSE UPTAKE

Cerebral glucose uptake was measured as previously described (Cholet et al., 1997) using the ($^{14}$C)2-deoxyglucose autoradiographic technique (Sokoloff, 1981) during mechanical stimulation (5 Hz) of the right whiskers. Rats ($n = 2$) were habituated to rest quietly on a Plexiglas support. Tygon catheters were inserted into the femoral vein and artery under isoflurane anesthesia. One hour after recovery from anesthesia, rats were injected i.v. with a ($^{14}$C)2-deoxyglucose solution (125 µCi/100 g in 0.9 ml NaCL 0.9%) 5 min after initiation of whisker stimulation. Body temperature was monitored and maintained at 37.5°C during the

experiment. At the end of the 45-min period, the animal was euthanized by a rapid blood injection of sodium pentobarbital. The brain was immediately removed and frozen, and 20 μm-thick coronal sections were processed for autoradiography using $^{14}$C standards (ARC 146C).

### IMAGE ANALYSIS

Analysis of autoradiograms was performed using a computer-based image analysis system (MCID). The metabolic response to whisker stimulation was calculated as the ratio of the 2DG uptake measured in activated and resting S1BF.

### BRAIN PERCHLORIC ACID EXTRACTS

The frozen cerebral tissues were weighed (around 30 mg) and a volume of 1 mL of 0.9 M perchloric acid was added. Sonication was then performed (4°C), followed by centrifugation (5000 g, 15 min, 4°C). The supernatant was neutralized with KOH to pH = 7.2 and centrifuged once more to eliminate potassium perchlorate salts. Samples were lyophilized and dissolved in 100 μL $D_2O$ containing ethylene glycol (0.04 M, peak at 63 ppm).

### NMR SPECTROSCOPY

#### *$^1$H-NMR spectroscopy*

NMR spectra were obtained with a Bruker DPX500 spectrometer equipped with an HRMAS probe. $^1$H-NMR spectra were acquired at 4°C with 90° flip angle (measured for each sample), 8 s relaxation delay, 5000 Hz sweep width and 32 K memory size. Residual water signal was suppressed by homonuclear presaturation. The $^{13}$C-enrichment of lactate C3 and that of glucose C1 in rat sera and tissue extracts were determined from satellite peak areas resulting from the heteronuclear spin-coupling patterns on spectra.

#### *$^{13}$C-NMR spectroscopy*

Proton-decoupled $^{13}$C-NMR spectra were acquired overnight using 60° flip angle, 20 s relaxation delay, 25063 Hz sweep width and 64 K memory size. Measurements were conducted at 4°C under bi-level broadband gated proton decoupling and $D_2O$ lock. From these spectra, the $^{13}$C content at the different carbon positions of compounds was determined as previously described (Bouzier et al., 1999). Briefly, incorporation of $^{13}$C into the different carbons in glutamate, glutamine, GABA, alanine, aspartate and lactate were determined from integration of the observed resonances relative to the ethylene glycol peak (63 ppm, external reference, known amount). Perchloric acid extract spectra were normalized thanks to ethylene glycol and protein contents.

#### *Proton-observed carbon-editing (POCE) sequence*

A POCE sequence was used to determine the $^{13}$C-specific enrichment at selected metabolite carbon positions using the ($^{13}$C-$^1$H) heteronuclear multiquanta correlation (Freeman et al., 1981; Rothman et al., 1985). The sequence enabled the successive acquisitions of a first scan corresponding to a standard spin-echo experiment without any $^{13}$C excitation and a second scan involving a $^{13}$C inversion pulse allowing coherence transfer between coupled $^{13}$C and $^1$H nuclei. Subtraction of two alternate scans resulted in the editing of $^1$H spins coupled to $^{13}$C spins with a scalar coupling constant $J_{CH} = 127$ Hz. $^{13}$C decoupling during the acquisition collapsed the $^1$H-$^{13}$C coupling to a single $^1$H resonance. Flip angles for rectangular pulses were carefully calibrated on both radiofrequency channels before each experiment. The relaxation delay was 8 s for a complete longitudinal relaxation. The fractional $^{13}$C-enrichment was calculated as the ratio of the area of a given resonance on the edited $^{13}$C-$^1$H spectrum to its area on the standard spin-echo spectrum. The reproducibility and accuracy of the method were assessed using several mixtures of $^{13}$C-labeled amino acids and lactate with known fractional enrichments. Both were better than 5%.

### DETERMINATION OF PROTEINS, GLUCOSE AND LACTATE CONTENTS

Protein content was determined according to the procedure of Lowry et al. (1951) using bovine serum albumin as standard.

Blood glucose concentrations were determined by enzymatic assays using the coupled reactions of glucose oxidase and peroxidase. Blood lactate concentrations were determined using lactate dehydrogenase (Sigma).

### STATISTICAL ANALYSIS

Data are given as mean ± SD values. They were analyzed by Student's *t*-test or the paired *t*-test. The level of significance was set at $p < 0.05$.

## RESULTS

### BLOOD LACTATE AND GLUCOSE EVOLUTIONS DURING INFUSION

Blood samples were collected periodically during infusion to determine the time evolution of both glucose and lactate concentrations (**Figure 1A**) and variations in $^{13}$C-enrichments of lactate C3 and glucose C1 (**Figure 1B**). Experiments were conducted both on anesthetized and awake rats in order to compare the kinetics of substrates in both conditions. Blood concentrations of glucose and lactate seemed to be slightly higher in awake rats compared to anesthetized ones, but no statistical difference (except for glucose, time point 5 min) was found. During [1-$^{13}$C]glucose + lactate infusion, the specific $^{13}$C-enrichment of glucose C1 was lower in the awake animals (**Figure 1B**). A very small part of the [1-$^{13}$C]glucose was converted into [3-$^{13}$C]lactate in anesthetized rats (maximum value: 1.8% after 10 min), whereas this conversion was 4-fold greater in awake rats. During glucose + [3-$^{13}$C]lactate infusion, the specific $^{13}$C-enrichment of lactate C3 was also lower in awake rats (**Figure 1B**). The specific enrichment of glucose C1 increased very slowly with infusion time, and more significantly in awake rats. At the end of infusion, it was 3.9% in anesthetized rats and 6.4% in awake rats.

### VALIDATION OF WHISKER ACTIVATION

Functional activation was performed by stimulating the right whiskers (5 Hz, 45 min) in awake rats, which led to a significant increase (40 ± 2%) in cerebral glucose uptake in the left (activated) S1BF area compared to the right (rest) one (**Figure 2**). This result validated the stimulation protocol, which was then used during $^{13}$C-labeled substrate infusion in the next experiments. The same S1BF area were dissected and analyzed by NMR spectroscopy.

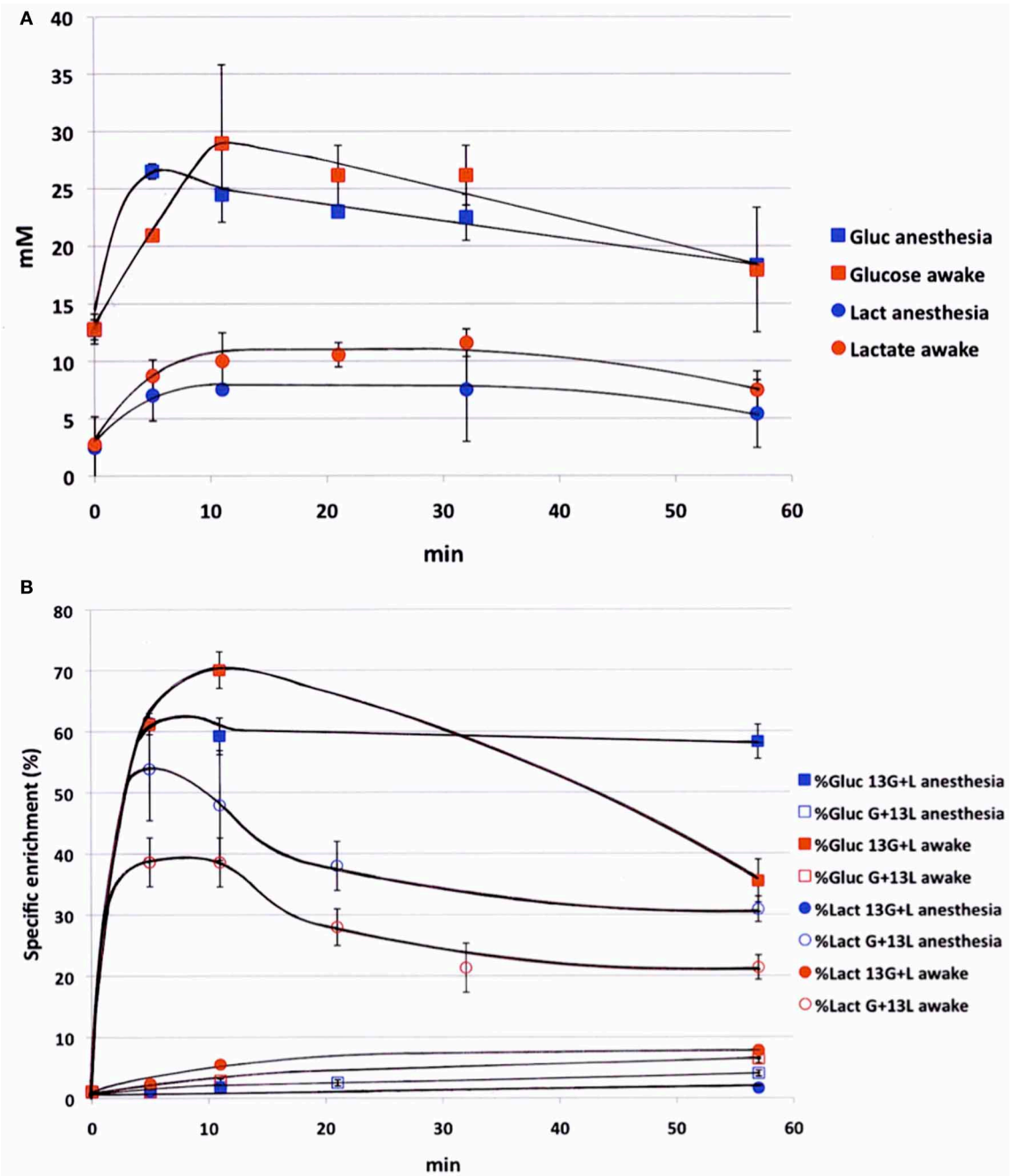


**FIGURE 1 | Time evolution of labeled glucose and lactate during infusion. (A)** Glucose (squares) and lactate (circles) concentrations (mM) were measured during infusion (glucose 750 mM and lactate 534 mM), both in anesthetized (blue) and awake (red) rats; $n = 4$. No statistical difference (except for glucose concentration, time point 5 min). **(B)** [1-$^{13}$C]glucose (squares) and [3-$^{13}$C]lactate (circles) specific enrichments (%) were measured during infusion with [1-$^{13}$C]glucose + lactate (filled dots, $n = 7$) or glucose + [3-$^{13}$C]lactate (open dots, $n = 7$), both in anesthetized (blue) and awake (red) rats. $p < 0.05$ between awake and anesthetized rats at the end of the infusion.

## COMPARISON OF $^{1}$H-NMR SPECTRA BETWEEN DIFFERENT SACRIFICE PROCEDURES

HRMAS $^{1}$H-NMR spectra of brain biopsies were compared with three methods of sacrifice: decapitation (**Figure 3A**), funnel freezing (**Figure 3B**) and rapid microwave fixation of the brain (**Figure 3C**). In all cases, brains were rapidly removed from the skull, dipped into liquid nitrogen and stored at −80°C before HRMAS analysis. Spectra were normalized to biopsy weights. Spectra clearly indicated that lactate peaks (red arrows) were the lowest after microwave fixation. There was a 19-fold increase in lactate content between the microwave and the decapitation biopsies, and a 2.2-fold increase between the microwave and the

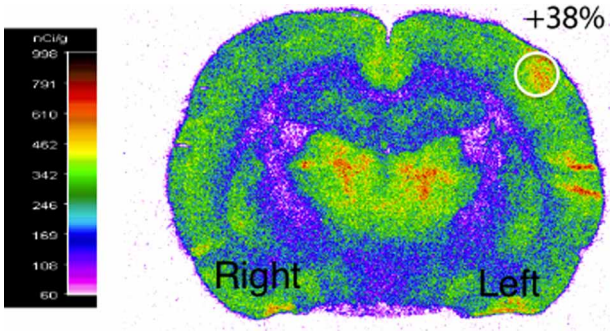


**FIGURE 2 | Functional activation of the brain during whisker stimulation.** Digitized, pseudocolored autoradiogram of the distribution of $^{14}$C-2-deoxyglucose uptake on representative brain section from awake and unilaterally stimulated rat. The region of interest is represented by the white circle.

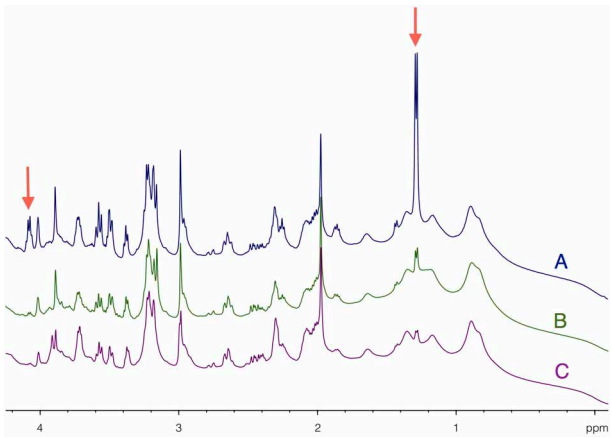


**FIGURE 3 | Determination of brain tissue lactate content as function of the sacrifice procedure.** HRMAS $^{1}$H-NMR spectra of brain biopsies rapidly removed after euthanasia by **(A)** decapitation, **(B)** funnel freezing, and **(C)** focused microwaves. Lactate can be detected on the spectra (red arrows) at 1.32 ppm (doublet, protons linked to carbon 3) and at 4.11 ppm (quadruplet, proton linked to carbon 2). Spectra were normalized thanks to biopsie weights and fumarate peak (6.9 ppm), added as an external reference.

funnel freezing biopsies. When fumarate was added as an external reference, lactate concentration was estimated to be around 1 mM in the microwave biopsy. This method of euthanasia is therefore required to prevent post-mortem metabolism, and thus anaerobic lactate production.

## COMPARISON OF $^{1}$H-NMR SPECTRA BETWEEN ACTIVATED AND REST AREAS

HRMAS $^{1}$H-NMR spectra of perchloric acid extracts of S1BF biopsies from microwave-treated brains are presented in **Figure 4**. Spectra were normalized to protein content on the ethylene glycol peak, added as an external reference. Lactate content was determined and the ratio between activation and rest was measured in each rat ($n = 14$). In 12 out of 14 rats, lactate content in the activated S1BF area increased compared to the rest one, the lowest ratio being 1.4 and the highest being 4.1. In the two other rats, no difference was observed (ratios were 0.95 and 0.99). The mean value of the ratio of lactate contents (activated area over rest area) was 2.4.

## $^{13}$C INCORPORATION INTO BRAIN METABOLITES IN ACTIVATED AND REST AREAS

The metabolism and fate of $^{13}$C from [1-$^{13}$C]glucose and [3-$^{13}$C]lactate is the same as both labeled substrates yields [3-$^{13}$C]pyruvate (for a scheme of the labeling, see (Bouzier et al., 1999; Bouzier-Sore et al., 2002, 2006)). However, since one mole of [1-$^{13}$C]glucose gives one mole of labeled [3-$^{13}$C]pyruvate and one mole of unlabeled pyruvate, there is an isotopic dilution of 50% when starting from [1-$^{13}$C]glucose, which is not the case when [3-$^{13}$C]lactate is the labeled substrate (one mole of [3-$^{13}$C]lactate gives one mole of [3-$^{13}$C]pyruvate). From [3-$^{13}$C]pyruvate, [3-$^{13}$C]alanine can be generated. [3-$^{13}$C]pyruvate enters the TCA cycle through two pathways: via the pyruvate dehydrogenase (PDH) or the pyruvate carboxylase (PC) route. According to the PDH pathway, [3-$^{13}$C]pyruvate is converted to [2-$^{13}$C]acetyl-CoA, which enters the TCA cycle to give [4-$^{13}$C]citrate. Within the first TCA cycle turn, the label is further transferred to α-[4-$^{13}$C]ketoglutarate and then to [2-$^{13}$C]- or [3-$^{13}$C]oxaloacetate. From α-[4-$^{13}$C]ketoglutarate, [4-$^{13}$C]glutamate and thereafter [4-$^{13}$C]glutamine and [2-$^{13}$C]GABA can be obtained, whereas [2-$^{13}$C]- or [3-$^{13}$C]oxaloacetate may give rise to [2-$^{13}$C]- or [3-$^{13}$C]aspartate. According to the PC pathway, which is present only in astrocytes (Norenberg and Martinez-Hernandez, 1979), [3-$^{13}$C]pyruvate is converted into [3-$^{13}$C]oxaloacetate, which enters the TCA cycle. Depending on the yield of cycling between oxaloacetate and fumarate, a fraction of the label can, however, be recovered as [2-$^{13}$C]oxaloacetate (Merle et al., 1996). At the next TCA cycle turn, the label entered by the PC route is mainly recovered as α-[2-$^{13}$C]ketoglutarate. From [3-$^{13}$C]oxaloacetate and α-[2-$^{13}$C]ketoglutarate, [3-$^{13}$C]aspartate, [2-$^{13}$C]glutamate and thereafter [2-$^{13}$C]glutamine are then principally formed.

Both [1-$^{13}$C]glucose + lactate and glucose + [3-$^{13}$C]lactate infusions induced the labeling of brain amino acids and lactate, as illustrated in the $^{13}$C-NMR spectra shown in **Figure 5**. These spectra were acquired on perchloric acid extracts of rest areas (**Figures 5A,C**) or activated areas (**Figures 5B,D**) after either a 1 h-infusion with glucose + [3-$^{13}$C]lactate (**Figures 5A,B**) or with [1-$^{13}$C]glucose + lactate (**Figures 5C,D**). Relative peak intensities and coupling figures were lower when glucose + [3-$^{13}$C]lactate were infused than in the [1-$^{13}$C]glucose + lactate condition, indicating a lower $^{13}$C incorporation. The lactate C3 peak was much higher in the activated area compared to the rest one in the [1-$^{13}$C]glucose + lactate condition, whereas this increase was much lower in the glucose + [3-$^{13}$C]lactate condition.

The specific enrichments of selected amino acid carbons were determined from spectra acquired with the POCE sequence. The values are reported in **Table 1**. Specific enrichment values were much higher in the [1-$^{13}$C]glucose + lactate condition compared to the one measured after glucose + [3-$^{13}$C]lactate infusion. In the latter condition, specific enrichments were indeed very low (natural abundance, 1.1%, was not subtracted). However,

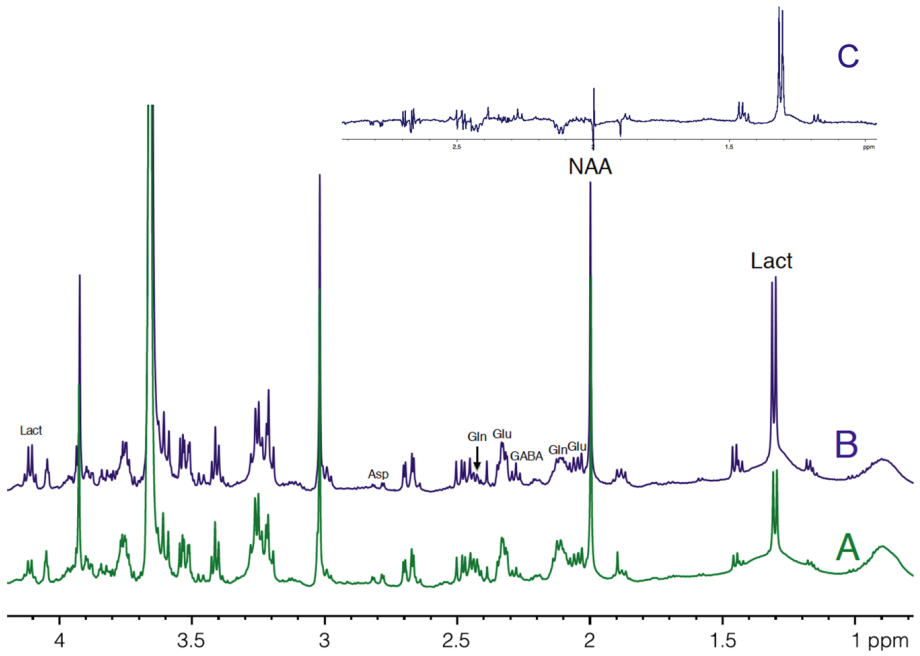


**FIGURE 4 | HRMAS $^{1}$H-NMR spectra of perchloric acid extracts of rest (A) and activated (B) S1BF areas.** Spectra were obtained from rat n°5, in which ratio of lactate between rest **(A)** and activated **(B)** S1BF was 2.6, representing the closer the mean ratio in the 14 rats. The difference between the two spectra is presented in **(C)**. Ethylen glycol was added as an internal reference. Lact, lactate; NAA, N-acetyl-aspartate; Glu, glutamate; Gln, glutamine; Asp, aspartate.

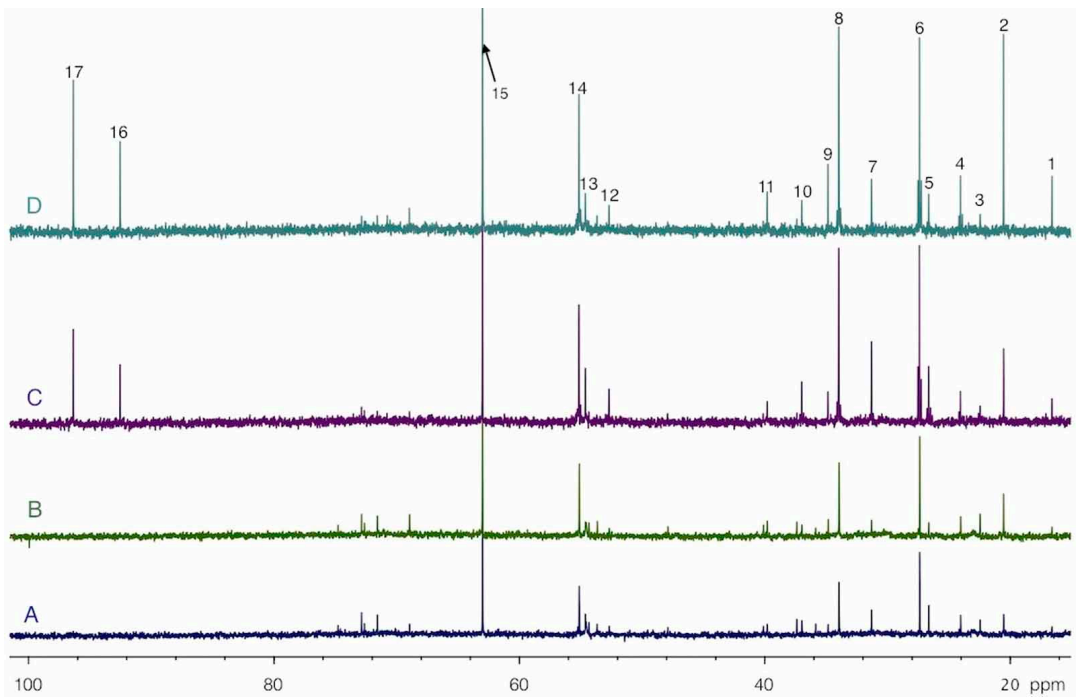


**FIGURE 5 | HRMAS $^{13}$C-NMR spectra of perchloric acid extracts of rest (A and C) and activated (B and D) S1BF areas, after infusion with glucose + [3-$^{13}$C]lactate (A and B) or [1-$^{13}$C]glucose + lactate (C and D).** Spectra were normalized owing to their protein contents and to the EG peak (15, 63 ppm). Peak assignments: 1: alanine C3, 2: lactate C3, 3: NAA C6, 4: GABA C3, 5: glutamine C3, 6: glutamate C3, 7: glutamine C4, 8: glutamate C4, 9: GABA C2, 10: aspartate C3, 11: GABA C4, 12: aspartate C2, 13: glutamine C2, 14: glutamate C2, 15: EG, 16: glucose C1α, 17: glucose C1β.

we found a statistical decrease in lactate C3-specific enrichment between rest and activated areas. After [1-13C]glucose + lactate infusion, lactate and alanine C3-specific enrichments were higher in the activated area compared to the rest one, whereas the opposite was found for glutamine C4.

The enrichments of the different carbons within glutamate and glutamine were evaluated relatively to carbon 4, the most labeled carbon (**Table 2**). In the [1-13C]glucose + lactate condition, no difference was found between glutamate C2 and C3 both at rest and during activation, whereas glutamine C2 was more enriched than C3, reflecting the PC activity, which is present only in astrocytes. In the glucose + [3-13C]lactate condition, no further difference between glutamine C2 and C3 could be evidenced, as shown previously (Bouzier et al., 2000), and indicating that [3-13C]lactate is more a neuronal substrate (no PC activity).

**Table 1 | Specific enrichments (%) of some carbon positions of brain metabolites, after infusion of [1-13C]glucose + lactate ($^{13}$G + L) or glucose + [3-13C]lactate (G + $^{13}$L).**

| | Specific enrichments (%) | | | |
|---|---|---|---|---|
| | $^{13}$G + L | | G + $^{13}$L | |
| | Rest | Activated | Rest | Activated |
| Lact C3 | 10.2 ± 0.4 | 13.5 ± 2.9* | 3.2 ± 0.8 | 2.7 ± 0.8* |
| Glu C4 | 19.1 ± 1.2 | 18.5 ± 2.4 | 4.0 ± 1.0 | 4.1 ± 0.9 |
| Asp C3 | 15.5 ± 1.3 | 15.4 ± 3.0 | 2.6 ± 0.3 | 3.0 ± 1.3 |
| GABA C2 | 18.3 ± 0.5 | 17.7 ± 1.1 | 2.6 ± 0.4 | 2.9 ± 0.3 |
| Gln C4 | 14.2 ± 1.1 | 11.4 ± 2.6* | 3.5 ± 0.9 | 3.6 ± 1.0 |
| Ala C3 | 15.5 ± 1.5 | 16.9 ± 0.6* | 3.8 ± 1.1 | 3.4 ± 0.9 |

*$p < 0.03$ between rest and activation, paired t-test.*

**Table 2 | Relative enrichments of glutamate and glutamine, after infusion of [1-13C]glucose + lactate ($^{13}$G + L) or glucose + [3-13C]lactate (G + $^{13}$L).**

| | Relative enrichments | | | |
|---|---|---|---|---|
| | Glu | | Gln | |
| | Rest | Activated | Rest | Activated |
| **$^{13}$G + L** | | | | |
| C4 | 1 | 1 | 1 | 1 |
| C2 | 0.72 ± 0.04 | 0.76 ± 0.04 | 0.81 ± 0.07 | 0.86 ± 0.07 |
| C3 | 0.75 ± 0.02 | 0.76 ± 0.05 | 0.63 ± 0.04# | 0.70 ± 0.06# |
| **C2/C3** | **0.96 ± 0.03** | **0.99 ± 0.05** | **1.28 ± 0.07°** | **1.24 ± 0.07°** |
| **G + $^{13}$L** | | | | |
| C4 | 1 | 1 | 1 | 1 |
| C2 | 0.95 ± 0.08 | 0.87 ± 0.10 | 0.91 ± 0.16 | 0.65 ± 0.20 |
| C3 | 1.02 ± 0.16 | 0.92 ± 0.12 | 0.95 ± 0.08 | 0.68 ± 0.05 |
| **C2/C3** | **0.93 ± 0.12** | **0.95 ± 0.11** | **0.96 ± 0.12*** | **0.95 ± 0.13*** |

*Enrichments of carbon 2 and 3 were measured relative to the most enriched carbon, which is carbon 4. #$p < 0.05$ between C3 and C2; °$p < 0.05$ between Glu and Gln C2/C3 ratios; *$p < 0.05$ between $^{13}$G + L and G + $^{13}$L infusions. The ratio C2/C3 (in bold) was then calculated and reflects the contribution of the pyruvate carboxylase (when PC activity is present, C2/C3 > 1).*

### CORRELATION BETWEEN LACTATE CONCENTRATION AND LACTATE C3-SPECIFIC ENRICHMENT INCREASES DURING BRAIN ACTIVATION

To our knowledge, this study is the first in which 13C-labeled substrate infusion was performed in awake and stimulated rats. This protocol was used to mimic physiological states as closely as possible. However, since the rats were awake, they were able to move their heads freely, leading to inter-individual variations. It was thus interesting to compare results obtained for each independent experiment (**Figure 6**). When infused with [1-13C]glucose + lactate, 6 out of 7 rats demonstrated an increase in lactate C3-specific enrichment. When infused with glucose + [3-13C]lactate, all rats underwent a decrease in lactate C3-specific enrichment, even if the enrichment values were low.

Interestingly, we found a correlation ($r^2 = 0.86$) between the increase in lactate concentration during activation (measured on 1H-NMR spectra and reflecting the total lactate content in the barrel field biopsy, at rest or activated) and the increase in lactate C3-specific enrichment measured between rest and activated states (when [1-13C]glucose + lactate was infused).

## DISCUSSION

The time course of glucose and lactate concentrations and that of glucose C1 and lactate C3 13C-enrichments (**Figure 1**) emphasize the intricate glucose-lactate metabolic relationship already shown in a previous study (Bouzier et al., 2000) and demonstrated here to be even more complex when rats are awake. Results indicated an active blood lactate metabolism, as already reported (Jenkins et al., 1993), and a recycling attributed to liver gluconeogenesis, which was greater in awake than in anesthetized rats. However, this conversion is minimized by the addition of glucose in the [3-13C]lactate infusion solution (Bouzier et al., 2000). In parallel, blood glucose can also be converted into lactate, as confirmed by the higher lactate concentration in awake rats than in anesthetized ones, as well as by the specific evolution in enrichment of [3-13C]lactate, i.e., an increase after [1-13C]glucose + lactate infusion and a decrease in the glucose + [3-13C]lactate condition. Therefore, working with awake and stimulated animals modifies glucose and lactate blood kinetics. However, in both infusion conditions, we were able to measure specific enrichment values and to find statistical differences between rest and stimulated S1BF in awake animals.

1H-NMR spectra showed a mean 2.4-fold increase in lactate content during brain activation. This lactate increase has already been observed in human visual cortex during photic stimulation using localized 1H-NMR spectroscopy (Prichard et al., 1991; Sappey-Marinier et al., 1992; Mangia et al., 2007) as well as in rats using microdialysis (Caesar et al., 2008). In the present study, the brain irradiation using focused microwaves was a key element. Indeed, **Figure 3** clearly shows that the lactate detected on our 1H-NMR spectra was the physiologic lactate present in brain tissue and was not that arising from post-mortem or anaerobic glycolysis. Note that the funnel freezing technique, the classical euthanasia procedure when studying brain metabolism, induced a 2.2-fold increase in lactate content compared to microwave irradiation. The lactate concentration in brain tissue relative to the NAA peak was found to be around 1 mM in the absence of activation, a value in accordance with data obtained either by

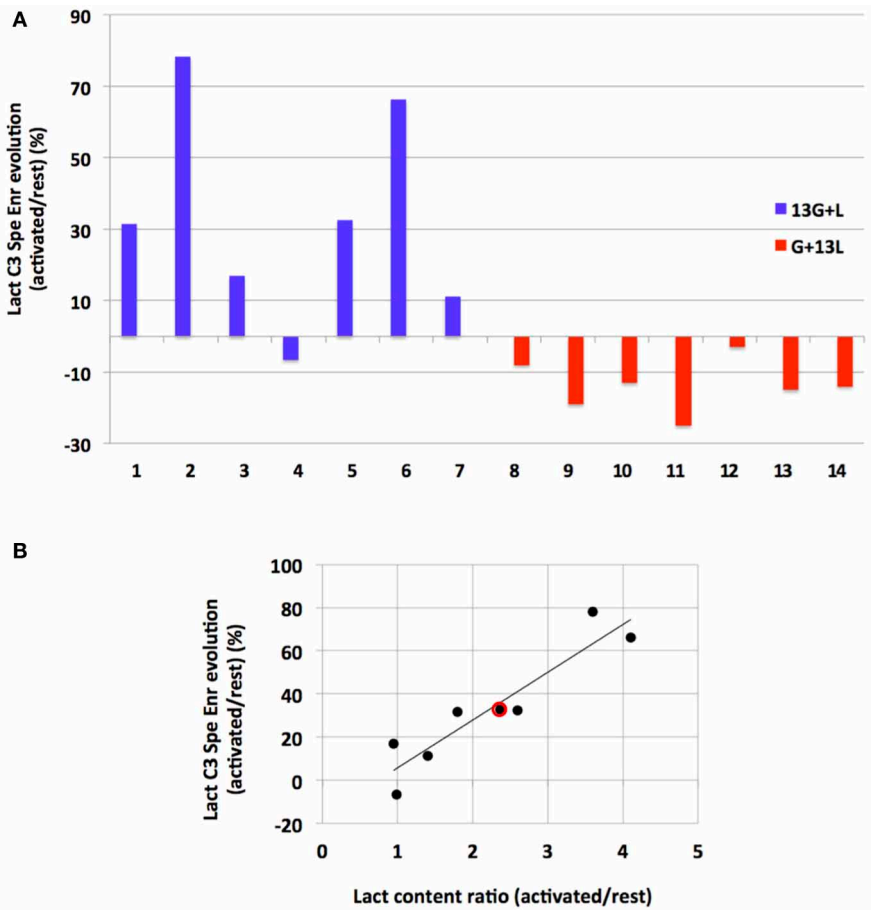


**FIGURE 6 | Evolution of lactate C3 specific enrichment for each rat (A) and correlation between its evolution and lactate content during activation (B). (A)** Evolutions of lactate C3 specific enrichment (activated over rest, %) are presented for each independent experiment after infusion with [1-$^{13}$C]glucose+lactate ($n = 7$, rat 1 to rat 7, blue) or with glucose + [3-$^{13}$C]lactate ($n = 7$, rat 8–14, red). **(B)** Linear regression between lactate concentration increase (ratio between lactate content measured in the activated S1BF and the one measured in the rest S1BF on $^{1}$H-NMR spectra) and lactate C3 specific enrichment increases (values in **A**, blue) for the [1-$^{13}$C]glucose + lactate condition (rat 1–7). Red dot represents the mean values in this latter condition (a 2.4-fold increase in the lactate content, and a 33% increase in lactate C3 specific enrichments). $r^2 = 0.86$.

microdialysis or NMR spectroscopy (Prichard et al., 1991; Fellows et al., 1992; Abi-Saab et al., 2002).

$^{13}$C-NMR spectra (**Figure 5**) indicate that the $^{13}$C-labeled substrate entered the brain and was metabolized in both infusion conditions. $^{13}$C was incorporated into amino acids such as glutamine, glutamate, alanine, aspartate and GABA. However, this incorporation was much lower when [3-$^{13}$C]lactate was the labeled substrate, leading to low specific enrichment values. Even under such conditions, variations between rest and activated states were statistically observed for lactate C3-specific enrichments. When resting and activated states were compared for each independent experiment (**Figure 6**), an increase in lactate C3-specific enrichment was observed in 6 out of 7 rats infused with [1-$^{13}$C]glucose + lactate, as well as a decrease in all rats infused with glucose + [3-$^{13}$C]lactate. This result indicates that during brain activation, glucose uptake increases (as confirmed by the 2-DG experiment), as well as endogenous lactate synthesis. When glucose is $^{13}$C-labeled, lactate C3-specific enrichment also increases. When unlabeled glucose + [3-$^{13}$C]lactate is infused, the same occurs: glucose uptake and lactate production increase. However, since the glucose is unlabeled, unlabeled lactate is synthesized and leads to the isotopic dilution of the [3-$^{13}$C]lactate also present in the infusion solution.

This study was performed in awake rats, so inter-individual variations were to be expected. Even though barrel fields can be activated in anesthetized animals (Castro-Alamancos, 2004; Krupa et al., 2004; Chakrabarti and Alloway, 2009), we wanted to avoid any modification in brain metabolism due to anesthetics. This inter-individual variation could be accounted for by more or less efficient whisker activation. Indeed, rats were awake and able to freely move their heads, even if restrained. The quieter the rat, the more whiskers were stimulated. Interestingly, a correlation between lactate concentration increase (measured on $^{1}$H-NMR spectra and reflecting the total lactate content in the biopsy containing the barrel field) and changes in lactate C3-specific enrichments between rest and activated states (when [1-$^{13}$C]glucose + lactate was infused) was obtained, confirming that the lactate appearing in the barrel field during brain activation

originated from [1-$^{13}$C]glucose breakdown ($r^2 = 0.86$) in an activity-dependent manner, as already proposed (Wyss et al., 2011).

When glucose + [3-$^{13}$C]lactate were the substrates, we also observed a higher lactate C3 peak on the $^{13}$C-NMR spectrum in the activated S1BF, even if this increase was much lower than in the [1-$^{13}$C]glucose + lactate condition. This was due to a combination of an increase in total lactate content and a decrease in lactate C3-specific enrichment, fewer lactate molecules being $^{13}$C-labeled. This confirms that lactate newly synthesized during brain activation arises from glucose (unlabeled in this case).

Like lactate C3, alanine C3-specific enrichment increased during brain activation under the condition [1-$^{13}$C]glucose + lactate infusion, which is not surprising as both metabolites are at the same metabolic node linked to pyruvate. On the contrary, glutamine C4-specific enrichment decreased during activation. This indicates that during whisker stimulation, the $^{13}$C arising from glucose, which ends up in [3-$^{13}$C]pyruvate at the end of the glycolysis, is less incorporated into the astrocytic TCA cycle and more probably converted into lactate by lactate dehydrogenase.

Concerning the relative enrichments, a difference in $^{13}$C-incorporation into glutamine carbon 2 and 3 is always detected after [1-$^{13}$C]glucose infusion, thus reflecting the PC activity present only in astrocytes (Norenberg and Martinez-Hernandez, 1979). This astrocytic enzyme leads to a higher enrichment of carbon 2 compared to carbon 3 (**Table 1**, Gln, $^{13}$G + L) (Bouzier et al., 1999). This imbalance disappears (**Table 1**, Gln, $^{13}$G + L compared to G + $^{13}$L) when lactate is the $^{13}$C-labeled substrate. No further difference in glutamine carbon 2 and 3 was detected. The absence of a higher $^{13}$C incorporation in glutamine carbon 2 compared to carbon 3 when [3-$^{13}$C]lactate is the labeled substrate reflects its metabolism in a PC-deprived compartment, i.e., in neurons. This specificity of lactate to be a neuronal substrate was already shown after [3-$^{13}$C]lactate infusion in anesthetized rats (Bouzier et al., 2000) and in humans (Boumezbeur et al., 2010). In another study where [3-$^{13}$C]lactate was administered in awake rats, the authors concluded that it enters the glutamatergic neurons preferentially (Qu et al., 2000).

The fact that lactate levels reliably increase with the onset of brain activation implies that regional glycolysis exceeds lactate utilization and/or clearance. Several *in vivo* studies using microdialysis (Caesar et al., 2008) or MRS (Mangia et al., 2007) have also shown an increase in lactate level that persists during the activation period, and not only during the first phase of brain activation. In our study, the whiskers were stimulated for 1 h, so it may be argued that a new higher steady state of lactate concentration is achieved during such sustained activation. This new steady state suggests that, in addition to being an energetic substrate, lactate could also have another role such as regulator of the cerebral blood flow (Mintun et al., 2004; Gordon et al., 2008). Indeed, in the latter studies, lactate was proposed to facilitate vasodilatation and increase cerebral blood flow. Recently, lactate was also suggested to act as a mediator of metabolic information for synapses (Bergersen and Gjedde, 2012).

The present findings clearly show that during brain activation, there is an increase in glucose uptake, an increase in glucose consumption and an increase in the production of lactate newly synthesized from blood glucose in the activated area. However, we were unable to determine in which compartment this metabolic conversion occurs; in astrocytes, as proposed by the ANLSH, or in neurons, as suggested by others in studies based on *in vitro* experiments (Bak et al., 2006). Nevertheless, in another study where the same whisker-to-barrel system was studied using a different approach (Voutsinos-Porche et al., 2003), the authors used 2DG autoradiography to establish that the enhanced glucose uptake during activation is dependent on the glutamate uptake occurring in astrocytes. More recently, Chuquet et al. (2010) using a fluorescent analog of 2DG and two-photon microscopy showed that the enhancement of glucose uptake in the barrel cortex upon whisker stimulation takes place essentially in the astrocytes. Combined with these previous findings, our results support the idea of a metabolic cooperation between the different cell types in the brain, i.e., astrocytes and neurons, the former becoming more glycolytic and the latter more oxidative during brain activation. Such metabolic interaction between neighboring cells is not unique as it has also been observed between different muscle fiber types (Brooks, 2009). Even if glucose is the main energetic substrate in adult mammals, lactate can no longer be considered as a metabolic end product but rather as a complementary and efficient substrate synthesized by one cellular type to supply energy to its neighbor.

## ACKNOWLEDGMENTS

This study was supported by a public grant from the French "Agence Nationale de la Recherche" within the context of the Investments for the Future Program, referenced ANR-10-LABX-57 and named TRAIL.

## REFERENCES

Abi-Saab, W. M., Maggs, D. G., Jones, T., Jacob, R., Srihari, V., Thompson, J., et al. (2002). Striking differences in glucose and lactate levels between brain extracellular fluid and plasma in conscious human subjects: effects of hyperglycemia and hypoglycemia. *J. Cereb. Blood Flow Metab.* 22, 271–279. doi: 10.1097/00004647-200203000-00004

Bak, L. K., Schousboe, A., Sonnewald, U., and Waagepetersen, H. S. (2006). Glucose is necessary to maintain neurotransmitter homeostasis during synaptic activity in cultured glutamatergic neurons. *J. Cereb. Blood Flow Metab.* 26, 1285–1297. doi: 10.1038/sj.jcbfm.9600281

Bakken, I. J., White, L. R., Aasly, J., Unsgard, G., and Sonnewald, U. (1998). [U-13C] aspartate metabolism in cultured cortical astrocytes and cerebellar granule neurons studied by NMR spectroscopy. *Glia* 23, 271–277. doi: 10.1002/(SICI)1098-1136(199807)23:3<271::AID-GLIA9>3.0.CO;2-7

Bergersen, L. H., and Gjedde, A. (2012). Is lactate a volume transmitter of metabolic states of the brain? *Front. Neuroenergetics* 4:5. doi: 10.3389/fnene.2012.00005

Bonvento, G., Herard, A. S., and Voutsinos-Porche, B. (2005). The astrocyte–neuron lactate shuttle: a debated but still valuable hypothesis for brain imaging. *J. Cereb. Blood Flow Metab.* 25, 1394–1399. doi: 10.1038/sj.jcbfm.9600127

Boumezbeur, F., Petersen, K. F., Cline, G. W., Mason, G. F., Behar, K. L., Shulman, G. I., et al. (2010). The contribution of blood lactate to brain energy metabolism in humans measured by dynamic 13C nuclear magnetic resonance spectroscopy. *J. Neurosci.* 30, 13983–13991. doi: 10.1523/JNEUROSCI.2040-10.2010

Bouzier, A. K., Quesson, B., Valeins, H., Canioni, P., and Merle, M. (1999). [1-(13)C]glucose metabolism in

the tumoral and nontumoral cerebral tissue of a glioma-bearing rat. *J. Neurochem.* 72, 2445–2455. doi: 10.1046/j.1471-4159.1999.0722445.x

Bouzier, A. K., Thiaudiere, E., Biran, M., Rouland, R., Canioni, P., and Merle, M. (2000). The metabolism of [3-(13)C]lactate in the rat brain is specific of a pyruvate carboxylase-deprived compartment. *J. Neurochem.* 75, 480–486. doi: 10.1046/j.1471-4159.2000.0750480.x

Bouzier-Sore, A. K., Merle, M., Magistretti, P. J., and Pellerin, L. (2002). Feeding active neurons: (re)emergence of a nursing role for astrocytes. *J. Physiol. Paris* 96, 273–282. doi: 10.1016/S0928-4257(02)00016-5

Bouzier-Sore, A. K., Voisin, P., Bouchaud, V., Bezancon, E., Franconi, J. M., and Pellerin, L. (2006). Competition between glucose and lactate as oxidative energy substrates in both neurons and astrocytes: a comparative NMR study. *Eur. J. Neurosci.* 24, 1687–1694. doi: 10.1111/j.1460-9568.2006.05056.x

Bouzier-Sore, A. K., Voisin, P., Canioni, P., Magistretti, P. J., and Pellerin, L. (2003). Lactate is a preferential oxidative energy substrate over glucose for neurons in culture. *J. Cereb. Blood Flow Metab.* 23, 1298–1306. doi: 10.1097/01.WCB.0000091761.61714.25

Brand, A., Engelmann, J., and Leibfritz, D. (1992). A 13C NMR study on fluxes into the TCA cycle of neuronal and glial tumor cell lines and primary cells. *Biochimie* 74, 941–948. doi: 10.1016/0300-9084(92)90078-S

Brooks, G. A. (2009). Cell-cell and intracellular lactate shuttles. *J. Physiol.* 587, 5591–5600. doi: 10.1113/jphysiol.2009.178350

Caesar, K., Hashemi, P., Douhou, A., Bonvento, G., Boutelle, M. G., Walls, A. B., et al. (2008). Glutamate receptor-dependent increments in lactate, glucose and oxygen metabolism evoked in rat cerebellum *in vivo*. *J. Physiol.* 586, 1337–1349. doi: 10.1113/jphysiol.2007.144154

Castro-Alamancos, M. A. (2004). Absence of rapid sensory adaptation in neocortex during information processing states. *Neuron* 41, 455–464. doi: 10.1016/S0896-6273(03)00853-5

Chakrabarti, S., and Alloway, K. D. (2009). Differential response patterns in the si barrel and septal compartments during mechanical whisker stimulation. *J. Neurophysiol.* 102, 1632–1646. doi: 10.1152/jn.91120.2008

Chih, C. P., Lipton, P., and Roberts, E. L. Jr. (2001). Do active cerebral neurons really use lactate rather than glucose? *Trends Neurosci.* 24, 573–578. doi: 10.1016/S0166-2236(00)01920-2

Chih, C. P., and Roberts, E. L. Jr. (2003). Energy substrates for neurons during neural activity: a critical review of the astrocyte-neuron lactate shuttle hypothesis. *J. Cereb. Blood Flow Metab.* 23, 1263–1281. doi: 10.1097/01.WCB.0000081369.51727.6F

Choi, H. B., Gordon, G. R., Zhou, N., Tai, C., Rungta, R. L., Martinez, J., et al. (2012). Metabolic communication between astrocytes and neurons via bicarbonate-responsive soluble adenylyl cyclase. *Neuron* 75, 1094–1104. doi: 10.1016/j.neuron.2012.08.032

Cholet, N., Seylaz, J., Lacombe, P., and Bonvento, G. (1997). Local uncoupling of the cerebrovascular and metabolic responses to somatosensory stimulation after neuronal nitric oxide synthase inhibition. *J. Cereb. Blood Flow Metab.* 17, 1191–1201. doi: 10.1097/00004647-199711000-00008

Chuquet, J., Quilichini, P., Nimchinsky, E. A., and Buzsaki, G. (2010). Predominant enhancement of glucose uptake in astrocytes versus neurons during activation of the somatosensory cortex. *J. Neurosci.* 30, 15298–15303. doi: 10.1523/JNEUROSCI.0762-10.2010

Cruz, F., Villalba, M., Garcia-Espinosa, M. A., Ballesteros, P., Bogonez, E., Satrustegui, J., et al. (2001). Intracellular compartmentation of pyruvate in primary cultures of cortical neurons as detected by (13)C NMR spectroscopy with multiple (13)C labels. *J. Neurosci. Res.* 66, 771–781. doi: 10.1002/jnr.10048

Dienel, G. A. (2012). Fueling and imaging brain activation. *ASN Neuro.* 4, 267–321. doi: 10.1042/AN20120021

Dienel, G. A., and Hertz, L. (2001). Glucose and lactate metabolism during brain activation. *J. Neurosci. Res.* 66, 824–838. doi: 10.1002/jnr.10079

Fellows, L. K., Boutelle, M. G., and Fillenz, M. (1992). Extracellular brain glucose levels reflect local neuronal activity: a microdialysis study in awake, freely moving rats. *J. Neurochem.* 59, 2141–2147.

Freeman, R., Mareci, T. H., and Morris, G. A. (1981). Weak satellite signals in high-resolution NMR spectra: separating the wheat from the chaff. *J. Magn. Reson.* 42, 341–345.

Giaume, C., Maravall, M., Welker, E., and Bonvento, G. (2009). The barrel cortex as a model to study dynamic neuroglial interaction. *Neuroscientist* 15, 351–366. doi: 10.1177/1073858409336092

Gordon, G. R., Choi, H. B., Rungta, R. L., Ellis-Davies, G. C., and MacVicar, B. A. (2008). Brain metabolism dictates the polarity of astrocyte control over arterioles. *Nature* 456, 745–749. doi: 10.1038/nature07525

Hassel, B., and Brathe, A. (2000). Cerebral metabolism of lactate *in vivo*: evidence for neuronal pyruvate carboxylation. *J. Cereb. Blood Flow Metab.* 20, 327–336. doi: 10.1097/00004647-200002000-00014

Hertz, L. (2004). The astrocyte-neuron lactate shuttle: a challenge of a challenge. *J. Cereb. Blood Flow Metab.* 24, 1241–1248. doi: 10.1097/00004647-200411000-00008

Jenkins, B. G., Koroshetz, W. J., Beal, M. F., and Rosen, B. R. (1993). Evidence for impairment of energy metabolism *in vivo* in Huntington's disease using localized 1H NMR spectroscopy. *Neurology* 43, 2689–2695.

Krupa, D. J., Wiest, M. C., Shuler, M. G., Laubach, M., and Nicolelis, M. A. (2004). Layer-specific somatosensory cortical activation during active tactile discrimination. *Science* 304, 1989–1992. doi: 10.1126/science.1093318

Leo, G. C., Driscoll, B. F., Shank, R. P., and Kaufman, E. (1993). Analysis of [1-13C]D-glucose metabolism in cultured astrocytes and neurons using nuclear magnetic resonance spectroscopy. *Dev. Neurosci.* 15, 282–288.

Lowry, O. H., Rosenbrough, N. J., Farr, A. L., and Randall, R. J. (1951). Protein measurement with the folin phenol reagent. *J. Biol. Chem.* 193, 265–275.

Magistretti, P. J., and Pellerin, L. (1999). Cellular mechanisms of brain energy metabolism and their relevance to functional brain imaging. *Philos. Trans. R. Soc. Lond. B Biol. Sci.* 354, 1155–1163. doi: 10.1098/rstb.1999.0471

Mangia, S., Tkac, I., Gruetter, R., Van de Moortele, P. F., Maraviglia, B., and Ugurbil, K. (2007). Sustained neuronal activation raises oxidative metabolism to a new steady-state level: evidence from 1H NMR spectroscopy in the human visual cortex. *J. Cereb. Blood Flow Metab.* 27, 1055–1063. doi: 10.1038/sj.jcbfm.9600401

Merle, M., Martin, M., Villegier, A., and Canioni, P. (1996). Mathematical modelling of the citric acid cycle for the analysis of glutamine isotopomers from cerebellar astrocytes incubated with [1(- 13)C]glucose. *Eur. J. Biochem.* 239, 742–751. doi: 10.1111/j.1432-1033.1996.0742u.x

Mintun, M. A., Vlassenko, A. G., Rundle, M. M., and Raichle, M. E. (2004). Increased lactate/pyruvate ratio augments blood flow in physiologically activated human brain. *Proc. Natl. Acad. Sci. U.S.A.* 101, 659–664. doi: 10.1073/pnas.0307457100

Norenberg, M. D., and Martinez-Hernandez, A. (1979). Fine structural localization of glutamine synthetase in astrocytes of rat brain. *Brain Res.* 161, 303–310. doi: 10.1016/0006-8993(79)90071-4

Pellerin, L., Bouzier-Sore, A. K., Aubert, A., Serres, S., Merle, M., Costalat, R., et al. (2007). Activity-dependent regulation of energy metabolism by astrocytes: an update. *Glia* 55, 1251–1262. doi: 10.1002/glia.20528

Pellerin, L., and Magistretti, P. J. (1994). Glutamate uptake into astrocytes stimulates aerobic glycolysis: a mechanism coupling neuronal activity to glucose utilization. *Proc. Natl. Acad. Sci. U.S.A.* 91, 10625–10629.

Pellerin, L., and Magistretti, P. J. (2012). Sweet sixteen for ANLS. *J. Cereb. Blood Flow Metab.* 32, 1152–1166. doi: 10.1038/jcbfm.2011.149

Pellerin, L., Pellegri, G., Bittar, P. G., Charnay, Y., Bouras, C., Martin, J. L., et al. (1998). Evidence supporting the existence of an activity-dependent astrocyte- neuron lactate shuttle. *Dev. Neurosci.* 20, 291–299.

Prichard, J., Rothman, D., Novotny, E., Petroff, O., Kuwabara, T., Avison, M., et al. (1991). Lactate rise detected by 1H NMR in human visual cortex during physiologic stimulation. *Proc. Natl. Acad. Sci. U.S.A.* 88, 5829–5831. doi: 10.1073/pnas.88.13.5829

Qu, H., Haberg, A., Haraldseth, O., Unsgard, G., and Sonnewald, U. (2000). (13)C MR spectroscopy study of lactate as substrate for rat brain. *Dev. Neurosci.* 22, 429–436. doi: 10.1159/000017472

Rothman, D. L., Behar, K. L., Hetherington, H. P., den Hollander, J. A., Bendall, M. R., Petroff, O. A., et al. (1985). 1H-Observe/13C-decouple spectroscopic measurements of lactate and

glutamate in the rat brain *in vivo*. *Proc. Natl. Acad. Sci. U.S.A.* 82, 1633–1637.

Sappey-Marinier, D., Calabrese, G., Fein, G., Hugg, J. W., Biggins, C., and Weiner, M. W. (1992). Effect of photic stimulation on human visual cortex lactate and phosphates using 1H and 31P magnetic resonance spectroscopy. *J. Cereb. Blood Flow Metab.* 12, 584–592. doi: 10.1038/jcbfm.1992.82

Schousboe, A., Westergaard, N., Waagepetersen, H. S., Larsson, O. M., Bakken, I. J., and Sonnewald, U. (1997). Trafficking between glia and neurons of TCA cycle intermediates and related metabolites. *Glia* 21, 99–105. doi: 10.1002/(SICI)1098-1136(199709)21:1<99::AID-GLIA11>3.0.CO;2-W

Schurr, A., and Rigor, B. M. (1998). Brain anaerobic lactate production: a suicide note or a survival kit? *Dev. Neurosci.* 20, 348–357.

Sokoloff, L. (1981). The deoxyglucose method for the measurement of local glucose utilization and the mapping of local functional activity in the central nervous system. *Int. Rev. Neurobiol.* 22, 287–333.

Voutsinos-Porche, B., Bonvento, G., Tanaka, K., Steiner, P., Welker, E., Chatton, J. Y., et al. (2003). Glial glutamate transporters mediate a functional metabolic crosstalk between neurons and astrocytes in the mouse developing cortex. *Neuron* 37, 275–286. doi: 10.1016/S0896-6273(02)01170-4

Waagepetersen, H. S., Bakken, I. J., Larsson, O. M., Sonnewald, U., and Schousboe, A. (1998a). Comparison of lactate and glucose metabolism in cultured neocortical neurons and astrocytes using 13C-NMR spectroscopy. *Dev. Neurosci.* 20, 310–320.

Waagepetersen, H. S., Bakken, I. J., Larsson, O. M., Sonnewald, U., and Schousboe, A. (1998b). Metabolism of lactate in cultured GABAergic neurons studied by 13C nuclear magnetic resonance spectroscopy. *J. Cereb. Blood Flow Metab.* 18, 109–117. doi: 10.1097/00004647-199801000-00011

Wyss, M. T., Jolivet, R., Buck, A., Magistretti, P. J., and Weber, B. (2011). *In vivo* evidence for lactate as a neuronal energy source. *J. Neurosci.* 31, 7477–7485. doi: 10.1523/JNEUROSCI.0415-11.2011

Zwingmann, C., Richter-Landsberg, C., Brand, A., and Leibfritz, D. (2000). NMR spectroscopic study on the metabolic fate of [3-(13)C]alanine in astrocytes, neurons, and cocultures: implications for glia-neuron interactions in neurotransmitter metabolism. *Glia* 32, 286–303. doi: 10.1002/1098-1136(200012)32:3<286::AID-GLIA80>3.0.CO;2-P

**Conflict of Interest Statement:** The authors declare that the research was conducted in the absence of any commercial or financial relationships that could be construed as a potential conflict of interest.

*Received: 27 March 2013; accepted: 13 May 2013; published online: 31 May 2013.*

*Citation: Sampol D, Ostrofet E, Jobin M-L, Raffard G, Sanchez S, Bouchaud V, Franconi J-M, Bonvento G and Bouzier-Sore A-K (2013) Glucose and lactate metabolism in the awake and stimulated rat: a $^{13}$C-NMR study. Front. Neuroenergetics* ***5****:5. doi: 10.3389/fnene.2013.00005*

frontiers in
NEUROENERGETICS

REVIEW ARTICLE
published: 13 June 2013
doi: 10.3389/fnene.2013.00006

# Hypothalamic metabolic compartmentation during appetite regulation as revealed by magnetic resonance imaging and spectroscopy methods

**Blanca Lizarbe[1], Ania Benitez[1,2], Gerardo A. Peláez Brioso[1,2], Manuel Sánchez-Montañés[2], Pilar López-Larrubia[1], Paloma Ballesteros[3] and Sebastián Cerdán[1]***

[1] Department of Experimental Models of Human diseases, Laboratory of Imaging and Spectroscopy by Magnetic Resonance, Instituto de Investigaciones Biomédicas "Alberto Sols" CSIC/UAM, Madrid, Spain
[2] Departmento de Informática, Escuela Politécnica Superior, Universidad Autónoma de Madrid, Cantoblanco, Madrid, Spain
[3] Laboratorio de Síntesis Orgánica e Imagen Molecular por Resonancia Magnética, Facultad de Ciencias, Universidad Nacional de Educación a Distancia, Unidad Asociada al CSIC, Madrid, Spain

**Edited by:**
Mary McKenna, University of Maryland, USA

**Reviewed by:**
Caroline Rae, University of New South Wales, Australia
Brenda Bartnik-Olson, Loma Linda University, USA

***Correspondence:**
Sebastián Cerdán, Department of Experimental Models of Human diseases, Instituto de Investigaciones Biomédicas "Alberto Sols" CSIC/UAM., c/ Arturo Duperier 4, Madrid 28029, Spain
e-mail: scerdan@iib.uam.es

We review the role of neuroglial compartmentation and transcellular neurotransmitter cycling during hypothalamic appetite regulation as detected by Magnetic Resonance Imaging (MRI) and Spectroscopy (MRS) methods. We address first the neurochemical basis of neuroendocrine regulation in the hypothalamus and the orexigenic and anorexigenic feed-back loops that control appetite. Then we examine the main MRI and MRS strategies that have been used to investigate appetite regulation. Manganese-enhanced magnetic resonance imaging (MEMRI), Blood oxygenation level-dependent contrast (BOLD), and Diffusion-weighted magnetic resonance imaging (DWI) have revealed $Mn^{2+}$ accumulations, augmented oxygen consumptions, and astrocytic swelling in the hypothalamus under fasting conditions, respectively. High field $^{1}H$ magnetic resonance *in vivo*, showed increased hypothalamic myo-inositol concentrations as compared to other cerebral structures. $^{1}H$ and $^{13}C$ high resolution magic angle spinning (HRMAS) revealed increased neuroglial oxidative and glycolytic metabolism, as well as increased hypothalamic glutamatergic and GABAergic neurotransmissions under orexigenic stimulation. We propose here an integrative interpretation of all these findings suggesting that the neuroendocrine regulation of appetite is supported by important ionic and metabolic transcellular fluxes which begin at the tripartite orexigenic clefts and become extended spatially in the hypothalamus through astrocytic networks becoming eventually MRI and MRS detectable.

**Keywords: appetite regulation, hypothalamus, neuroendocrine signaling, neuroglial compartmentation, magnetic resonance imaging, magnetic resonance spectroscopy**

The hypothalamus is a small cerebral structure responsible for the integral homeostasis of vital systemic functions including global energy metabolism, appetite, thirst and osmoregulation, thermoregulation, circadian rhythms, and some fundamental survival responses such as aggressiveness (Swaab et al., 1992; Ganong, 1993; Lin et al., 2011). It operates as a highly sophisticated neuroendocrine transducer, sensing peripheral endocrine signals and transforming them in intracerebral excitatory or inhibitory neurotransmitter events that deliver the homeostatic response back to the periphery (McEwen, 1989; Levin et al., 2011). Hypothalamic function involves frequently the operation of highly elaborated feed-back control loops (**Figure 1**).

Activation of the hypothalamic interface is thought to proceed essentially in two steps, an initial endocrine activation, involving the receptor-mediated interaction of the hormone or neuropeptide with the presynaptic terminal, followed either by the activation or inhibition of excitatory or inhibitory neurotransmitter release at the postsynaptic cleft. The neurotransmitters glutamate and GABA play a central role in this process mediating glutamatergic (Tong et al., 2007) or GABAergic (Xu et al., 2012) neurotransmissions through specific neuronal pathways of the hypothalamus. These pathways trigger eventually the release of hypothalamic neuropeptides or hormones to the blood stream, to other hypothalamic structures and the hypophysis (McEwen, 1989; Thorburn and Proietto, 1998) or activate the brain stem autonomic neurocircuitry (Palkovits, 1999), all these events geared to maintain systemic homeostasis.

In the last decades, important progress has been reached characterizing the initial endocrine step, identifying the corresponding systemic and intrahypothalamic neuropeptides and receptors or the morphological pathways and tracts transmitting these signals within the different hypothalamic nuclei or even to extra-hypothalamic structures (McEwen, 1989; Lantos et al., 1995). Progress has been slower, however, in the characterization

**Abbreviations:** MRI, Magnetic Resonance Imaging; MRS, Magnetic Resonance Spectroscopy; MEMRI, Manganese-enhanced Magnetic Resonance Imaging; BOLD, Blood Oxygenation Level-dependent contrast; DWI, Diffusion-weighted Imaging; DIA, Dehydration-induced Anorexia.

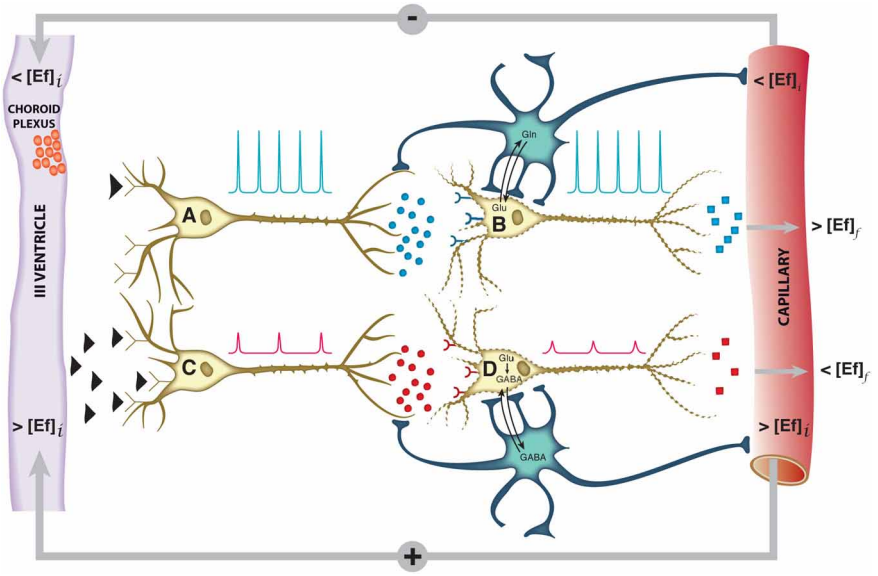


**FIGURE 1 | Schematic representation of the neuroendocrine interface and feed-back control loops.** Neuroendocrine integration may involve both, neurons receiving endocrine signals and releasing neurotransmitters (A, C) or neurons receiving neurotransmitter signals and releasing neuropeptides or hormones (B, D). A typical feed-back control loop is illustrated. The initial decrease in plasma concentration of an endocrine inhibitory effector (<[Ef]$_i$), passes the blood brain barrier, releasing the inhibition of neuron A and triggering action potentials (blue spikes) and the synaptic release of an excitatory neurotransmitter as glutamate (blue circles). This activates neuron B and triggers the release of an endocrine signal resulting eventually in an increase in the final plasma concentration of the effector (>[Ef]$_f$). Glutamatergic neurotransmission involves necessarily the operation of the neuroglial glutamine cycle. The initial increase in the plasma concentration of the effector (>[Ef]$_i$) inhibits neuron C, decreasing the frequency and amplitude of the action potentials and triggering the release of an inhibitory neurotransmitter as GABA (red circles). This causes neuron D to reduce or suspend the release of the effector Ef, resulting eventually in an homeostatic reduction in the plasma concentration of (<[Ef]$_f$),. GABAergic neurotransmission involves necessarily the neuroglial glutamate-GABA cycle. Both negative and positive feed-back loops tend to maintain the plasma concentration of the effector Ef stable within a narrow range. Glu, glutamate; Gln, glutamine; GABA, $\gamma$-aminobutyric acid.

of the neurotransmitter events underlying the neuroendocrine response. In this respect, early interpretations conceived the hypothalamic response as a neuronal only event. The evolution of the tripartite synapse concept (Araque et al., 1999; Halassa et al., 2007; Santello et al., 2012), however, revealed the essential role of astroglia in the modulation of synaptic neurotransmission, gaining for astrocytes a fundamental role in neuroendocrine signaling (Garcia-Ovejero et al., 2005; Garcia-Segura et al., 2008). In some important cases, as in thyroid hormones, astrocytes are even required not only to modulate synaptic transmission, but to generate the active endocrine response (Mohacsik et al., 2011). Furthermore, glutamatergic or GABAergic neurotransmissions involve necessarily the operation of transcellular cycles of glutamate and GABA between neurons and astrocytes (Hertz, 2004; Dienel and Hertz, 2005), stressing the fundamental role of neuroglial compartmentation in hypothalamic function. However, further improvements in our understanding of the role of metabolic compartmentation in neuroendocrine function have been often hampered by the limited accessibility of sufficiently robust non-invasive methods to monitor neuronal activation and transcellular neurotransmitter cycling in the hypothalamus *in vivo*.

Magnetic Resonance Imaging (MRI) and Spectroscopy (MRS) approaches are known to be well endowed to observe hypothalamic morphology and function. Briefly, Manganese-enhanced MRI (MEMRI) techniques allow to monitor neuronal activation through the accumulation of $Mn^{2+}$ and its effects in $T_1$-weighted images (Koretsky and Silva, 2004), Blood Oxygen Level-dependent (BOLD) methods detect cerebral activation through associated hemoglobin deoxygenation and perfusion changes (Zhu et al., 1998; Logothetis and Wandell, 2004) and Diffusion-weighted Imaging (DWI) visualize microstructural changes in the diffusion coefficient of water (Le Bihan, 2003), reflecting most probably activation induced neurocellular swelling events. In addition, $^1$H MRS *in vivo* is able to characterize the metabolic profile of the hypothalamus and its changes during activation (Duarte et al., 2012) and $^{13}$C MRS provides comprehensive information on neuroglial oxidative metabolism and neurotransmitter cycling (Cruz and Cerdan, 1999; Gruetter et al., 2003; Rothman et al., 2003). Taken together, these techniques are beginning to yield precious information on hypothalamic physiology. However, a critical overview of the information gained with the different methods and an integrative interpretation of the results obtained becomes currently necessary, to be able to recapitulate and design more precisely the protocols of future strategies.

In this review, we examine the information gained thus far with these approaches and provide an integrative interpretation that highlights the vital role of hypothalamic neuroglial compartmentation in the cerebral control of global energy homeostasis *in vivo*.

## HYPOTHALAMIC CONTROL OF APPETITE

Recent years have witnessed an important development in the understanding of the hypothalamic mechanisms involved in appetite control and global energy homeostasis (Coll et al., 2007). Appetite control is currently understood to operate on the balance of positive and negative peripheral signals from the adipose tissue, the pancreas, and the gastrointestinal tract, modulating intrahypothalamic and brain stem autonomic activities that determine the early hunger or satiety responses and the long-term body weight and energy balance (Schwartz and Morton, 2002; Morton et al., 2006). Peripheral signals from the gut include mainly peptide YY (PYY), oxyntomodulin (OXM), ghrelin, glucagon-like peptide 1 (GLP-1), and colecystokinin (CCK). Adipose tissue, pancreatic, and gut-derived peptides influence the hypothalamic circuitry providing short-term hunger or satiety signals and resulting in the long term in anabolic (−) or catabolic (+) effects in energy expenditure, increasing or decreasing body weight. In particular, these mediators modulate the activation of the arcuate (ARC), paraventricular (PVN), dorsomedial nuclei (DMN), and ventromedial nuclei (VMN) of the hypothalamus which control food intake through a delicate balance of orexigenic and anorexigenic pathways operated by specific neurons and neuropeptides (Stanley et al., 2005).

**Figure 2** illustrates our current views on the mechanism of appetite control within the hypothalamus. Hypothalamic control of energy homeostasis involves the modulation of orexigenic (stimulation of food intake) and anorexigenic (satiety signals) pathways, that determine the positive or negative balance between food intake and energy expenditure (Schwartz et al., 2000; Schwartz and Morton, 2002; Morton et al., 2006). Briefly, leptin and insulin produced by fat tissues and pancreas, circulate in blood in amounts proportional to body fat and blood glucose. These long-term systemic effectors reach easily the hypothalamic ARC nucleus, an area of relatively permeable Blood Brain Barrier (BBB) and thus highly accessible to activation by systemic effectors. Insulin and leptin, inhibit the orexigenic Neuropeptide Y (NPY) and Agouti-related Peptide (AgRP) neurons (purple) and activate the anorexigenic neurons (green) of the melanocortin (α-MSH)/cocaine and amphetamine-regulated transcript (CART) pathways, resulting in decreased food intake and increased energy expenditure. Long-term increases in leptin or insulin lead to receptor desensitization

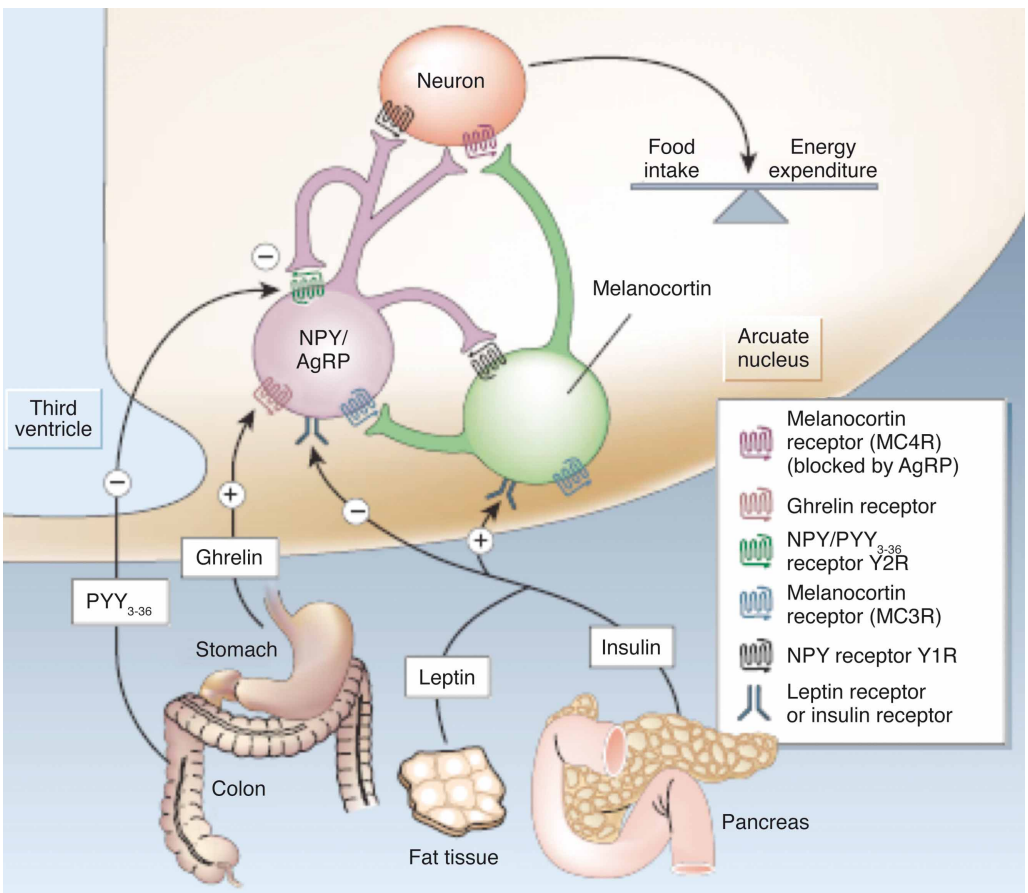


**FIGURE 2 | Hypothalamic control of global energy balance.** Appetite is regulated by a complex feed-back loop involving endocrine signals originated in peripheral tissues and intrahypothalamic peptides. Leptin and insulin inhibit the orexigenic NPY/AgRP neurons (purple) and stimulate the anorexigenic melanocortin neurons (green), resulting in a reduction of food intake. Ghrelin or $PYY_{3–36}$ activate or inhibit the NPY/AgRP neurons resulting in orexigenic or anorexigenic responses, respectively. Taken from Schwartz and Morton (2002). Reproduced with permission of the publisher.

and insulin or leptin "resistance" increasing plasma glucose levels and fat accumulation, producing eventually obesity and diabetes. Ghrelin and peptide $PYY_{3-36}$, released by the stomach and the colon, respectively, provide the Arcuate with positive or negative short-term signals of appetite or satiety through the selective activation or inhibition of the NPY/AgRP neurons, resulting in hunger or satiety, respectively (Tang-Christensen et al., 2004).

Despite these important advances in the understanding of the endocrine processes controlling food intake and energy expenditure, less is known on how these modify the neuroglial metabolic coupling mechanisms supporting the activation or inhibition of the orexigenic or anorexigenic pathways. However, important evidence supports the crucial role of glutamatergic or GABAergic neurotransmissions on hypothalamic function (Collin et al., 2003; Hentges et al., 2004). In particular, intracerebral glutamate administration is known to elicit an intense orexigenic response (Stanley et al., 1993) while knock out mice in glutamate or GABA vesicular transporters are known to exhibit altered feeding behavior (Tong et al., 2007; Xu et al., 2012). Notably, how glutamatergic or GABAergic neurotransmissions are modulated by orexigenic or anorexigenic stimuli *in vivo* has not been directly addressed.

## MAGNETIC RESONANCE IMAGING STUDIES OF HYPOTHALAMIC APPETITE REGULATION

### MANGANESE-ENHANCED MAGNETIC RESONANCE IMAGING (MEMRI)

MEMRI is currently thought to directly reflect the neuronal accumulation of $Mn^{2+}$ through Voltage-dependent Calcium Channels in stimulated brain areas, an event that extends transynaptically and enables MEMRI to map neuronal connectivities (Pautler, 2004). $Mn^{2+}$ accumulation may actually exceed the neuronal tracts and extend to surrounding astrocytes and astrocytic networks, since abundant gap junctions exist in astrocytes (Andrew et al., 1981) and neuronal activation has shown to elicit astrocytic intracellular and intercellular $Ca^{2+}$ waves (Jaffe, 2006, 2008, 2010). Paramagnetic $Mn^{2+}$ ions mimic closely the size of diamagnetic $Ca^{2+}$, thus providing an ideal surrogate probe to monitor $Ca^{2+}$ dynamics during neuronal activation. Hydrated $Mn^{2+}$ ions are classically known to induce a strong reduction in the $T_1$ of water, resulting in bright contrast in $T_1$-weighted images in those activated areas accumulating $Mn^{2+}$ (Lee et al., 2005). MEMRI is not devoid from limitations, since $Mn^{2+}$ administration is known to become neurotoxic, competing with endogenous $Ca^{2+}$ fluxes, pertubing hypothalamic levels of metabolites and interfering with the operation of vital metabolic pathways as the tricarboxylic acid cycle and neurotransmitter cycles (Zwingmann et al., 2003, 2004).

Despite these limitations, MEMRI has been successfully used to detect brain activity (Aoki et al., 2002) and neuronal architecture (Aoki et al., 2004) in rodents since the early 2000s, when the first application to the study of hypothalamic functionality appeared (Morita et al., 2002). Morita et al. detected increases in $T_1$-weighted images in the rat brain after intravenously infusing $MnCl_2$, but they had to disrupt the BBB for manganese to diffuse properly through the brain. As an activation agent, they injected NaCl to the rat brain and found signal increases in areas involved in central osmotic regulation, including the hypothalamic area. Their observations were validated by a positive correlation with c-Fos expression levels in the activated areas and demonstrated, for the first time to our knowledge, the possibility of studying hypothalamic functionality with $Mn^{2+}$-enhanced MRI, although this required BBB disruption. Later on, in 2006, MEMRI was successfully implemented without compromising the BBB (Yu et al., 2005) to map regions of accumulated sound-evoked activity in mice, after intraperitoneal administration of $MnCl_2$. Soon after, the first MEMRI study of hypothalamic activation associated with feeding, without compromising the BBB (Kuo et al., 2006) was published. Authors infused intravenously $MnCl_2$ during the MRI acquisition protocol and compared signal enhancement in the hypothalamus of fed or overnight-fasted mice, obtaining significant differences in different hypothalamic nuclei. This revealed that region-specific $Mn^{2+}$ enhancement in the mouse brain could be modulated by fasting. Since then, several MEMRI studies have focused on the hypothalamic functionality associated to feeding, by studying the effect of peptide administration and its pathways of activation (Chaudhri et al., 2006; Parkinson et al., 2009; Hankir et al., 2011), cerebral activation in transgenic mice (Delgado et al., 2011) and hypothalamic response to alterations of food intake (Just and Gruetter, 2011; Anastasovska et al., 2012).

Finally, recent years have witnessed growing interest on MEMRI applications, geared to a better understanding of the molecular mechanisms by which $Mn^{2+}$ produces alterations of the hypothalamic physiological processes. In particular, a significant number of publications focused on studies combing MEMRI with other imaging or spectroscopic techniques (Delgado et al., 2011; Just et al., 2011; Gutman et al., 2012), or even using MEMRI information to understand other functional techniques (Silva, 2012).

**Figure 3** provides a useful frame for these concepts illustrating the use of MEMRI in the hypothalamus of control and obese mice. $Mn^{2+}$ infused in the tail vein of normal and obese mice resulted in a larger increase in the intensity of the Arcuate and VMN of obese animals as compared to the controls, a circumstance revealing the orexigenic stimulation of obese animals and the high anatomical and neurophysiological resolution of the approach.

### BLOOD OXYGENATION LEVEL DEPENDENT (BOLD) CONTRAST

BOLD imaging is one of the most widely used techniques to study brain function in animals and man, based on detecting increases in oxygen consumption and associated hemodynamic responses during neuronal activation. In the neuronal activation process, the ratio between deoxyhemoglobin (paramagnetic) and oxyhemoglobin (diamagnetic) changes, and by studying this ratio, BOLD (Ogawa et al., 1990) can successfully map brain activity.

The use of functional neuroimaging in the study of appetite control started in the late nineties, by monitoring the hypothalamic function after glucose uptake in obese or lean humans (Matsuda et al., 1999), demonstrating for the first time the existence of differential hypothalamic function between lean and obese subjects. Almost at the same time, BOLD imaging

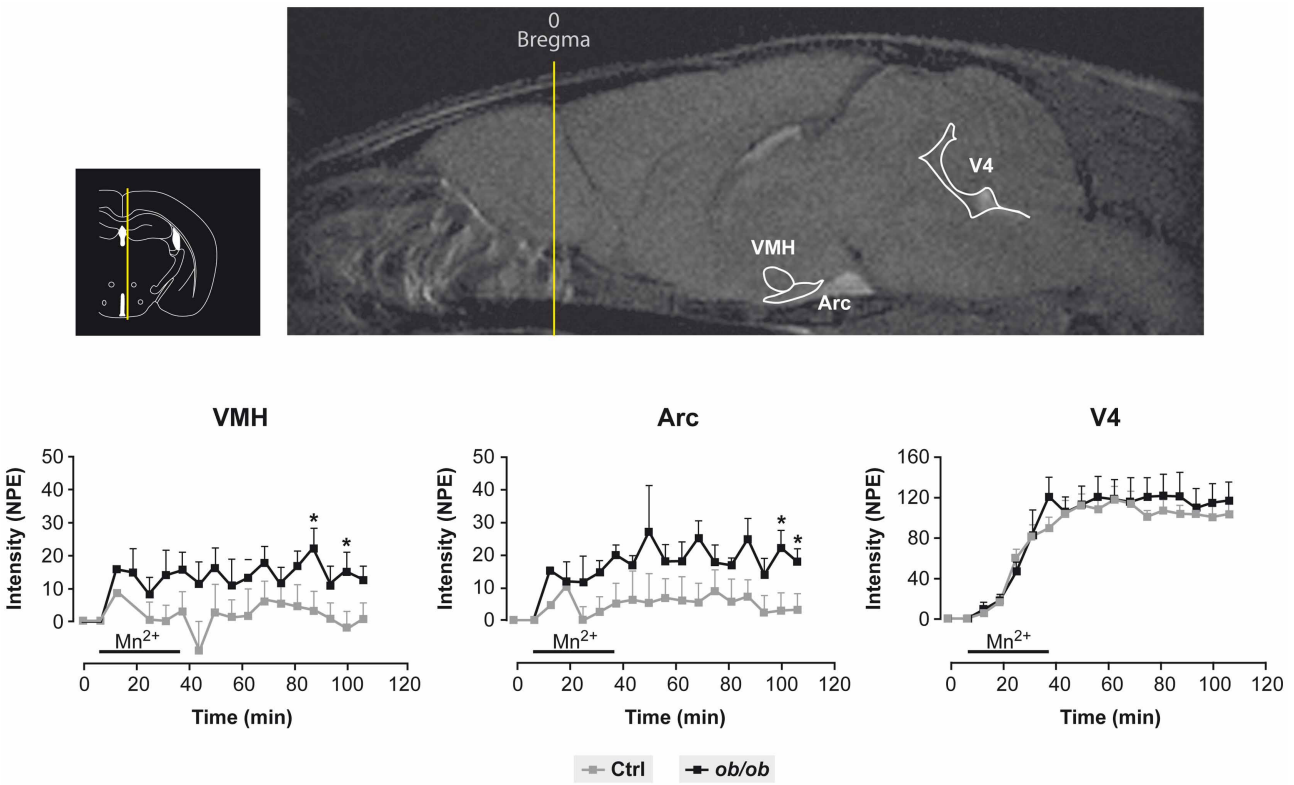


**FIGURE 3 | Representative MEMRI response in obese and control mice.** Inset upper left: Localization of the hypothalamus, third and fourth ventricles in an anatomical atlas (Paxinos and Franklin, 2001). Upper right: $Mn^{2+}$ induced increase in MR signal intensity (MEMRI) in the arcuate nucleus (Arc), ventromedial nucleus (VMH) and the fourth ventricle (V4). Lower panels: Kinetics of MEMRI increase in VMH, Arc and V4 during and after $Mn^{2+}$ infusion. Note that the obese animals (black squares) show a larger increase in MEMRI than the controls (gray squares) in VMH and Arc, but not in V4, revealing a specific obesity effect in these hypothalamic nuclei. Taken from Delgado et al. (2011). Reproduced with permission of the publisher.

detected hypothalamic functionality in a rat model following intraperitoneal glucose administration (Mahankali et al., 2000) by recording significant decreases of the MRI signal in the hypothalamic region after the injection. A few years later, a positive correlation between blood-oxygenation-level-dependent (BOLD) contrast fMRI and c-fos protein expression was established in activated areas of the rat brain after the administration of anorexigenic agents (Stark et al., 2006), thus validating the use of BOLD in anesthetized rats to identify the pathways of brain response to appetite-modulating signals. Also in rats, different hypothalamic response to glucose administration was detected in lean and obese animals (Chen et al., 2007), with an attenuated BOLD response in obese rats that was positively correlated with the percentage of positive NPY cells in the hypothalamus, and with significantly lower levels of 5-hydroxytryptamine (5-HT). Since then, the use of BOLD imaging for the study of appetite regulation in animals has generated an important number of contributions, mainly related to the effects on hypothalamic activation after the administration of different diets or peptides to rats (Min et al., 2011; Li et al., 2012) and its correlation with endogenous levels of neuropeptides.

In humans, early fMRI studies started investigating cerebral activation with food pictures (Killgore et al., 2003) and the hypothalamic response to different tastes and calories (Smeets et al., 2005). It soon became clear that appetite in humans was the result of very complex and interrelated neuronal circuits, including not only hypothalamus and brainstem, which are the principal homeostatic brain areas regulating body weight, but also corticolimbic and higher cortical regions. Consequently, different authors investigated the neuronal networks that responded to specific orexigenic or anorexigenic signals (Batterham et al., 2007; Miller et al., 2007; Malik et al., 2008). Currently, the applications of BOLD fMRI on studies of appetite regulation are mainly dedicated to the study of hypothalamic response to glucose (Vidarsdottir et al., 2007; Purnell et al., 2011), to the establishment of differences between fMRI responses in obese and non-obese humans (Tomasi et al., 2009), and to the effects of appetite modulating hormones derived from the gastrointestinal tract and adipose tissue, mainly ghrelin (Jones et al., 2012), insulin (Guthoff et al., 2010) and leptin (Baicy et al., 2007; Farooqi et al., 2007).

**Figure 4** illustrates a representative application of BOLD imaging to appetite regulation in a study that monitored hypothalamic activation in humans, as induced by a paradigm that showed images of high- and low-calorie foods. Briefly, fMRI was applied to investigate cerebral responses of 13 healthy women by

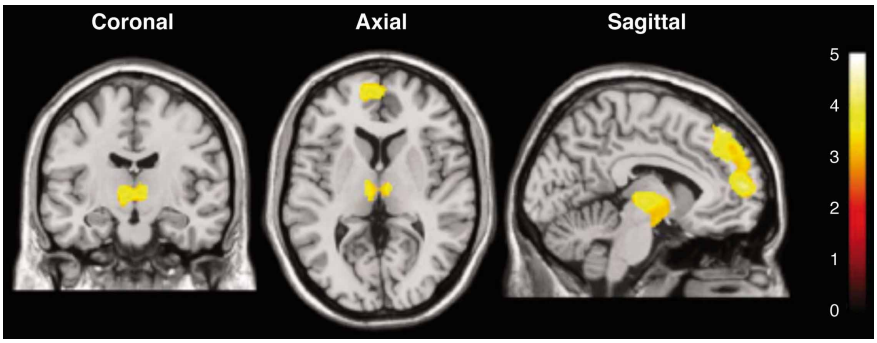


**FIGURE 4 | Statistical parametric maps of brain activated regions in the human brain, as measured by BOLD, during the presentation of high-calorie food images.** The color bar reflects the scale of the SPM statistic used for the analysis. The dorsolateral and medial prefrontal cortex, the thalamus and the hypothalamus showed significant activation ($P < 0.005$) relative to the control pictures of non-edible food related utensils Reproduced from Killgore et al. (2003) with permission of the publisher.

presenting three categories of images: high-calorie, low-calorie and non-edible food-related utensils. They found areas of activation common to food stimuli regardless of the calorie content, such as the bilateral amygdala/hippocampus region. Besides, high-calorie food stimuli were found to be associated with significant clusters of activation within the medial and dorsolateral prefrontal cortex, medial dorsal thalamus, hypothalamus, corpus callosum, and cerebellum.

#### DIFFUSION-WEIGHTED IMAGING (DWI)

Diffusion-weighted Imaging (DWI) provides information on the diffusion behavior of water molecules in biological tissues, and can be used to probe and define tissue structures at microscopic scales (Le Bihan, 2003). Since its introduction in 1985, it is the modality of choice for the assessment of stroke in patients (Schellinger et al., 2000) and for studies of white matter diseases (Hagmann et al., 2007).

The interpretation of the biophysical models underlying diffusion changes observed in physiological or pathological states has been a matter of debate in the last decades. Indeed, several models that overcome the conventional monoexponential approach of diffusion (Le Bihan, 2003) have been proposed (Assaf et al., 2002; Jensen and Helpern, 2010; Grinberg et al., 2011).

Conventional DWI has been used to the study of appetite regulation in the hypothalamus (Alkan et al., 2008). This study compared apparent diffusion coefficients (ADC) values in brain regions of obese and non-obese human subjects. Among other areas, the hypothalamus of obese subjects was found to have higher ADC values than the hypothalamic areas of lean patients. Results were explained as an alteration of fluid distribution in obese subjects due to a vasogenic edema. In fact, it has been demonstrated that consumption of fat-rich diets activates proinflammatory responses in the hypothalamus (De Souza et al., 2005), and that, in mice, the ability of high fat diets to induce obesity depends upon the neuronal expression of the mediator of inflammatory signaling MyD88 (Kleinridders et al., 2009). Furthermore, the relationship between hypothalamic inflammation and obesity has become a matter of study and debate (Wisse and Schwartz, 2009; Wang et al., 2012), and DWI is ideally endowed to evaluate its existence *in vivo* (Cazettes et al., 2011). Recent results from our laboratories (Lizarbe et al., 2013) suggest that hypothalamic inflammation may occur not only in obesity, but also transiently during fasting states.

Some years ago, the behavior of diffusion in biological tissues was suggested to represent slow and fast diffusion phases of water that were modified during neuronal activation process (Niendorf et al., 1996; Le Bihan et al., 2006). Since then, several contributions have used the biphasic model to detect and describe more precisely brain activation using DWI in man and studies *in vitro* (Flint et al., 2009; Kohno et al., 2009; Aso et al., 2013). Even model-free approaches have been proposed that confirm and extend the results obtained with the biexponential model (Lizarbe et al., 2013). The use of functional DWI (fDWI) in the study of hypothalamic activation associated to feeding came also from this study. Our results showed that the diffusion coefficients of water in the hypothalamus changed with fasting in both mice and humans. In mice, it became possible to detect changes in individual hypothalamic nuclei, including the ARC, the DMN and the VMN. On these grounds, the application of fDWI to the study of brain activation in general and hypothalamic activity in particular, appears to open a new avenue within the functional neuroimaging field, even in humans. Diffusion changes associated to activation are thought to occur closer -temporally and spatially- to the activated areas than the physiological changes detected with BOLD (Le Bihan et al., 2006), avoiding the use of potentially toxic $Mn^{+2}$ doses. Besides, the possibility of using DWI to detect directional differences through the implementation of Diffusion Tensor Imaging approaches (Le Bihan et al., 2001; Ahn and Lee, 2011) may allow the investigation of neuronal tracts and their potential alterations under different kinds of appetite-related disturbances.

An example on the use of DWI imaging in the study of hypothalamic activation is illustrated in **Figure 5**, through the changes observed in the diffusion parameters of water in different hypothalamic nuclei including the ARC, VMN, and DMN, depicted in **Figure 5A** (Lizarbe et al., 2013). Panels **5B**,**D**,**F**,

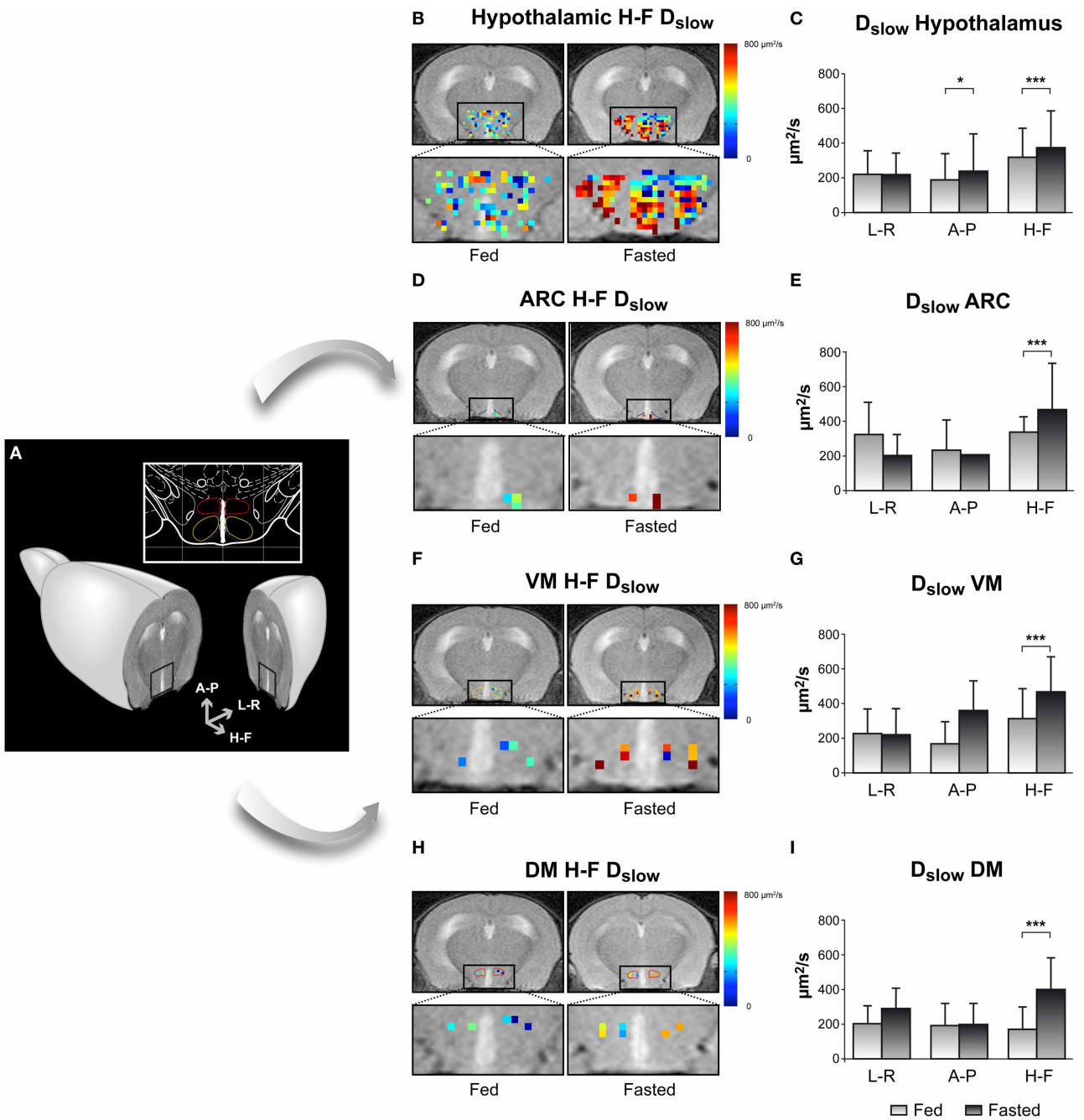


**FIGURE 5 | Imaging appetite by fDWI in the hypothalamic nuclei of the mouse brain. (A)** Axial MRI section containing the hypothalamus in a representative mouse brain and in a brain atlas (inset) showing the localization of the main periventricular hypothalamic nuclei: Dorsomedial Nucleus (DMN, red), Ventromedial Nucleus (VMN, yellow), and Arcuate Nucleus (Arc, blue). **(B,D,F,H)** Hypothalamic color maps of diffusion parameters from fed or fasted mice, superimposed to $T_{2w}$ images in different hypothalamic nuclei. The hypothalamic region is depicted enlarged in the corresponding lower panels. **(C,E,G,I)** $D_{slow}$ bar graphs of parameter values corresponding to the **(B,D,F,H)** panels, respectively. $^{*}p < 0.05$, $^{***}p < 0.001$. Reproduced from Lizarbe et al. (2013) with permission of the publisher.

and **H** show parameter maps of the slow diffusion coefficient ($D_{slow}$) of a representative mouse in the fed (left) or overnight-fasted (right) state, in the hypothalamus, ARC, VMN, and DMN nuclei, respectively. Bar graphs in panels **5C,E,G,** and **I** show mean values of the same parameter in six mice. The significant increase of $D_{slow}$ with fasting in all nuclei may be interpreted as the consequence of activation-induced astrocytic swelling.

## MULTINUCLEAR MAGNETIC RESONANCE SPECTROSCOPY STUDIES OF APPETITE REGULATION

The use of imaging methods may be complemented by several advanced spectroscopy strategies including mainly $^{1}$H MRS *in vivo* and *ex vivo* $^{1}$H and $^{13}$C HRMAS. These methods have been shown to overcome the need to use large voxel volumes, a limitation precluding earlier the applications of MRS *in vivo* to hypothalamic physiology.

### HIGH FIELD $^{1}$H MRS *in vivo*

High field $^{1}$H MRS (14.1 Tesla) has been shown to be able to obtain high quality metabolic profiles from the mouse hypothalamus *in vivo* either unilaterally (2.2 μL voxels) or bilaterally (4.4 μL voxels) (Lei et al., 2010; Duarte et al., 2012). Authors reported that the metabolic profile of the hypothalamus is different from other cerebral structures as the hippocampus, containing larger concentration of γ-aminobutyric acid and myo-inositol and lower concentrations of taurine (**Figure 6A**). High field $^{1}$H MRS was used to characterize the effects of $Mn^{2+}$ in the metabolic profile of the rat hypothalamus under the paradigm of Dehydration-induced Anorexia (DIA) (Just and Gruetter, 2011). Results showed that γ-aminobutyric acid had an essential role in the maintenance of energy homeostasis in the hypothalamus, independently of the condition investigated. Glutamate, glutamine, and taurine, however, appeared to respond more accurately to $Mn^{2+}$ exposure. When comparing DIA and overnight fasting, GABA levels increased in both, but lactate increased significantly only in DIA. Taken together, these studies showed that high field $^{1}$H MRS *in vivo* coupled with MEMRI, could provide very relevant information on the hypothalamic mechanisms involved in the control of food intake, global energy balance, and body weight control in rodents.

### $^{13}$C AND $^{1}$H HIGH RESOLUTION MAGIC ANGLE SPINNING SPECTROSCOPY

$^{13}$C Magnetic Resonance Spectroscopy is a method that has shown previously an enormous potential in the investigation of neuroglial coupling mechanisms, both *in vivo* and *in vitro* (Cruz and Cerdan, 1999; Gruetter et al., 2003; Rothman et al., 2003; Rodrigues et al., 2009). However, the low natural abundance of $^{13}$C (1.1%) and the reduced sensitivity of the method, imposed the use of relatively large voxel sizes *in vivo*, exceeding significantly the dimensions of the hypothalamus. To overcome this, a novel collection of High Resolution Magic Angle Spinning (HRMAS) $^{13}$C methods *ex vivo* were implemented recently. By acquiring NMR spectra of biopsy samples, inclined 54.7° with respect to the static magnetic field, the dipolar couplings that broaden the resonances *in vivo* are removed and high resolution spectra similar to those obtained in solution, can be obtained from samples as small as 5–10 mg, a size comparable with that of the rodent brain hypothalamus. Using this technology, authors investigated (**Figure 6B**) the effects of overnight fasting and ghrelin administration on the metabolic profile and the incorporation of $^{13}$C from (1-$^{13}$C) glucose into hypothalamic metabolites (Violante et al., 2009). Overnight fasting induced significant increases in $^{13}$C incoporation into (2-$^{13}$C) GABA and (3-$^{13}$C) lactate, while the infusion of the orexigenic peptide ghrelin did not affect $^{13}$C labeling in these metabolites. These results revealed that overnight fasting appears to increase GABAergic neurotrasmission and glycolysis, but additional factors other

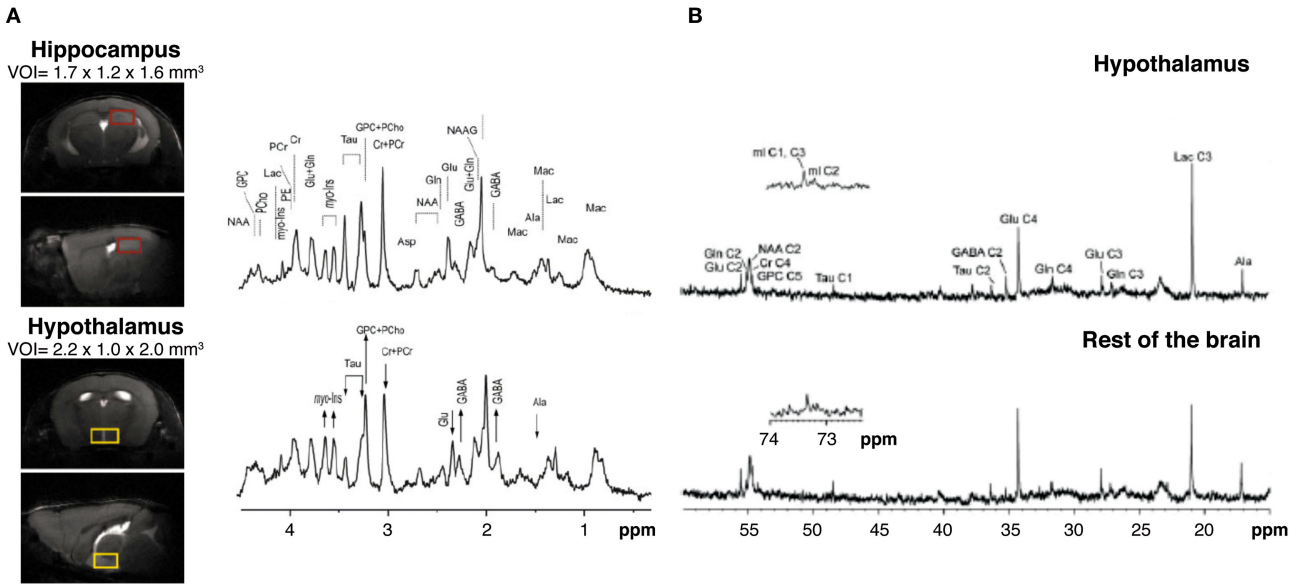


**FIGURE 6 | Multinuclear NMR spectroscopy of the hypothalamus. (A)** $^{1}$H MRI *in vivo* from selected voxels of mouse hypothalamus (lower panels, yellow region) as compared to the hippocampus (upper panels, red region) and corresponding 1H NMR spectra. Note the relative increases in hypothalamic GABA and myo-inositol (arrow up) and the decreases in glutamate and taurine content (arrow down). Taken from Lei et al. (2010) and reproduced with permission of the publisher. **(B)** Representative $^{13}$C HRMAS of hypothalamic biopsies (top) prepared after (1-$^{13}$C) glucose infusion as compared to the rest of the brain (bottom) in a fasted mouse. Reproduced from Violante et al. (2009) with permission of the publisher.

than ghrelin were required to elicit this complex hypothalamic response.

The neuroglial mechanisms underlying leptin signaling in the hypothalamus were recently investigated in control and ob/ob mice, combining MEMRI with $^{1}$H and $^{13}$C HRMAS and infusions of (1-$^{13}$C) glucose, a primarily neuronal substrate or (2-$^{13}$C) acetate, a predominantly glial substrate (Delgado et al., 2011). Leptin defficient obese mice showed increased MEMRI contrast in the ARC and VMN (**Figure 3**) and augmented $^{13}$C accumulation in the hypothalamic glutamate and glutamine carbons from (1-$^{13}$C) glucose, but not from $^{13}$C acetate. Together, this evidence showed for the first time that the increased MEMRI effect associated to neuronal activation of the orexigenic pathways in the obese mice was accompanied by increased oxidative metabolism and glutamate-glutamine cycling. Together with earlier $^{13}$C HRMAS evidences on increased GABAergic performance after overnight fasting, the picture emerges that orexigenic stimulation results in increased glutamatergic and GABAergic neurotransmission, implying augmented transcellular cycling of glutamate-glutamine and GABA between neurons and astrocytes. Present results support the view that the synaptic transmission events supporting neuroendocrine signaling in the hypothalamus follow similar neuroglial compartmentation mechanisms to other types of cerebral sensorial or motor activations.

## RECAPITULATION

In summary, the evidence accumulated recently by MRI and MRS methodologies has contributed importantly to investigate the role of metabolic compartmentation during neuroendocrine regulation in the hypothalamus. **Figure 7** provides an integrative interpretation on the role of neuroglial compartmentation during appetite regulation, as revealed by MEMRI, BOLD, DWI as well as by $^{1}$H and $^{13}$C NMR spectroscopy.

Briefly, the firing of orexigenic neurons involves voltage dependent $Na^{+}$ and $Ca^{2+}$ channels. $Mn^{2+}$ substitutes $Ca^{2+}$, accumulating in excited neurons during depolarization (Koretsky and Silva, 2004; Silva et al., 2004). In addition, glutamatergic neurotransmission is known to be associated to intracellular and intercellular astrocyte to astrocyte calcium waves transmitted through gap junctions (Jaffe, 2006, 2008). $Mn^{2+}$ could thus accumulate in astrocytic networks as well. These astrocytic arrangements may reach millimeter sizes, becoming then detectable under conventional MRI resolution conditions. At present it is not clear which neuronal or astroglial mechanism is predominant, but it can be safely thought that both contribute to the observed MEMRI effect. Excess glutamate released to the orexigenic cleft under fasting or obese conditions, is recaptured by surrounding astrocytes, by $Na^{+}$ dependent cotransport mainly through the GLAST/EAAT1 and GLT-1/EAAT2 transporters, in a $3Na^{+}$ per glutamate stoichiometry (Anderson and Swanson, 2000). The three sodium ions incorporated in this way, are extruded to the extracellular space, in exchange with two potassium ions entering the astrocytic interior through the electrogenic $Na^{+}/K^{+}$ ATPase (Glynn, 1993; Pellerin and Magistretti, 1994). The astrocytic ATP required for the operation of the $Na^{+}/K^{+}$ ATPase and glutamine synthesis during activation by fasting, is thought to be derived from increased glucose consumption and metabolism by oxidative and glycolytic pathways in neurons and astrocytes (Cerdan et al., 2006; Violante et al., 2009; Delgado et al., 2011). Indeed, orexigenic stimulation results in lactate accumulation in the hypothalamus and increased labeling of glutamate, glutamine and GABA from (1-$^{13}$C) glucose as reflected by $^{13}$C HRMAS. This reveals that hypothalamic activation by fasting involves the excitation of both glutamatergic (activatory) and GABAergic (inhibitory) terminals, as expected for an hypothalamic feed-back loop mechanism (**Figure 1**). In addition, the increased metabolic demand in the hypothalamus induced by fasting, results in an increased microvascular blood flow and hemoglobin deoxygenation, a circumstance underlying the changes observed by BOLD and DWI imaging (Lizarbe et al., 2013).

The volume changes inferred in the hypothalamus during orexigenic activation merit further attention. The $K^{+}$ ions accumulated in the extracellular space during the orexigenic action potentials, may enter surrounding astrocytes through stimulation of the $Na^{+}/K^{+}/2Cl^{-}$ cotransporter (Hertz et al., 2007), a circumstance that might trigger concomitant water influx and astrocytic volume increase (Jayakumar and Norenberg, 2010), primarily-mediated through the highly abundant aquaporin AQP-4 of astrocytic membranes (Badaut et al., 2002). It should be noted here that increased $K^{+}$ concentrations are known to be tightly coupled to neuronal activation, and have been detected using metallographic microscopic imaging approaches (Goldschmidt et al., 2004). In addition, EAAT1 glutamate sodium cotransporter has been shown to cause water influx together with glutamate transport (MacAulay et al., 2001) and the activation of the GABA receptors $GABA_{A}$Rs has been recently proposed to be involved with cell volume regulation processes and water exchange in the brain (Cesetti et al., 2011). On these grounds, increased astrocytic volume may become an important determinant of the alterations in diffusion parameters observed by DWI. The osmotic swelling response associated to orexigenic stimulation, is proposed here to occur initially in the few astrocytes surrounding the activated orexigenic clefts (**Figure 1**), but can be rapidly extended, to a plethora of neighboring astrocytes, through the numerous interconnecting gap junctions of the network arrangement (Halassa and Haydon, 2010) as mentioned above for $Mn^{2+}$ accumulations.

The volume changes inferred by DWI find an adequate support when considering the increases in hypothalamic *myo*-inositol levels detected by high field $^{1}$H MRS (Lei et al., 2010). The relative increases in osmolite content between the hypothalamus and other areas of the brain as detected by $^{1}$H MRS *in vivo*, indicate that volume regulation processes in the hypothalamus may play an important role in hypothalamic function.

In summary, the above sections indicate that MRI and MRS methodologies have provided important insight into the hypothalamic mechanisms underlying appetite regulation. Briefly, MEMRI approaches reveal neuroglial manganese accumulation, BOLD shows concomitant oxygen consumption and associated hemodynamic responses and DWI discloses water diffusion changes compatible with glial swelling. $^{1}$H and $^{13}$C MRS have revealed osmolite accumulation and increased glutamatergic

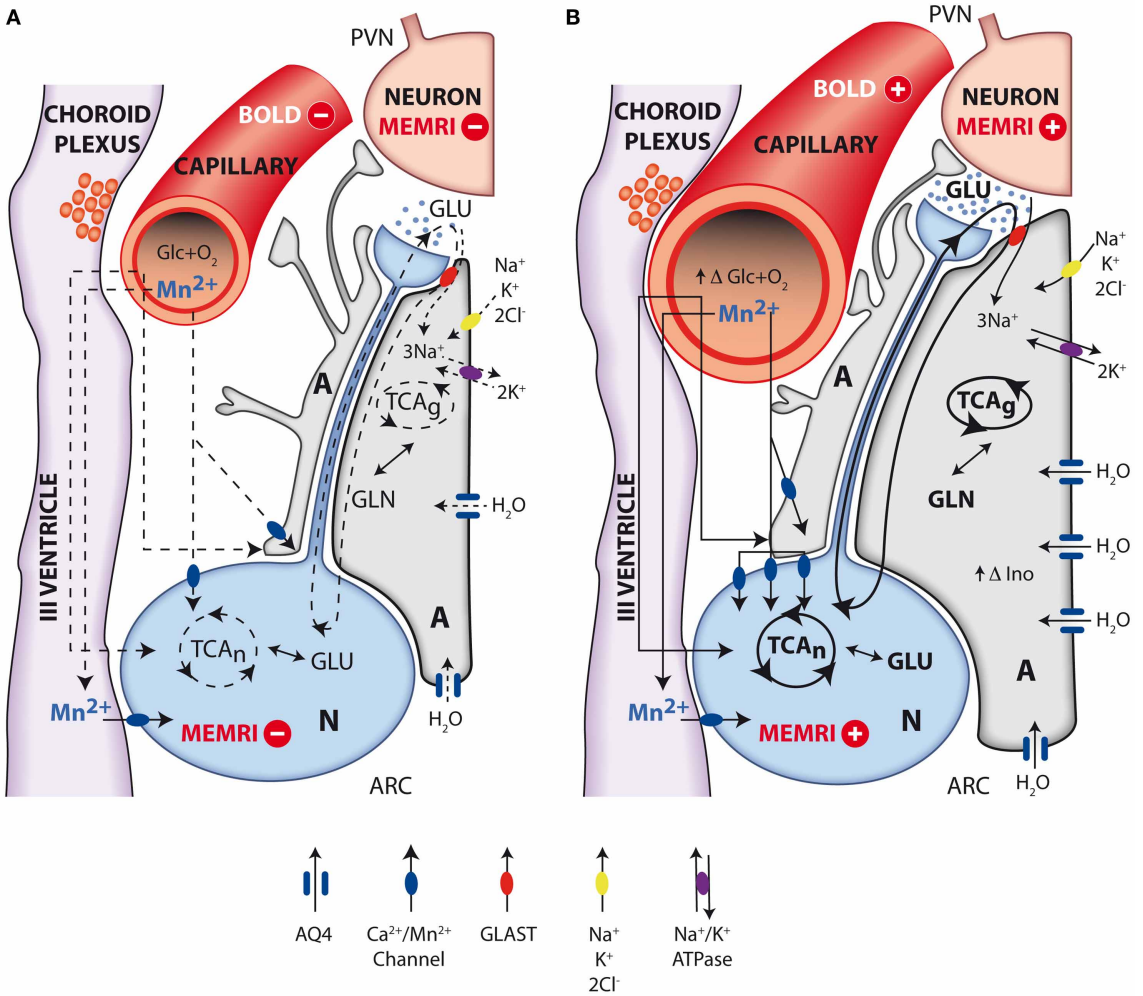


**FIGURE 7 | Integrative interpretation of orexigenic activation in the hypothalamus as detected by MEMRI, BOLD, fDWI, and multinuclear magnetic resonance spectroscopy.** Neuroglial metabolic coupling mechanisms and volume changes in astrocytes and capillaries of the hypothalamus underlie the orexigenic response from resting **(A)** to activated **(B)** states. Briefly, during orexigenic neurotransmission, excess glutamate released to the synaptic cleft by AGRP/NPYY neurons (N, blue) is recaptured by surrounding astrocytes (A, gray), together with $3Na^+$. Intracellular sodium ions incorporated are extruded to the extracellular space, through the electrogenic $Na^+/K^+$ATPase, incorporating two intracellular $K^+$ ions. Astrocytic glutamate produces glutamine, through glutamine synthase, which is later recaptured by the neurons to operate the glutamate-glutamine cycle. Additional $K^+$ ions may be incorporated to the astrocyte through the $Na^+K^+2Cl^-$ cotransporter, resulting in increased intracellular $K^+$ concentrations and thus triggering an osmotically driven, aquaporin 4 (AQP4) mediated (blue channel), water transport, producing astrocytic swelling. Glucose and oxygen are delivered through capillary to astrocytes and neurons, and $Mn^{2+}$ ions enter neurons and astrocytes through calcium channels. Under resting conditions **(A)**, oxidative metabolism and glutamatergic neurotransmission depict basal levels (dotted lines). Under activated orexigenic conditions **(B)**, oxidative metabolism and glutamatergic neurotransmission are increased (darker lines, increased glutamate in the synaptic cleft) as revealed by $^{13}C$ HRMAS, resulting in augmented ionic and water trafficking to astrocytes (darker arrows, increased water influx through AQP4). The accumulated $K^+$ in one synaptic astrocyte may be transferred to the neighboring astroglia, through gap junctions, providing a spreading mechanism for the swelling response through the astrocyte syncytium, becoming measurable by fDWI. Astrocytic volume changes are thought to underlie the increased hypothalamic myo-inostol content observed by $^1H$ HRMAS. Glucose and oxygen demand increase (increasing capillary volume) during neuronal activation, and the ratio between deoxyhemoglobin and oxyhemoglobin changes causing the BOLD effect and the increased $^{13}C$ labeling of glutamate and GABA. Neuronal accumulation of $Mn^{2+}$ through voltage dependent calcium channels increase with neuronal activation (higher number of channels and darker lines), causing the MEMRI effect.

and GABAergic neurotransmissions. Taken together, these results suggest an important role for hypothalamic metabolic compartmentation during appetite regulation, as in other cerebral activations. Naturally, these interpretations do not exclude additional contributions to MRI or MRS from other potential mechanisms.

Finally, the approaches reviewed here may provide a valuable tool to further investigate glutamatergic or GABAergic neurotransmissions in the hypothalamic control of global energy balance and in the development of improved treatments against feeding disorders, obesity, and diabetes. In addition, this arsenal of new methodologies may be easily extended to explore other

hypothalamic functions, opening a new avenue in the research of hypothalamic performance *in vivo*.

## ACKNOWLEDGMENTS

This work was supported in part by grants SAF-2008-01327 and SAF2011-23622 to Sebastián Cerdán, grant CTQ-2010-20960-C02-02 to Pilar López, grants S-BIO-2006-0170 and S2010/BMD-2349 to Sebastián Cerdán, Pilar López-Larrubia, and Manuel Sánchez-Montañés. Blanca Lizarbe and Ania Benitez held predoctoral fellowships from the Spanish Ministry of Science and Technology (BES 2009-027615) and the Spanish Agency for International Cooperation and Development. The expert assistance of Mr. Javier Pérez, CSIC with the final drafting of the illustrations is gratefully acknowledged.

## REFERENCES

Ahn, S., and Lee, S. K. (2011). Diffusion tensor imaging: exploring the motor networks and clinical applications. *Korean J. Radiol.* 12, 651–661. doi: 10.3348/kjr.2011.12.6.651

Alkan, A., Sahin, I., Keskin, L., Cikim, A. S., Karakas, H. M., Sigirci, A., et al. (2008). Diffusion-weighted imaging features of brain in obesity. *Magn. Reson. Imaging* 26, 446–450. doi: 10.1016/j.mri.2007.10.004

Anastasovska, J., Arora, T., Sanchez Canon, G. J., Parkinson, J. R., Touhy, K., Gibson, G. R., et al. (2012). Fermentable carbohydrate alters hypothalamic neuronal activity and protects against the obesogenic environment. *Obesity (Silver Spring)* 20, 1016–1023. doi: 10.1038/oby.2012.6

Anderson, C. M., and Swanson, R. A. (2000). Astrocyte glutamate transport: review of properties, regulation, and physiological functions. *Glia* 32, 1–14. doi: 10.1002/1098-1136(200010)32:1<1::AID-GLIA10>3.0.CO;2-W

Andrew, R. D., MacVicar, B. A., Dudek, F. E., and Hatton, G. I. (1981). Dye transfer through gap junctions between neuroendocrine cells of rat hypothalamus. *Science* 211, 1187–1189. doi: 10.1126/science.7466393

Aoki, I., Tanaka, C., Takegami, T., Ebisu, T., Umeda, M., Fukunaga, M., et al. (2002). Dynamic activity-induced manganese-dependent contrast magnetic resonance imaging (DAIM MRI). *Magn. Reson. Med.* 48, 927–933. doi: 10.1002/mrm.10320

Aoki, I., Wu, Y. J., Silva, A. C., Lynch, R. M., and Koretsky, A. P. (2004). *In vivo* detection of neuroarchitecture in the rodent brain using manganese-enhanced MRI. *Neuroimage* 22, 1046–1059. doi: 10.1016/j.neuroimage.2004.03.031

Araque, A., Parpura, V., Sanzgiri, R. P., and Haydon, P. G. (1999). Tripartite synapses: glia, the unacknowledged partner. *Trends Neurosci.* 22, 208–215. doi: 10.1016/S0166-2236(98)01349-6

Aso, T., Urayama, S., Fukuyama, H., and Le Bihan, D. (2013). Comparison of diffusion-weighted fMRI and BOLD fMRI responses in a verbal working memory task. *Neuroimage* 67, 25–32. doi: 10.1016/j.neuroimage.2012.11.005

Assaf, Y., Ben-Bashat, D., Chapman, J., Peled, S., Biton, I. E., Kafri, M., et al. (2002). High b-value q-space analyzed diffusion-weighted MRI: application to multiple sclerosis. *Magn. Reson. Med.* 47, 115–126. doi: 10.1002/mrm.10040

Badaut, J., Lasbennes, F., Magistretti, P. J., and Regli, L. (2002). Aquaporins in brain: distribution, physiology, and pathophysiology. *J. Cereb. Blood Flow Metab.* 22, 367–378. doi: 10.1097/00004647-200204000-00001

Baicy, K., London, E. D., Monterosso, J., Wong, M. L., Delibasi, T., Sharma, A., et al. (2007). Leptin replacement alters brain response to food cues in genetically leptin-deficient adults. *Proc. Natl. Acad. Sci. U.S.A.* 104, 18276–18279. doi: 10.1073/pnas.0706481104

Batterham, R. L., Ffytche, D. H., Rosenthal, J. M., Zelaya, F. O., Barker, G. J., Withers, D. J., et al. (2007). PYY modulation of cortical and hypothalamic brain areas predicts feeding behaviour in humans. *Nature* 450, 106–109. doi: 10.1038/nature06212

Cazettes, F., Cohen, J. I., Yau, P. L., Talbot, H., and Convit, A. (2011). Obesity-mediated inflammation may damage the brain circuit that regulates food intake. *Brain Res.* 1373, 101–109. doi: 10.1016/j.brainres.2010.12.008

Cerdan, S., Rodrigues, T. B., Sierra, A., Benito, M., Fonseca, L. L., Fonseca, C. P., et al. (2006). The redox switch/redox coupling hypothesis. *Neurochem. Int.* 48, 523–530. doi: 10.1016/j.neuint.2005.12.036

Cesetti, T., Ciccolini, F., and Li, Y. (2011). GABA not only a neurotransmitter: osmotic regulation by GABA(A)R signaling. *Front. Cell Neurosci.* 6:3. doi: 10.3389/fncel.2012.00003

Chaudhri, O. B., Parkinson, J. R., Kuo, Y. T., Druce, M. R., Herlihy, A. H., Bell, J. D., et al. (2006). Differential hypothalamic neuronal activation following peripheral injection of GLP-1 and oxyntomodulin in mice detected by manganese-enhanced magnetic resonance imaging. *Biochem. Biophys. Res. Commun.* 350, 298–306. doi: 10.1016/j.bbrc.2006.09.033

Chen, M., Zhang, T. M., Luo, S. L., Zhou, C., Wu, X. M., Zhou, N. N., et al. (2007). Functional magnetic resonance imaging and immunohistochemical study of hypothalamic function following oral glucose ingestion in rats. *Chin. Med. J.* 120, 1232–1235.

Coll, A. P., Farooqi, I. S., and O'Rahilly, S. (2007). The hormonal control of food intake. *Cell* 129, 251–262. doi: 10.1016/j.cell.2007.04.001

Collin, M., Backberg, M., Ovesjo, M. L., Fisone, G., Edwards, R. H., Fujiyama, F., et al. (2003). Plasma membrane and vesicular glutamate transporter mRNAs/proteins in hypothalamic neurons that regulate body weight. *Eur. J. Neurosci.* 18, 1265–1278. doi: 10.1046/j.1460-9568.2003.02840.x

Cruz, F., and Cerdan, S. (1999). Quantitative 13C NMR studies of metabolic compartmentation in the adult mammalian brain. *NMR Biomed.* 12, 451–462. doi: 10.1002/(SICI)1099-1492(199911)12:7<451::AID-NBM571>3.0.CO;2-E

De Souza, C. T., Araujo, E. P., Bordin, S., Ashimine, R., Zollner, R. L., Boschero, A. C., et al. (2005). Consumption of a fat-rich diet activates a proinflammatory response and induces insulin resistance in the hypothalamus. *Endocrinology* 146, 4192–4199. doi: 10.1210/en.2004-1520

Delgado, T. C., Violante, I. R., Nieto-Charques, L., and Cerdan, S. (2011). Neuroglial metabolic compartmentation underlying leptin deficiency in the obese ob/ob mice as detected by magnetic resonance imaging and spectroscopy methods. *J. Cereb. Blood Flow Metab.* 31, 2257–2266. doi: 10.1038/jcbfm.2011.134

Dienel, G. A., and Hertz, L. (2005). Astrocytic contributions to bioenergetics of cerebral ischemia. *Glia* 50, 362–388. doi: 10.1002/glia.20157

Duarte, J. M., Lei, H., Mlynarik, V., and Gruetter, R. (2012). The neurochemical profile quantified by *in vivo* 1H NMR spectroscopy. *Neuroimage* 61, 342–362. doi: 10.1016/j.neuroimage.2011.12.038

Farooqi, I. S., Bullmore, E., Keogh, J., Gillard, J., O'Rahilly, S., and Fletcher, P. C. (2007). Leptin regulates striatal regions and human eating behavior. *Science* 317, 1355. doi: 10.1126/science.1144599

Flint, J., Hansen, B., Vestergaard-Poulsen, P., and Blackband, S. J. (2009). Diffusion weighted magnetic resonance imaging of neuronal activity in the hippocampal slice model. *Neuroimage* 46, 411–418. doi: 10.1016/j.neuroimage.2009.02.003

Ganong, W. F. (1993). "Central regulation of visceral function," in *Review of Medical Physiology*, ed W. F. Ganong (Connecticut, CT: Appleton and Lange Pub.), 208–230.

Garcia-Ovejero, D., Azcoitia, I., Doncarlos, L. L., Melcangi, R. C., and Garcia-Segura, L. M. (2005). Glia-neuron crosstalk in the neuroprotective mechanisms of sex steroid hormones. *Brain Res. Brain Res. Rev.* 48, 273–286. doi: 10.1016/j.brainresrev.2004.12.018

Garcia-Segura, L. M., Lorenz, B., and Doncarlos, L. L. (2008). The role of glia in the hypothalamus: implications for gonadal steroid feedback and reproductive neuroendocrine output. *Reproduction* 135, 419–429. doi: 10.1530/REP-07-0540

Glynn, I. M. (1993). Annual review prize lecture. 'All hands to the sodium pump'. *J. Physiol.* 462, 1–30.

Goldschmidt, J., Zuschratter, W., and Scheich, H. (2004). High-resolution mapping of neuronal activity by thallium autometallography. *Neuroimage* 23, 638–647. doi: 10.1016/j.neuroimage.2004.05.023

Grinberg, F., Farrher, E., Kaffanke, J., Oros-Peusquens, A. M., and

Shah, N. J. (2011). Non-Gaussian diffusion in human brain tissue at high b-factors as examined by a combined diffusion kurtosis and biexponential diffusion tensor analysis. *Neuroimage* 57, 1087–1102. doi: 10.1016/j.neuroimage.2011.04.050

Gruetter, R., Adriany, G., Choi, I. Y., Henry, P. G., Lei, H., and Oz, G. (2003). Localized *in vivo* 13C NMR spectroscopy of the brain. *NMR Biomed.* 16, 313–338. doi: 10.1002/nbm.841

Guthoff, M., Grichisch, Y., Canova, C., Tschritter, O., Veit, R., Hallschmid, M., et al. (2010). Insulin modulates food-related activity in the central nervous system. *J. Clin. Endocrinol. Metab.* 95, 748–755. doi: 10.1210/jc.2009-1677

Gutman, D. A., Magnuson, M., Majeed, W., Keifer, O. P. Jr., Davis, M., Ressler, K. J., et al. (2012). Mapping of the mouse olfactory system with manganese-enhanced magnetic resonance imaging and diffusion tensor imaging. *Brain Struct. Funct.* 218, 527–537. doi: 10.1007/s00429-012-0413-6

Hagmann, P., Kurant, M., Gigandet, X., Thiran, P., Wedeen, V. J., Meuli, R., et al. (2007). Mapping human whole-brain structural networks with diffusion MRI. *PLoS ONE* 2:e597. doi: 10.1371/journal.pone.0000597

Halassa, M. M., and Haydon, P. G. (2010). Integrated brain circuits: astrocytic networks modulate neuronal activity and behavior. *Annu. Rev. Physiol.* 72, 335–355. doi: 10.1146/annurev-physiol-021909-135843

Halassa, M. M., Fellin, T., and Haydon, P. G. (2007). The tripartite synapse: roles for gliotransmission in health and disease. *Trends Mol. Med.* 13, 54–63. doi: 10.1016/j.molmed.2006.12.005

Hankir, M. K., Parkinson, J. R., Minnion, J. S., Addison, M. L., Bloom, S. R., and Bell, J. D. (2011). Peptide YY 3-36 and pancreatic polypeptide differentially regulate hypothalamic neuronal activity in mice *in vivo* as measured by manganese-enhanced magnetic resonance imaging. *J. Neuroendocrinol.* 23, 371–380. doi: 10.1111/j.1365-2826.2011.02111.x

Hentges, S. T., Nishiyama, M., Overstreet, L. S., Stenzel-Poore, M., Williams, J. T., and Low, M. J. (2004). GABA release from proopiomelanocortin neurons. *J. Neurosci.* 24, 1578–1583. doi: 10.1523/JNEUROSCI.3952-03.2004

Hertz, L. (2004). Intercellular metabolic compartmentation in the brain: past, present and future. *Neurochem. Int.* 45, 285–296. doi: 10.1016/j.neuint.2003.08.016

Hertz, L., Peng, L., and Dienel, G. A. (2007). Energy metabolism in astrocytes: high rate of oxidative metabolism and spatiotemporal dependence on glycolysis/glycogenolysis. *J. Cereb. Blood Flow Metab.* 27, 219–249. doi: 10.1038/sj.jcbfm.9600343

Jaffe, L. (2006). The discovery of calcium waves. *Semin. Cell Dev. Biol.* 17, 229. doi: 10.1016/j.semcdb.2006.02.003

Jaffe, L. F. (2008). Calcium waves. *Philos. Trans. R. Soc. Lond. B Biol. Sci.* 363, 1311–1316. doi: 10.1098/rstb.2007.2249

Jaffe, L. F. (2010). Fast calcium waves. *Cell Calcium* 48, 102–113. doi: 10.1016/j.ceca.2010.08.007

Jayakumar, A. R., and Norenberg, M. D. (2010). The Na-K-Cl Co-transporter in astrocyte swelling. *Metab. Brain Dis.* 25, 31–38. doi: 10.1007/s11011-010-9180-3

Jensen, J. H., and Helpern, J. A. (2010). MRI quantification of non-Gaussian water diffusion by kurtosis analysis. *NMR Biomed.* 23, 698–710. doi: 10.1002/nbm.1518

Jones, R. B., McKie, S., Astbury, N., Little, T. J., Tivey, S., Lassman, D. J., et al. (2012). Functional neuroimaging demonstrates that ghrelin inhibits the central nervous system response to ingested lipid. *Gut* 61, 1543–1551. doi: 10.1136/gutjnl-2011-301323

Just, N., Cudalbu, C., Lei, H., and Gruetter, R. (2011). Effect of manganese chloride on the neurochemical profile of the rat hypothalamus. *J. Cereb. Blood Flow Metab.* 31, 2324–2333. doi: 10.1038/jcbfm.2011.92

Just, N., and Gruetter, R. (2011). Detection of neuronal activity and metabolism in a model of dehydration-induced anorexia in rats at 14.1 T using manganese-enhanced MRI and 1H MRS. *NMR Biomed.* 24, 1326–1336. doi: 10.1002/nbm.1694

Killgore, W. D., Young, A. D., Femia, L. A., Bogorodzki, P., Rogowska, J., and Yurgelun-Todd, D. A. (2003). Cortical and limbic activation during viewing of high- versus low-calorie foods. *Neuroimage* 19, 1381–1394. doi: 10.1016/S1053-8119(03)00191-5

Kleinridders, A., Schenten, D., Konner, A. C., Belgardt, B. F., Mauer, J., Okamura, T., et al. (2009). MyD88 signaling in the CNS is required for development of fatty acid-induced leptin resistance and diet-induced obesity. *Cell Metab.* 10, 249–259. doi: 10.1016/j.cmet.2009.08.013

Kohno, S., Sawamoto, N., Urayama, S., Aso, T., Aso, K., Seiyama, A., et al. (2009). Water-diffusion slowdown in the human visual cortex on visual stimulation precedes vascular responses. *J. Cereb. Blood Flow Metab.* 29, 1197–1207. doi: 10.1038/jcbfm.2009.45

Koretsky, A. P., and Silva, A. C. (2004). Manganese-enhanced magnetic resonance imaging (MEMRI). *NMR Biomed.* 17, 527–531. doi: 10.1002/nbm.940

Kuo, Y. T., Herlihy, A. H., So, P. W., and Bell, J. D. (2006). Manganese-enhanced magnetic resonance imaging (MEMRI) without compromise of the blood-brain barrier detects hypothalamic neuronal activity *in vivo*. *NMR Biomed.* 19, 1028–1034. doi: 10.1002/nbm.1070

Lantos, T. A., Gorcs, T. J., and Palkovits, M. (1995). Immunohistochemical mapping of neuropeptides in the premamillary region of the hypothalamus in rats. *Brain Res. Brain Res. Rev.* 20, 209–249. doi: 10.1016/0165-0173(94)00013-F

Le Bihan, D. (2003). Looking into the functional architecture of the brain with diffusion MRI. *Nat. Rev. Neurosci.* 4, 469–480. doi: 10.1038/nrn1119

Le Bihan, D., Mangin, J. F., Poupon, C., Clark, C. A., Pappata, S., Molko, N., et al. (2001). Diffusion tensor imaging: concepts and applications. *J. Magn. Reson. Imaging* 13, 534–546. doi: 10.1002/jmri.1076

Le Bihan, D., Urayama, S., Aso, T., Hanakawa, T., and Fukuyama, H. (2006). Direct and fast detection of neuronal activation in the human brain with diffusion MRI. *Proc. Natl. Acad. Sci. U.S.A.* 103, 8263–8268. doi: 10.1073/pnas.0600644103

Lee, J. H., Silva, A. C., Merkle, H., and Koretsky, A. P. (2005). Manganese-enhanced magnetic resonance imaging of mouse brain after systemic administration of MnCl2: dose-dependent and temporal evolution of T1 contrast. *Magn. Reson. Med.* 53, 640–648. doi: 10.1002/mrm.20368

Lei, H., Poitry-Yamate, C., Preitner, F., Thorens, B., and Gruetter, R. (2010). Neurochemical profile of the mouse hypothalamus using *in vivo* 1H MRS at 14.1T. *NMR Biomed.* 23, 578–583. doi: 10.1002/nbm.1498

Levin, B. E., Magnan, C., Dunn-Meynell, A., and Le Foll, C. (2011). Metabolic sensing and the brain: who, what, where, and how? *Endocrinology* 152, 2552–2557.

Li, J., An, R., Zhang, Y., Li, X., and Wang, S. (2012). Correlations of macronutrient-induced functional magnetic resonance imaging signal changes in human brain and gut hormone responses. *Am. J. Clin. Nutr.* 96, 275–282. doi: 10.3945/ajcn.112.037440

Lin, D., Boyle, M. P., Dollar, P., Lee, H., Lein, E. S., Perona, P., et al. (2011). Functional identification of an aggression locus in the mouse hypothalamus. *Nature* 470, 221–226. doi: 10.1038/nature09736

Lizarbe, B., Benitez, A., Sanchez-Montanes, M., Lago-Fernandez, L. F., Garcia-Martin, M. L., Lopez-Larrubia, P., et al. (2013). Imaging hypothalamic activity using diffusion weighted magnetic resonance imaging in the mouse and human brain. *Neuroimage* 64, 448–457. doi: 10.1016/j.neuroimage.2012.09.033

Logothetis, N. K., and Wandell, B. A. (2004). Interpreting the BOLD signal. *Annu. Rev. Physiol.* 66, 735–769. doi: 10.1146/annurev.physiol.66.082602.092845

MacAulay, N., Gether, U., Klaerke, D. A., and Zeuthen, T. (2001). Water transport by the human $Na^+$-coupled glutamate cotransporter expressed in Xenopus oocytes. *J. Physiol.* 530, 367–378. doi: 10.1111/j.1469-7793.2001.0367k.x

Mahankali, S., Liu, Y., Pu, Y., Wang, J., Chen, C. W., Fox, P. T., et al. (2000). *In vivo* fMRI demonstration of hypothalamic function following intraperitoneal glucose administration in a rat model. *Magn. Reson. Med.* 43, 155–159. doi: 10.1002/(SICI)1522-2594(200001)43:1<155::AID-MRM20>3.0.CO;2-5

Malik, S., McGlone, F., Bedrossian, D., and Dagher, A. (2008). Ghrelin modulates brain activity in areas that control appetitive behavior. *Cell Metab.* 7, 400–409. doi: 10.1016/j.cmet.2008.03.007

Matsuda, M., Liu, Y., Mahankali, S., Pu, Y., Mahankali, A., Wang, J., et al. (1999). Altered hypothalamic function in response to glucose ingestion in obese humans. *Diabetes* 48, 1801–1806. doi: 10.2337/diabetes.48.9.1801

McEwen, B. S. (1989). "Endocrine effects on the brain and their relationship to behavior," in

*Basic Neurochemistry,* eds G. Siegel, B. Agranoff, R. W. Albers, and P. Molinoff (New York, NY: Raven Press), 893–913.

Miller, J. L., James, G. A., Goldstone, A. P., Couch, J. A., He, G., Driscoll, D. J., et al. (2007). Enhanced activation of reward mediating prefrontal regions in response to food stimuli in Prader-Willi syndrome. *J. Neurol. Neurosurg. Psychiatry* 78, 615–619. doi: 10.1136/jnnp.2006.099044

Min, D. K., Tuor, U. I., Koopmans, H. S., and Chelikani, P. K. (2011). Changes in differential functional magnetic resonance signals in the rodent brain elicited by mixed-nutrient or protein-enriched meals. *Gastroenterology* 141, 1832–1841. doi: 10.1053/j.gastro.2011.07.034

Mohacsik, P., Zeold, A., Bianco, A. C., and Gereben, B. (2011). Thyroid hormone and the neuroglia: both source and target. *J. Thyroid. Res.* 2011:215718. doi: 10.4061/2011/215718

Morita, H., Ogino, T., Seo, Y., Fujiki, N., Tanaka, K., Takamata, A., et al. (2002). Detection of hypothalamic activation by manganese ion contrasted T(1)-weighted magnetic resonance imaging in rats. *Neurosci. Lett.* 326, 101–104. doi: 10.1016/S0304-3940(02)00330-0

Morton, G. J., Cummings, D. E., Baskin, D. G., Barsh, G. S., and Schwartz, M. W. (2006). Central nervous system control of food intake and body weight. *Nature* 443, 289–295. doi: 10.1038/nature05026

Niendorf, T., Dijkhuizen, R. M., Norris, D. G., Van Lookeren Campagne, M., and Nicolay, K. (1996). Biexponential diffusion attenuation in various states of brain tissue: implications for diffusion-weighted imaging. *Magn. Reson. Med.* 36, 847–857. doi: 10.1002/mrm.1910360607

Ogawa, S., Lee, T. M., Kay, A. R., and Tank, D. W. (1990). Brain magnetic resonance imaging with contrast dependent on blood oxygenation. *Proc. Natl. Acad. Sci. U.S.A.* 87, 9868–9872. doi: 10.1073/pnas.87.24.9868

Palkovits, M. (1999). Interconnections between the neuroendocrine hypothalamus and the central autonomic system. Geoffrey Harris Memorial Lecture, Kitakyushu, Japan, October 1998. *Front. Neuroendocrinol.* 20:4. doi: 10.1006/frne.1999.0186

Parkinson, J. R., Chaudhri, O. B., and Bell, J. D. (2009). Imaging appetite-regulating pathways in the central nervous system using manganese-enhanced magnetic resonance imaging. *Neuroendocrinology* 89, 121–130. doi: 10.1159/000163751

Pautler, R. G. (2004). *In vivo*, trans-synaptic tract-tracing utilizing manganese-enhanced magnetic resonance imaging (MEMRI). *NMR Biomed.* 17, 595–601. doi: 10.1002/nbm.942

Paxinos, G., and Franklin, K. (2001). *The Mouse Brain in Stereotaxic Coordinates.* New York, NY: Academic Press.

Pellerin, L., and Magistretti, P. J. (1994). Glutamate uptake into astrocytes stimulates aerobic glycolysis: a mechanism coupling neuronal activity to glucose utilization. *Proc. Natl. Acad. Sci. U.S.A.* 91, 10625–10629. doi: 10.1073/pnas.91.22.10625

Purnell, J. Q., Klopfenstein, B. A., Stevens, A. A., Havel, P. J., Adams, S. H., Dunn, T. N., et al. (2011). Brain functional magnetic resonance imaging response to glucose and fructose infusions in humans. *Diabetes. Obes. Metab.* 13, 229–234. doi: 10.1111/j.1463-1326.2010.01340.x

Rodrigues, T. B., Fonseca, C. P., Castro, M. M., Cerdan, S., and Geraldes, C. F. (2009). 13C NMR tracers in neurochemistry: implications for molecular imaging. *Q. J. Nucl. Med. Mol. Imaging* 53, 631–645.

Rothman, D. L., Behar, K. L., Hyder, F., and Shulman, R. G. (2003). *In vivo* NMR studies of the glutamate neurotransmitter flux and neuroenergetics: implications for brain function. *Annu. Rev. Physiol.* 65, 401–427. doi: 10.1146/annurev.physiol.65.092101.142131

Santello, M., Cali, C., and Bezzi, P. (2012). Gliotransmission and the tripartite synapse. *Adv. Exp. Med. Biol.* 970, 307–331. doi: 10.1007/978-3-7091-0932-8_14

Schellinger, P. D., Jansen, O., Fiebach, J. B., Pohlers, O., Ryssel, H., Heiland, S., et al. (2000). Feasibility and practicality of MR imaging of stroke in the management of hyperacute cerebral ischemia. *AJNR* 21, 1184–1189.

Schwartz, M. W., and Morton, G. J. (2002). Obesity: keeping hunger at bay. *Nature* 418, 595–597. doi: 10.1038/418595a

Schwartz, M. W., Woods, S. C., Porte, D. Jr., Seeley, R. J., and Baskin, D. G. (2000). Central nervous system control of food intake. *Nature* 404, 661–671.

Silva, A. C. (2012). Using manganese-enhanced MRI to understand BOLD. *Neuroimage* 62, 1009–1013. doi: 10.1016/j.neuroimage.2012.01.008

Silva, A. C., Lee, J. H., Aoki, I., and Koretsky, A. P. (2004). Manganese-enhanced magnetic resonance imaging (MEMRI): methodological and practical considerations. *NMR Biomed.* 17, 532–543. doi: 10.1002/nbm.945

Smeets, P. A., De Graaf, C., Stafleu, A., Van Osch, M. J., and Van Der Grond, J. (2005). Functional magnetic resonance imaging of human hypothalamic responses to sweet taste and calories. *Am. J. Clin. Nutr.* 82, 1011–1016.

Stanley, B., Ha, L., Spears, L., Dee, M. (1993). Lateral hypothalamic injections of glutamate, kainic acid, D, L-alpha-amino-3-hydroxy–5-methyl-isoxazole propionic acid or N-methyl-D-aspartic acid rapidly elicit transient eating in rats. *Brain Res.* 613, 88–95. doi: 10.1016/0006-8993(93)90458-Y

Stanley, S., Wynne, K., McGowan, B., and Bloom, S. (2005). Hormonal regulation of food intake. *Physiol. Rev.* 85, 1131–1158. doi: 10.1152/physrev.00015.2004

Stark, J. A., Davies, K. E., Williams, S. R., and Luckman, S. M. (2006). Functional magnetic resonance imaging and c-Fos mapping in rats following an anorectic dose of m-chlorophenylpiperazine. *Neuroimage* 31, 1228–1237. doi: 10.1016/j.neuroimage.2006.01.046

Swaab, D. F., Hofman, M. A., Mirmiran, M., Ravid, R., and Van Leewen, F. W. (Eds.). (1992). *The Human Hypothalamus in Health and Disease*, Vol. 93 (Progress in Brain Research). Amsterdam, Elsevier, 3–455.

Tang-Christensen, M., Vrang, N., Ortmann, S., Bidlingmaier, M., Horvath, T. L., and Tschop, M. (2004). Central administration of ghrelin and agouti-related protein (83-132) increases food intake and decreases spontaneous locomotor activity in rats. *Endocrinology* 145, 4645–4652. doi: 10.1210/en.2004-0529

Thorburn, A. W., and Proietto, J. (1998). Neuropeptides, the hypothalamus and obesity: insights into the central control of body weight. *Pathology* 30, 229–236. doi: 10.1080/00313029800169366

Tomasi, D., Wang, G. J., Wang, R., Backus, W., Geliebter, A., Telang, F., et al. (2009). Association of body mass and brain activation during gastric distention: implications for obesity. *PLoS ONE* 4:e6847. doi: 10.1371/journal.pone.0006847

Tong, Q., Ye, C., McCrimmon, R. J., Dhillon, H., Choi, B., Kramer, M. D., et al. (2007). Synaptic glutamate release by ventromedial hypothalamic neurons is part of the neurocircuitry that prevents hypoglycemia. *Cell Metab.* 5, 383–393. doi: 10.1016/j.cmet.2007.04.001

Vidarsdottir, S., Smeets, P. A., Eichelsheim, D. L., van Osch, M. J., Viergever, M. A., Romijn, J. A., et al. (2007). Glucose ingestion fails to inhibit hypothalamic neuronal activity in patients with type 2 diabetes. *Diabetes* 56, 2547–2550. doi: 10.2337/db07-0193

Violante, I. R., Anastasovska, J., Sanchez-Canon, G. J., Rodrigues, T. B., Righi, V., Nieto-Charques, L., et al. (2009). Cerebral activation by fasting induces lactate accumulation in the hypothalamus. *Magn. Reson. Med.* 62, 279–283. doi: 10.1002/mrm.22010

Wang, X., Ge, A., Cheng, M., Guo, F., Zhao, M., Zhou, X., et al. (2012). Increased hypothalamic inflammation associated with the susceptibility to obesity in rats exposed to high-fat diet. *Exp. Diabetes Res.* 2012:847246. doi: 10.1155/2012/847246

Wisse, B. E., and Schwartz, M. W. (2009). Does hypothalamic inflammation cause obesity? *Cell Metab.* 10, 241–242.

Xu, Y., O'Brien, W. G. 3rd, Lee, C. C., Myers, M. G. Jr., and Tong, Q. (2012). Role of GABA release from leptin receptor-expressing neurons in body weight regulation. *Endocrinology* 153, 2223–2233. doi: 10.1210/en.2011-2071

Yu, X., Wadghiri, Y. Z., Sanes, D. H., and Turnbull, D. H. (2005). *In vivo* auditory brain mapping in mice with Mn-enhanced MRI. *Nat. Neurosci.* 8, 961–968. doi: 10.1038/nn1477

Zhu, X. H., Kim, S. G., Andersen, P., Ogawa, S., Ugurbil, K., and Chen, W. (1998). Simultaneous oxygenation and perfusion imaging study of functional activity in primary visual cortex at different visual stimulation frequency: quantitative correlation between BOLD and CBF changes. *Magn. Reson. Med.* 40, 703–711. doi: 10.1002/mrm.1910400510

Zwingmann, C., Leibfritz, D., and Hazell, A. S. (2003). Energy metabolism in astrocytes and

neurons treated with manganese: relation among cell-specific energy failure, glucose metabolism, and intercellular trafficking using multinuclear NMR-spectroscopic analysis. *J. Cereb. Blood Flow Metab.* 23, 756–771. doi: 10.1097/01.WCB.0000056062.25434.4D

Zwingmann, C., Leibfritz, D., and Hazell, A. S. (2004). Brain energy metabolism in a sub-acute rat model of manganese neurotoxicity: an *ex vivo* nuclear magnetic resonance study using [1-13C]glucose. *Neurotoxicology* 25, 573–587. doi: 10.1016/j.neuro.2003.08.002

**Conflict of Interest Statement:** The authors declare that the research was conducted in the absence of any commercial or financial relationships that could be construed as a potential conflict of interest.

*Received: 12 March 2013; accepted: 28 May 2013; published online: 13 June 2013.*

*Citation: Lizarbe B, Benitez A, Peláez Brioso GA, Sánchez-Montañés M, López-Larrubia P, Ballesteros P and Cerdán S (2013) Hypothalamic metabolic compartmentation during appetite regulation as revealed by magnetic resonance imaging and spectroscopy methods. Front. Neuroenergetics* ***5****:6. doi: 10.3389/fnene.2013.00006*

frontiers in
NEUROENERGETICS

MINI REVIEW ARTICLE
published: 04 October 2013
doi: 10.3389/fnene.2013.00008

# Insights into the metabolic response to traumatic brain injury as revealed by $^{13}$C NMR spectroscopy

***Brenda L. Bartnik-Olson[1]*, Neil G. Harris[2], Katsunori Shijo[2†] and Richard L. Sutton[2]***

[1] *Department of Radiology, Loma Linda University School of Medicine, Loma Linda, CA, USA*
[2] *Department of Neurosurgery, David Geffen School of Medicine at University of California Los Angeles, Los Angeles, CA, USA*

***Edited by:***
*Sebastian Cerdan, Instituto de Investigaciones Biomedicas Alberto Sols, Spain*

***Reviewed by:***
*Sebastian Cerdan, Instituto de Investigaciones Biomedicas Alberto Sols, Spain*
*Susanna Scafidi, Johns Hopkins University School of Medicine, USA*

****Correspondence:***
*Brenda L. Bartnik-Olson, Department of Radiology, Loma Linda University Medical Center, 11234 Anderson Street, Room B623, Loma Linda, CA 92354, USA*
*e-mail: bbartnik@llu.edu*

***† Present address:***
*Katsunori Shijo, Department of Neurological Surgery, Nihon University School of Medicine, Tokyo, Japan*

The present review highlights critical issues related to cerebral metabolism following traumatic brain injury (TBI) and the use of $^{13}$C labeled substrates and nuclear magnetic resonance (NMR) spectroscopy to study these changes. First we address some pathophysiologic factors contributing to metabolic dysfunction following TBI. We then examine how $^{13}$C NMR spectroscopy strategies have been used to investigate energy metabolism, neurotransmission, the intracellular redox state, and neuroglial compartmentation following injury. $^{13}$C NMR spectroscopy studies of brain extracts from animal models of TBI have revealed enhanced glycolytic production of lactate, evidence of pentose phosphate pathway (PPP) activation, and alterations in neuronal and astrocyte oxidative metabolism that are dependent on injury severity. Differential incorporation of label into glutamate and glutamine from $^{13}$C labeled glucose or acetate also suggest TBI-induced adaptations to the glutamate-glutamine cycle.

**Keywords: acetate, glucose, glutamate-glutamine cycle, magnetic resonance spectroscopy, neuroglial compartmentation, oxidative metabolism, pentose phosphate pathway**

## INTRODUCTION

A significant body of work has shown that traumatic brain injury (TBI) initiates a cascade of cellular events including potassium efflux (Katayama et al., 1990; Kawamata et al., 1995), $Ca^{++}$ accumulation (Fineman et al., 1993; Osteen et al., 2001), glutamate release (Katayama et al., 1990; Nilsson et al., 1990; Rose et al., 2002), and increased oxidative stress (Hall et al., 1993; Lewen and Hillered, 1998; Vagnozzi et al., 1999; Tyurin et al., 2000; Marklund et al., 2001) that contribute to reduced ATP production. In addition, TBI results in an immediate increase in cerebral metabolic rates for glucose (CMRglc) (Yoshino et al., 1991; Sutton et al., 1994; Lee et al., 1999; Kelly et al., 2000) that can endure for days in TBI patients (Bergsneider et al., 1997). This increase is thought to represent an increase in glycolysis (hyperglycolysis) in an attempt to meet the cellular energy demand required to restore ionic balance and maintain the neuronal membrane potential (Hovda, 1996). Studies have shown that the duration and severity of regional decreases in ATP are dependent upon TBI severity (Lee et al., 1999; Aoyama et al., 2008; Signoretti et al., 2010), and during the post-injury period where ATP production is reduced, secondary insults or activation of the injured brain can further reduce ATP levels and result in secondary cellular damage (Ip et al., 2003; Zanier et al., 2003; Aoyama et al., 2008). A secondary and enduring reduction of CMRglc (metabolic "depression") is a common finding in models of experimental TBI (Hovda et al., 1991; Yoshino et al., 1991; Sutton et al., 1994; Jiang et al., 2000; Moore et al., 2000; Prins and Hovda, 2001) and after human TBI (Langfitt et al., 1986; Yamaki et al., 1996; Bergsneider et al., 2000, 2001). Moreover, an increase in energy demand or decreased glucose availability after TBI would potentially compromise neuronal viability and functional outcomes (Vespa et al., 2003, 2007; Parkin et al., 2005; Marcoux et al., 2008).

**Abbreviations:** ATP, adenosine triphosphate; $Ca^{++}$, calcium; CCI, controlled cortical impact; CMRglc, cerebral metabolic rate of glucose; FPI, fluid percussion injury; G6PDH, glyceraldehyde-6-phosphate dehydrogenase; GAPDH, glyceraldehyde-3-phosphate dehydrogenase; GC-MS, gas chromatography-mass spectrometry; GLAST, glutamate-aspartate transporter; GLT-1, glutamate transporter 1; GLT-1v, glutamate transporter 1 variant; $NAD^+$, nicotinamide adenine dinucleotide phosphate; $NADP^+$, nicotinamide adenine dinucleotide phosphate; NMR, nuclear magnetic resonance spectroscopy; PARP, poly(ADP) ribose polymerases; PC, pyruvate carboxylase; PDH, pyruvate dehydrogenase; PPP, pentose phosphate pathway; TCA, tricarboxylic acid cycle; TBI, traumatic brain injury.

## POTENTIAL FACTORS CONTRIBUTING TO THE METABOLIC DEPRESSION AFTER TBI

Some underlying mechanisms responsible for the hypometabolic response following TBI are the overproduction of reactive oxygen and nitrogen species which can lead to poly(ADP) ribose polymerases (PARP) activation (Laplaca et al., 1999; Clark et al., 2001; Arundine et al., 2004; Mendez et al., 2004; Kauppinen, 2007; Besson, 2009) and related reductions of nicotinamide adenine dinucleotide ($NAD^+$) and nicotinamide adenine dinucleotide phosphate ($NADP^+$; Satchell et al., 2003; Clark et al., 2007; Signoretti et al., 2010). Consequently, a diminished supply of reducing equivalents for oxidoreductive reactions involved

in glucose metabolism, such as glyceraldehyde-3-phosphate dehydrogenase (GAPDH) and pyruvate dehydrogenase (PDH), could inhibit glycolysis and the entry of pyruvate into the TCA cycle resulting in energy depletion and cell death. Reduced GAPDH activity has also been shown to act as a "molecular switch" resulting in increased flux of glucose into the PPP (Ralser et al., 2007; Grant, 2008). Direct evidence for reduced activity of these enzyme complexes following TBI is an active area of research, and to date, studies have shown PDH nitrosylation (Opii et al., 2007) and alterations in the expression and phosphorylation of PDH E1alpha1 subunit (Sharma et al., 2009; Xing et al., 2009, 2012). Both increased intracellular $Ca^{++}$ or PARP activity (Lai et al., 2008) following TBI can also lead to an uncoupling of the mitochondrial electron transport chain (Dugan et al., 1995) and mitochondrial permeability transition (Gunter et al., 1994; Schinder et al., 1996; Zamzami et al., 1997), with decreases in state 3 respiratory rates (Xiong et al., 1997, 1998; Verweij et al., 2000) that would contribute to energy loss and cell death. Studies have shown that PARP inhibitors can attenuate $NAD^+$ reductions, decrease neuronal damage, and improve behavioral outcome following experimental TBI (Laplaca et al., 2001; Komjati et al., 2005; Clark et al., 2007; Besson, 2009).

## $^{13}$C STUDIES OF TBI

To more finely resolve the TBI-induced changes in glucose metabolic pathways, a number of studies have employed the use of stable isotopes ($^{13}$C) of glucose, lactate and acetate to determine the metabolic fate of these fuels and characterize changes in oxidative metabolism and neuroglia metabolic compartmentation during the acute and hypometabolic periods following experimental and clinical TBI (Bartnik et al., 2005, 2007; Dusick et al., 2007; Gallagher et al., 2009; Scafidi et al., 2009; Bartnik-Olson et al., 2010; Clausen et al., 2011). In most studies these isotopes were used in conjunction with *ex vivo* $^{13}$C nuclear magnetic resonance (NMR) spectroscopy, which allows for the simultaneous assessment of multiple metabolic pathways. The primary advantage of this technique arises from its ability to distinguish $^{13}$C incorporation into multiple metabolites as well as into the specific carbon positions within the same metabolite, resulting in a detailed analysis of the metabolic "fate" of the $^{13}$C label (Bachelard and Badar-Goffer, 1993; Cruz and Cerdan, 1999). The relative $^{13}$C enrichment at each carbon position and the ratios between isotopomers of glutamate and glutamine gives additional information regarding enzyme usage, neurotransmitter synthesis, and neuroglia metabolic compartmentation (Badar-Goffer et al., 1990; Shank et al., 1993; Hassel et al., 1995; Aureli et al., 1997). As shown in **Figure 1**, $^{13}$C NMR spectroscopy can be used to measure TBI-induced changes in glycolysis ($^{13}$C lactate labeling), oxidative metabolism within, and interactions between, the neuron and astrocyte compartments (glutamate and glutamine labeling). By using [1, 2 $^{13}C_2$] glucose as the substrate, injury-induced changes in the activity of the pentose phosphate pathway (PPP) can be assessed using the ratio between the lactate labeled in two carbon positions (doublet) via glycolysis (C2 and C3) and lactate labeled in the singlet C3 carbon position (Cruz et al., 1998; Lee et al., 1998). However, the formation of a lactate C3 singlet also results via the pyruvate recycling pathway (Hassel and Sonnewald, 1995). In contrast, lactate labeling using [1, 2 $^{13}C_2$] acetate is derived exclusively from the pyruvate recycling pathway and comparisons between the lactate C3 singlet/doublet ratio from [1, 2 $^{13}C_2$] glucose and the lactate labeling from [1, 2 $^{13}C_2$] acetate could provide a valid method for more accurately measuring the contribution of the PPP to the post-injury response. The cytosolic $NAD^+$/NADH redox state of the injured tissue can be estimated by the ratio of glutamate labeled in two carbon positions via glycolysis (C3 and C4) to the labeling of glutamate labeled in the C4 position via the recycling of pyruvate from labeled oxaloacetate via malic enzyme using either [1, 2 $^{13}C_2$] glucose or [1, 2 $^{13}C_2$] acetate (ME; Cruz et al., 1998; Cerdan et al., 2006). This more finely-grained approach to monitoring the fate of labeled fuels provides an ideal platform from which to determine how fuel supplementation after injury may prevent on-going metabolic deficits.

### EXPERIMENTAL MODELS USED IN $^{13}$C STUDIES OF TBI

To date $^{13}$C studies have been conducted using the lateral fluid percussion injury (FPI) or the unilateral controlled cortical impact (CCI) injury models of TBI. The FPI model can produce a diffuse pattern of neuronal and axonal injury, while CCI is often termed a more focal injury model due to the contusion induced (Cernak, 2005) although widespread axonal injury occurs after CCI (Hall et al., 2008). With moderate injury severity the period of hyperglycolysis and the extent of ATP reduction in cortex is reduced in the FPI model compared to CCI (Lee et al., 1999), but in both TBI models a widespread reduction in CMRglc is observed throughout the injured hemisphere within a few hours (Hovda et al., 1991; Yoshino et al., 1991; Sutton et al., 1994; Moore et al., 2000). Although CMRglc recovers to baseline within 10 days after FPI (Yoshino et al., 1991; Moore et al., 2000) substantial reductions of CMRglc are still present by 15 days following CCI injury (Moro et al., 2011).

### GLYCOLYSIS AND PPP METABOLISM FOLLOWING TBI

Numerous experimental studies have reported an acute increase in extracellular lactate levels consistent with hyperglycolysis following TBI (Inao et al., 1988; Kawamata et al., 1995; Chen et al., 2000). In keeping with these observations, studies using *ex vivo* $^{13}$C NMR spectroscopy have reported increased $^{13}$C labeling of lactate from $^{13}$C glucose in the injured cortex within the first 6 h following a CCI injury in both the adult (Bartnik et al., 2005) and immature rat brain (Scafidi et al., 2009). In the adult brain this increase was seen at 3.5 h after injury which then normalized by 24 h (Bartnik et al., 2005). Increased lactate labeling from $^{13}$C-labeled glucose was also detected by gas chromatography/mass spectroscopy (GC-MS) from microdialysis samples of CCI injured cerebral cortex in rats (Clausen et al., 2011) and in blood samples from moderate-severe human TBI patients (Dusick et al., 2007). In adult rats with FPI, lactate $^{13}$C labeling was reduced at 24 h post-injury (Bartnik et al., 2007) indicating reduced glucose metabolism via glycolysis in this more diffuse TBI model. It remains to be determined whether this finding is the result of reduced GAPDH activity and whether similar findings are replicated at all developmental stages.

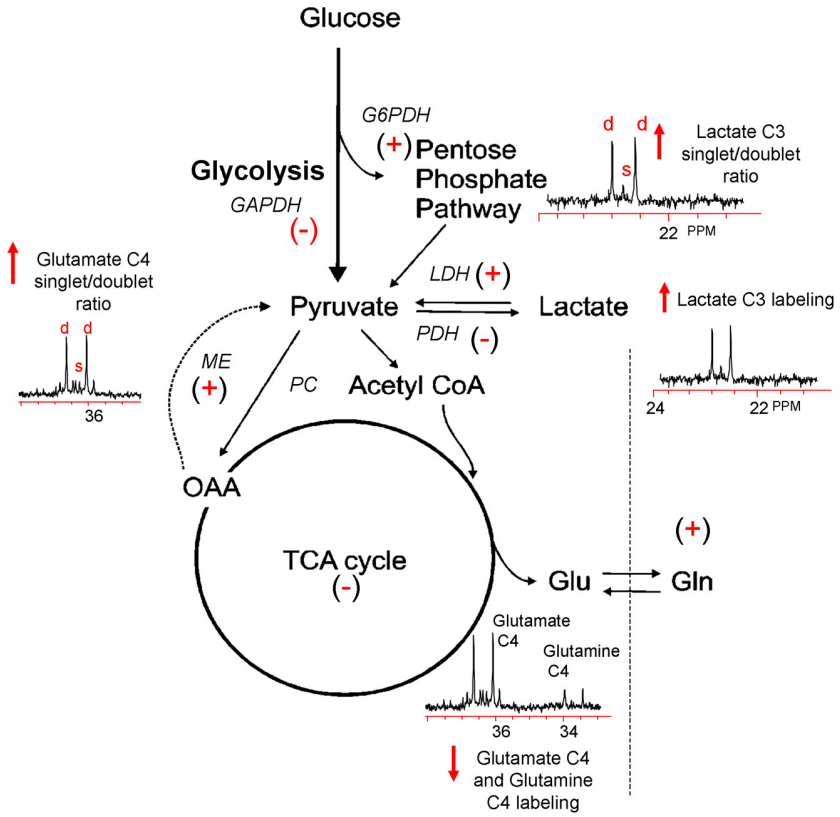


**FIGURE 1 | Simplified illustration of the metabolic response to TBI as determined by $^{13}$C NMR spectroscopy using [1, 2 $^{13}C_2$] glucose.** TBI-induced ion fluxes and neurotransmitter release can increase anaerobic metabolism and initiate an injury cascade including increased oxidative/nitrosative stress, PARP-1 activation, and $NAD^+$ and/or $NAPD^+$ reductions. These in turn are thought to result in the activation (+) or inhibition (−) of enzymes contributing to the metabolic response to TBI (see text). Using [1, 2 $^{13}C_2$] glucose as a precursor, $^{13}$C NMR spectroscopy can be used to measure increases (↑) or decreases (↓) in glycolysis, the PPP, oxidative metabolism in the TCA cycle, and the pyruvate recycling system by monitoring the production of [2, 3 $^{13}C_2$] lactate, [2 $^{13}$C] lactate, and [4, 5 $^{13}C_2$] glutamate and [4 $^{13}$C] glutamate.

*Ex vivo* $^{13}$C NMR spectroscopy studies of cerebral cortex after CCI or FPI using [1, 2 $^{13}C_2$] glucose also reported a significant increase in lactate labeling via the PPP (Bartnik et al., 2005, 2007). This finding was supported by a clinical study of severe TBI patients, where evidence of increased glucose metabolism via the PPP was detected in blood samples using GC-MS following an infusion of [1, 2 $^{13}C_2$] glucose (Dusick et al., 2007). The PPP functions in producing reducing equivalents of NADPH for biosynthetic reactions (Baquer et al., 1988) and it has been demonstrated that this pathway has an enormous reserve capacity that can be drawn on during periods of oxidative stress to act as a proton donor during the redox cycling of glutathione (Hothersall et al., 1982; Schrader et al., 1993). Peroxynitrite has been shown to activate glucose-6-phosphate dehydrogenase (G6PDH), the enzyme catalyzing the rate limiting step of the oxidative branch of the PPP, resulting in the rapid activation of the PPP and increased NADPH accumulation in astrocytes and neurons (Garcia-Nogales et al., 2003). In addition, *in vitro* studies of neurons and astrocytes in high glucose environments show increased PPP activity and glutathione levels in astrocytes, which can reduce levels of oxidative stress and protect neurons in mixed cultures (Takahashi et al., 2012). Recently, it was shown that pyruvate generated from metabolism via the PPP can be metabolized in the TCA cycle and contributes to the formation of glutamate in neurons (Brekke et al., 2012). Thus, it is tempting to hypothesize, but remains to be proven that increased PPP activity following TBI reflects a response by injured cells to combat oxidative/nitrosative stress and/or provide additional substrates for oxidative metabolism.

## OXIDATIVE METABOLISM FOLLOWING TBI

As previously described, mitochondrial dysfunction is thought to play a key role in the pathophysiology of TBI. Studies using cytochrome C oxidase histochemistry as a measure of oxidative phosphorylation on the mitochondrial membrane, show a diffuse decrease in staining throughout the injured hemisphere of both FPI (Hovda et al., 1991) and CCI (Moro and Sutton, 2010) injured adult rats. Moreover, measurements of mitochondrial respiration rates have shown TBI-induced reductions in mitochondrial state 3 respiratory rates in immature and adult rat experimental models and humans (Xiong et al., 1997; Verweij et al., 2000; Kilbaugh et al., 2011). Neuroprotective strategies

targeting mitochondrial dysfunction such as cyclosporin A (or its analog), oxidative/nitrosative species scavengers, or alternative metabolic substrates to glucose have shown reduced cell death, improvements in mitochondrial function, and/or functional outcome (Fukushima et al., 2009; Moro and Sutton, 2010; Mustafa et al., 2010; Kilbaugh et al., 2011; Readnower et al., 2011; Singh et al., 2013). Mitochondrial dysfunction, specifically changes in the oxidative metabolism of metabolic fuels, can be measured using $^{13}$C NMR spectroscopy by determining the amount of $^{13}$C incorporation into glutamate and glutamine. However, oxidative metabolism in astrocytes and the specific contribution of glutamine to metabolic compartmentation is more accurately measured using acetate, a glial specific substrate (Waniewski and Martin, 1998; Lebon et al., 2002; Deelchand et al., 2009; Shen, 2013) or [2 $^{13}$C] glucose that preferentially labels glutamine via pyruvate carboxylase (PC).

Using an adult rat CCI injury model (Bartnik et al., 2005), the amount of $^{13}$C label incorporated into the glutamate C2, C3, and C4 isotopomers did not differ from naive, suggesting that oxidative metabolism and the activity of PDH in glutamatergic neurons is maintained in the injured cortex over the first 24 h after injury. In the same study, a significant increase in $^{13}$C labeling of the glutamine C3 isotopomer was detected at 3.5 h after injury. Since the specific contribution of glutamine labeling via oxidative metabolism in astrocytes is difficult to ascertain using [1, 2 $^{13}C_2$] labeled glucose, this study could not clarify if the increased labeling of glutamine reflected the *de novo* synthesis of glutamine or increased glutamate uptake by astrocytes in response to injury. In support of the latter mechanism, increased glutamate metabolism via the astrocytic TCA cycle occurs when extracellular glutamate concentrations are increased (McKenna et al., 1996) and during ischemia (Haberg et al., 1998; Pascual et al., 1998). Also, excitotoxic injury in rats alters glutamate-glutamine cycle enzymes to favor increased glutamine synthesis (Ramonet et al., 2004). In contrast to CCI, adult rats with FPI showed reduced $^{13}$C labeling of all glutamate and glutamine isotopomers at 3.5 h post injury, indicating reduced oxidative metabolism in both neurons and astrocytes in the injured cortex (Bartnik et al., 2007). In this model, the $^{13}$C labeling of glutamate returned to non-injury levels by 24 h while reductions in glutamine labeling persisted. The divergent pattern of $^{13}$C labeling between these two injury models likely represents previously reported differences in the extent and severity of CMRglc changes in the two models (Yoshino et al., 1991; Sutton et al., 1994; Lee et al., 1999; Moore et al., 2000).

In contrast to what is observed in studies using adult models, a $^{13}$C NMR spectroscopy study of the injured immature rat brain found increased labeling of glutamate and glutamine C3 and C4 isotopomers at 5.5 and 6 h following CCI injury (Scafidi et al., 2009). Scafidi et al. (2009) proposed that there could be an accumulation of glutamate due to impaired glutamate entry into the mitochondria via reduced activity of the aspartate-glutamate carrier (McKenna et al., 2006; McKenna, 2007), or reduced glutamate oxidation to α-ketoglutarate via decreased activity of α-ketoglutarate dehydrogenase due to oxidative stress (Starkov et al., 2004). The delayed increase in labeling also suggests a delay in the metabolic response in the immature brain and highlight important developmental differences in the response to injury (Scafidi et al., 2009).

## ASTROCYTE METABOLISM AND NEUROGLIA METABOLIC COMPARTMENTATION FOLLOWING TBI

Astrocytes show pronounced changes in gene expression, cellular hypertrophy and proliferation, in a degree relative to the severity of brain injury. Studies in both experimental and human brain injury have demonstrated the presence of reactive astrocytes (Bourke et al., 1980; Cortez et al., 1989; Castejón, 1998). Reactive astrocytes play dual roles following injury, one that may result in a detrimental increase in glutamate excitotoxicity or inflammation, the other being brain protection or repair (Laird et al., 2008). A transient down regulation of glutamate transporters GLT-1, GLT-1v, and GLAST on astrocytes after experimental (Rao et al., 1998, 2001; Yi and Hazell, 2006) and human TBI (van Landeghem et al., 2006; Beschorner et al., 2007) may well contribute to the injury process. However, ablation of reactive astrocytes following experimental CCI in transgenic mice resulted in greater loss of cortical tissue and inflammation, suggesting an essential protective role for astrocytes after TBI (Myer et al., 2006).

Determining the role that astrocytes play in the metabolic response to TBI is an important research direction. Astrocytes play a pivotal role in meeting the energy requirements of neurons through the glutamate-glutamine cycle that links the exchange of glutamate and glutamine between glutamatergic neurons and astrocytes (Van den Berg et al., 1969). Another proposed mechanism of metabolite trafficking between these cells is the lactate shuttle, where astrocytes preferentially metabolize glucose via glycolysis and transfer lactate to neurons during high metabolic demand (Magistretti and Pellerin, 1999; Bouzier-Sore et al., 2002; Pellerin et al., 2007), although yet to be proven and a topic of ongoing debate (Jolivet et al., 2010; Mangia et al., 2011). The net synthesis of glutamate in neurons also requires a compensatory flux of TCA cycle intermediates, notably glutamine from astrocytes (Schousboe et al., 1997), as neurons lack the capacity to generate TCA cycle intermediates. This net synthesis of TCA cycle intermediates, glutamate and glutamine depends upon the entry of pyruvate, via an anaplerotic pathway, into the TCA cycle. In the brain this is exclusively achieved by PC, an astrocyte specific enzyme (Yu et al., 1983; Shank et al., 1985). Numerous *in vitro* studies have shown that astrocytes supply TCA cycle substrates to neurons during periods of glucose and/or oxygen deprivation (Hertz, 2003; Bambrick et al., 2004; Peng et al., 2007), suggesting that astrocytes may play an even greater nutritional role for neurons in the injured state. Given the essential role of neuroglia metabolic coupling in normal brain, a greater appreciation of the effect of TBI on metabolic coupling is an important and necessary contribution to understanding the metabolic response to TBI.

The $^{13}$C NMR studies detailed in section Glycolysis and PPP Metabolism Following TBI suggest that neuroglia metabolic coupling is altered in two different rat models of TBI. To more clearly define the contribution of this metabolic coupling over

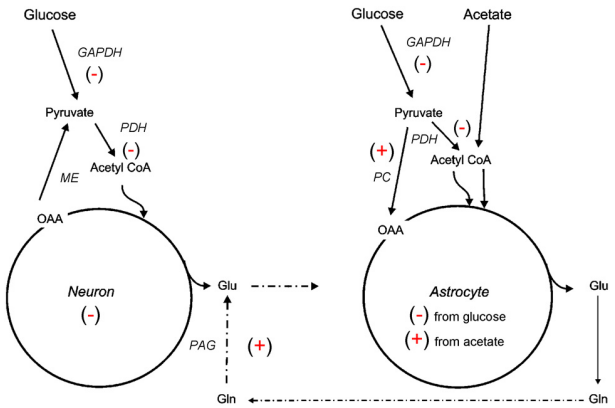


**FIGURE 2 | Simplified illustration of changes in neuroglial metabolic coupling following FPI as determined using $^{13}$C labeled glucose and acetate.** Findings show reduced (–) glucose metabolism in both neuron and astrocyte metabolic compartments, possibly due to reduced activity of GAPDH and/or PDH. The capacity for oxidative metabolism was retained (+) in the astrocyte compartment as $^{13}$C labeling was detected in glutamine isotopomers resulting from acetate metabolism via the TCA cycle and PC. Labeling of glutamate from $^{13}$C acetate indicates continued activity (+) of the glutamate-glutamine cycle and phosphate activated glutaminase (PAG). These findings could be interpreted to mean that astrocytes have a supportive metabolic role to neurons following TBI.

the hypometabolic period, a $^{13}$C NMR spectroscopy study using [1 $^{13}$C] glucose, which is consumed in both neuronal and glial compartments, and [1, 2 $^{13}C_2$] acetate, which is metabolized solely within the glial compartment, was undertaken using an adult rat FPI model (Bartnik-Olson et al., 2010). **Figure 2** illustrates the metabolic alterations to neuronal and astrocyte metabolism determined using this strategy. Similar to previous findings, decreased $^{13}$C labeling of all glutamate isotopomers from the metabolism of glucose was observed early post-injury, but recovered over time, indicating that injury-induced decreases in the oxidative metabolism of glucose in neurons is consistent with the time course of reduced CMRglc following FPI (Yoshino et al., 1991; Moore et al., 2000). Although the $^{13}$C labeling of glutamine C4 from glucose in the first turn of the astrocyte TCA cycle was reduced, the labeling of glutamine C2 and C3 remained unchanged, indicating that the metabolism of glucose via PC was unaffected by FPI. In addition, the incorporation of $^{13}$C label from acetate into glutamine and glutamate C4 was maintained, indicating that oxidative metabolism in astrocytes and the functional activity of the glutamate-glutamine cycle were preserved during the hypometabolic period following FPI. $^{13}$C labeling of glutamine from $^{13}$C acetate was also demonstrated following human TBI using microdialysis samples and $^{13}$C NMR spectroscopy (Gallagher et al., 2009), although glutamate labeling was seen in only a few patients. It is important to note that acetate enters the astrocyte TCA cycle as acetyl CoA, bypassing any dysfunction in glycolysis or at the level of PDH, which may relate to the ability of an acetate precursor to improve ATP and improve motor performance after CCI (Arun et al., 2010).

### LIMITATIONS AND FUTURE DIRECTIONS

The studies reviewed above highlight alterations to a number of key metabolic processes during the period of metabolic depression following experimental TBI. Although these studies are valuable in their contributions linking the period of metabolic depression to qualitative changes in a number of metabolic processes, they are limited by their descriptive nature. *In vivo* metabolic reactions are dynamic and future studies making use of mathematical models to extract quantitative flux rates would vastly improve our understanding of TBI-induced changes in neuroglia compartmentation and neurotransmission. Moreover, clinical (human) studies using dynamic $^{13}$C NMR spectroscopy is a logical next step in advancing our understanding brain function after TBI.

One goal of future animal and clinical $^{13}$C studies should be to understand the cellular basis of metabolic alterations following TBI. It is important to establish how individual cell types respond to TBI. For example, studies employing compartment specific labels (singly or in combination) could delineate a cell-type specific preference for a metabolic fuel that would preferentially enhance outcome. In addition, future studies of metabolic flux during the acute period of hyperglycolysis could provide direct evidence of the metabolic forces (increased neurotransmission and/or energetics) driving this need. Moreover, comparisons between findings from the acute period of hyperglycolysis and the period of metabolic depression could establish key time points and potential targets for metabolic intervention.

## CONCLUSION

TBI induces multiple primary and secondary injury mechanisms that can impact the supply of fuels and/or alter the functions of metabolic enzymes and proteins which can lead to deficits in energy availability. $^{13}$C NMR spectroscopy can be utilized to probe multiple aspects of the metabolic response to TBI, including changes in glycolysis, PPP activity, oxidative metabolism, and neuroglial metabolic compartmentation. As illustrated in the materials reviewed above, numerous experimental treatments that improve cerebral metabolism, reduce neuronal injury, and improve functional outcomes after TBI are currently being investigated, and future studies using $^{13}$C NMR spectroscopy to evaluate the metabolic responses to such treatments should provide valuable insights into the mechanisms of actions.

## AUTHOR CONTRIBUTIONS

Dr's. Bartnik-Olson and Sutton prepared the initial draft of this manuscript, Dr's. Harris and Shijo contributed additions and edits to the final versions of the manuscript.

## ACKNOWLEDGMENTS

This work was supported by the UCLA Brain Injury Research Center and P01NS058489 from the National Institute of Neurological Disorders and Stroke (NINDS). The content is the sole responsibility of the authors and does not necessarily represent official views of the NINDS or the National Institutes of Health.

## REFERENCES


Aoyama, N., Lee, S. M., Moro, N., Hovda, D. A., and Sutton, R. L. (2008). Duration of ATP reduction affects extent of CA1 cell death in rat models of fluid percussion injury combined with secondary ischemia. *Brain Res.* 1230, 310–319. doi: 10.1016/j.brainres.2008.07.006

Arun, P., Ariyannur, P. S., Moffett, J. R., Xing, G., Hamilton, K., Grunberg, N. E., et al. (2010). Metabolic acetate therapy for the treatment of traumatic brain injury. *J. Neurotrauma* 27, 293–298. doi: 10.1089/neu.2009.0994

Arundine, M., Aarts, M., Lau, A., and Tymianski, M. (2004). Vulnerability of central neurons to secondary insults after *in vitro* mechanical stretch. *J. Neurosci.* 24, 8106–8123. doi: 10.1523/JNEUROSCI.1362-04.2004

Aureli, T., Di Cocco, M. E., Calvani, M., and Conti, F. (1997). The entry of [1-13C] glucose into biochemical pathways reveals a complex compartmentation and metabolite trafficking between glia and neurons: a study by 13C-NMR spectroscopy. *Brain Res.* 765, 218–227. doi: 10.1016/S0006-8993(97)00514-3

Bachelard, H. S., and Badar-Goffer, R. S. (1993). NMR spectroscopy in neurochemistry. *J. Neurochem.* 61, L412–L429. doi: 10.1111/j.1471-4159.1993.tb02141.x

Badar-Goffer, R. S., Bachelard, H. S., and Morris, P. G. (1990). Cerebral metabolism of acetate and glucose studied by 13C-n.m.r. spectroscopy. A technique for investigating metabolic compartmentation in the brain. *Biochem. J.* 266, 133–139.

Bambrick, L., Kristian, T., and Fiskum, G. (2004). Astrocyte mitochondrial mechanisms of ischemic brain injury and neuroprotection. *Neurochem. Res.* 29, 601–608. doi: 10.1023/B:NERE.0000014830.06376.e6

Baquer, N. Z., Hothersall, J. S., and McLean, P. (1988). Function and regulation of the pentose phosphate pathway in brain. *Curr. Top. Cell. Regul.* 29, 265–289.

Bartnik, B. L., Lee, S. M., Hovda, D. A., and Sutton, R. L. (2007). The fate of glucose during the period of decreased metabolism after fluid percussion injury: a 13C NMR study. *J. Neurotrauma* 24, 1079–1092. doi: 10.1089/neu.2006.0210

Bartnik, B. L., Sutton, R. L., Fukushima, M., Harris, N. G., Hovda, D. A., and Lee, S. M. (2005). Upregulation of pentose phosphate pathway and preservation of tricarboxylic acid cycle flux after experimental brain injury. *J. Neurotrauma* 22, 1052–1065. doi: 10.1089/neu.2005.22.1052

Bartnik-Olson, B. L., Oyoyo, U., Hovda, D., and Sutton, R. L. (2010). Astrocyte oxidative metabolism and metabolite trafficking after fluid percussion brain injury in adult rats. *J. Neurotrauma* 27, 2191–2202. doi: 10.1089/neu.2010.1508

Bergsneider, M., Hovda, D. A., Lee, S. M., Kelly, D. F., McArthur, D. L., Vespa, P. M., et al. (2000). Dissociation of cerebral glucose metabolism and level of consciousness during the period of metabolic depression following human traumatic brain injury. *J. Neurotrauma* 17, 389–401. doi: 10.1089/neu.2000.17.389

Bergsneider, M., Hovda, D. A., McArthur, D. L., Etchepare, M., Huang, S.-C., Sehati, N., et al. (2001). Metabolic recovery following human traumatic brain injury based on FDG-PET: time course and relationship to neurological disability. *J. Head Trauma Rehabil.* 16, 135–148. doi: 10.1097/00001199-200104000-00004

Bergsneider, M., Hovda, D. A., Shalmon, E., Kelly, D. F., Vespa, P. M., Martin, N. A., et al. (1997). Cerebral hyperglycolysis following severe traumatic brain injury in humans: a positron emission tomography study. *J. Neurosurg.* 86, 241–251. doi: 10.3171/jns.1997.86.2.0241

Beschorner, R., Dietz, K., Schauer, N., Mittelbronn, M., Schluesener, H. J., Trautmann, K., et al. (2007). Expression of EAAT1 reflects a possible neuroprotective function of reactive astrocytes and activated microglia following human traumatic brain injury. *Histol. Histopathol.* 22, 515–526.

Besson, V. C. (2009). Drug targets for traumatic brain injury from poly(ADP-ribose)polymerase pathway modulation. *Br. J. Pharmacol.* 157, 695–704. doi: 10.1111/j.1476-5381.2009.00229.x

Bourke, R. S., Kimelberg, H. K., Nelson, L. R., Barron, K. D., Auen, E. L., Popp, A. J., et al. (1980). Biology of glial swelling in experimental brain edema. *Adv. Neurol.* 28, 99–109.

Bouzier-Sore, A. K., Merle, M., Magistretti, P. J., and Pellerin, L. (2002). Feeding active neurons: (re)emergence of a nursing role for astrocytes. *J. Physiol. Paris* 96, 273–282. doi: 10.1016/S0928-4257(02)00016-5

Brekke, E. M., Walls, A. B., Schousboe, A., Waagepetersen, H. S., and Sonnewald, U. (2012). Quantitative importance of the pentose phosphate pathway determined by incorporation of (13)C from [2-(13)C]- and [3-(13)C]glucose into TCA cycle intermediates and neurotransmitter amino acids in functionally intact neurons. *J. Cereb. Blood Flow Metab.* 32, 1788–1799. doi: 10.1038/jcbfm.2012.85

Castejón, O. J. (1998). Morphological astrocytic changes in complicated human brain trauma. A light and electron microscopic study. *Brain Inj.* 12, 409–427. doi: 10.1080/026990598122539

Cerdan, S., Rodrigues, T. B., Sierra, A., Benito, M., Fonseca, L. L., Fonseca, C. P., et al. (2006). The redox switch/redox coupling hypothesis. *Neurochem. Int.* 48, 523–530. doi: 10.1016/j.neuint.2005.12.036

Cernak, I. (2005). Animal models of head trauma. *NeuroRx.* 2, 410–422. doi: 10.1602/neurorx.2.3.410

Chen, T., Qian, Y. Z., Di, X., Rice, A., Zhu, J. P., and Bullock, R. (2000). Lactate/glucose dynamics after rat fluid percussion brain injury. *J. Neurotrauma* 17, 135–142. doi: 10.1089/neu.2000.17.135

Clark, R. S., Vagni, V. A., Nathaniel, P. D., Jenkins, L. W., Dixon, C. E., and Szabo, C. (2007). Local administration of the poly(ADP-ribose) polymerase inhibitor INO-1001 prevents $NAD^+$ depletion and improves water maze performance after traumatic brain injury in mice. *J. Neurotrauma* 24, 1399–1405. doi: 10.1089/neu.2007.0305

Clark, R. S. B., Chen, M., Kochanek, P. M., Watkins, S. C., Jin, K. L., Draviam, R., et al. (2001). Detection of single- and double-strand DNA breaks after traumatic brain injury in rats: comparison of *in situ* labeling techniques using DNA polymerase I, the Klenow fragment of DNA polymerase I, and terminal deoxynucleotidyl transferase. *J. Neurotrauma* 18, 675–689. doi: 10.1089/089771501750357627

Clausen, F., Hillered, L., and Gustafsson, J. (2011). Cerebral glucose metabolism after traumatic brain injury in the rat studied by 13C-glucose and microdialysis. *Acta Neurochir.(Wien.)* 153, 653–658. doi: 10.1007/s00701-010-0871-7

Cortez, S. C., McIntosh, T. K., and Noble, L. J. (1989). Experimental fluid percussion brain injury: vascular disruption and neuronal and glial alterations. *Brain Res.* 482, 271–282. doi: 10.1016/0006-8993(89)91190-6

Cruz, F., Scott, S. R., Barroso, I., Santisteban, P., and Cerdan, S. (1998). Ontogeny and cellular localization of the pyruvate recycling system in rat brain. *J. Neurochem.* 70, 2613–2619. doi: 10.1046/j.1471-4159.1998.70062613.x

Cruz, F., and Cerdan, S. (1999). Quantitative 13C NMR studies of metabolic compartmentation in the adult mammalian brain. *NMR Biomed.* 12, 451–462. doi: 10.1002/(SICI)1099-1492(199911)12:7<451::AID-NBM571>3.3.CO;2-5

Deelchand, D. K., Shestov, A. A., Koski, D. M., Uğurbil, K., and Henry, P. G. (2009). Acetate transport and utilization in the rat brain. *J. Neurochem.* 109, 46–54. doi: 10.1111/j.1471-4159.2009.05895.x

Dugan, L. L., Sensi, S. L., Canzoniero, L. M., Handran, S. D., Rothman, S. M., Lin, T. S., et al. (1995). Mitochondrial production of reactive oxygen species in cortical neurons following exposure to N-methyl-D-aspartate. *J. Neurosci.* 15, 6377–6388.

Dusick, J. R., Glenn, T. C., Lee, W. N., Vespa, P. M., Kelly, D. F., Lee, S. M., et al. (2007). Increased pentose phosphate pathway flux after clinical traumatic brain injury: a [1,2-(13)C(2)]glucose labeling study in humans. *J. Cereb. Blood Flow Metab.* 27, 1593–1602. doi: 10.1038/sj.jcbfm.9600458

Fineman, I., Hovda, D. A., Smith, M., Yoshino, A., and Becker, D. P. (1993). Concussive brain injury is associated with a prolonged accumulation of calcium: a 45 Ca autoradiographic study. *Brain Res.* 624, 94–102. doi: 10.1016/0006-8993(93)90064-T

Fukushima, M., Lee, S. M., Moro, N., Hovda, D. A., and Sutton, R. L. (2009). Metabolic and histologic effects of sodium pyruvate treatment in the rat after cortical contusion injury. *J. Neurotrauma* 26, 1095–1110. doi: 10.1089/neu.2008.0771

Gallagher, C. N., Carpenter, K. L., Grice, P., Howe, D. J., Mason, A., Timofeev, I., et al. (2009). The human brain utilizes lactate via the tricarboxylic acid cycle: a 13C-labelled microdialysis and high-resolution nuclear magnetic resonance study. *Brain* 132, 2839–2849. doi: 10.1093/brain/awp202

Garcia-Nogales, P., Almeida, A., and Bolanos, J. P. (2003). Peroxynitrite protects neurons against nitric oxide-mediated apoptosis. A key role for glucose-6-phosphate dehydrogenase

activity in neuroprotection. *J. Biol. Chem*. 278, 864–874. doi: 10.1074/jbc.M206835200

Grant, C. M. (2008). Metabolic reconfiguration is a regulated response to oxidative stress. *J. Biol.* 7, 1. doi: 10.1186/jbiol63

Gunter, T. E., Gunter, K. K., Sheu, S. S., and Gavin, C. E. (1994). Mitochondrial calcium transport: physiological and pathological relevance. *Am. J. Physiol*. 267, C313–C339.

Haberg, A., Qu, H., Haraldseth, O., Unsgard, G., and Sonnewald, U. (1998). *In vivo* injection of [1-13C]glucose and [1,2-13C]acetate combined with *ex vivo* 13C nuclear magnetic resonance spectroscopy: a novel approach to the study of middle cerebral artery occlusion in the rat. *J. Cereb. Blood Flow Metab.* 18, 1223–1232. doi: 10.1097/00004647-199811000-00008

Hall, E. D., Andrus, P. K., and Yonkers, P. A. (1993). Brain hydroxyl radical generation in acute experimental head injury. *J. Neurochem*. 60, 588–594. doi: 10.1111/j.1471-4159.1993.tb03189.x

Hall, E. D., Bryant, Y. D., Cho, W., and Sullivan, P. G. (2008). Evolution of post-traumatic neurodegeneration after controlled cortical impact traumatic brain injury in mice and rats as assessed by the de olmos silver and fluorojade staining methods. *J. Neurotrauma* 25, 235–247. doi: 10.1089/neu.2007.0383

Hassel, B., Sonnewald, U., and Fonnum, F. (1995). Glial-neuronal interactions as studied by cerebral metabolism of [2-13C]acetate and [1-13C]glucose: an *ex vivo* 13C NMR spectroscopic study. *J. Neurochem*. 64, 2773–2782. doi: 10.1046/j.1471-4159.1995.64062773.x

Hassel, B., and Sonnewald, U. (1995). Glial formation of pyruvate and lactate from TCA cycle intermediates: implications for the inactivation of transmitter amino acids. *J. Neurochem*. 65, 2227–2234. doi: 10.1046/j.1471-4159.1995.65052227.x

Hertz, L. (2003). Astrocytic amino acid metabolism under control conditions and during oxygen and/or glucose deprivation. *Neurochem. Res*. 28, 243–258. doi: 10.1023/A:1022377100379

Hothersall, J. S., Greenbaum, A. L., and McLean, P. (1982). The functional significance of the pentose phosphate pathway in synaptosomes: protection against peroxidative damage by catecholamines and oxidants. *J. Neurochem*. 39, 1325–1332. doi: 10.1111/j.1471-4159.1982.tb12574.x

Hovda, D. A. (1996). "Metabolic dysfunction," in *Neurotrauma,* eds R. K.Narayan, J. E. Wilberger, and J. T. Povlishock (New York, NY: McGraw-Hill, Inc.), 1459–1478.

Hovda, D. A., Yoshino, A., Kawamata, T., Katayama, Y., and Becker, D. P. (1991). Diffuse prolonged depression of cerebral oxidative metabolism following concussive brain injury in the rat: a cytochrome oxidase histochemistry study. *Brain Res.* 567, 1–10. doi: 10.1016/0006-8993(91)91429-5

Inao, S., Marmarou, A., Clarke, G. D., Andersen, B. J., Fatouros, P. P., and Young, H. F. (1988). Production and clearance of lactate from brain tissue, cerebrospinal fluid, and serum following experimental brain injury. *J. Neurosurg*. 69, 736–744. doi: 10.3171/jns.1988.69.5.0736

Ip, E. Y., Zanier, E. R., Moore, A. H., Lee, S. M., and Hovda, D. A. (2003). Metabolic, neurochemical, and histologic responses to vibrissa motor cortex stimulation after traumatic brain injury. *J. Cereb. Blood Flow Metab*. 23, 900–910. doi: 10.1097/01.WCB.0000076702.71231.F2

Jiang, X. B., Ohno, K., Qian, L., Tominaga, B., Kuroiwa, T., Nariai, T., et al. (2000). Changes in local cerebral blood flow, glucose utilization, and mitochondrial function following traumatic brain injury in rats. *Neurol. Med. Chir. (Tokyo)* 40, 16–28. doi: 10.2176/nmc.40.16

Jolivet, R., Allaman, I., Pellerin, L., Magistretti, P. J., and Weber, B. (2010). Comment on recent modeling studies of astrocyte-neuron metabolic interactions. *J. Cereb. Blood Flow Metab*. 30, 1982–1986. doi: 10.1038/jcbfm.2010.132

Katayama, Y., Becker, D. P., Tamura, T., and Hovda, D. A. (1990). Massive increases in extracellular potassium and the indiscriminate release of glutamate following concussive brain injury. *J. Neurosurg*. 73, 889–900. doi: 10.3171/jns.1990.73.6.0889

Kauppinen, T. M. (2007). Multiple roles for poly(ADP-ribose)polymerase-1 in neurological disease. *Neurochem. Int.* 50, 954–958. doi: 10.1016/j.neuint.2006.11.010

Kawamata, T., Katayama, Y., Hovda, D. A., Yoshino, A., and Becker, D. P. (1995). Lactate accumulation following concussive brain injury: the role of ionic fluxs induced by excitatory amino acids. *Brain Res.* 674, 196–204. doi: 10.1016/0006-8993(94)01444-M

Kelly, D. F., Kozlowski, D. A., Haddad, E., Echiverri, A., Hovda, D. A., and Lee, S. M. (2000). Ethanol reduces metabolic uncoupling following experimental head injury. *J. Neurotrauma* 17, 261–272. doi: 10.1089/neu.2000.17.261

Kilbaugh, T. J., Bhandare, S., Lorom, D. H., Saraswati, M., Robertson, C. L., and Margulies, S. S. (2011). Cyclosporin a preserves mitochondrial function after traumatic brain injury in the immature rat and piglet. *J. Neurotrauma* 28, 763–774. doi: 10.1089/neu.2010.1635

Komjati, K., Besson, V. C., and Szabo, C. (2005). Poly (adp-ribose) polymerase inhibitors as potential therapeutic agents in stroke and neurotrauma. *Curr. Drug Targets CNS Neurol. Disord*. 4, 179–194. doi: 10.2174/1568007053544138

Lai, Y., Chen, Y., Watkins, S. C., Nathaniel, P. D., Guo, F., Kochanek, P. M., et al. (2008). Identification of poly-ADP-ribosylated mitochondrial proteins after traumatic brain injury. *J. Neurochem.* 104, 1700–1711. doi: 10.1111/j.1471-4159.2007.05114.x

Laird, M. D., Vender, J. R., and Dhandapani, K. M. (2008). Opposing roles for reactive astrocytes following traumatic brain injury. *Neurosignals* 16, 154–164. doi: 10.1159/000111560

Langfitt, T. W., Obrist, W. D., Alavi, A., Grossman, R. I., Zimmerman, R., Jaggi, J., et al. (1986). Computerized tomography, magnetic resonance imaging, and positron emission tomography in the study of brain trauma. Preliminary observations. *J. Neurosurg.* 64, 760–767. doi: 10.3171/jns.1986.64.5.0760

Laplaca, M. C., Raghupathi, R., Verma, A., Pieper, A. A., Saatman, K. E., Snyder, S. H., et al. (1999). Temporal patterns of poly(ADP-ribose) polymerase activation in the cortex following experimental brain injury in the rat. *J. Neurochem*. 73, 205–213. doi: 10.1046/j.1471-4159.1999.0730205.x

Laplaca, M. C., Zhang, J., Raghupathi, R., Li, J. H., Smith, F., Bareyre, F. M., et al. (2001). Pharmacologic inhibition of poly(ADP-ribose) polymerase is neuroprotective following traumatic brain injury in rats. *J. Neurotrauma* 18, 369–376. doi: 10.1089/089771501750170912

Lebon, V., Petersen, K. F., Cline, G. W., Shen, J., Mason, G. F., Dufour, S., et al. (2002). Astroglial contribution to brain energy metabolism in humans revealed by 13C nuclear magnetic resonance spectroscopy: elucidation of the dominant pathway for neurotransmitter glutamate repletion and measurement of astrocytic oxidative metabolism. *J. Neurosci*. 22, 1523–1531.

Lee, S. M., Wong, D. A., Samii, A., and Hovda, D. A. (1999). Evidence for energy failure following irreversible traumatic brain injury. *Ann. N.Y. Acad. Sci*. 893, 337–340. doi: 10.1111/j.1749-6632.1999.tb07849.x

Lee, W. N., Boros, L. G., Puigjaner, J., Bassilian, S., Lim, S., and Cascante, M. (1998). Mass isotopomer study of the nonoxidative pathways of the pentose cycle with [1,2-13C2]glucose. *Am. J. Physiol.* 274, E843–E851.

Lewen, A., and Hillered, L. (1998). Involvement of reactive oxygen species in membrane phospholipid breakdown and energy perturbation after traumatic brain injury in the rat. *J. Neurotrauma* 15, 521–530. doi: 10.1089/neu.1998.15.521

Magistretti, P. J., and Pellerin, L. (1999). Cellular mechanisms of brain energy metabolism and their relevance to functional brain imaging. *Philos. Trans. R. Soc. Lond. B. Biol. Sci*. 354, 1155–1163. doi: 10.1098/rstb.1999.0471

Mangia, S., DiNuzzo, M., Giove, F., Carruthers, A., Simpson, I. A., and Vannucci, S. J. (2011). Response to 'comment on recent modeling studies of astrocyte-neuron metabolic interactions': much ado about nothing. *J. Cereb. Blood Flow Metab*. 31, 1346–1353. doi: 10.1038/jcbfm.2011.29

Marcoux, J., McArthur, D. A., Miller, C., Glenn, T. C., Villablanca, P., Martin, N. A., et al. (2008). Persistent metabolic crisis as measured by elevated cerebral microdialysis lactate-pyruvate ratio predicts chronic frontal lobe brain atrophy after traumatic brain injury. *Crit. Care Med.* 36, 2871–2877. doi: 10.1097/CCM.0b013e318186a4a0

Marklund, N., Clausen, F., Ander, T. L., and Hillered, L. (2001). Monitoring of reactive oxygen species production after traumatic brain injury in rats with microdialysis and the 4-hydroxybenzoic acid trapping method. *J. Neurotrauma* 18, 1217–1227. doi: 10.1089/089771501317095250

McKenna, M. C. (2007). The glutamate-glutamine cycle is not stoichiometric: fates of glutamate in brain. *J. Neurosci. Res.* 85, 3347–3358. doi: 10.1002/jnr.21444

McKenna, M. C., Sonnewald, U., Huang, X., Stevenson, J., and Zielke, H. R. (1996). Exogenous

glutamate concentration regulates the metabolic fate of glutamate in astrocytes. *J. Neurochem.* 66, 386–393. doi: 10.1046/j.1471-4159.1996.66010386.x

McKenna, M. C., Waagepetersen, H. S., Schousboe, A., and Sonnewald, U. (2006). Neuronal and Astrocytic shuttle mechanisms for cytosolic-mitochondrial transfer of reducing equivalents current evidence and pharmacological tools. *Biochem. Pharmacol*. 71, 399–407. doi: 10.1016/j.bcp.2005.10.011

Mendez, D. R., Cherian, L., Moore, N., Arora, T., Liu, P. K., and Roberstson, C. S. (2004). Oxidative DNA lesions in a rodent model of traumatic brain injury. *J. Trauma* 56, 1235–1240. doi: 10.1097/01.TA.0000130759.62286.0E

Moore, A. H., Osteen, C. L., Chatziioannou, A. F., Hovda, D. A., and Cherry, S. R. (2000). Quantitative assessment of longitudinal metabolic changes *in vivo* after traumatic brain injury in the adult rat using FDG-microPET. *J. Cereb. Blood Flow Metab.* 20, 1492–1501. doi: 10.1097/00004647-200010000-00011

Moro, N., Ghavim, S., Hovda, D. A., and Sutton, R. L. (2011). Delayed sodium pyruvate treatment improves working memory following experimental traumatic brain injury. *Neurosci. Lett*. 491, 158–162. doi: 10.1016/j.neulet.2011.01.029

Moro, N., and Sutton, R. L. (2010). Beneficial effects of sodium or ethyl pyruvate after traumatic brain injury in the rat. *Exp. Neurol.* 225, 391–401. doi: 10.1016/j.expneurol.2010.07.013

Mustafa, A. G., Singh, I. N., Wang, J., Carrico, K. M., and Hall, E. D. (2010). Mitochondrial protection after traumatic brain injury by scavenging lipid peroxyl radicals. *J. Neurochem*. 114, 271–280. doi: 10.1111/j.1471-4159.2010.06749.x

Myer, D. J., Gurkoff, G. G., Lee, S. M., Hovda, D. A., and Sofroniew, M. V. (2006). Essential protective roles of reactive astrocytes in traumatic brain injury. *Brain* 129, 2761–2772. doi: 10.1093/brain/awl165

Nilsson, P., Hillered, L., Ponten, U., and Ungerstedt, U. (1990). Changes in cortical extracellular levels of energy-related metabolites and amino acids following concussive brain injury in rats. *J. Cereb. Blood Flow Metab*. 10, 631–637. doi: 10.1038/jcbfm.1990.115

Opii, W. O., Nukala, V. N., Sultana, R., Pandya, J. D., Day, K. M., Merchant, M. L., et al. (2007). Proteomic identification of oxidized mitochondrial proteins following experimental traumatic brain injury. *J. Neurotrauma* 24, 772–789. doi: 10.1089/neu.2006.0229

Osteen, C. L., Moore, A. H., Prins, M. L., and Hovda, D. A. (2001). Age-dependency of 45 calcium accumulation following lateral fluid percussion: acute and delayed patterns. *J. Neurotrauma* 18, 141–162. doi: 10.1089/08977150150502587

Parkin, M., Hopwood, S., Jones, D. A., Hashemi, P., Landolt, H., Fabricius, M., et al. (2005). Dynamic changes in brain glucose and lactate in pericontusional areas of the human cerebral cortex, monitored with rapid sampling on-line microdialysis: relationship with depolarisation-like events. *J. Cereb. Blood Flow Metab.* 25, 402–413. doi: 10.1038/sj.jcbfm.9600051

Pascual, J. M., Carceller, F., Roda, J. M., and Cerdan, S. (1998). Glutamate, glutamine, and GABA as substrates for the neuronal and glial compartments after focal cerebral ischemia in rats. *Stroke* 29, 1048–1056. doi: 10.1161/01.STR.29.5.1048

Pellerin, L., Bouzier-Sore, A. K., Aubert, A., Serres, S., Merle, M., Costalat, R., et al. (2007). Activity-dependent regulation of energy metabolism by astrocytes: an update. *Glia* 55, 1251–1262. doi: 10.1002/glia.20528

Peng, L., Gu, L., Zhang, H., Huang, X., Hertz, E., and Hertz, L. (2007). Glutamine as an energy substrate in cultured neurons during glucose deprivation. *J. Neurosci. Res*. 85, 3480–3486. doi: 10.1002/jnr.21262

Prins, M. L., and Hovda, D. A. (2001). Mapping cerebral glucose metabolism during spatial learning: interactions of development and traumatic brain injury. *J. Neurotrauma* 18, 31–46. doi: 10.1089/089771501750055758

Ralser, M., Wamelink, M. M., Kowald, A., Gerisch, B., Heeren, G., Struys, E. A., et al. (2007). Dynamic rerouting of the carbohydrate flux is key to counteracting oxidative stress. *J. Biol*. 6, 10. doi: 10.1186/jbiol61

Ramonet, D., Rodriguez, M. J., Fredriksson, K., Bernal, F., and Mahy, N. (2004). *In vivo* neuroprotective adaptation of the glutamate/glutamine cycle to neuronal death. *Hippocampus* 14, 586–594. doi: 10.1002/hipo.10188

Rao, V. L., Baskaya, M. K., Dogan, A., Rothstein, J. D., and Dempsey, R. J. (1998). Traumatic brain injury down-regulates glial glutamate transporter (GLT-1 and GLAST) proteins in rat brain. *J. Neurochem.* 70, 2020–2027. doi: 10.1046/j.1471-4159.1998.70052020.x

Rao, V. L., Dogan, A., Bowen, K. K., Todd, K. G., and Dempsey, R. J. (2001). Antisense knockdown of the glial glutamate transporter GLT-1 exacerbates hippocampal neuronal damage following traumatic injury to rat brain. *Eur. J. Neurosci.* 13, 119–128. doi: 10.1046/j.1460-9568.2001.01367.x

Readnower, R. D., Pandya, J. D., McEwen, M. L., Pauly, J. R., Springer, J. E., and Sullivan, P. G. (2011). Post-injury administration of the mitochondrial permeability transition pore inhibitor, NIM811, is neuroprotective and improves cognition after traumatic brain injury in rats. *J. Neurotrauma* 28, 1845–1853. doi: 10.1089/neu.2011.1755

Rose, M. E., Huerbin, M. B., Melick, J., Marion, D. W., Palmer, A. M., Schiding, J. K., et al. (2002). Regulation of interstitial excitatory amino acid concentrations after cortical contusion injury. *Brain Res.* 935, 40–46. doi: 10.1016/S0006-8993(02)02445-9

Satchell, M. A., Zhang, X., Kochanek, P. M., Dixon, C. E., Jenkins, L. W., Melick, J., et al. (2003). A dual role for poly-ADP-ribosylation in spatial memory acquisition after traumatic brain injury in mice involving $NAD^+$ depletion and ribosylation of 14-13-3gamma. *J. Neurochem.* 85, 697–708. doi: 10.1046/j.1471-4159.2003.01707.x

Scafidi, S., O'Brien, J., Hopkins, I., Robertson, C., Fiskum, G., and McKenna, M. (2009). Delayed cerebral oxidative glucose metabolism after traumatic brain injury in young rats. *J. Neurochem.* 109(Suppl. 1), 189–197. doi: 10.1111/j.1471-4159.2009.05896.x

Schinder, A. F., Olson, E. C., Spitzer, N. C., and Montal, M. (1996). Mitochondrial dysfunction is a primary event in glutamate neurotoxicity. *J. Neurosci*. 16, 6125–6133.

Schrader, M. C., Eskey, C. J., Simplaceanu, V., and Ho, C. (1993). A carbon-13 nuclear magnetic resonance investigation of the metabolic fluxes associated with glucose metabolism in human erythrocytes. *Biochim. Biophys. Acta* 1182, 162–178. doi: 10.1016/0925-4439(93)90138-Q

Schousboe, A., Westergaard, N., Waagepetersen, H. S., Larsson, O. M., Bakken, I. J., and Sonnewald, U. (1997). Trafficking between glia and neurons of TCA cycle intermediates and related metabolites. *Glia* 21, 99–105. doi: 10.1002/(SICI)1098-1136(199709)21:1<99::AID-GLIA11>3.0.CO;2-W

Shank, R. P., Leo, G. C., and Zilkha, E. (1993). Cerebral metabolic compartmentation as revealed by nuclear magnetic resonance analysis of D- [1-$1^3$C] glucose metabolism. *J. Neurochem.* 61, 315–323. doi: 10.1111/j.1471-4159.1993.tb03570.x

Shank, R. P., Bennett, G. S., Freytag, S. O., and Campbell, G. L. (1985). Pyruvate carboxylase: an astrocyte-specific enzyme implicated in the replenishment of amino acid neurotransmitter pools. *Brain Res.* 329, 364–367. doi: 10.1016/0006-8993(85)90552-9

Sharma, P., Benford, B., Li, Z. Z., and Ling, G. S. (2009). Role of pyruvate dehydrogenase complex in traumatic brain injury and measurement of pyruvate dehydrogenase enzyme by dipstick test. *J. Emerg.Trauma Shock* 2, 67–72. doi: 10.4103/0974-2700.50739

Shen, J. (2013). Modeling the glutamate-glutamine neurotransmitter cycle. *Front. Neuroenergetics* 5:1. doi: 10.3389/fnene.2013.00001

Signoretti, S., Vagnozzi, R., Tavazzi, B., and Lazzarino, G. (2010). Biochemical and neurochemical sequelae following mild traumatic brain injury: summary of experimental data and clinical implications. *Neurosurg. Focus* 29, E1. doi: 10.3171/2010.9.FOCUS10183

Singh, I. N., Gilmer, L. K., Miller, D. M., Cebak, J. E., Wang, J. A., and Hall, E. D. (2013). Phenelzine mitochondrial functional preservation and neuroprotection after traumatic brain injury related to scavenging of the lipid peroxidation-derived aldehyde 4-hydroxy-2-nonenal. *J. Cereb. Blood Flow Metab.* 33, 593–599. doi: 10.1038/jcbfm.2012.211

Starkov, A. A., Fiskum, G., Chinopoulos, C., Lorenzo, B. J., Browne, S. E., Patel, M. S., et al. (2004). Mitochondrial alpha-ketoglutarate dehydrogenase complex generates reactive oxygen species. *J. Neurosci.* 24, 7779–7788. doi: 10.1523/JNEUROSCI.1899-04.2004

Sutton, R. L., Hovda, D. A., Adelson, P. D., Benzel, E. C., and Becker, D. P. (1994). Metabolic changes following cortical contusion: relationships to edema and morphological changes. *Acta Neurochir. Suppl.(Wien.)* 60, 446–448.

Takahashi, S., Izawa, Y., and Suzuki, N. (2012). Astroglial pentose phosphate pathway rates in response to high-glucose environments. *ASN Neuro*. 4, 71–88. doi: 10.1042/AN20120002

Tyurin, V. A., Tyurina, Y. Y., Borisenko, G. G., Sokolova, T. V., Ritov, V. B., Quinn, P. J., et al. (2000). Oxidative stress following traumatic brain injury in rats: quantitation of biomarkers and detection of free radical intermediates. *J. Neurochem.* 75, 2178–2189. doi: 10.1046/j.1471-4159.2000.0752178.x

Vagnozzi, R., Marmarou, A., Tavazzi, B., Signoretti, S., Di Pierro, D., del Bolgia, F., et al. (1999). Changes of cerebral energy metabolism and lipid peroxidation in rats leading to mitochondrial dysfunction after diffuse brain injury. *J. Neurotrauma* 16, 903–913. doi: 10.1089/neu.1999.16.903

Van den Berg, C. J., Krzalic, L. J., Mela, P., and Waelsch, H. (1969). Compartmentation of glutamate metabolism in brain. Evidence for the existence of two different tricarboxylic acid cycles in brain. *Biochem. J.* 113, 281–290.

van Landeghem, F. K. H., Weiss, T., Oehmichen, M., and von Deimling, A. (2006). Decreased expression of glutamate transporters in astrocytes after human traumatic brain injury. *J. Neurotrauma* 23, 1518–1528. doi: 10.1089/neu.2006.23.1518

Verweij, B. H., Muizelaar, J. P., Vinas, F. C., Peterson, P. L., Xiong, Y., and Lee, C. P. (2000). Impaired cerebral mitochondrial function after traumatic brain injury in humans. *J. Neurosurg.* 93, 815–820. doi: 10.3171/jns.2000.93.5.0815

Vespa, P. M., McArthur, D., O'Phelan, K., Glenn, T., Etchepare, M., Kelly, D., et al. (2003). Persistently low extracellular glucose correlates with poor outcome 6 months after human traumatic brain injury despite a lack of increased lactate: a microdialysis study. *J. Cereb. Blood Flow Metab.* 23, 865–877. doi: 10.1097/01.WCB.0000076701.45782.EF

Vespa, P. M., Miller, C., McArthur, D., Eliseo, M., Etchepare, M., Hirt, D., et al. (2007). Nonconvulsive electrographic seizures after traumatic brain injury result in a delayed, prolonged increase in intracranial pressure and metabolic crisis. *Crit. Care Med.* 35, 2830–2836. doi: 10.1097/01.CCM.0000295667.66853.BC

Waniewski, R. A., and Martin, D. L. (1998). Preferential utilization of acetate by astrocytes is attributable to transport. *J. Neurosci.* 18, 5225–5233.

Xing, G., Ren, M., O'Neill, J. T., Sharma, P., Verma, A., and Watson, W. D. (2012). Pyruvate dehydrogenase phosphatase1 mRNA expression is divergently and dynamically regulated between rat cerebral cortex, hippocampus and thalamus after traumatic brain injury: a potential biomarker of TBI-induced hyper- and hypo-glycaemia and neuronal vulnerability. *Neurosci. Lett.* 525, 140–145. doi: 10.1016/j.neulet.2012.07.055

Xing, G., Ren, M., Watson, W. A., O'Neil, J. T., and Verma, A. (2009). Traumatic brain injury-induced expression and phosphorylation of pyruvate dehydrogenase: a mechanism of dysregulated glucose metabolism. *Neurosci. Lett.* 454, 38–42. doi: 10.1016/j.neulet.2009.01.047

Xiong, Y., Gu, Q., Peterson, P. L., Muizelaar, J. P., and Lee, C. P. (1997). Mitochondrial dysfunction and calcium perturbation induced by traumatic brain injury. *J. Neurotrauma* 14, 23–34. doi: 10.1089/neu.1997.14.23

Xiong, Y., Peterson, P. L., Verweij, B. H., Vinas, F. C., Muizelaar, J. P., and Lee, C. P. (1998). Mitochondrial dysfunction after experimental traumatic brain injury: combined efficacy of SNX-111 and U-101033E. *J. Neurotrauma* 15, 531–544. doi: 10.1089/neu.1998.15.531

Yamaki, T., Yoshino, E., Fujimoto, M., Ohmori, Y., Imahori, Y., and Ueda, S. (1996). Chronological positron emission tomographic study of severe diffuse brain injury in the chronic stage. *J. Trauma* 40, 50–56. doi: 10.1097/00005373-199601000-00010

Yi, J. H., and Hazell, A. S. (2006). Excitotoxic mechanisms and the role of astrocytic glutamate transporters in traumatic brain injury. *Neurochem. Int.* 48, 394–403. doi: 10.1016/j.neuint.2005.12.001

Yoshino, A., Hovda, D. A., Kawamata, T., Katayama, Y., and Becker, D. P. (1991). Dynamic changes in local cerebral glucose utilization following cerebral concussion in rats: evidence of a hyper- and subsequent hypometabolic state. *Brain Res.* 561, 106–119. doi: 10.1016/0006-8993(91)90755-K

Yu, A. C., Drejer, J., Hertz, L., and Schousboe, A. (1983). Pyruvate carboxylase activity in primary cultures of astrocytes and neurons. *J. Neurochem.* 41, 1484–1487. doi: 10.1111/j.1471-4159.1983.tb00849.x

Zamzami, N., Hirsch, T., Dallaporta, B., Petit, P. X., and Kroemer, G. (1997). Mitochondrial implication in accidental and programmed cell death: apoptosis and necrosis. *J. Bioenerg. Biomembr.* 29, 185–193. doi: 10.1023/A:1022694131572

Zanier, E. R., Lee, S. M., Vespa, P. M., Giza, C. C., and Hovda, D. A. (2003). Increased hippocampal CA3 vulnerability to low-level kainic acid following lateral fluid percussion injury. *J. Neurotrauma* 20, 409–420. doi: 10.1089/089771503765355496

**Conflict of Interest Statement:** The authors declare that the research was conducted in the absence of any commercial or financial relationships that could be construed as a potential conflict of interest.

*Received: 31 July 2013; accepted: 12 September 2013; published online: 04 October 2013.*

*Citation: Bartnik-Olson BL, Harris NG, Shijo K and Sutton RL (2013) Insights into the metabolic response to traumatic brain injury as revealed by $^{13}C$ NMR spectroscopy. Front. Neuroenergetics* ***5****:8. doi: 10.3389/fnene.2013.00008*

*This article was submitted to the journal Frontiers in Neuroenergetics.*

frontiers in
NEUROENERGETICS

MINI REVIEW ARTICLE
published: 28 March 2013
doi: 10.3389/fnene.2013.00003

# Neurophysiological, metabolic and cellular compartments that drive neurovascular coupling and neuroimaging signals

***Andrea Moreno[1], Pierrick Jego[1], Feliberto de la Cruz[2] and Santiago Canals[1]****

[1] *Instituto de Neurociencias, Consejo Superior de Investigaciones Científicas, Universidad Miguel Hernández, San Juan de Alicante, Spain*
[2] *Centro de Estudios Avanzados de Cuba, Ministerio de Ciencia Tecnología y Medio Ambiente, Habana, Cuba*

***Edited by:***
*Sebastian Cerdan, Instituto de Investigaciones Biomedicas Alberto Sols, Spain*

***Reviewed by:***
*Sebastian Cerdan, Instituto de Investigaciones Biomedicas Alberto Sols, Spain*
*Tiago B. Rodrigues, Cambridge Research Institute and University of Cambridge, UK*

***Correspondence:**
*Santiago Canals, Instituto de Neurociencias, Consejo Superior de Investigaciones Científicas, Universidad Miguel Hernández, Campus de San Juan, Avenida Ramón y Cajal, s/n, 03550 San Juan de Alicante, Spain.*
*e-mail: scanals@umh.es*

Complete understanding of the mechanisms that coordinate work and energy supply of the brain, the so called neurovascular coupling, is fundamental to interpreting brain energetics and their influence on neuronal coding strategies, but also to interpreting signals obtained from brain imaging techniques such as functional magnetic resonance imaging. Interactions between neuronal activity and cerebral blood flow regulation are largely compartmentalized. First, there exists a functional compartmentalization in which glutamatergic peri-synaptic activity and its electrophysiological events occur in close proximity to vascular responses. Second, the metabolic processes that fuel peri-synaptic activity are partially segregated between glycolytic and oxidative compartments. Finally, there is cellular segregation between astrocytic and neuronal compartments, which has potentially important implications on neurovascular coupling. Experimental data is progressively showing a tight interaction between the products of energy consumption and neurotransmission-driven signaling molecules that regulate blood flow. Here, we review some of these issues in light of recent findings with special attention to the neuron-glia interplay on the generation of neuroimaging signals.

**Keywords: neurovascular coupling, fMRI, neurophysiology, astrocytes, glycolysis**

## INTRODUCTION

By the end of the nineteenth century, two scientists provided the first evidence in support of coordination between brain work and energy supply. Mosso (1881), on measuring brain pulsations over the right prefrontal cortex in a subject with abnormally thinned skull, reported increased pulsations when the subject performed a mathematical task. In 1890, Sherrington, using a more direct approach, showed that stimulation of the sensory nerves, or the medulla oblongata, produced an increase in brain blood pressure (Roy and Sherrington, 1890). This hemodynamic response that accompanies brain activation was later found to also exist in pathological situations such as ischemia (Ames et al., 1968). This vascular response was interpreted as a compensatory mechanism that fuels the brain either during increased energy expenditure or during restriction of metabolic substrate delivery.

Brain energy is mainly used for restoring the resting membrane potential of activated neurons (Ames, 2000; Attwell and Laughlin, 2001). It is well established that the metabolic processes that fuel energy consumption are distributed in different cell types (neurons and glia) and subcellular compartments with predominantly either glycolytic or oxidative metabolisms. This segregation allows a functional compartmentalization of energy expenditure and is critical in understanding the mechanisms that coordinate brain work and energy supply, the so called neurovascular coupling. As such, is also fundamental in interpreting the signals obtained from brain imaging techniques as functional magnetic resonance imaging (fMRI).

Functional MRI based on blood oxygen level-dependent (BOLD) signal is the principal neuroimaging technique for basic and clinical research in humans. It is based on the paramagnetic nature of deoxygenated hemoglobin (Pauling and Coryell, 1936) and the overcompensation of blood supply in response to brain activation that produces a net increase in oxygenated hemoglobin (Fox and Raichle, 1986). This is accompanied by an enhancement of the MRI signal (Ogawa and Lee, 1990; Ogawa et al., 1990).While the physical origin of the signal is clear, both the triggering mechanisms and its relation to neuronal activity are still controversial.

## NEUROPHYSIOLOGY

An important matter for neuroimaging is to understand which aspects of neuronal work are reflected in increased cerebral blood flow (CBF). Experiments simultaneously combining fMRI and electrophysiological recordings in the primary visual cortex of anesthetized monkeys showed that the imaging signal evoked by visual stimulation maximally correlates with the local field potential (LFP), an aggregate measure of synaptic and active dendritic currents (Logothetis et al., 2001). Although the correlation of the BOLD signal was only slightly higher toward LFP compared with spiking activity (multiunit and single unit activity), the LFP signal was the only predictor of the hemodynamic response when long stimulation protocols that habituate spiking activity were used. Consistent with these findings were studies in the rat cerebellar cortex which convincingly showed that local CBF can indeed be dissociated from spiking activity while

strongly correlated with LFPs (Mathiesen et al., 1998, 2000; Thomsen et al., 2004).

Based on the above results, it has been argued that neuroimaging signals reflect the local processing of incoming neuronal activity to a particular area, rather than the output message being sent in outgoing efferent neuronal activity. Recent support of this view comes from combined fMRI-electrophysiology experiments, demonstrating that local synaptic plasticity modulates the amplitude of the BOLD signal (Canals et al., 2009). In anesthetized rats, the dentate gyrus was activated with electrical microstimulation of the perforant pathway, while simultaneously recording electrophysiological and high resolution fMRI signals (**Figures 1** and **2**). Of note, in the hippocampus, the axial organization of the cellular elements, with a rather precise alignment of dendritic trees and somas, minimizes the cancellation of current sources form the LFP generators and facilitates the neurophysiological interpretation of the electrically-evoked field potentials, such as synaptic currents reflected in the excitatory post-synaptic potential (EPSP) and spiking activity in the population spike. Using this preparation, we showed that the glutamate-evoked post-synaptic currents were a precise predictor of BOLD signal amplitude, better than either the population spike or the electrical current used for stimulation (Canals et al., 2008, 2009). This result has recently been confirmed in experiments combining electrophysiological recordings with hippocampal CBF measurements based on Laser-Doppler flowmetry (Hamadate et al., 2011). Interestingly, the extension of the functional maps correlated better with the spiking activity than the EPSP recorded in the dentate gyrus (Canals et al., 2009). This result indicated, perhaps not surprisingly, that while the local BOLD signal follows the synaptic input, the output (spiking) activity of a particular region predicts the activity propagation in the network connected to that region (**Figures 1** and **2E**).

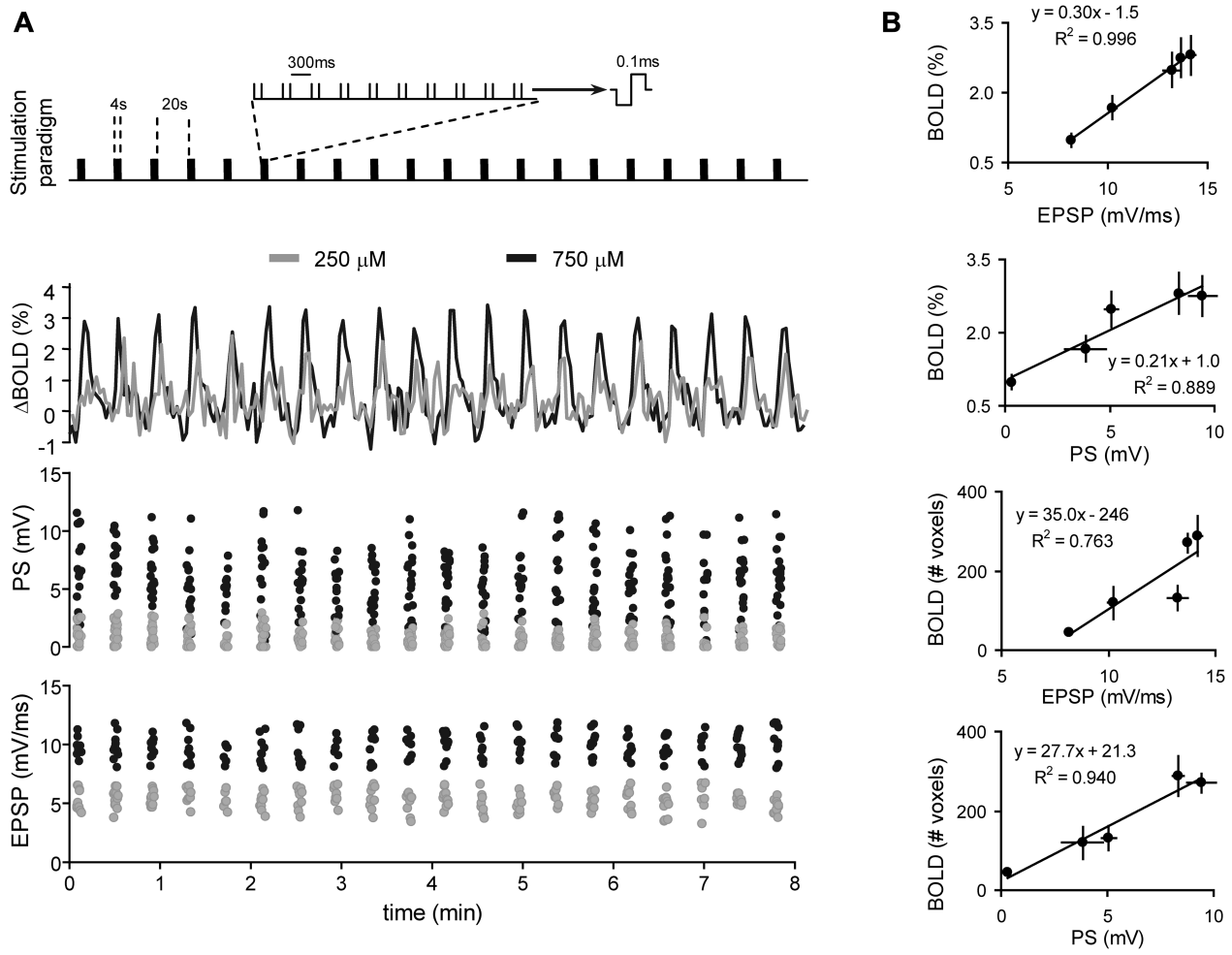


**FIGURE 1 | Correlation of BOLD and electrophysiological signals. (A)** Simultaneous recordings of BOLD (middle panel) and electrophysiological signals (PS and EPSP; lower two panels, respectively) during a typical block-design protocol of electric-stimulation fMRI (upper panel). Two stimulation intensities in one animal are shown. **(B)** The amplitude of the BOLD signal in the dentate gyrus (%, two upper panels) or the volume of brain activated during perforant path stimulation (#, number of activated voxels, two lower panels) is plotted against the EPSP in the dentate gyrus or the corresponding PS. BOLD, EPSP and PS represent the mean ± SEM of all hemodynamic, synaptic and spiking responses, respectively, during a complete experiment ($n = 5$ experiments, collected in four different animals). Data is fitted with linear regression. Adapted with permission from Canals et al. (2009).

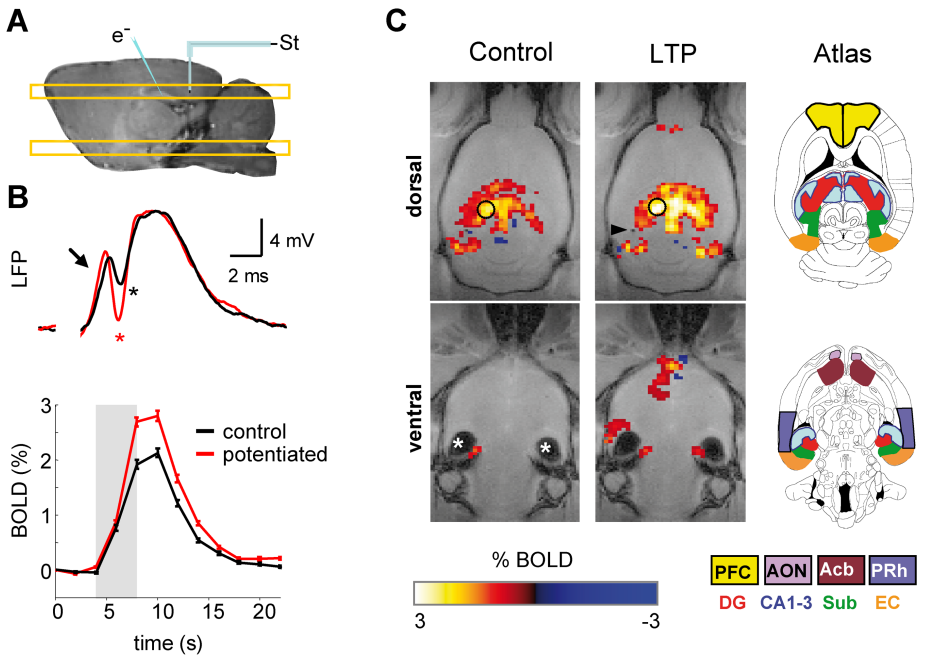


**FIGURE 2 | Potentiation of the synaptic strength is accompanied by enhancement of the BOLD-fMRI signal. (A)** Schematic representation of the experimental preparation. The placement of the stimulating and recording electrodes is shown on a sagital T1-weighted image acquired with manganese-enhanced MRI. The location of the dorsal and ventral MRI slices shown in **(C)** is also illustrated. **(B)** LFP (upper panel) and BOLD signal time course (lower panel) recorded in the dentate gyrus during perforant pathway stimulation, before (black) and after (red) induction of long-term potentiation (LTP) of the synaptic strength. Arrow points toward the EPSP and asterisks mark the PS. **(C)** Functional maps thresholded and overlaid on horizontal FLASH anatomical scans, showing brain active areas during perforant path stimulation before (control) and after synaptic potentiation (LTP). New structures are recruited after LTP. Asterisks "*" mark image artifacts due to the ear channel. The color-coded scale represents positive and negative BOLD response in percent change from baseline. The position of the tip of the stimulation electrode is marked by the black arrowhead. The inset drawings, modified from the Paxinos and Watson rat brain atlas (Paxinos and Watson, 2007), delineate different regions of interest. **(D)** Quantification of EPSP, PS and the amplitude of the BOLD signal (%) in the dentate gyrus, and the total number of activated fMRI voxels in the brain (#). **(E)** Electrophysiological and fMRI responses to different stimulation intensities measured in the dentate gyrus and the subiculum. Synaptic input (EPSP) and local BOLD signal amplitude in the dentate evolve together and diverge from the spiking output (PS) and its propagation to the subiculum. PFC, prefrontal cortex; AON, anterior olfactory nucleus; Acb, accumbens; PRh, perirhinal cortex; DG, dentate gyrus; Sub, subiculum; EC, entorhinal cortex. **(A–D)** adapted with permission from Canals et al. (2009).

It must be noted, however, that the local synaptic input of a volume of tissue relevant for the spatial resolution of fMRI (2–3 mm in human studies and 0.2–0.5 mm in small animal studies) is also contributed to by synaptic currents driven by recurrent spiking activity. Therefore, input and output activities are somehow mixed to some extent. What is the relative contribution to the BOLD signal of the synaptic inputs driven by recurrent spiking activity? In hippocampal preparations, when the strength of the synapses in the dentate gyrus was experimentally increased by means of a tetanic stimulation of the perforant pathway (long-term potentiation, LTP), the BOLD signal concomitantly increased (Canals et al., 2009). Both, the EPSP and BOLD signal potentiations were of comparable magnitude and two to three times smaller than the spike potentiation. The dissociated evolution of the spiking activity vs. the BOLD signal and EPSP becomes even clearer in the small proportion of experiments in which, as originally described by Bliss and Lomo (1973), the tetanization of the perforant pathway is followed by an increase in the spiking probability without changing the EPSP (EPSP-to-spike or E-S potentiation). In these cases of increased tissue excitability, the local BOLD signal evoked by perforant path stimulation remains almost unaffected, like the EPSP, while the population spike amplitude increases two- to threefold (Benito et al., unpublished results). These results indicate that the effect of extrinsic synaptic inputs on the hyperemic response in the hippocampus outweigh the effect of synapses on recurrent axon collaterals, and suggest the intriguing possibility that not all glutamatergic synapses are equally suited to initiate a vascular response.

In summary, the above observations indicate that between the electrophysiological events constituting neuronal computations, glutamate evoked synaptic currents critically contribute to neuroimaging signals. It is intuitively appealing that the supply of energy substrates could be coupled to the process that, as mentioned earlier, consumes most of the energy used for neuronal signaling (Ames, 2000; Attwell and Laughlin, 2001). However, the nature of the coupling mechanisms is under intense debate.

## METABOLISM vs. NEUROTRANSMISSION

Two major concepts have been put forward to mechanistically explain the coupling between neuronal activity and hyperemia. A classical view supports a feed-back mechanism in which the

byproducts of energy expenditure act as signaling molecules to increase blood supply and restore energy buffers. In a more recent view, a feed-forward mechanism controlled by neurotransmitter-mediated signaling has a major role in CBF regulation. While neurotransmitter signaling is intrinsically correlated with energy consumption, the feed-forward model maintains that a causal link with CBF regulation only exists for the first. A large body of recent experimental data, mainly from *in vitro* preparations (see below), is shifting the field in favor of the feed-forward model (Attwell et al., 2010; Petzold and Murthy, 2011). Both models, however, are mutually non-exclusive and may coexist in specific physiological states.

## METABOLIC FEED-BACK MECHANISM

Initial observations challenging the feed-back model came from studies showing that experimental manipulations of metabolic substrates such as $O_2$ (Mintun et al., 2001; Lindauer et al., 2010) or glucose (Powers et al., 1996) *in vivo* have little effect on CBF regulation. However, other metabolic byproducts such as adenosine can regulate CBF, linking the action of the $Na^+/K^+$ ATPase pump to local vasodilatation. Extracellular adenosine acting on $A_{2A}$ receptors in vascular smooth muscle inhibits the arteriolar vasoconstriction mediated by the arachidonic acid (AA) metabolite 20-hydroxy-eicosatetraenoic acid (20-HETE; Gordon et al., 2008). This vasodilatory effect has been demonstrated in the cortex (Ko et al., 1990) and the cerebellum (Li and Iadecola, 1994) following neuronal stimulation. Adenosine effects on CBF regulation mediated by $A_{2B}$ receptors have also been reported and involve interaction with $Ca^{2+}$ signaling in astrocytes and probably AA metabolism (Shi et al., 2008). A caveat in interpreting the source of extracellular adenosine is that ATP used as a gliotransmitter is also hydrolyzed to adenosine by extracellular ectonucleotidases (Latini and Pedata, 2001). Therefore, depending on its origin, adenosine will couple CBF to energy consumption or neuronal signaling through glio-transmission. An additional unsolved question of adenosine-mediated functional hyperemia is the concomitant synaptic depressing effect that adenosine may exert on pre- and post-synaptic $A_1$ receptors (Greene and Haas, 1991), to which it binds with highest affinity (Fredholm et al., 2001). The dual effect of adenosine may help maintain a safety energy level for neuronal integrity under conditions of transient energy limitations such as ischemia (Dunwiddie and Masino, 2001; Canals et al., 2008), but it may interfere with neuronal computations in physiological conditions. The functional compartmentalization of adenosine release may constitute a solution to this potential problem (Pelligrino et al., 2011).

One key energy metabolite in the brain which reinforces the feed-back model of neurovascular coupling is lactate. Important work on the special role of glycolysis in brain energy production provided the concept that glycolytic increase during brain activation (Raichle and Mintun, 2006) results from the uptake of synaptically-released glutamate into astrocytes together with $Na^+$ (Magistretti and Pellerin, 1999; Pellerin and Magistretti, 2004). In the astrocyte, glutamate is converted into glutamine and the excess $Na^+$ is released to the extracellular space, both processes consuming ATP (Erecinska and Silver, 1994). Refilling of the energy buffer seems to critically depend on glycolysis (Raichle and Mintun, 2006), and glycolysis is linked to blood flow modulation through lactate. Accordingly, it has been convincingly shown that CBF response to an increase in neuronal activity is modulated by changes in the plasma lactate/pyruvate ratio in experimental animals (Ido et al., 2001, 2004) and humans (Mintun et al., 2004; Vlassenko et al., 2006). Accordingly, it has been recently shown that lactate indeed modulates the BOLD fMRI signal in the early visual cortex of non-human primates (von Pfostl et al., 2012). These results and others (Kasischke et al., 2004) support a direct metabolic (glycolytic) effect on CBF regulation and identify astrocytes as important players in the generation of neuroimaging signals.

Glutamate recycling is not the only mechanism linking astrocytes to functional hyperemia (see below), nor is metabolic compartmentalization of glycolytic enzymes restricted to astrocytes. Of potential functional (and imaging) relevance is also the discovery of glycolytic enzymes in the post-synaptic density of glutamatergic synapses (Wu et al., 1997) and GABA receptors (Laschet et al., 2004), potentially linking post-synaptic activations, glycolysis, and neuroimaging signals.

## NEUROTRANSMITTER-MEDIATED FEED-FORWARD SIGNALING

The feed-forward model is mainly represented by nitric oxide (NO) and AA metabolites released from neurons and glial cells as a consequence of glutamatergic neurotransmission. While vasoactive peptides and GABA ($\gamma$-aminobutyric acid) released by interneurons have been shown to contribute to the functional hyperemia in some systems (Cauli et al., 2004; Kocharyan et al., 2008), and therefore contribute to the feed-forward neurovascular coupling mechanism, the experimental evidence accumulated to date is less abundant (Lauritzen et al., 2012).

Synaptically-released glutamate acting on NMDA receptors increases post-synaptic $Ca^{2+}$ levels and activates neuronal NO synthase (nNOS), which translates into NO release. NO mediates vasodilation in the brain, as repeatedly demonstrated in slice and *in vivo* preparations (Busija et al., 2007). It has to be noted, however, that NO contribution to blood flow regulation presents regional differences in the brain (Sokoloff et al., 1977). In the cortex (but not the cerebellum), while NO is required for functional hyperemia, it does not directly mediate the neuron-to-vessel signaling (Lindauer et al., 1999). Its role in the cortex has been suggested to be the modulation of the AA metabolic pathways in astrocytes (Attwell et al., 2010). There is strong evidence supporting blood flow regulation through the production and release of AA metabolites in response to synaptic glutamate. The supported mechanisms start with an mGluR-dependent increase in the astrocytic $[Ca^{2+}]i$ that activates phospholipase $A_2$ and releases AA from membrane phospholipids. Subsequently, AA metabolites with vasodilatory activity, such as prostaglandins and epoxyeicosatrienoic acids, are produced and released. Interestingly, vasoconstrictions induced by increases in astrocytic $[Ca^{2+}]i$ have also been reported *in vitro* (Mulligan and MacVicar, 2004; Metea and Newman, 2006) and are also mediated by the AA metabolite 20-HETE (Behm et al., 2009). This conflicting result was elegantly explained by demonstrating that the metabolic state of the tissue ultimately determines the sign of the astrocytic control over vascular responses (Gordon et al., 2008), with decreasing $O_2$ concentrations favoring the production

of vasodilatory responses. This interaction may therefore reflect the combination of feed-back and feed-forward mechanisms of blood flow regulation. Although conceptually attractive, it must be noted that the above *in vitro* results are challenged by previous (Mintun et al., 2001) and recent (Lindauer et al., 2010) studies showing no effect of $O_2$ concentration on CBF regulation *in vivo* (see above).

A tight interaction between feed-back and feed-forward mechanism of neurovascular coupling starts to be clear as their respective counterparts are found to be closely related in the biochemical pathways supporting functional hyperemia. For example, the vasodilatory effect of adenosine at $A_{2A}$ receptors is coupled to AA signaling pathway by interfering with 20-HETE vasoconstriction, a mechanism that also mediates part of the NO vasodilatory effect (Roman, 2002). Furthermore, the mechanism linking lactate to vasodilation involves the inhibition of the prostaglandin transporter, increasing the extracellular concentration of PGE2 released from astrocytes and potentiating vasodilation (Gordon et al., 2008). The vasodilatory effects of glutamate on astrocytes is reduced by blocking glutamate uptake (Raichle, 1998; Bernardinelli et al., 2004), suggesting a metabolic contribution to the signaling effect. Therefore, activity-driven energy expenditure and neuronal or astrocytic-initiated signaling seem to be the two ends of the same rope. This may explain why inhibitory cocktails combining antagonists for the different pathways (AA, NO, adenosine) do not show additive blocking of functional hyperemia (Koehler et al., 2006).

An additional level of interaction arises when considering that NO and AA have also been involved in the mechanism that strengthens synaptic currents after LTP induction and learning (Schuman and Madison, 1991; Hardingham and Fox, 2006; DeCostanzo et al., 2010; Dachtler et al., 2011), protocols shown to increase the hyperemic response (Canals et al., 2009; Hamadate et al., 2011). An intriguing possibility then is that the same set of molecules acting on converging signaling pathways is coordinating the strength of synaptic currents and energy consumption with the level of local blood supply. Whether a long-lasting increase in synaptic efficacy is accompanied by a similarly-lasting enhancement of neurovascular coupling efficacy is an important yet unsolved question, with potentially relevant implications on neuroimaging signal interpretation.

## ASTROCYTES

In light of the reviewed results and their strategic location between synapses and blood vessels, astrocytes have often been regarded as key players in the neurovascular coupling (Ramón y Cajal, 1899). Astrocytes seem to be the compartment where many of the biochemical processes that determine the magnitude and direction of the vascular response to neuronal activation take place. Increases in astrocytic $[Ca^{2+}]$i linked to AA metabolism is the principal mechanism thought to contribute to hyperemia. However, $Ca^{2+}$ fluctuation in astrocytes not only occurs in response to neuronal activity (i.e., spontaneous events may also trigger astrocytic $Ca^{2+}$ waves; Perea and Araque, 2005; Wang et al., 2009). Therefore, it has been suggested that a significant contribution to the neuroimaging signals may arise from the activation of astrocytes independently of neuronal signaling (Wang et al., 2009). Nevertheless, a number of issues regarding $Ca^{2+}$-mediated astrocyte-dependent neurovascular coupling still need to be clarified before a quantitative contribution of astrocytes to neuroimaging signals can be ascertained. First, functional hyperemia occurs less than 2 sec after the onset of the stimulation, whereas astrocytic $Ca^{2+}$ elevation is slower, typically delayed by more than 2–3 sec (Wang et al., 2006; Schummers et al., 2008). Based on this finding it was suggested that the astrocyte-$Ca^{2+}$ response might be more important for sustaining the vasodilation during prolonged activation rather than as an initiating signal (Koehler et al., 2009), an argument that has recently found some experimental support in simultaneous fMRI and fiber-optic $Ca^{2+}$ recordings in rat neocortex (Schulz et al., 2012). Second, and more importantly, neither spontaneous nor evoked $[Ca^{2+}]$i increases in astrocytes are affected by ionotropic glutamate receptor antagonists such us CNQX (6-cyano-7-nitroquinoxaline-2,3-dione) and APV [(2R)-amino-5-phosphonovaleric acid; Takano et al., 2006; Thrane et al., 2012]. This pharmacological manipulation, however, eliminates both post-synaptic electrophysiological activity and the coupled vascular response.

## CONCLUDING REMARKS

Interactions between neuronal activity and CBF are largely compartmentalized. First, a functional compartmentalization that situates glutamatergic peri-synaptic activity and its electrophysiological events exists in close proximity to vascular coupling. Whether all glutamatergic synapses are equally suited for neurovascular coupling is an interesting yet unsolved question. In this direction, it is also important to acknowledge that heterogeneity in coupling mechanisms between different brain regions has already been reported and requires further attention. Second, the metabolic processes fueling peri-synaptic activity are partially segregated in glycolytic vs. oxidative compartments, with lactate production in response to increased neuronal activity as a key metabolite for energy supply, but also vascular coupling. A distinction between feed-back (metabolic) and feed-forward (signaling) mechanisms appears diffuse, since both mechanisms closely interact in the mediating biochemical pathways. An important issue to be clarified is whether a constant metabolic baseline and a constant neurovascular coupling efficiency can be assumed across brain states and synaptic plasticity. The quantitative value of neuroimaging signals may otherwise be affected by fluctuations in the reference baseline. Finally, a third level of segregation occurs at the cellular level, with astrocytic and neuronal compartments involved in vascular coupling through different but converging signaling pathways (NO, AA, adenosine, lactate/pyruvate ratio). Still, the actual relevance of astrocytes to neuroimaging signals needs to be clarified.

## ACKNOWLEDGMENTS

The work is Santiago Canals lab is supported by grants of the Spanish Ministry of Science and Innovation BFU2009-09938 and PIM2010ERN-00679 (part of the coordinated ERA-Net NEURON project TRANSALC). Pierrick Jego has been supported by the "Symbad" Marie Curie ITN program and Feliberto de la Cruz was supported by a fellowship from CSIC-CITMA.

## REFERENCES


Ames, A. III. (2000). CNS energy metabolism as related to function. *Brain Res. Brain Res. Rev.* 34, 42–68.

Ames, A. III, Wright, R. L., Kowada, M., Thurston, J. M., and Majno, G. (1968). Cerebral ischemia. II. The no-reflow phenomenon. *Am. J. Pathol.* 52, 437–453.

Attwell, D., Buchan, A. M., Charpak, S., Lauritzen, M., Macvicar, B. A., and Newman, E. A. (2010). Glial and neuronal control of brain blood flow. *Nature* 468, 232–243.

Attwell, D., and Laughlin, S. B. (2001). An energy budget for signaling in the grey matter of the brain. *J. Cereb. Blood Flow Metab.* 21, 1133–1145.

Behm, D. J., Ogbonna, A., Wu, C., Burns-Kurtis, C. L., and Douglas, S. A. (2009). Epoxyeicosatrienoic acids function as selective, endogenous antagonists of native thromboxane receptors: identification of a novel mechanism of vasodilation. *J. Pharmacol. Exp. Ther.* 328, 231–239.

Bernardinelli, Y., Magistretti, P. J., and Chatton, J. Y. (2004). Astrocytes generate Na+-mediated metabolic waves. *Proc. Natl. Acad. Sci. U.S.A.* 101, 14937–14942.

Bliss, T. V., and Lomo, T. (1973). Long-lasting potentiation of synaptic transmission in the dentate area of the anaesthetized rabbit following stimulation of the perforant path. *J. Physiol.* 232, 331–356.

Busija, D. W., Bari, F., Domoki, F., and Louis, T. (2007). Mechanisms involved in the cerebrovascular dilator effects of *N*-methyl-D-aspartate in cerebral cortex. *Brain Res. Rev.* 56, 89–100.

Canals, S., Beyerlein, M., Keller, A. L., Murayama, Y., and Logothetis, N. K. (2008). Magnetic resonance imaging of cortical connectivity in vivo. *Neuroimage* 40, 458–472.

Canals, S., Beyerlein, M., Merkle, H., and Logothetis, N. K. (2009). Functional MRI evidence for LTP-induced neural network reorganization. *Curr. Biol.* 19, 398–403.

Cauli, B., Tong, X. K., Rancillac, A., Serluca, N., Lambolez, B., Rossier, J., et al. (2004). Cortical GABA interneurons in neurovascular coupling: relays for subcortical vasoactive pathways. *J. Neurosci.* 24, 8940–8949.

Dachtler, J., Hardingham, N. R., Glazewski, S., Wright, N. F., Blain, E. J., and Fox, K. (2011). Experience-dependent plasticity acts via GluR1 and a novel neuronal nitric oxide synthase-dependent synaptic mechanism in adult cortex. *J. Neurosci.* 31, 11220–11230.

DeCostanzo, A. J., Voloshyna, I., Rosen, Z. B., Feinmark, S. J., and Siegelbaum, S. A. (2010). 12-Lipoxygenase regulates hippocampal long-term potentiation by modulating L-type Ca2+ channels. *J. Neurosci.* 30, 1822–1831.

Dunwiddie, T. V., and Masino, S. A. (2001). The role and regulation of adenosine in the central nervous system. *Annu. Rev. Neurosci.* 24, 31–55.

Erecinska, M., and Silver, I. A. (1994). Ions and energy in mammalian brain. *Prog. Neurobiol.* 43, 37–71.

Fox, P. T., and Raichle, M. E. (1986). Focal physiological uncoupling of cerebral blood flow and oxidative metabolism during somatosensory stimulation in human subjects. *Proc. Natl. Acad. Sci. U.S.A.* 83, 1140–1144.

Fredholm, B. B., Ap, I. J., Jacobson, K. A., Klotz, K. N., and Linden, J. (2001). International Union of Pharmacology. XXV. Nomenclature and classification of adenosine receptors. *Pharmacol. Rev.* 53, 527–552.

Gordon, G. R., Choi, H. B., Rungta, R. L., Ellis-Davies, G. C., and Macvicar, B. A. (2008). Brain metabolism dictates the polarity of astrocyte control over arterioles. *Nature* 456, 745–749.

Greene, R. W., and Haas, H. L. (1991). The electrophysiology of adenosine in the mammalian central nervous system. *Prog. Neurobiol.* 36, 329–341.

Hamadate, N., Yamaguchi, T., Sugawara, A., Tsujimatsu, A., Izumi, T., Yoshida, T., et al. (2011). Regulation of cerebral blood flow in the hippocampus by neuronal activation through the perforant path: relationship between hippocampal blood flow and neuronal plasticity. *Brain Res.* 1415, 1–7.

Hardingham, N., and Fox, K. (2006). The role of nitric oxide and GluR1 in presynaptic and postsynaptic components of neocortical potentiation. *J. Neurosci.* 26, 7395–7404.

Ido, Y., Chang, K., and Williamson, J. R. (2004). NADH augments blood flow in physiologically activated retina and visual cortex. *Proc. Natl. Acad. Sci. U.S.A.* 101, 653–658.

Ido, Y., Chang, K., Woolsey, T. A., and Williamson, J. R. (2001). NADH: sensor of blood flow need in brain, muscle, and other tissues. *FASEB J.* 15, 1419–1421.

Kasischke, K. A., Vishwasrao, H. D., Fisher, P. J., Zipfel, W. R., and Webb, W. W. (2004). Neural activity triggers neuronal oxidative metabolism followed by astrocytic glycolysis. *Science* 305, 99–103.

Ko, K. R., Ngai, A. C., and Winn, H. R. (1990). Role of adenosine in regulation of regional cerebral blood flow in sensory cortex. *Am . J. Physiol.* 259, H1703–H1708.

Kocharyan, A., Fernandes, P., Tong, X. K., Vaucher, E., and Hamel, E. (2008). Specific subtypes of cortical GABA interneurons contribute to the neurovascular coupling response to basal forebrain stimulation. *J. Cereb. Blood Flow Metab.* 28, 221–231.

Koehler, R. C., Gebremedhin, D., and Harder, D. R. (2006). Role of astrocytes in cerebrovascular regulation. *J. Appl. Physiol.* 100, 307–317.

Koehler, R. C., Roman, R. J., and Harder, D. R. (2009). Astrocytes and the regulation of cerebral blood flow. *Trends Neurosci.* 32, 160–169.

Laschet, J. J., Minier, F., Kurcewicz, I., Bureau, M. H., Trottier, S., Jeanneteau, F., et al. (2004). Glyceraldehyde-3-phosphate dehydrogenase is a GABAA receptor kinase linking glycolysis to neuronal inhibition. *J. Neurosci.* 24, 7614–7622.

Latini, S., and Pedata, F. (2001). Adenosine in the central nervous system: release mechanisms and extracellular concentrations. *J. Neurochem.* 79, 463–484.

Lauritzen, M., Mathiesen, C., Schaefer, K., and Thomsen, K. J. (2012). Neuronal inhibition and excitation, and the dichotomic control of brain hemodynamic and oxygen responses. *Neuroimage* 62, 1040–1050.

Li, J., and Iadecola, C. (1994). Nitric oxide and adenosine mediate vasodilation during functional activation in cerebellar cortex. *Neuropharmacology* 33, 1453–1461.

Lindauer, U., Leithner, C., Kaasch, H., Rohrer, B., Foddis, M., Fuchtemeier, M., et al. (2010). Neurovascular coupling in rat brain operates independent of hemoglobin deoxygenation. *J. Cereb. Blood Flow Metab.* 30, 757–768.

Lindauer, U., Megow, D., Matsuda, H., and Dirnagl, U. (1999). Nitric oxide: a modulator, but not a mediator, of neurovascular coupling in rat somatosensory cortex. *Am. J. Physiol.* 277, H799–H811.

Logothetis, N. K., Pauls, J., Augath, M., Trinath, T., and Oeltermann, A. (2001). Neurophysiological investigation of the basis of the fMRI signal. *Nature* 412, 150–157.

Magistretti, P. J., and Pellerin, L. (1999). Cellular mechanisms of brain energy metabolism and their relevance to functional brain imaging. *Philos. Trans. R. Soc. Lond. B Biol. Sci.* 354, 1155–1163.

Mathiesen, C., Caesar, K., Akgoren, N., and Lauritzen, M. (1998). Modification of activity-dependent increases of cerebral blood flow by excitatory synaptic activity and spikes in rat cerebellar cortex. *J. Physiol.* 512(Pt 2), 555–566.

Mathiesen, C., Caesar, K., and Lauritzen, M. (2000). Temporal coupling between neuronal activity and blood flow in rat cerebellar cortex as indicated by field potential analysis. *J. Physiol.* 523(Pt 1), 235–246.

Metea, M. R., and Newman, E. A. (2006). Glial cells dilate and constrict blood vessels: a mechanism of neurovascular coupling. *J. Neurosci.* 26, 2862–2870.

Mintun, M. A., Lundstrom, B. N., Snyder, A. Z., Vlassenko, A. G., Shulman, G. L., and Raichle, M. E. (2001). Blood flow and oxygen delivery to human brain during functional activity: theoretical modeling and experimental data. *Proc. Natl. Acad. Sci. U.S.A.* 98, 6859–6864.

Mintun, M. A., Vlassenko, A. G., Rundle, M. M., and Raichle, M. E. (2004). Increased lactate/pyruvate ratio augments blood flow in physiologically activated human brain. *Proc. Natl. Acad. Sci. U.S.A.* 101, 659–664.

Mosso, A. (1881). *Ueber den Kreislauf des Blutes im menschlichen Gehirn.* Leipzig: Veit.

Mulligan, S. J., and MacVicar, B. A. (2004). Calcium transients in astrocyte endfeet cause cerebrovascular constrictions. *Nature* 431, 195–199.

Ogawa, S., and Lee, T. M. (1990). Magnetic resonance imaging of blood vessels at high fields: in vivo and in vitro measurements and image simulation. *Magn. Reson. Med.* 16, 9–18.

Ogawa, S., Lee, T. M., Kay, A. R., and Tank, D. W. (1990). Brain magnetic resonance imaging with contrast dependent on blood oxygenation. *Proc. Natl. Acad. Sci. U.S.A.* 87, 9868–9872.

Pauling, L., and Coryell, C. D. (1936). The Magnetic properties and structure of hemoglobin, oxyhemoglobin and carbonmonoxyhemoglobin. *Proc. Natl. Acad. Sci. U.S.A.* 22, 210–216.

Paxinos, G., and Watson, C. (2007). *The Rat Brain in Stereotaxic Coordinates.* Amsterdam: Elsevier.

Pellerin, L., and Magistretti, P. J. (2004). Neuroenergetics: calling upon astrocytes to satisfy hungry neurons. *Neuroscientist* 10, 53–62.

Pelligrino, D. A., Vetri, F., and Xu, H. L. (2011). Purinergic mechanisms in gliovascular coupling. *Semin. Cell Dev. Biol* . 22, 229–236.

Perea, G., and Araque, A. (2005). Synaptic regulation of the astrocyte calcium signal. *J. Neural. Transm.* 112, 127–135.

Petzold, G. C., and Murthy, V. N. (2011). Role of astrocytes in neurovascular coupling. *Neuron* 71, 782–797.

Powers, W. J., Hirsch, I. B., and Cryer, P. E. (1996). Effect of stepped hypoglycemia on regional cerebral blood flow response to physiological brain activation. *Am. J. Physiol.* 270, H554–H559.

Raichle, M. E. (1998). Behind the scenes of functional brain imaging: a historical and physiological perspective. *Proc. Natl. Acad. Sci. U.S.A.* 95, 765–772.

Raichle, M. E., and Mintun, M. A. (2006). Brain work and brain imaging. *Annu. Rev. Neurosci.* 29, 449–476.

Ramón y Cajal, S. (1899). *Textura del sistema nervioso del hombre y de los vertebrados : estudios sobre el plan estructural y composición histológica de los centros nerviosos adicionados de consideraciones fisiológicas fundadas en los nuevos descubrimientos.* Madrid: N. Moya.

Roman, R. J. (2002). P-450 metabolites of arachidonic acid in the control of cardiovascular function. *Physiol. Rev.* 82, 131–185.

Roy, C. S., and Sherrington, C. S. (1890). On the regulation of the blood-supply of the brain. *J. Physiol.* 11, 85–158.

Schulz, K., Sydekum, E., Krueppel, R., Engelbrecht, C. J., Schlegel, F., Schroter, A., et al. (2012). Simultaneous BOLD fMRI and fiber-optic calcium recording in rat neocortex. *Nat. Methods* 9, 597–602.

Schuman, E. M., and Madison, D. V. (1991). A requirement for the intercellular messenger nitric oxide in long-term potentiation. *Science* 254, 1503–1506.

Schummers, J., Yu, H., and Sur, M. (2008). Tuned responses of astrocytes and their influence on hemodynamic signals in the visual cortex. *Science* 320, 1638–1643.

Shi, Y., Liu, X., Gebremedhin, D., Falck, J. R., Harder, D. R., and Koehler, R. C. (2008). Interaction of mechanisms involving epoxyeicosatrienoic acids, adenosine receptors, and metabotropic glutamate receptors in neurovascular coupling in rat whisker barrel cortex. *J. Cereb. Blood Flow Metab.* 28, 111–125.

Sokoloff, L., Reivich, M., Kennedy, C., Des Rosiers, M. H., Patlak, C. S., Pettigrew, K. D., et al. (1977). The [14C]deoxyglucose method for the measurement of local cerebral glucose utilization: theory, procedure, and normal values in the conscious and anesthetized albino rat. *J. Neurochem.* 28, 897–916.

Takano, T., Tian, G. F., Peng, W., Lou, N., Libionka, W., Han, X., et al. (2006). Astrocyte-mediated control of cerebral blood flow. *Nat. Neurosci.* 9, 260–267.

Thomsen, K., Offenhauser, N., and Lauritzen, M. (2004). Principal neuron spiking: neither necessary nor sufficient for cerebral blood flow in rat cerebellum. *J. Physiol.* 560, 181–189.

Thrane, A. S., Rangroo Thrane, V., Zeppenfeld, D., Lou, N., Xu, Q., Nagelhus, E. A., et al. (2012). General anesthesia selectively disrupts astrocyte calcium signaling in the awake mouse cortex. *Proc. Natl. Acad. Sci. U.S.A.* 109, 18974–18979.

Vlassenko, A. G., Rundle, M. M., Raichle, M. E., and Mintun, M. A. (2006). Regulation of blood flow in activated human brain by cytosolic NADH/NAD+ ratio. *Proc. Natl. Acad. Sci. U.S.A.* 103, 1964–1969.

von Pfostl, V., Li, J., Zaldivar, D., Goense, J., Zhang, X., Serr, N., et al. (2012). Effects of lactate on the early visual cortex of non-human primates, investigated by pharmaco-MRI and neurochemical analysis. *Neuroimage* 61, 98–105.

Wang, X., Lou, N., Xu, Q., Tian, G. F., Peng, W. G., Han, X., et al. (2006). Astrocytic $Ca^{2+}$ signaling evoked by sensory stimulation in vivo. *Nat. Neurosci.* 9, 816–823.

Wang, X., Takano, T., and Nedergaard, M. (2009). Astrocytic calcium signaling: mechanism and implications for functional brain imaging. *Methods Mol. Biol.* 489, 93–109.

Wu, K., Aoki, C., Elste, A., Rogalski-Wilk, A. A., and Siekevitz, P. (1997). The synthesis of ATP by glycolytic enzymes in the postsynaptic density and the effect of endogenously generated nitric oxide. *Proc. Natl. Acad. Sci. U.S.A.* 94, 13273–13278.

**Conflict of Interest Statement:** The authors declare that the research was conducted in the absence of any commercial or financial relationships that could be construed as a potential conflict of interest.

*Received: 14 February 2013; accepted: 13 March 2013; published online: 28 March 2013.*

*Citation: Moreno A, Jego P, de la Cruz F and Canals S (2013) Neurophysiological, metabolic and cellular compartments that drive neurovascular coupling and neuroimaging signals. Front. Neuroenergetics* ***5****:3. doi: 10.3389/fnene.2013.00003*

frontiers in
NEUROENERGETICS

REVIEW ARTICLE
published: 26 April 2013
doi: 10.3389/fnene.2013.00004

# Astroglial networking contributes to neurometabolic coupling

***Carole Escartin*** [1] ***and Nathalie Rouach*** [2] *******

[1] *CEA DSV I2BM MIRCen and CNRS URA2210, Fontenay-aux-Roses, Paris, France*
[2] *Neuroglial Interactions in Cerebral Physiopathology, Center for Interdisciplinary Research in Biology, CNRS UMR 7241, INSERM U1050, Collège de France, Paris, France*

***Edited by:***
*Sebastian Cerdan, Instituto de Investigaciones Biomedicas Alberto Sols, Spain*

***Reviewed by:***
*Sebastian Cerdan, Instituto de Investigaciones Biomedicas Alberto Sols, Spain*
*Anne-Karine Bouzier-Sore, CNRSUniversité Victor Segalen, France*

****Correspondence:***
*Nathalie Rouach, Neuroglial Interactions in Cerebral Physiopathology, Center for Interdisciplinary Research in Biology, CNRS UMR 7241, INSERM U1050, Collège de France, 11 place Marcelin Berthelot, 75005 Paris, France.*
*e-mail: nathalie.rouach@college-de-france.fr*

The strategic position of astrocytic processes between blood capillaries and neurons, provided the early insight that astrocytes play a key role in supplying energy substrates to neurons in an activity-dependent manner. The central role of astrocytes in neurometabolic coupling has been first established at the level of single cell. Since then, exciting recent work based on cellular imaging and electrophysiological recordings has provided new mechanistic insights into this phenomenon, revealing the crucial role of gap junction (GJ)-mediated networks of astrocytes. Indeed, astrocytes define the local availability of energy substrates by regulating blood flow. Subsequently, in order to efficiently reach distal neurons, these substrates can be taken up, and distributed through networks of astrocytes connected by GJs, a process modulated by neuronal activity. Astrocytic networks can be morphologically and/or functionally altered in the course of various pathological conditions, raising the intriguing possibility of a direct contribution from these networks to neuronal dysfunction. The present review upgrades the current view of neuroglial metabolic coupling, by including the recently unravelled properties of astroglial metabolic networks and their potential contribution to normal and pathological neuronal activity.

**Keywords: astrocytes, neuroglial interactions, gap junctions, astroglial networks, energy metabolism, neurometabolic coupling, neurodegenerative diseases, epilepsy**

## INTRODUCTION

Brain information processing comes with important energetic costs (Harris et al., 2012). Consequently, although representing only 2% of the body mass, the brain consumes 20% of the oxygen and glucose supplied by blood. One of the oldest functions attributed to astrocytes consists in providing metabolic support to neurons. As early as 1886, Camilio Golgi described the strategic position that astrocytes occupy between blood vessels and neurons, and from which the concept of neuroglial metabolic coupling originates. Astrocytes take up glucose, which can then be stored as glycogen or metabolized into lactate, an energy substrate that can be shuttled to neurons and fuel their TCA cycle (Pellerin et al., 2007). Astrocytes can also regulate glucose neuronal supply through the modulation of blood flow via vasodilatation or vasoconstriction of blood vessels, which respectively increases or decreases glucose supply (Attwell et al., 2010). Thus, astrocytes play an important role in the local supply of energy substrates to neurons, via regulation of blood microcirculation as well as glucose uptake and metabolization. However, the molecular mechanisms enabling energy substrates delivery from astrocytes to neurons and the actual role such supply undertakes in sustaining neuronal activity are still matter of intense debates. For decades, the contribution of astrocytes to neuronal metabolic support has mainly been examined at the level of an individual astrocyte as part of the neuro-glia-vascular unit, thus overlooking the extraordinary network properties of astrocytes connected by gap junctions (GJ). However, recent data have unravelled the unique properties of GJ-mediated astroglial networks and their role in neurometabolic coupling. The existing model of astroglial metabolic support to neuronal activity should therefore be upgraded to encompass GJ-mediated astroglial networks, which not only influence local synapses, but also modulate distal neuronal circuits. We here review recent data revealing the main properties of astroglial networks, and describe the current understanding of their contribution to the neurometabolic coupling, at both synaptic and circuit level, in normal and pathological situations. The current review therefore aims at extending the classical model of neuroglial metabolic coupling to the network level.

## ASTROCYTES HAVE UNIQUE METABOLIC FEATURES AND FORM A DYNAMIC NETWORK

### PIVOTAL ROLE OF ASTROCYTES IN BRAIN ENERGY METABOLISM

Glucose oxidation in the brain is almost exclusively directed toward fulfilling the high energy cost of synaptic transmission. Enhanced neuronal activity translates into an increased uptake of glucose in the active regions (Belanger et al., 2011). Because very little local energetic reserves are available in the central nervous system (CNS), such activity is highly dependent on the finely regulated supply of glucose from the bloodstream. Astrocytes play a central role in this process. They express glucose transporters at their endfeet, which come into close contact with

brain capillaries (Belanger et al., 2011). The astrocyte to neuron lactate shuttle (ANLS) hypothesis states that enhanced neuronal activity at glutamatergic synapses stimulates the uptake of glutamate, which is co-transported with sodium ($Na^+$) in astrocytes. Restoration of the $Na^+$ gradient by the Na/K ATPase pump consumes ATP, whose levels are recovered by an enhanced uptake and glycolysis of glucose in astrocytes. Glycolysis in astrocytes leads to rapid production of lactate, which is then transported to neurons, thereby fueling their energy needs (Pellerin and Magistretti, 1994). Glutamate is also exported back to neurons in the form of glutamine. Since the first description of the ANLS, the molecular mechanisms subtending the tight cooperation between astrocytes and neurons for glucose oxidation in conditions of enhanced neuronal activity have been further detailed and complexified (Belanger et al., 2011). Notably, it was demonstrated that $K^+$ released during neurotransmission is an important additional inducer of astrocyte glycolysis and lactate export (Bittner et al., 2011; Ruminot et al., 2011; Choi et al., 2012).

Another possible fate for glucose in astrocytes is its transformation into glycogen, the major energy reserve of the CNS. Glycogen granules are stored exclusively in astrocytes (Magistretti et al., 1993) and can be mobilized rapidly in conditions of aglycemia to sustain neuronal function (Brown et al., 2005). Most importantly, glycogen, and the lactate derived from its degradation, also play a role in non-pathological conditions, as they have been shown to be required for learning and memory (Suzuki et al., 2011).

Glucose is by far the primary metabolic substrate of the brain, but alternative substrates such as ketone bodies (KB) may also be metabolized, provided their concentrations are sufficiently high relatively to that of glucose. This occurs during the neonatal pre-weaning period, during fasting, or when KB plasma levels are artificially increased by a ketogenic diet (Maalouf et al., 2009; Prins, 2012). KB may also be produced locally by astrocytes as these cells have been shown in culture to synthetize KB from fatty acids (Guzman and Blazquez, 2001). Moreover, in particular conditions, astrocytes may overexpress enzymes involved in KB and fatty acid metabolism and increase their oxidation as alternative substrates to glucose (Escartin et al., 2007).

Overall, astrocytes are perfectly equipped to orchestrate a tight regulation of glucose metabolism in response to neuronal activity. They express a large variety of receptors that allow them to sense and respond to neuronal activity. In addition, they exhibit a complex machinery of transporters and enzymes enabling them to metabolize, store and transfer multiple metabolic substrates. Interestingly, astrocytes are primarily oriented toward glucose uptake and oxidation or storage in the form of glycogen, but they also display a marked metabolic versatility, being able to metabolize efficiently KB, fatty acids and glutamate (Escartin et al., 2007; McKenna, 2007). Importantly, most of the aforementioned metabolites are small enough to transit through GJ, hence conveying the intriguing possibility that these substrates may be shuttled between astrocytes in an activity-dependent manner.

## WIDESPREAD AND REGULATED GAP JUNCTION-MEDIATED NETWORKS OF ASTROCYTES

Individual astrocytes play a major role in synaptic physiology by controlling a large number of synapses, in part through gliotransmission, or glutamate and $K^+$ uptake (Nedergaard and Verkhratsky, 2012). However, another key property of astrocytes is their extensive network communication via intercellular GJ channels (**Figures 1B**,**C**). Astrocytes express indeed high levels of connexins, the proteins forming GJ channels, which are poorly selective channels allowing direct cytoplasmic exchange of a variety of small molecules, with a molecular weight up to 1.5 kDa. These include ions ($K^+$, $Ca^{2+}$, $Na^+$), second messengers (cAMP, IP3), neurotransmitters (glutamate) or energy metabolites (glucose, lactate) (Giaume et al., 2010). Each GJ channel is formed by the alignment of two hemichannels, the connexons, provided by two neighboring astrocytes, and composed of six transmembrane

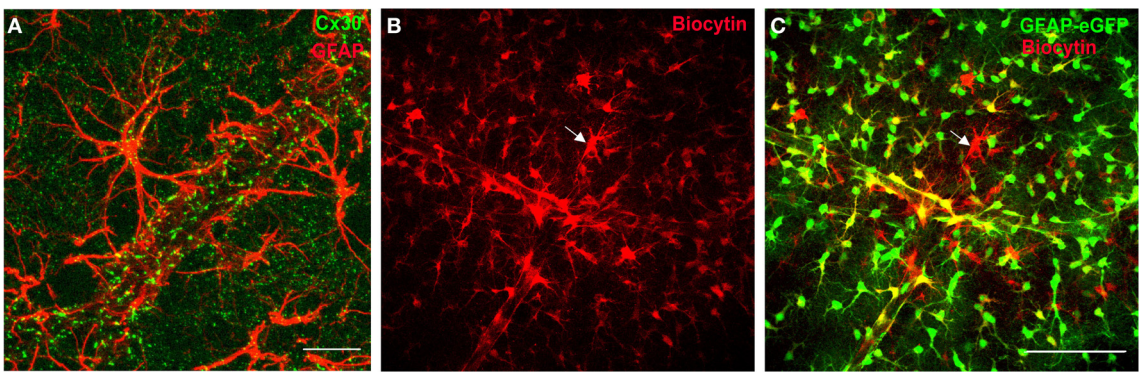


**FIGURE 1 | Connexins define a functional network of astrocytes at the gliovascular interface. (A)** Staining of Cx30, one of the two main GJ protein in astrocytes, in mouse hippocampus co-localizes with astrocyte endfeet, labeled with the glial fibrillary acidic protein marker (GFAP), enwrapping blood vessels. Scale bar, 25 μm. **(B,C)** Functional coupling of perivascular astrocytes in GFAP-eGFP mice visualized by diffusion of biocytin (red, **B**; overlay with GFAP-eGFP, **C**), a tracer permeable to GJ channels, dialyzed for 20 min by whole-cell recording of a perivascular astrocyte (see arrow), revealing an extensive coupling of neighboring astrocytes. Note that some EGFP-positive cells near the dialyzed cell do not stain for biocytin, which indicates the presence of a preferential network of astrocytes. Scale bar, 100 μm. Adapted, with permission, from Giaume et al. (2010) (**A**) and Rouach et al. (2008) (**B**,**C**).

proteins, the connexins. In astrocytes, the two main connexins expressed are connexin 43, present from embryonic stages to adulthood, and connexin 30, expressed after postnatal day 10 (Nagy et al., 1999). GJ channels mediate the formation of large cellular ensembles reaching millimeter size in different brain regions, encompassing hundreds to thousands of astrocytes (Ball et al., 2007; Giaume et al., 2010).

Astroglial networks display several typical properties. Although GJ mediate an extensive intercellular communication between neighboring cells, these connections can be selective and preferential. Indeed, adjacent astrocytes are not always functionally connected, as assessed by dye coupling experiments (Houades et al., 2006, 2008; Roux et al., 2011) (**Figures 1B,C**). This may result from heterogeneous expression of connexins in astrocytes, or to short-term regulation of astroglial GJ permeability. Astroglial networks are also finely organized in anatomical and functional compartments, similarly to neuronal networks, as recently shown in different brain areas (Houades et al., 2006, 2008; Roux et al., 2011). For instance, in the hippocampus, astrocytes form extensive and nearly non-overlapping networks in the *stratum radiatum* and *oriens*, respectively, under and above the pyramidal cell layer; this is partly attributable to the non-homogeneous distribution of astrocytes and connexins. More strikingly, in markedly compartmentalized cerebral structures such as the somatosensory cortex or the olfactory bulb, the structural organization of astroglial networks does overlap with the anatomical and functional units of associated neurons. In the somatosensory cortex, astrocytes located between barrels, in the septa, are weakly connected, in contrast to astrocytes located in the barrel, which show significant coupling almost exclusively within a single barrel (Houades et al., 2006). Similarly, in the olfactory bulb, extraglomerular astrocytes show reduced coupling compared to intraglomerular astrocytes, which are mainly coupled within the limits of a single glomerulus (Roux et al., 2011). Confinement of astroglial networks in the reach of a given structural and functional neuronal network may favor specific neuroglial interactions. This might contribute to local and precise processing of neuronal signals, favoring circuit independence by restricting information transfer to distal neurons, belonging to other networks. This region-dependent organization of astroglial networks may also directly influence how distant neurons with high energy needs, within a specific network, are supplied with metabolites taken up by perivascular astrocytes.

## NEUROMETABOLIC COUPLING WITH NETWORKS OF ASTROCYTES

### ACTIVITY-DEPENDENT TRAFFICKING OF ENERGY METABOLITES THROUGH ASTROGLIAL NETWORKS

A striking feature of Cx43 and Cx30, the two main GJ subunit proteins in astrocytes, is their enrichment in perivascular astrocytic endfeet and delineation of blood vessel walls (Nagy et al., 1999; Simard et al., 2003; Rouach et al., 2008) (**Figure 1A**). The functional connectivity of perivascular astrocytic networks has thus been hypothesized to contribute to neurometabolic coupling. The first step in demonstrating such hypothesis consisted in visualizing online energy metabolite trafficking through astroglial networks and determining whether it could be subject to activity dependent regulations. This was achievable through the use of fluorescent glucose analogs, such as 2-NBDG (2-[*N*-(7-nitrobenz-2-oxa-1,3-diazol-4-yl)amino]-2 deoxyglucose), infused in single astrocytes lining blood vessels. Diffusion of such molecules revealed that astroglial connexins mediate an activity-dependent glucose distribution through intercellular astroglial networks (Rouach et al., 2008) (**Figure 2**). The possible contribution of connexin hemichannels in glucose intercellular trafficking was ruled out, because they were shown not to be functional under these physiological conditions (Rouach et al., 2008). Interestingly, glucose trafficking through astroglial networks was found to be specifically regulated, as it occurs within a preferential pathway along interconnected astrocyte endfeet around blood vessels and depends on neuronal activity (Rouach et al., 2008). The molecular mechanism underlying the activity-dependent regulation of astroglial metabolic networks remains, however, unclear. Regulations of astroglial networks have been investigated almost exclusively using passive dye coupling, instead of bioactive molecules. Such approach has enabled to show that the permeability and selectivity of GJ channels control the extent of astroglial network diffusion and are regulated by a variety of endogenous molecules such as ions, peptides, and neurotransmitters, released by various brain cell types and acting on membrane channels and receptors (Giaume et al., 2010). Thus, astroglial networks are functionally plastic and are regulated by neuronal activity, as shown in several brain regions (Fischer and Kettenmann, 1985; Marrero and Orkand, 1996; Rouach et al., 2000, 2002b, 2008; Roux et al., 2011). Although mostly assessed by GJ coupling for passive dyes, a few pathways have been proposed to control activity-dependent astroglial networking. For instance, depolarization mediated by activity-dependent $K^+$ release has been suggested to enhance astroglial GJ coupling (Enkvist and McCarthy, 1994; De Pina-Benabou et al., 2001; Roux et al., 2011) through Cx43 phosphorylation by CAMKII (De Pina-Benabou et al., 2001). Glutamate has also been proposed as an important regulator of astroglial GJ permeability, although different effects have been described, depending on the preparation and the receptor subtype involved (Giaume et al., 2010). Glutamate released at hippocampal synapses increases glucose trafficking through astroglial GJs via activation of postsynaptic AMPA receptors, but not astroglial glutamate transporters (Rouach et al., 2008). Interestingly, this activity-dependent regulation of glucose trafficking does not result from a direct action on the permeability of GJ channels, because astroglial GJ coupling for passive tracers is unchanged by glutamate. Thus, glucose trafficking through GJ-mediated astroglial networks may follow a gradient from sites of high concentration, near blood vessels, to sites of low concentration, where active neurons requiring a large consumption reside. This hypothesis is supported by the observation that neuronal stimulation in a given hippocampal layer selectively increases glucose diffusion into this layer via an astroglial network originating from a distant layer (Rouach et al., 2008). Thus, astroglial metabolic networks can be reshaped by local glutamatergic activity from active neurons, which act as a signal for energy demand.

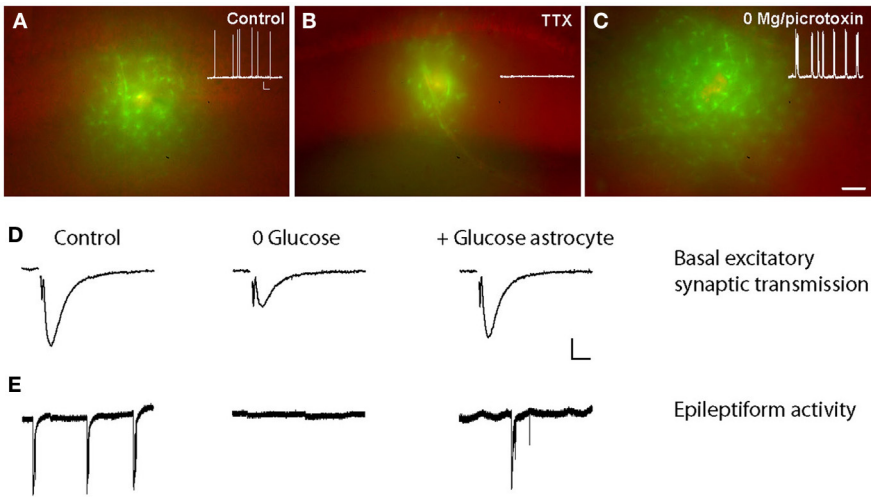


**FIGURE 2 | Activity-dependent glucose trafficking through astroglial networks sustain normal and pathological neuronal activity.** **(A)** Sample pictures showing that the fluorescent glucose derivative 2-[N-(7-nitrobenz-2-oxa-1,3-diazol-4-yl)amino]-2-deoxyglucose (2-NBDG, green) trafficking in astrocytes is decreased when neuronal activity is inhibited with tetrodotoxin (TTX) **(B)** and increased during epileptiform activity (in 0 $Mg^{2+}$-picrotoxin) **(C)** as compared with control conditions **(A)**. Scale bar, 50 μm. Insets, corresponding spontaneous activity of hippocampal CA1 pyramidal cells recorded in current clamp in control, TTX (0.5 μm, 1–4 h), and 0 $Mg^{2+}$-picrotoxin (100 μm, 1–4 h) conditions. Scale bar, 20 mV, 9 s. **(D,E)** Glucose supply through astrocytic networks sustains basal synaptic transmission and epileptiform activity during exogenous glucose deprivation (EGD). Sample traces of extracellular field potentials recorded in hippocampal slices showing that intracellular glucose (20 mM) delivery to astrocytic networks (+Glucose astrocytes) through the patch pipette inhibits the depression of fEPSP amplitude **(D)** and epileptiform activity **(E)** induced by exogenous glucose deprivation (0 glucose, 30 min) in wild-type mice. Scale bars **(D)** 0.2 mV, 5 ms and **(E)** 0.3 mV, 20 s. Adapted, with permission, from Rouach et al. (2008) **(A–E)**.

## METABOLIC SUPPORT OF SYNAPTIC ACTIVITY

The second step required for probing the role of astroglial networks in neurometabolic coupling was to determine whether intercellular glucose trafficking through astroglial networks could in turn affect synaptic activity. To do so, field excitatory postsynaptic potentials were monitored in the context of exogenous glucose deprivation whilst a remote astrocyte was loaded, via a patch pipette, with glucose or lactate. Exogenous glucose deprivation expectedly induced a slow depression of synaptic transmission, which could be rescued by glucose or lactate supply to a single astrocyte connected to the astroglial network via GJs. Remarkably, such metabolic support was not observed when glucose was administrated to disconnected astrocytes, lacking both Cx30 and Cx43 (Rouach et al., 2008). This body of work therefore suggests that GJ-mediated astroglial networks play a crucial role in the supportive function of astrocytes by providing an activity-dependent intercellular pathway for glucose delivery from blood vessels to neurons. Hence, glutamate increases both glucose uptake and trafficking in astrocytic networks, and is likely to be the key signal for adequate supply of energy metabolites to sites of neuronal demand. The classic model of neurometabolic coupling, in which astrocytes are considered as single entities controlling metabolic substrates supply to neurons, is therefore revisited and now includes GJ-mediated metabolic networks of astrocytes, which provide energy metabolites in a remote yet efficient manner toward sites of active neurotransmission. However up to now, these networks have been characterized *in vitro* and *ex vivo*. Thus, it is still unknown whether extensive astroglial metabolic networks occur *in vivo* and contribute to functional neuroimaging responses observed with *in vivo* techniques such as functional magnetic resonance imaging and positron emission tomography using [$^{18}$F]-fluorodeoxyglucose.

## AMPLIFICATION OF METABOLIC RESPONSES

One of the key element of the ANLS model is the $Na^+$ influx in astrocytes though glutamate transporters, which stimulates glucose uptake. Interestingly, bringing such model to the level of astroglial networks now implies the notion of metabolic response amplification. Indeed, neuronal glutamate has been shown *in vitro* to generate $Na^+$-mediated metabolic waves, enabling the coordination of glucose uptake by astrocytes connected by GJ channels (Bernardinelli et al., 2004). This amplification system requires intercellular $Ca^{2+}$ waves to trigger astroglial release of glutamate, which is taken up by glutamate/$Na^+$ cotransporters, and results in regenerative intracellular astroglial $Na^+$ waves. The recent identification of astroglial intracellular $Na^+$ waves *in situ* in the hippocampus (Langer et al., 2012) suggests that this mechanism occurs in physiological conditions. However, generation of $Na^+$ waves *in situ* was found to depend on GJ, but not on $Ca^{2+}$ waves. Such observation is reminiscent of the current debate questioning the actual occurrence of astrocytic $Ca^{2+}$ waves in physiological conditions *in situ* and *in vivo*. Nevertheless, a recent study reported that such waves, named glissandi, do occur in physiological conditions *in vivo* in the hippocampus and depend on neuronal activity and GJ channels (Kuga et al., 2011). However, the GJ dependence was demonstrated using carbenoxolone, a non-specific GJ channel blocker targeting as well other

ionic channels, which directly regulate neuronal activity (Rouach et al., 2003; Vessey et al., 2004). Whether $Na^+$ waves translate into metabolic waves (i.e., waves of enhanced glucose uptake or metabolism) remains to be demonstrated *in situ*. In sum, the generations of metabolic waves through astroglial networks are likely to occur in both, physiological and pathological conditions, and would contribute to neurometabolic coupling over extensive distances.

## ASTROGLIAL METABOLIC NETWORKS IN PATHOLOGICAL CONDITIONS

In physiological conditions, GJ-mediated networks of astrocytes play a pivotal role in $K^+$ and glutamate buffering, as well as in energy substrate trafficking from blood vessels to distant active neurons. Alterations in GJ permeability are known to exacerbate $K^+$ and glutamate dysregulations in pathological conditions such as ischemia (Nakase et al., 2003; Farahani et al., 2005) or epilepsy (Coulter and Eid, 2012; Steinhauser et al., 2012). Intriguingly, the opening of connexin hemichannel is now starting to emerge as a contributing factor to brain diseases (Bennett et al., 2012; Orellana et al., 2012). However, since recent articles have reviewed these two topics in great details (Bennett et al., 2012; Coulter and Eid, 2012; Orellana et al., 2012; Steinhauser et al., 2012), we shall thereafter focus on how changes in GJ-mediated astroglial metabolic networks might influence neuronal dysfunction in several brain diseases such as ischemia, epilepsy or neurodegenerative conditions.

### WHICH SIGNALS THROUGH GJs IN PATHOLOGICAL CONDITIONS?

Although the concept of "kiss of death", whereby apoptotic signals can transit through GJs from a dying cell to a healthy connected cell, was the first put forward (Lin et al., 1998), it remains somewhat controversial. Such process was proposed to account for the amplification of cell death following cerebral ischemia (Frantseva et al., 2002b; Farahani et al., 2005), traumatic brain injury (Frantseva et al., 2002a; Cronin et al., 2008) and infection of astrocytes by HIV (Eugenin and Berman, 2007; Eugenin et al., 2011). Yet the nature of the toxic signals that propagate through the network in each of these specific conditions still remains to be identified to substantiate this hypothesis.

GJ-mediated networks of astrocytes also contribute to the transfer of survival signals such as metabolic substrates, which could supply distal neurons no longer connected to the bloodstream. This might particularly apply to acute local pathological conditions such as ischemia, traumatic brain injury, or infections. In these conditions, local resources are rapidly exhausted and the gap junctional network then represents an invaluable pathway for delivery of glucose metabolites originating from distant sources. For instance, after ischemia, the transfer of energy metabolites from spared regions to the ischemic region might help neurons to overcome local metabolic dearth. However, the shape and extent of astroglial networks being different between brain structures (Theis and Giaume, 2012), the ability of GJ-mediated networks to counteract the deleterious consequences of ischemia may depend on the affected brain region. Interestingly, this might partly explain the discrepancies of the literature regarding the beneficial versus detrimental role of GJs in these diseases.

### HOW DO ASTROGLIAL METABOLIC NETWORKS FUNCTION IN PATHOLOGICAL CONDITIONS?

Numerous pathologies have been associated with alterations of astroglial networks and GJ permeability. In particular, changes in connexin expression occur following acute injuries or in the process of chronic diseases, including demyelinating and neurodegenerative diseases (Kielian and Esen, 2004; Giaume et al., 2010; Cotrina and Nedergaard, 2012). Both increases and decreases in astrocyte connexin expression and GJ permeability to passive dyes have been reported, depending on the model, species, and connexin type (Giaume et al., 2010). In neurodegenerative diseases such as Alzheimer's disease (AD), Cx43 expression increases (Koulakoff et al., 2012), resulting in enhanced dye coupling in the cortex of aged transgenic AD mice (Peters et al., 2009). This may contribute to increased astroglial $Ca^{2+}$ waves, as observed in the cortex of transgenic mice with amyloid beta plaques (Kuchibhotla et al., 2009). However, the functional impact of connexin expression alterations on metabolite trafficking through astrocytic networks has never been directly assessed in any of the aforementioned pathologies.

To our knowledge, the contribution of astroglial metabolic networks in the sustaining of neuronal activity in pathological conditions has only been directly assessed in the context of epileptiform activity. In a slice model of acute aberrant discharges (0 $Mg^{2+}$ and picrotoxin), the astroglial network remains functional and the degree of glucose trafficking through the network actually increases, as a consequence of enhanced neuronal activity (**Figure 2**). Crucially in such context, infusion of glucose or lactate through the astrocytic network, while depriving the acute hippocampal slices from glucose, partially maintained epileptiform activity (**Figure 2**) (Rouach et al., 2008). This unique study thus suggests that astrocyte metabolic networks are still functional in conditions of acute epileptiform activity and contribute to fuel abnormal neuronal activity.

In other pathological conditions involving, on the contrary, a chronic deficit in energy metabolism, such as neurodegenerative diseases (Lin and Beal, 2006), an increased permeability of GJ-mediated network might represent a beneficial mechanism of resistance, as it may indeed enhance metabolites supply to vulnerable neurons. Once distributed through the network, glucose may be metabolized into lactate to sustain neuronal energy needs, or give rise to reducing equivalents through the pentose phosphate pathway (Allaman et al., 2011; Belanger et al., 2011). Given the involvement of oxidative stress in neuronal demise (Lin and Beal, 2006), such enhancement of the antioxidant machinery would also represent a beneficial aspect.

Metabolic networks of astrocytes therefore combine multiple positive features that might shoulder the compromised neurons in a variety of pathological conditions. Besides neuronal activity, astroglial metabolic networks likely also sustain neuronal survival in many pathological conditions in which GJ channels do still operate (Cotrina et al., 1998; Rouach et al., 2008). Such networks thus represent potent therapeutic targets. However, the current knowledge of astrocytic network functioning in pathological conditions is insufficient and further investigations are required to experimentally assess GJ functions and their impact on disease progression. In addition,

targeting GJ metabolic networks demands to identify in these diseases the molecular regulators of connexin expression and GJ permeability.

### THE ASTROCYTE NETWORK AS A THERAPEUTIC TARGET

The signaling pathways mediating changes in connexin expression in diseases are still elusive. Pro-inflammatory cytokines such as IL-1β and TNFα decrease the expression of Cx43 and Cx30 *in vitro* (Meme et al., 2006), while the neurotrophic cytokine ciliary neurotrophic factor increases Cx43 expression in reactive astrocytes *in vivo* (Escartin et al., 2006). As a rule, most molecules released in neuroinflammatory conditions impact connexin expression and GJ permeability (Kielian and Esen, 2004). A number of other signals including second messengers, endogenous lipids, and changes in osmolarity or pH also modulate GJ permeability, as assessed using passive dyes (Rouach et al., 2002a). Such changes in permeability are likely to affect GJ network function more transiently than changes in connexin expression, and would hence be a better target to alleviate acute pathological conditions. Besides transcriptional regulation of connexin expression, the molecular cascades governing connexin insertion at the plasma membrane, connexon apposition, and GJ opening probability could also represent relevant targets to modulate network function in brain affections.

## CONCLUSIONS AND PERSPECTIVES

Astrocytes have been recognized as major players in neurometabolic coupling for decades. One of the typical features of astrocytes is their massive direct intercellular communication mediated by GJ channels. However, the role of astroglial network organization in their supporting function has only been recently addressed. GJ-connected astrocytes amplify metabolic responses by generating $Na^+$-mediated metabolic waves, resulting in coordinated astroglial glucose uptake. In addition, energy substrates, such as glucose and lactate, can traffick in an activity-dependent manner through astroglial networks to sustain distal neuronal activity. Thus, astroglial metabolic networks play a crucial role in neurometabolic coupling, by supplying efficiently and distally energy substrates to active neurons. Given that astroglial metabolic networks are able to provide energy metabolites from distant sources, they likely play important roles in physiological situations associated with increased metabolic demand related to high neuronal activity that exceeds local glucose supply, or pathological conditions with altered substrate availability (such as hypoglycemia, anoxia, ischemia, glucose transporter deficiency).

However, our understanding of the properties and function of astroglial metabolic networks remains insufficient. What might be the advantage of a coordinated glucose uptake and metabolite delivery through astroglial metabolic networks? Theoretically, each astrocyte should be in the reach of a local source of glucose, since the high density of the vascular network within the hippocampus enables every astrocyte to contact a capillary. However, glucose uptake by a single astrocyte in response to energy needs, might be metabolically less proficient than coordinated glucose supply from distal source through astroglial networks in conditions of high neuronal activity. Thus, astroglial metabolic networks may represent an energetically efficient mechanism for glucose delivery to active neurons. In addition, although capillaries are a local source of glucose, the capacity of each astrocyte to take up and deliver glucose to neurons may not be homogeneous within a given brain area. This depends on several factors including the capillary coverage by astrocytic endfeet, the density of glucose transporters in these endfeet, the astroglial metabolic machinery, and the strength of neuroglial interactions (i.e. density of receptors on astrocytes, astrocytic coverage of neurons). These parameters are likely to be heterogeneous among astrocytes (Matyash and Kettenmann, 2010), and thus astroglial GJs may offer a mean to equilibrate neuronal glucose supply in basal or pathological conditions.

Another unknown matter is whether astroglial metabolic networks only operate with excitatory neurons. Astrocytes take up GABA through $Na^+$-dependent transporters. Nevertheless, inhibitory activity is associated with lower metabolic demand than excitatory activity (Chatton et al., 2003; Hyder et al., 2006). Therefore, the role played by astroglial metabolic networks at inhibitory synapses remains to be established.

In addition, it is uncertain whether other energy metabolites, such as KBs, known to have a therapeutic effect on epileptic activity, can also traffick through GJs in astrocytes to sustain neuronal activity. The development of fluorescent KBs and other metabolic substrates should help investigating this issue.

Finally, the few studies investigating astroglial metabolic network properties and function have been performed in culture or in brain slices with relatively low temporal and spatial resolution. In addition, they used fluorescent derivatives of glucose, such as 2-NBDG, which are highly bleachable molecules, as well as non-selective blockers of GJ channels, targeting also connexin and pannexin hemichannels, or connexin knockout mouse model chronically disrupting astroglial GJ networks. Hence, the dynamics and moment to moment contribution of astroglial networks to neurotransmission *in vivo* during specific tasks in physiological or pathological situations are still open questions. To solve these issues and better understand brain functions and dysfunctions, the development of novel pharmacological and molecular tools is required, including new stable fluorescent derivatives of metabolite substrates, as well as pharmacological inhibitors and mouse models, timely and selectively targeting the GJ channel function of astroglial connexins. Only then, we shall fully understand the pivotal role played by astroglial networks in neurometabolic coupling.

## ACKNOWLEDGMENTS

We would like to thank Glenn Dallérac for comments on the manuscript and Annette Koulakoff for **Figure 1A**. This work was supported by grants from the Human Frontier Science Program Organization (Career Development Award), French Research Agency (ANR, Programme Jeunes chercheurs and Programme Blanc), FRC (Fédération pour la Recherche sur le Cerveau), City of Paris (Programme Emergence), La Pitié Salpêtrière hospital (Translational research contract) and INSERM to Nathalie Rouach, and French Research Agency (ANR, Programme Jeunes chercheurs and Programme Blanc) to Carole Escartin.

## REFERENCES


Allaman, I., Belanger, M., and Magistretti, P. J. (2011). Astrocyte-neuron metabolic relationships: for better and for worse. *Trends Neurosci.* 34, 76–87.

Attwell, D., Buchan, A. M., Charpak, S., Lauritzen, M., Macvicar, B. A., and Newman, E. A. (2010). Glial and neuronal control of brain blood flow. *Nature* 468, 232–243.

Ball, K. K., Gandhi, G. K., Thrash, J., Cruz, N. F., and Dienel, G. A. (2007). Astrocytic connexin distributions and rapid, extensive dye transfer via gap junctions in the inferior colliculus: implications for [(14)C]glucose metabolite trafficking. *J. Neurosci. Res.* 85, 3267–3283.

Belanger, M., Allaman, I., and Magistretti, P. J. (2011). Brain energy metabolism: focus on astrocyte-neuron metabolic cooperation. *Cell Metab.* 14, 724–738.

Bennett, M. V., Garre, J. M., Orellana, J. A., Bukauskas, F. F., Nedergaard, M., and Saez, J. C. (2012). Connexin and pannexin hemichannels in inflammatory responses of glia and neurons. *Brain Res.* 1487, 3–15.

Bernardinelli, Y., Magistretti, P. J., and Chatton, J. Y. (2004). Astrocytes generate Na+-mediated metabolic waves. *Proc. Natl. Acad. Sci. U.S.A.* 101, 14937–14942.

Bittner, C. X., Valdebenito, R., Ruminot, I., Loaiza, A., Larenas, V., Sotelo-Hitschfeld, T., et al. (2011). Fast and reversible stimulation of astrocytic glycolysis by K+ and a delayed and persistent effect of glutamate. *J. Neurosci.* 31, 4709–4713.

Brown, A. M., Sickmann, H. M., Fosgerau, K., Lund, T. M., Schousboe, A., Waagepetersen, H. S., et al. (2005). Astrocyte glycogen metabolism is required for neural activity during aglycemia or intense stimulation in mouse white matter. *J. Neurosci. Res.* 79, 74–80.

Chatton, J. Y., Pellerin, L., and Magistretti, P. J. (2003). GABA uptake into astrocytes is not associated with significant metabolic cost: implications for brain imaging of inhibitory transmission. *Proc. Natl. Acad. Sci. U.S.A.* 100, 12456–12461.

Choi, H. B., Gordon, G. R., Zhou, N., Tai, C., Rungta, R. L., Martinez, J., et al. (2012). Metabolic communication between astrocytes and neurons via bicarbonate-responsive soluble adenylyl cyclase. *Neuron* 75, 1094–1104.

Cotrina, M. L., Kang, J., Lin, J. H., Bueno, E., Hansen, T. W., He, L., et al. (1998). Astrocytic gap junctions remain open during ischemic conditions. *J. Neurosci.* 18, 2520–2537.

Cotrina, M. L., and Nedergaard, M. (2012). Brain connexins in demyelinating diseases: therapeutic potential of glial targets. *Brain Res.* 1487, 61–68.

Coulter, D. A., and Eid, T. (2012). Astrocytic regulation of glutamate homeostasis in epilepsy. *Glia* 60, 1215–1226.

Cronin, M., Anderson, P. N., Cook, J. E., Green, C. R., and Becker, D. L. (2008). Blocking connexin43 expression reduces inflammation and improves functional recovery after spinal cord injury. *Mol. Cell Neurosci.* 39, 152–160.

De Pina-Benabou, M. H., Srinivas, M., Spray, D. C., and Scemes, E. (2001). Calmodulin kinase pathway mediates the K+-induced increase in Gap junctional communication between mouse spinal cord astrocytes. *J. Neurosci.* 21, 6635–6643.

Enkvist, M. O., and McCarthy, K. D. (1994). Astroglial gap junction communication is increased by treatment with either glutamate or high K+ concentration. *J. Neurochem.* 62, 489–495.

Escartin, C., Brouillet, E., Gubellini, P., Trioulier, Y., Jacquard, C., Smadja, C., et al. (2006). Ciliary neurotrophic factor activates astrocytes, redistributes their glutamate transporters GLAST and GLT-1 to raft microdomains, and improves glutamate handling *in vivo*. *J. Neurosci.* 26, 5978–5989.

Escartin, C., Pierre, K., Colin, A., Brouillet, E., Delzescaux, T., Guillermier, M., et al. (2007). Activation of astrocytes by CNTF induces metabolic plasticity and increases resistance to metabolic insults. *J. Neurosci.* 27, 7094–7104.

Eugenin, E. A., and Berman, J. W. (2007). Gap junctions mediate human immunodeficiency virus-bystander killing in astrocytes. *J. Neurosci.* 27, 12844–12850.

Eugenin, E. A., Clements, J. E., Zink, M. C., and Berman, J. W. (2011). Human immunodeficiency virus infection of human astrocytes disrupts blood-brain barrier integrity by a gap junction-dependent mechanism. *J. Neurosci.* 31, 9456–9465.

Farahani, R., Pina-Benabou, M. H., Kyrozis, A., Siddiq, A., Barradas, P. C., Chiu, F. C., et al. (2005). Alterations in metabolism and gap junction expression may determine the role of astrocytes as "good samaritans" or executioners. *Glia* 50, 351–361.

Fischer, G., and Kettenmann, H. (1985). Cultured astrocytes form a syncytium after maturation. *Exp. Cell Res.* 159, 273–279.

Frantseva, M. V., Kokarovtseva, L., Naus, C. G., Carlen, P. L., Macfabe, D., and Perez Velazquez, J. L. (2002a). Specific gap junctions enhance the neuronal vulnerability to brain traumatic injury. *J. Neurosci.* 22, 644–653.

Frantseva, M. V., Kokarovtseva, L., and Perez Velazquez, J. L. (2002b). Ischemia-induced brain damage depends on specific gap-junctional coupling. *J. Cereb. Blood Flow Metab.* 22, 453–462.

Giaume, C., Koulakoff, A., Roux, L., Holcman, D., and Rouach, N. (2010). Astroglial networks: a step further in neuroglial and gliovascular interactions. *Nat. Rev. Neurosci.* 11, 87–99.

Guzman, M., and Blazquez, C. (2001). Is there an astrocyte-neuron ketone body shuttle? *Trends Endocrinol. Metab.* 12, 169–173.

Harris, J. J., Jolivet, R., and Attwell, D. (2012). Synaptic energy use and supply. *Neuron* 75, 762–777.

Houades, V., Koulakoff, A., Ezan, P., Seif, I., and Giaume, C. (2008). Gap junction-mediated astrocytic networks in the mouse barrel cortex. *J. Neurosci.* 28, 5207–5217.

Houades, V., Rouach, N., Ezan, P., Kirchhoff, F., Koulakoff, A., and Giaume, C. (2006). Shapes of astrocyte networks in the juvenile brain. *Neuron Glia Biol.* 2, 3–14.

Hyder, F., Patel, A. B., Gjedde, A., Rothman, D. L., Behar, K. L., and Shulman, R. G. (2006). Neuronal-glial glucose oxidation and glutamatergic-GABAergic function. *J. Cereb. Blood Flow Metab.* 26, 865–877.

Kielian, T., and Esen, N. (2004). Effects of neuroinflammation on glia-glia gap junctional intercellular communication: a perspective. *Neurochem. Int.* 45, 429–436.

Koulakoff, A., Mei, X., Orellana, J. A., Saez, J. C., and Giaume, C. (2012). Glial connexin expression and function in the context of Alzheimer's disease. *Biochim. Biophys. Acta* 1818, 2048–2057.

Kuchibhotla, K. V., Lattarulo, C. R., Hyman, B. T., and Bacskai, B. J. (2009). Synchronous hyperactivity and intercellular calcium waves in astrocytes in Alzheimer mice. *Science* 323, 1211–1215.

Kuga, N., Sasaki, T., Takahara, Y., Matsuki, N., and Ikegaya, Y. (2011). Large-scale calcium waves traveling through astrocytic networks *in vivo*. *J. Neurosci.* 31, 2607–2614.

Langer, J., Stephan, J., Theis, M., and Rose, C. R. (2012). Gap junctions mediate intercellular spread of sodium between hippocampal astrocytes *in situ*. *Glia* 60, 239–252.

Lin, J. H., Weigel, H., Cotrina, M. L., Liu, S., Bueno, E., Hansen, A. J., et al. (1998). Gap-junction-mediated propagation and amplification of cell injury. *Nat. Neurosci.* 1, 494–500.

Lin, M. T., and Beal, M. F. (2006). Mitochondrial dysfunction and oxidative stress in neurodegenerative diseases. *Nature* 443, 787–795.

Maalouf, M., Rho, J. M., and Mattson, M. P. (2009). The neuroprotective properties of calorie restriction, the ketogenic diet, and ketone bodies. *Brain Res. Rev.* 59, 293–315.

Magistretti, P. J., Sorg, O., and Martin, J. L. (1993). "Regulation of glycogen metabolism in astrocytes: physiological, pharmacological, and pathological aspects," in *Astrocytes: Pharmacology and Function*, ed S. Murphy (San Diego, CA: Academic Press), 243–265.

Marrero, H., and Orkand, R. K. (1996). Nerve impulses increase glial intercellular permeability. *Glia* 16, 285–289.

Matyash, V., and Kettenmann, H. (2010). Heterogeneity in astrocyte morphology and physiology. *Brain Res. Rev.* 63, 2–10.

McKenna, M. C. (2007). The glutamate-glutamine cycle is not stoichiometric: fates of glutamate in brain. *J. Neurosci. Res.* 85, 3347–3358.

Meme, W., Calvo, C. F., Froger, N., Ezan, P., Amigou, E., Koulakoff, A., et al. (2006). Proinflammatory cytokines released from microglia inhibit gap junctions in astrocytes: potentiation by beta-amyloid. *FASEB J.* 20, 494–496.

Nagy, J. I., Patel, D., Ochalski, P. A., and Stelmack, G. L. (1999). Connexin30 in rodent, cat and human brain: selective expression in gray matter astrocytes, co-localization with connexin43 at gap junctions and late developmental appearance. *Neuroscience* 88, 447–468.

Nakase, T., Fushiki, S., Sohl, G., Theis, M., Willecke, K., and Naus, C. C. (2003). Neuroprotective role of astrocytic gap junctions in ischemic stroke. *Cell Commun. Adhes.* 10, 413–417.

Nedergaard, M., and Verkhratsky, A. (2012). Artifact versus reality–how astrocytes contribute to synaptic events. *Glia* 60, 1013–1023.

Orellana, J. A., Von Bernhardi, R., Giaume, C., and Saez, J. C. (2012).

Glial hemichannels and their involvement in aging and neurodegenerative diseases. *Rev. Neurosci.* 23, 163–177.

Pellerin, L., Bouzier-Sore, A. K., Aubert, A., Serres, S., Merle, M., Costalat, R., et al. (2007). Activity-dependent regulation of energy metabolism by astrocytes: an update. *Glia* 55, 1251–1262.

Pellerin, L., and Magistretti, P. J. (1994). Glutamate uptake into astrocytes stimulates aerobic glycolysis: a mechanism coupling neuronal activity to glucose utilization. *Proc. Natl. Acad. Sci. U.S.A.* 91, 10625–10629.

Peters, O., Schipke, C. G., Philipps, A., Haas, B., Pannasch, U., Wang, L. P., et al. (2009). Astrocyte function is modified by Alzheimer's disease-like pathology in aged mice. *J. Alzheimers Dis.* 18, 177–189.

Prins, M. L. (2012). Cerebral ketone metabolism during development and injury. *Epilepsy Res.* 100, 218–223.

Rouach, N., Avignone, E., Meme, W., Koulakoff, A., Venance, L., Blomstrand, F., et al. (2002a). Gap junctions and connexin expression in the normal and pathological central nervous system. *Biol. Cell* 94, 457–475.

Rouach, N., Tence, M., Glowinski, J., and Giaume, C. (2002b). Costimulation of N-methyl-D-aspartate and muscarinic neuronal receptors modulates gap junctional communication in striatal astrocytes. *Proc. Natl. Acad. Sci. U.S.A.* 99, 1023–1028.

Rouach, N., Glowinski, J., and Giaume, C. (2000). Activity-dependent neuronal control of gap-junctional communication in astrocytes. *J. Cell Biol.* 149, 1513–1526.

Rouach, N., Koulakoff, A., Abudara, V., Willecke, K., and Giaume, C. (2008). Astroglial metabolic networks sustain hippocampal synaptic transmission. *Science* 322, 1551–1555.

Rouach, N., Segal, M., Koulakoff, A., Giaume, C., and Avignone, E. (2003). Carbenoxolone blockade of neuronal network activity in culture is not mediated by an action on gap junctions. *J. Physiol.* 553, 729–745.

Roux, L., Benchenane, K., Rothstein, J. D., Bonvento, G., and Giaume, C. (2011). Plasticity of astroglial networks in olfactory glomeruli. *Proc. Natl. Acad. Sci. U.S.A.* 108, 18442–18446.

Ruminot, I., Gutierrez, R., Pena-Munzenmayer, G., Anazco, C., Sotelo-Hitschfeld, T., Lerchundi, R., et al. (2011). NBCe1 mediates the acute stimulation of astrocytic glycolysis by extracellular K+. *J. Neurosci.* 31, 14264–14271.

Simard, M., Arcuino, G., Takano, T., Liu, Q. S., and Nedergaard, M. (2003). Signaling at the gliovascular interface. *J. Neurosci.* 23, 9254–9262.

Steinhauser, C., Seifert, G., and Bedner, P. (2012). Astrocyte dysfunction in temporal lobe epilepsy: K+ channels and gap junction coupling. *Glia* 60, 1192–1202.

Suzuki, A., Stern, S. A., Bozdagi, O., Huntley, G. W., Walker, R. H., Magistretti, P. J., et al. (2011). Astrocyte-neuron lactate transport is required for long-term memory formation. *Cell* 144, 810–823.

Theis, M., and Giaume, C. (2012). Connexin-based intercellular communication and astrocyte heterogeneity. *Brain Res.* 1487, 88–98.

Vessey, J. P., Lalonde, M. R., Mizan, H. A., Welch, N. C., Kelly, M. E., and Barnes, S. (2004). Carbenoxolone inhibition of voltage-gated Ca channels and synaptic transmission in the retina. *J. Neurophysiol.* 92, 1252–1256.

**Conflict of Interest Statement:** The authors declare that the research was conducted in the absence of any commercial or financial relationships that could be construed as a potential conflict of interest.

*Received: 31 January 2013; paper pending published: 12 February 2013; accepted: 18 March 2013; published online: 26 April 2013.*

*Citation: Escartin C and Rouach N (2013) Astroglial networking contributes to neurometabolic coupling. Front. Neuroenergetics **5**:4. doi: 10.3389/fnene.2013.00004*

frontiers in
NEUROENERGETICS

PERSPECTIVE ARTICLE
published: 19 March 2012
doi: 10.3389/fnene.2012.00005

# Is lactate a volume transmitter of metabolic states of the brain?

***Linda H. Bergersen*[1,2,3]* *and Albert Gjedde*[2,3,4,5,6]**

[1] *The Brain and Muscle Energy Group, Centre for Molecular Biology and Neuroscience, Institute for Basic Medical Sciences, University of Oslo, Oslo, Norway*

[2] *Department of Neuroscience and Pharmacology, University of Copenhagen, Copenhagen, Denmark*

[3] *Center for Healthy Aging, Faculty of Health Sciences, University of Copenhagen, Copenhagen, Denmark*

[4] *Center of Functionally Integrative Neuroscience, Aarhus University, Aarhus, Denmark*

[5] *McConnell Brain Imaging Center, Montreal Neurological Institute, McGill University, Montreal, QC, Canada*

[6] *Department of Radiology and Radiological Science, Johns Hopkins University, Baltimore, MD, USA*

***Edited by:***
*Sebastian Cerdan, Instituto de Investigaciones Biomedicas Alberto Sols, Spain*

***Reviewed by:***
*Vladimir Parpura, University of Alabama, USA*
*Sebastian Cerdan, Instituto de Investigaciones Biomedicas Alberto Sols, Spain*
*Anne-Karine Bouzier-Sore, CNRS/Université Victor Segalen, France*

***Correspondence:**
*Linda H. Bergersen, The Brain and Muscle Energy Group, Centre for Molecular Biology and Neuroscience and Institute for Basic Medical Sciences, University of Oslo, P.O. Box 1105 Blindern, No-0317 Oslo, Norway.*
*e-mail: l.h.bergersen@medisin.uio.no*

We present the perspective that lactate is a volume transmitter of cellular signals in brain that acutely and chronically regulate the energy metabolism of large neuronal ensembles. From this perspective, we interpret recent evidence to mean that lactate transmission serves the maintenance of network metabolism by two different mechanisms, one by regulating the formation of cAMP via the lactate receptor GPR81, the other by adjusting the NADH/$NAD^+$ redox ratios, both linked to the maintenance of brain energy turnover and possibly cerebral blood flow. The role of lactate as mediator of metabolic information rather than metabolic substrate answers a number of questions raised by the controversial oxidativeness of astrocytic metabolism and its contribution to neuronal function.

**Keywords: lactate, lactate receptor, central fatigue, metabolic information, volume transmission**

Here, we present the perspective that lactate acts as a volume transmitter in brain tissue by distributing cellular signals that are relevant to the metabolic support of large neuronal ensembles. We interpret recent evidence to mean that lactate transmission is involved in the maintenance of network homeostasis by two different mechanisms; one by regulation of neuronal cAMP formation through the lactate receptor GPR81, the other by adjustment of the NADH/$NAD^+$ redox ratio. Lactate is an intermediary metabolite in brain energy metabolism, the role of which is controversial (Dienel, 2011). Traditionally, lactate was considered a waste product with no certain function in the metabolic housekeeping when eukaryotic cells have sufficient oxygen. However, it is also held to be a "preferred" substrate of energy metabolism, in muscle (Brooks, 2009) as well as in brain (Bouzier-Sore et al., 2003; Smith et al., 2003; Wyss et al., 2011). This alleged preference revives an ancient claim of lactate's service as nutrient for neurons that do not phosphorylate glucose to the extent required by neuronal energy metabolism (Andriezen, 1893; DiNuzzo et al., 2011). A cue to the notion of a signaling role of lactate, irrespective of any role as intermediary metabolite, is the observation that lactate regulates cerebral blood flow (Gordon et al., 2008).

## VOLUME TRANSMISSION

The concept of volume transmission, introduced by Luigi Agnati and Kjell Fuxe in 1986, designates is a form of communication in brain tissue in which modulators act across wide distances when their sites of release and removal are further apart than for "wired" transmission, characteristic of focused synaptic action (Fuxe et al., 2010). Volume transmission affects large volumes of tissue and undergoes change more slowly than wired transmission. The concept of volume transmission in brain therefore overlaps with forms of paracrine and autocrine signaling. The canonical volume transmitters are monoamines, released from varicosities along the fibers of monoaminergic neurons and removed by transporters at sites reached after variable distances of diffusion. However, the list of potential agents of volume transmission is long, as any molecule that engages receptors, transporters, or enzymes far from a place of synthesis or release may qualify as a volume transmitter, including the archetypical wired transmitter glutamate (Okubo and Iino, 2011). Another potential volume transmitter is L-DOPA, which shares with lactate the ability to move across cellular membranes and reach cells far from the sites of generation (Gjedde et al., 1993; Ugrumov, 2009).

## LACTATE RECEPTOR GPR81

The G-protein-coupled 7TM receptor (GPR) family includes members that mediate specific actions of hydroxyl carboxylic acids (HCA), including GPR81, also known as HCA1 receptor (Blad et al., 2011), which serves lactate's downregulation of cAMP, as shown in adipocytes (Ahmed et al., 2009). The GPR81

is prominent in adipose tissue, where it inhibits lipolysis, but it is known also to be expressed in a wider range of organs such as liver, kidney, skeletal muscle, spleen, and testis (Gantz et al., 1997; Ge et al., 2008; Liu et al., 2009; Rooney and Trayhurn, 2011). Evidence from *in situ* hybridization show a widespread distribution of GPR81 mRNA in the brain, predominantly in neurons, including the principal neurons in cortex, hippocampus (pyramidal and granule cells), and cerebellum (granule cells), while labeling of astrocytes cannot be excluded (The Allen Institute for Brain Science[1], GENSTAT[2], St. Jude Children's Research Hospital[3]). The receptor's reported affinities for L-lactate range from 1.3 to 5 mM (Cai et al., 2008; Liu et al., 2009), which is consistent with the range of lactate concentrations measured in brain tissue *in vivo* (Abi-Saab et al., 2002). The binding of lactate to GPR81 attenuates the formation of cAMP, which in turn inhibits protein kinase A and hence glycogenolysis, leading to decreases of glucose-1-phosphate and glucose-6-phosphate (G6P) that affect glycolysis in the cytosol, as recently shown by kinetic modeling (DiNuzzo et al., 2010). The decrease of G6P affects its role as allosteric regulator of hexokinase (HK), including the association of HK with the voltage dependent anion channel (VDAC) in the outer mitochondrial membrane, with important consequences for the efficiency of oxidative phosphorylation of ADP (Wilson, 2003; Mailloux and Harper, 2011). The main thrust of this perspective is the importance of any physical separation of HK and pyruvate dehydrogenase (PDH) activities, which would lead to diffusion of lactate between the sites. As such, this concept is not limited to major compartments or cell types but applies equally well to subdivisions of cells, such as distal vs proximal dendrites and astrocytic processes vs cell bodies rather than to astrocyte/neuron differences (**Figure 1**).

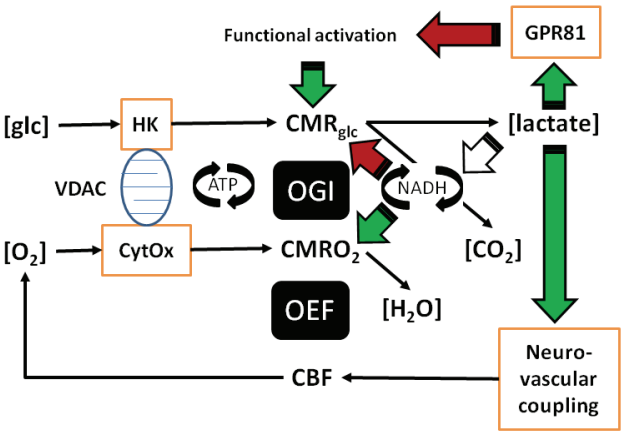


**FIGURE 1 | In this illustration you can follow the two different mechanisms proposed:** (a) Lactate regulates the formation of cAMP via the lactate receptor GPR81. (b) Lactate adjusts the NADH/$NAD^+$ redox ratio. (c) Both the formation of cAMP and the adjustment of NADH/$NAD^+$ redox ratio can be linked to the maintenance of brain energy turnover and neurovascular coupling. The role of lactate in neurovascular coupling is included in the figure, but not dealt with in the text, which focuses on cellular effects of lactate in brain tissue. The roles of lactate as mediator of metabolic information rather than metabolic substrate answer a number of questions raised by the aerobic glycolysis of astrocytes and its controversial contribution to neuronal function.

## CYTOSOLIC AND MITOCHONDRIAL NADH/$NAD^+$ REDOX RATIOS AND LACTATE DEHYDROGENASES

Lactic and pyruvic acids interact through the actions of the cytosolic near-equilibrium lactate dehydrogenase (LDH) isozymes, which reflect the cytosolic NADH/$NAD^+$ ratios in cytosol. The cytosolic and the mitochondrial redox states are linked through a network of redox reactions and inner membrane transport processes, but the exact relation between cytosolic and mitochondrial NADH/$NAD^+$ ratios is not known. There are reports of mitochondrial LDH activity (Brooks, 2009) and therefore potential for coupling of lactate–pyruvate and NADH/$NAD^+$ ratios in the mitochondrial matrix. Changes of the NADH/$NAD^+$ redox ratios trigger several intracellular responses, including expression of genes by modification of histone deacetylases, which profoundly affect the regulation of protein synthesis. For example sirtuins, gene-regulating histone deacetylases with effects on regulation of caloric intake, metabolism and age-related diseases (Finkel et al., 2009), are tightly redox regulated through the NADH/$NAD^+$ ratio (Gambini et al., 2011). Genes activated by lactate through lactate-sensitive response elements include c-fos, c-jun, c-ets, Hyal-1, Hyal-2, CD44, and caveolin-1 (Formby and Stern, 2003). The DNA binding of the transcription factor fos–jun heterodimer AP-1 depends on a specific cysteine residue being in the reduced sate (Abate et al., 1990), acting as a redox sensor. In addition, pyruvate, which interacts closely with lactate as dictated by the NADH/$NAD^+$ ratio, is a gene regulator through histone deacetylase inhibition (Thangaraju et al., 2009; Rajendran et al., 2011).

## NEAR-EQUILIBRIUM REACTIONS AND LACK OF COMPARTMENTATION

Both the LDH isozymes and the monocarboxylic acid transporters (MCT) of the blood–brain barrier and cell membranes of brain tissue mediate near-equilibrium transfer of lactate (Bergersen et al., 2001; Bergersen, 2007) when unidirectional fluxes exceed net fluxes by several orders of magnitude. Therefore LDH and MCT proteins serve to dissipate lactate concentration differences across cell membranes and tissue volumes. Thus, changes of pyruvate and lactate concentrations in one place lead to similar changes of lactate concentrations across large volumes of brain tissue over long times. In turn, any effects of changes of lactate on the NADH/$NAD^+$ ratio in one place lead to similar effects in widely distributed populations of cells (cf. Cerdán et al., 2006; Ramírez et al., 2007; Rodrigues et al., 2009). In fact, the transfer of lactate is so efficient that it is difficult to observe any differences of lactate concentrations across cell membranes in brain tissue (Gjedde and Marrett, 2001; Ido et al., 2001, 2004; Gjedde et al., 2002), such that significant cellular compartmentation of lactate is unlikely to exist under normal conditions, except briefly. The high concentration of MCT2 at the PSD of fast excitatory synapses co-localized with glutamate receptors (Bergersen et al.,

[1]http://www.brain-map.org
[2]http://www.ncbi.nlm.nih.gov/gensat
[3]http://www.stjudebgem.org

2001, 2005) suggests a particular need for lactate transfer at these synapses perhaps involved in volume transmission signaling. In addition to moving through brain tissue by facilitated transfer across plasma membranes of all cells through MCT1, MCT2, and MCT4, and by diffusion through the extracellular space, lactate spreads through the astroglial network in which individual astrocytes are connected by gap junctions (Dienel, 2011; Mathiesen et al., 2011). One puzzle is the kinetic differences among the isozymes of LDH (O'Brien et al., 2007), the physiological role of which at near-equilibrium is not yet understood (Ross et al., 2010; Quistorff and Grunnet, 2011; Ross, 2011), but may be related to the proposed function of lactate as a volume transmitter in cytosolic and perhaps mitochondrial environments with widely differing NADH/$NAD^+$ ratios (**Figure 1**).

## NON-STEADY-STATES AND ACTIVATION

The purported changes of lactate concentrations and the consequent redistribution of lactate happen whenever and wherever sites of generation and metabolic conversion of pyruvate are unmatched or physically separated. Pyruvate is the main end product of aerobic glycolysis, which is controlled by the concerted action of the HK and phosphofructokinase (PFK) enzyme complex, while the fate of pyruvate is determined by the PDH complex in mitochondria. The two enzyme complexes are the main flux-generating determinants of brain energy metabolism as controlled by allosteric effectors, and both therefore define the path that is open to the respective so-called "pathway substrates," glucose in the case of the HK–PFK complex, pyruvate in the case of the PDH complex (Gjedde, 2007). The temporal and spatial integration of the activities of these enzyme complexes is then the key to the dynamics of lactate inside and among the cells of brain tissue. Both the oxygen–glucose index (OGI) and the oxygen extraction fraction (OEF) decline during the temporary departures from steady-state associated with functional activation of brain regions, attributed to increased aerobic glycolysis (Madsen et al., 1999; Schmalbruch et al., 2002). The declines are signs of focal disintegration of the HK–PFK and PDH activities, resulting in increased lactate–pyruvate ratios, redistribution of lactate and adjustment of NADH/$NAD^+$ ratios within the sphere of action of the redistributed lactate. This process seems to be so efficient that it leaves no oxygen deficit or abnormal ATP, ADP, or AMP levels, even in seizures (Larach et al., 2011).

Extracellular lactate concentrations increase during neuronal and synaptic activation *in vivo*, as determined by microdialysis (Uehara et al., 2008; Bero et al., 2011), and proton magnetic resonance spectroscopy minutes after stimulation (Prichard et al., 1991; Sappey-Marinier et al., 1992; Maddock et al., 2006), following a transient decrease 5 s after stimulation (Mangia et al., 2003). These observations are consistent with adjustments that follow the perturbation of an existing steady-state and the subsequent return to a potential new steady-state, depending on conditions, such as the intensity of the continuing neuronal activation. The lactate dynamics are uniquely dependent on the shifts among these steady- and non-steady-states of brain energy metabolism. The observations that the OGI declines during the non-steady-state of the early stages of functional brain activation, signifies increased lactate production in the tissue as a whole, evidently due to increased glucose consumption relative to oxygen consumption. The observations are consistent with changes of glucose consumption that match the changes of blood flow during activation, while changes of oxygen consumption generally do not (Gjedde et al., 2002; Paulson et al., 2010). Recent evidence also shows that the changes of glucose consumption exceed the changes of oxygen consumption at specific regional locations (Vaishnavi et al., 2010), rather than everywhere, creating the gradients of lactate concentration that serve to redistribute lactate inside as well as outside cells and across the blood–brain barrier. The regional variation of the OGI (Vaishnavi et al., 2010) may possibly be related to different ratios of cell types (low in cortex with numerous astrocytes, high in cerebellum with numerous neurons). Any separation of the sites of lactate generation and lactate metabolism inside or among cells therefore must result in shuttling of lactate among its sites of generation and metabolism. The fluxes alter the interactions with enzymes and transporters that qualify as volume transmission. Thus, the temporal and spatial mismatches of lactate generation and metabolism arise because different cellular and subcellular compartments react differently to activating stimuli (Gjedde et al., 2005; Vaishnavi et al., 2010).

## CENTRAL vs PERIPHERAL FATIGUE

Physical exertion generates considerable increases of lactate concentration in the circulation. It has been shown by MR spectroscopy that blood lactate is an efficient substrate for the brain, and especially for neurons, both in rat (Bouzier et al., 2000; Hassel and Bråthe, 2000) and in humans (Boumezbeur et al., 2010). The increased lactate also has effects on brain metabolism, which are characterized by reduction of the cerebral OGI in the context of a state known as "central fatigue" (Dalsgaard, 2006; Dalsgaard and Secher, 2007; Rasmussen et al., 2010). Central fatigue precedes the muscle fatigue that also relates to increased lactate (van Hall, 2010). The mechanism responsible for the onset of central fatigue is not known with certainty but appears to be related to decreased oxygen delivery, which in turn may be due to increased lactate in brain tissue and possible effects on lactate's receptor GPR81 (Rasmussen et al., 2010; Gam et al., 2011). The down-regulation of cAMP formation by binding of lactate to GPR81 offers a novel explanation of central fatigue and "over-training" distress (Lehmann et al., 1993), and possibly in part the asthenia seen in advanced cancer, a condition that is known to be characterized by chronically increased blood lactate levels (Koppenol et al., 2011). Chronically increased lactate levels similarly are held to be characteristic of old age and dementia, based on the properties of a mtDNA mutator mouse model (Ross et al., 2010). These effects contrast with the upregulation of cAMP by noradrenaline with effects such as arousal and enhanced brain performance (Berridge, 2008).

Many other observed effects of lactate on neuronal function may result from enzyme- or receptor-mediated responses rather than from the direct actions of lactate as a metabolic substrate. For example, the observation that lactate administration protects against ischemia (Schurr et al., 1997, 2001; Cureton et al., 2010) has been ascribed to enhanced neuronal energy turnover. However, this is not readily explained by metabolic effects, as lactate metabolism cannot raise energy turnover under ischemic

conditions, although after ischemia and in the penumbra of vascular occlusion, the availability of lactate for oxidation may assist in alleviating ischemia induced damage (Schurr et al., 2001; Berthet et al., 2009). Similarly, the observed protective effect of lactate on glutamate toxicity in the brain (Ros et al., 2001) may be due to receptor-mediated inhibition, rather than the simple satisfaction of the metabolic demands of neurons exposed to high concentrations of glutamate (Schurr et al., 1999). In microdialysis of the cerebral cortex, excitotoxic concentrations of glutamate raised lactate at the expense of glucose in the dialysate. The addition of L-lactate caused the lesion to become smaller and abolished the decrease of glucose. Replacing L-lactate with the non-physiological D-lactate isomer expanded the lesion and raised L-lactate in the dialysate above the level observed with glutamate alone (Ros et al., 2001), consistent with the claim that endogenously produced lactate is neuroprotective by means of receptor interaction.

The suppression of noradrenalin and adrenalin releases by blood lactate clamps at 4 mM (Fattor et al., 2005) also suggests a receptor mechanism, consistent with the postulated reduction of cAMP formation by GRP81 activation. Interestingly, also β-adrenoceptor blockers, which presumably act by reducing intracellular cAMP, are neuroprotective in stroke and other brain injuries, and also lower extracellular glutamate levels, which may further limit excitotoxic cell damage (Goyagi et al., 2011).

## CONCLUSION

The proposed role of lactate as a mediator of information on changing NADH/$NAD^+$ ratios among the cells of brain tissue has implications for the understanding of regulation of brain energy metabolism, including the communication between cytosol and mitochondria in large populations of cells (Xu et al., 2007). Lactate's inhibition of cAMP formation through G-protein-coupled receptors may be a factor in the development of central fatigue. An action of lactate may therefore be to "smooth" the non-steady-states that underlie the mismatches of glycolysis and oxidative phosphorylation, induced by needs for aerobic glycolysis that satisfy the short time constants of ATP turnover required for maintenance of rapid de- and repolarizations. The redistribution of lactate by the volume transmission is both temporal and spatial and potentially reaches large volumes of tissue, aided by the extended syncytium of astrocytic networks connected by gap junctions. The role of lactate as informant of metabolic states rather than substrate of metabolism solves a number of puzzles that contribute to the controversy surrounding the understanding of astrocytic metabolism and its contribution to neuronal function.

## REFERENCES


Abate, C., Patel, L., Rauscher, F. J., and Curran, T. (1990). Redox regulation of fos and jun DNA-binding activity in vitro. *Science* 249, 1157–1161.

Abi-Saab, W. M., Maggs, D. G., Jones, T., Jacob, R., Srihari, V., Thompson, J., Kerr, D., Leone, P., Krystal, J. H., Spencer, D. D., During, M. J., and Sherwin, R. S. (2002). Striking differences in glucose and lactate levels between brain extracellular fluid and plasma in conscious human subjects: effects of hyperglycemia and hypoglycemia. *J. Cereb. Blood Flow Metab.* 22, 271–279.

Ahmed, K., Tunaru, S., and Offermanns, S. (2009). GPR109A, GPR109B and GPR81, a family of hydroxycarboxylic acid receptors. *Trends Pharmacol. Sci.* 30, 557–562.

Andriezen, W. L. (1893). The neuroglia elements in the human brain. *Br. Med. J.* 29, 227–230.

Bergersen, L. H. (2007). Is lactate food for neurons? Comparison of monocarboxylate transporter subtypes in brain and muscle. *Neuroscience* 145, 11–19.

Bergersen, L., Waerhaug, O., Helm, J., Thomas, M., Laake, p., Davies, A. J., Wilson, M. C., Halestrap, A. P., and Ottersen, O. P. (2001). A novel postsynaptic density protein: the monocarboxylate transporter MCT2 is co-localized with delta-glutamate receptors in postsynaptic densities of parallel fiber-Purkinje cell synapses. *Exp. Brain Res.* 136, 523–534.

Bergersen, L. H., Magistretti, P. J., and Pellerin, L. (2005). Selective postsynaptic co-localization of MCT2 with AMPA receptor GluR2/3 subunits at excitatory synapses exhibiting AMPA receptor trafficking. *Cereb. Cortex* 15, 361–370.

Bero, A. W., Yan, P., Roh, J. H., Cirrito, J. R., Stewart, F. R., Raichle, M. E., Lee, J. M., and Holtzman, D. M. (2011). Neuronal activity regulates the regional vulnerability to amyloid-β deposition. *Nat. Neurosci.* 14, 750–756.

Berridge, C. W. (2008). Noradrenergic modulation of arousal. *Brain Res. Rev.* 58, 1–17.

Berthet, C., Lei, H., Thevenet, J., Gruetter, R., Magistretti, P. J., and Hirt, L. (2009). Neuroprotective role of lactate after cerebral ischemia. *J. Cereb. Blood Flow Metab.* 29, 1780–1789.

Blad, C. C., Ahmed, K., Ijzerman, A. P., and Offermanns, S. (2011). Biological and pharmacological roles of HCA receptors. *Adv. Pharmacol* 62, 219–250.

Boumezbeur, F., Mason, G. F., de Graaf, R. A., Behar, K. L., Cline, G. W., Shulman, G. I., Rothman, D. L., and Petersen, K. F. (2010). Altered brain mitochondrial metabolism in healthy aging as assessed by in vivo magnetic resonance spectroscopy. *J. Cereb. Blood Flow Metab.* 30, 211–221.

Bouzier, A. K., Thiaudiere, E., Biran, M., Rouland, R., Canioni, P., and Merle, M. (2000). The metabolism of [3-(13)C]lactate in the rat brain is specific of a pyruvate carboxylase-deprived compartment. *J. Neurochem.* 75, 480–486.

Bouzier-Sore, A. K., Serres, S., Canioni, P., and Merle, M. (2003). Lactate involvement in neuron-glia metabolic interaction: (13)C-NMR spectroscopy contribution. *Biochimie* 85, 841–848.

Brooks, G. A. (2009). Cell–cell and intracellular lactate shuttles. *J. Physiol.* 587, 5591–5600.

Cai, T. Q., Ren, N., Jin, L., Cheng, K., Kash, S., Chen, R., Wright, S. D., Taggart, A. K., and Waters, M. G. (2008). Role of GPR81 in lactate-mediated reduction of adipose lipolysis. *Biochem. Biophys. Res. Commun.* 377, 987–991.

Cerdán, S., Rodrigues, T. B., Sierra, A., Benito, M., Fonseca, L. L., Fonseca, C. P., and García-Martín, M. L. (2006). The redox switch/redox coupling hypothesis. *Neurochem. Int.* 48, 523–530.

Cureton, E. L., Kwan, R. O., Dozier, K. C., Sadjadi, J., Pal, J. D., and Victorino, G. P. (2010). A different view of lactate in trauma patients: protecting the injured brain. *J. Surg. Res.* 159, 468–473.

Dalsgaard, M. K. (2006). Fuelling cerebral activity in exercising man. *J. Cereb. Blood Flow Metab.* 26, 731–750.

Dalsgaard, M. K., and Secher, N. H. (2007). The brain at work: a cerebral metabolic manifestation of central fatigue? *J. Neurosci. Res.* 85, 3334–3339.

Dienel, G. A. (2011). Brain lactate metabolism: the discoveries and the controversies. *J. Cereb. Blood Flow Metab.* doi: 10.1038/jcbfm.2011.175 [Epub ahead of print].

DiNuzzo, M., Gili, T., Maraviglia, B., and Giove, F. (2011). Modeling the contribution of neuron-astrocyte cross talk to slow blood oxygenation level-dependent signal oscillations. *J. Neurophysiol.* 106, 3010–3018.

DiNuzzo, M., Mangia, S., Maraviglia, B., and Giove, F. (2010). Glycogenolysis in astrocytes supports blood-borne glucose channeling not glycogen-derived lactate shuttling to neurons: evidence from mathematical modeling. *J. Cereb. Blood Flow Metab.* 1895–1904.

Fattor, J. A., Miller, B. F., Jacobs, K. A., and Brooks, G. A. (2005). Catecholamine response is attenuated during moderate-intensity exercise in response to the "lactate clamp". *Am. J. Physiol. Endocrinol. Metab.* 288, 143–147.

Finkel, T., Deng, C. X., and Mostoslavsky, R. (2009). Recent progress in the biology and physiology of sirtuins. *Nature* 460, 587–591.

Formby, B., and Stern, R. (2003). Lactate-sensitive response elements in genes involved in hyaluronan catabolism. *Biochem. Biophys. Res. Commun.* 305, 203–208.

Fuxe, K., Dahlström, A. B., Jonsson, G., Marcellino, D., Guescini, M., Dam, M., Manger, P., and Agnati, L. (2010). The discovery of central monoamine neurons gave volume transmission to the wired brain. *Prog. Neurobiol.* 90, 82–100.

Gam, C. M. B., Nielsen, H. B., Secher, N. H., Larsen, F. S., Ott, P., and Quistorff, B. (2011). In cirrhotic patients reduced muscle strength is unrelated to muscle capacity for ATP turnover suggesting a central limitation. *Clin. Physiol. Funct. Imaging* 31, 169–174.

Gambini, J., Gomez-Cabrera, M. C., Borras, C., Valles, S. L., Lopez-Grueso, R., Martinez-Bello, V. E., Herranz, D., Pallardo, F. V., Tresguerres, J. A., Serrano, M., and Viña, J. (2011). Free [NADH]/[NAD(+)] regulates sirtuin expression. *Arch. Biochem. Biophys.* 512, 24–29.

Gantz, I., Muraoka, A., Yang, Y. K., Samuelson, L. C., Zimmerman, E. M., Cook, H., and Yamada, T. (1997). Cloning and chromosomal localization of a gene (GPR18) encoding a novel seven transmembrane receptor highly expressed in spleen and testis. *Genomics* 42, 462–466.

Ge, H., Weiszmann, J., Reagan, J. D., Gupte, J., Baribault, H., Gyuris, T., Chen, J., Tian, H., and Li, Y. (2008). Elucidation of signaling and functional activities of an orphan GPCR, GPR81. *J. Lipid Res.* 49, 797–803.

Gjedde, A. (2007). "Coupling of brain function to metabolism: evaluation of energy requirements (Chapter 4.4)," in *Handbook of Neurochemistry: Brain Energetics from Genes to Metabolites to Cells: Integration of Molecular and Cellular Processes*, 3rd Edn, eds A. Lajtha, G. Gibson, and G. Dienel (Heidelberg/New York: Springer Verlag), 400p, 40 illus.

Gjedde, A., Johannsen, P., Cold, J. E., and Østergaard, L. (2005). Cerebral metabolic response to low blood flow: possible role of cytochrome oxidase inhibition. *J. Cereb. Blood Flow Metab.* 25, 1083–1096.

Gjedde, A., Léger, G. C., Cumming, P., Yasuhara, Y., Evans, A. C., Guttman, M., and Kuwabara, H. (1993). Striatal L-DOPA decarboxylase activity in Parkinson's disease in vivo: implications for the regulation of dopamine synthesis. *J. Neurochem.* 61, 1538–1541.

Gjedde, A., and Marrett, S. (2001). Glycolysis in neurons, not astrocytes, delays oxidative metabolism of human visual cortex during sustained checkerboard stimulation in vivo. *J. Cereb. Blood Flow Metab.* 21, 1384–1392.

Gjedde, A., Marrett, S., and Vafaee, M. (2002). Oxidative and nonoxidative metabolism of excited neurons and astrocytes. *J. Cereb. Blood Flow Metab.* 22, 1–14.

Gordon, G. R., Choi, H. B., Rungta, R. L., Ellis-Davies, G. C., and MacVicar, B. A. (2008). Brain metabolism dictates the polarity of astrocyte control over arterioles. *Nature* 456, 745–749.

Goyagi, T., Nishikawa, T., and Tobe, Y. (2011). Neuroprotective effects and suppression of ischemia-induced glutamate elevation by β1-adrenoreceptor antagonists administered before transient focal ischemia in rats. *J. Neurosurg. Anesthesiol.* 23, 131–137.

Hassel, B., and Bråthe, A. (2000). Cerebral metabolism of lactate in vivo: evidence for neuronal pyruvate carboxylation. *J. Cereb. Blood Flow Metab.* 20, 327–336.

Ido, Y., Chang, K., and Williamson, J. R. (2004). NADH augments blood flow in physiologically activated retina and visual cortex. *Proc. Natl. Acad. Sci. U.S.A.* 101, 653–658.

Ido, Y., Chang, K., Woolsey, T. A., and Williamson, J. R. (2001). NADH: sensor of blood flow need in brain, muscle, and other tissues. *FASEB J.* 15, 1419–1421.

Koppenol, W. H., Bounds, P. L., and Dang, C. V. (2011). Otto Warburg's contributions to current concepts of cancer metabolism. *Nat. Rev. Cancer* 11, 325–337.

Larach, D. B., Kofke, W. A., and Le Roux, P. (2011). Potential non-hypoxic/ischemic causes of increased cerebral interstitial fluid lactate/pyruvate ratio: a review of available literature. *Neurocrit. Care* 15, 609–622.

Lehmann, M., Foster, C., and Keul, J. (1993). Overtraining in endurance athletes: a brief review. *Med. Sci. Sports Exerc.* 25, 854–862.

Liu, C., Wu, J., Zhu, J., Kuei, C., Yu, J., Shelton, J., Sutton, S. W., Li, X., Yun, S. J., Mirzadegan, T., Mazur, C., Kamme, F., and Lovenberg, T. W. (2009). Lactate inhibits lipolysis in fat cells through activation of an orphan G-protein-coupled receptor, GPR81. *J. Biol. Chem.* 284, 2811–2822.

Maddock, R. J., Buonocore, M. H., Lavoie, S. P., Copeland, L. E., Kile, S. J., Richards, A. L., and Ryan, J. M. (2006). Brain lactate responses during visual stimulation in fasting and hyperglycemic subjects: a proton magnetic resonance spectroscopy study at 1.5 Tesla. *Psychiatry Res.* 148, 47–54.

Madsen, P. L., Cruz, N. F., Sokoloff, L., and Dienel, G. A. (1999). Cerebral oxygen/glucose ratio is low during sensory stimulation and rises above normal during recovery: excess glucose consumption during stimulation is not accounted for by lactate efflux from or accumulation in brain tissue. *J. Cereb. Blood Flow Metab.* 19, 393–400.

Mailloux, R. J., and Harper, M. E. (2011). Uncoupling proteins and the control of mitochondrial reactive oxygen species production. *Free Radic. Biol. Med.* 51, 1106–1115.

Mangia, S., Garreffa, G., Bianciardi, M., Giove, F., Di Salle, F., and Maraviglia, B. (2003). The aerobic brain: lactate decrease at the onset of neural activity. *Neuroscience* 118, 7–10.

Mathiesen, C., Caesar, K., Thomsen, K., Hoogland, T. M., Witgen, B. M., Brazhe, A., and Lauritzen, M. (2011). Activity-dependent increases in local oxygen consumption correlate with postsynaptic currents in the mouse cerebellum in vivo. *J. Neurosci.* 31, 18327–18337.

O'Brien, J., Kla, K. M., Hopkins, I. B., Malecki, E. A., and McKenna, M. C. (2007). Kinetic parameters and lactate dehydrogenase isozyme activities support possible lactate utilization by neurons. *Neurochem. Res.* 32, 597–607.

Okubo, Y., and Iino, M. (2011). Visualization of glutamate as a volume transmitter. *J. Physiol.* 589, 481–488.

Paulson, O. B., Hasselbalch, S. G., Rostrup, E., Knudsen, G. M., and Pelligrino, D. (2010). Cerebral blood flow response to functional activation *J. Cereb. Blood Flow Metab.* 30, 2–14.

Prichard, J., Rothman, D., Novotny, E., Petroff, O., Kuwabara, T., Avison, M., Howseman, A., Hanstock, C., and Shulman, R. (1991). Lactate rise detected by 1H NMR in human visual cortex during physiologic stimulation. *Proc. Natl. Acad. Sci. U.S.A.* 88, 5829–5831.

Quistorff, B., and Grunnet, N. (2011). The isoenzyme pattern of LDH does not play a physiological role; except perhaps during fast transitions in energy metabolism. *Aging* 3, 457–460.

Rajendran, P., Williams, D. E., Ho, E., and Dashwood, R. H. (2011). Metabolism as a key to histone deacetylase inhibition. *Crit. Rev. Biochem. Mol. Biol.* 46, 181–199.

Ramírez, B. G., Rodrigues, T. B., Violante, I. R., Cruz, F., Fonseca, L. L., Ballesteros, P., Castro, M. M., García-Martín, M. L., and Cerdán, S. (2007). Kinetic properties of the redox switch/redox coupling mechanism as determined in primary cultures of cortical neurons and astrocytes from rat brain. *J. Neurosci. Res.* 85, 3244–3253.

Rasmussen, P., Nielsen, J., Overgaard, M., Krogh-Madsen, R., Gjedde, A., Secher, N. H., and Petersen, N. C. (2010). Reduced muscle activation during exercise related to brain oxygenation and metabolism in humans. *J. Physiol.* 58, 1985–1995.

Rodrigues, T. B., López-Larrubia, P., and Cerdán, S. (2009). Redox dependence and compartmentation of [13C]pyruvate in the brain of deuterated rats bearing implanted C6 gliomas. *J. Neurochem.* 109, 237–245.

Rooney, K., and Trayhurn, P. (2011). Lactate and the GPR81 receptor in metabolic regulation: implications for adipose tissue function and fatty acid utilisation by muscle during exercise. *Br. J. Nutr.* 106, 1310–1316.

Ros, J., Pecinska, N., Alessandri, B., Landolt, H., and Fillenz, M. (2001). Lactate reduces glutamate-induced neurotoxicity in rat cortex. *J. Neurosci. Res.* 66, 790–794.

Ross, J. M. (2011). Visualization of mitochondrial respiratory function using cytochrome C oxidase/succinate dehydrogenase (COX/SDH) double-labeling histochemistry. *J. Vis. Exp.* 23, 57.

Ross, J. M., Öberg, J., Brené, S., Coppotelli, G., Terzioglu, M., Pernold, K., Goiny, M., Sitnikov, R., Kehr, J., Trifunovic, A., Larsson, N. G., Hoffer, B. J., and Olson, L. (2010). High brain lactate is a hallmark of aging and caused by a shift in the lactate dehydrogenase A/B ratio. *Proc. Natl. Acad. Sci. U.S.A.* 107, 20087–20092.

Sappey-Marinier, D., Calabrese, G., Fein, G., Hugg, J. W., Biggins, C., and Weiner, M. W. (1992). Effect of photic stimulation on human visual cortex lactate and phosphates using 1H and 31P magnetic resonance spectroscopy. *J. Cereb. Blood Flow Metab.* 12, 584–592.

Schmalbruch, I. K., Linde, R., Paulson, O. B., and Madsen, P. L. (2002). Activation-induced resetting of cerebral metabolism and flow is abolished by beta-adrenergic blockade with propranolol. *Stroke* 33, 251–255.

Schurr, A., Miller, J. J., Payne, R. S., and Rigor, B. M. (1999). An increase in lactate output by brain tissue serves to meet the energy needs of glutamate-activated neurons. *J. Neurosci.* 19, 34–39.

Schurr, A., Payne, R. S., Miller, J. J., and Rigor, B. M. (1997). Brain lactate is an obligatory aerobic energy substrate for functional recovery after hypoxia: further in vitro validation. *J. Neurochem.* 69, 423–426.

Schurr, A., Payne, R. S., Miller, J. J., Tseng, M. T., and Rigor, B. M. (2001). Blockade of lactate transport exacerbates delayed neuronal damage in a rat model of cerebral ischemia. *Brain Res.* 895, 268–272.

Smith, D., Pernet, A., Hallett, W. A., Bingham, E., Marsden, P. K., and Amiel, S. A. (2003). Lactate: a preferred fuel for human brain metabolism in vivo. *J. Cereb. Blood Flow Metab.* 23, 658–664.

Thangaraju, M., Carswell, K. N., Prasad, P. D., and Ganapathy, V. (2009). Colon cancer cells maintain low levels of pyruvate to avoid cell death caused by inhibition of HDAC1/HDAC3. *Biochem. J.* 417, 379–389.

Uehara, T., Sumiyoshi, T., Itoh, H., and Kurata, K. (2008). Lactate production and neurotransmitters; evidence from microdialysis studies. *Pharmacol. Biochem. Behav.* 90, 273–281.

Ugrumov, M. V. (2009). Non-dopaminergic neurons partly expressing dopaminergic phenotype: distribution in the brain, development and functional significance. *J. Chem. Neuroanat.* 38, 241–256.

Vaishnavi, S. N., Vlassenko, A. G., Rundle, M. M., Snyder, A. Z., Mintun, M. A., and Raichle, M. E. (2010). Regional aerobic glycolysis in the human brain. *Proc. Natl. Acad. Sci. U.S.A.* 107, 17757–17762.

van Hall, G. (2010). Lactate kinetics in human tissues at rest and during exercise *Acta. Physiol.* 199, 499–508.

Wilson, J. E. (2003). Isozymes of mammalian hexokinase: structure, subcellular localization and metabolic function. *J. Exp. Biol.* 206(Pt. 12), 2049–2057.

Wyss, M. T., Jolivet, R., Buck, A., Magistretti, P. J., and Weber, B. (2011). In vivo evidence for lactate as a neuronal energy source. *J. Neurosci.* 31, 7477–7485.

Xu, Y., Ola, M. S., Berkich, D. A., Gardner, T. W., Barber, A. J., Palmieri, F., Hutson, S. M., and LaNoue, K. F. (2007). Energy sources for glutamate neurotransmission in the retina: absence of the aspartate/glutamate carrier produces reliance on glycolysis in glia. *J. Neurochem.* 101, 120–131.

**Conflict of Interest Statement:** The authors declare that the research was conducted in the absence of any commercial or financial relationships that could be construed as a potential conflict of interest.

*Received: 14 January 2012; accepted: 01 March 2012; published online: 19 March 2012.*

*Citation: Bergersen LH and Gjedde A (2012) Is lactate a volume transmitter of metabolic states of the brain? Front. Front. Neuroenerg.* ***4****:5. doi: 10.3389/fnene.2012.00005*